UNIVERSITÉ DU QUÉBEC À MONTRÉAL

GREYWICK, A NEW, HIGHLY REPRESENTATIVE, TRANSGENIC MOUSE MODEL FOR POLYCYSTIC OVARY SYNDROME WITH A NEW THERAPEUTIC TARGET

THESIS
PRESENTED
AS PARTIAL REQUIREMENT OF
THE DOCTORATE IN BIOCHEMISTRY

BY
MOSTAFA ESMAEL

NOVEMBER 2022

UNIVERSITÉ DU QUÉBEC À MONTRÉAL

GREYWICH EST UN NOUVEAU MODÈLE DE SOURIS TRANSGÉNIQUE QUI REPRÉSENTE FORTEMENT LE SYNDROME DES OVAIRES POLYKYSTIQUES AVEC UNE NOUVELLE CIBLE THÉRAPEUTIQUE

THÈSE
PRÉSENTÉE
COMME EXIGENCE PARTIELLE
DU DOCTORAT EN BIOCHIMIE

PAR
MOSTAFA ESMAEL

NOVEMBRE 2022

ACKNOWLEDGEMENT

I would like to pass my sincere gratitude to everyone who helped me to produce this work in this shape. Names are countless, honestly, but I would love to give particular thanks to Dr. Nicolas Pilon, Dr. Catherine Mounier, and Dr. Robert Viger for their enormous help. Dr. Francois Ouellet, Dr. Claire Bénard, Dr. Tatiana Scorza, and Dr. Ali Jenabian, your teaching and directions made a vast difference in my progress and career.

My dear friend Guillaume Bernas is one of the brightest minds I ever met and one of the most helpful people. Karl-F Bergeron, and Rodolphe Soret, my brilliant genetics and molecular biology references. Ouliana Souchkova, Baptiste Charrier, and Benoit Grondin, I cannot thank you enough for all your help and guidance and the many times you backed me on work and troubleshoot errors with me.

Tatiana Cardinal, Félix Antoine Bérubé, Catherine Bélanger, and Grégoire Bonnamour, you made my stay at the lab a delight, thanks a lot. The list goes very long; thank you for your help to everyone who passed through my Ph.D.

DEDICATION

To my late dad, my mom, my family, and

my fiancé, when I started the Ph.D., who is now my lovely wife.

TABLE OF CONTENTS

FIGURES LIST

TABLES LIST

Table Page

ABBREVIATIONS AND ACRONYMS LIST

AgRP	Agouti-related peptide
AMH	Anti-Mullerian hormone
AMPK	Adenosine monophosphate-activated protein kinase
AR	Androgen receptor
ARC	Arcuate nucleus
ART	Assisted reproductive technologies
ATP	Adenosine triphosphate
BMI	Body mass index
CC	Clomiphene citrate
Chr2	Chromosome 2
Chr9	Chromosome 9
CHOP	C/EBP homologous protein
CL	Corpus luteum
COC	Combined oral contraceptive
COS7	African green monkey kidney fibroblast-like cell
CRISPR	Clustered regularly interspaced short palindromic repeats
Ct	Cycle threshold
DAPI	4',6-diamidino-2-phenylindole
DENND1A	Differentially expressed in normal and neoplastic development isoform 1A
DENND1A.V2	DENND1A variant 2

DHT	Dihydrotestosterone
DMH	Dorsomedial hypothalamus
DNA	Deoxyribonucleic acid
DR5	Death receptor 5
Dyn	Dynorphin
E2	Estradiol
ELISA	Enzyme-linked immunosorbent assay
ER	Endoplasmic reticulum
Era	E2 receptor alpha
FBS	Fasting blood sugar
FDFT1	Farnesyl-diphosphate farnesyltransferase
FFAs	Free fatty acids
FOH	Functional ovarian hyperandrogenism
FOXO1	Forkhead box O1
FSH	Follicle-stimulating hormone
FSHB	Follicle-stimulating hormone subunit beta
FSHR	Follicular-stimulating hormone receptor
GABA	Gamma-aminobutyric acid
GCs	Granulosa cells
GDNA	Genomic deoxyribonucleic acid
GFP	Green fluorescent protein
GLCs	Granulosa-lutein cells
GLUT	Glucose transporter proteins
GnRH	Gonadotrophin-releasing hormone
GRP78	BiP/glucose-regulated protein 78
GWAS	Genome-wide association studies
HCG	Human chorionic gonadotropin
HPG	Hypothalamic–pituitary-gonadal

IF	Immunofluorescence
IO	Induction of ovulation
IP	Intra-peritoneal
IRE-1	Inositol-requiring kinase/endoribonuclease 1
IRS	Insulin receptor substrate
IVF	*In vitro* fertilization
JNK	C-jun n-terminal kinase
KNDy	Kisspeptin, neurokinin B, and dynorphin
KO	Knock-out
LET	Letrozole
LH	Luteinizing hormone
LHCGR	Luteinizing hormone/choriogonadotropin receptor
mRNA	Messenger ribonucleic acid
N2A	Neuroblastoma cells
NGF	Nerve growth factor
NIH	National Institutes of Health
NKB	Neurokinin B
NPY	Neuropeptide Y
NSE	Neuron-specific enhancer
ORF	Open reading frame
P4	Progesterone
PAI-1	Plasminogen activator inhibitor-1
PAM	Protospacer adjacent motif
PAMH	Prenatally treated with anti-Mullerian hormone
PBS	Phosphate-buffered saline
PCOM	Polycystic ovary morphology
PCOS	Polycystic ovary syndrome
PCR	Polymerase chain reaction

PeN	Periventricular nucleus
PERK	Protein kinase R-like endoplasmic reticulum kinase
PI3K	Phosphatidylinositol-3-kinase
PIRO	Progranulin-induced receptor-like gene during osteoclastogenesis
PitERtgKO	Complete E2 receptor-alpha knock-out
PKC	Protein kinase C
PNA	Prenatally androgenized
POA	Preoptic area
POMC	Pro-opiomela-nocortin
POU	Pit-oct-unc
PR	Progesterone receptor
RACE	Rapid amplification of cDNA ends
RAD50	DNA repair protein RAD50
ROS	Reactive oxygen species
RT	Reverse transcription
Ser/Thr	Serine/Threonine
SHBG	Sex hormones binding globulins
SNPs	Single-nucleotide polymorphisms
SOCS	Suppressor of cytokine signalling
T	Testosterone
T2D	Type II diabetes
Tac2	Tachykinin 2
TNF-α	Tumour necrosis factor-alpha
TUDCA	Tauroursodeoxycholic acid
Tyr	Tyrosine
UPR	Unfolding protein response
US	Ultrasound
USA	United States of America

VMH	Ventromedial hypothalamus
WHO	World Health Organization

SYMBOLS AND UNITS LIST

<	Less than
ΔCt	Delta cycle threshold
≤	Less than or equal to
©	Copyright
10X	Ten times
H	Hour
IU	International unit
KDa	Kilo Dalton
Min	Minute
°C	Degree Celsius
α-	Alpha
β-	Beta
κ-	Kappa

RÉSUMÉ

Le syndrome des ovaires polykystiques (SOPK) est l'une des causes les plus communes d'infertilité féminine dans le monde. Les critères diagnostiques les plus couramment utilisés pour le détecter sont ceux de Rotterdam. Ces « critères de diagnostic » identifient le syndrome par la présence de deux de ces trois caractéristiques : des kystes multiples dans les ovaires, de l'hyperandrogénie et de l'oligo / anovulation. Greywick (*Gw*) est une lignée de souris transgénique portant un rapporteur fluorescent sous le contrôle du promoteur de *Gata4*, qui permet notamment de marquer les cellules de la crête neurale pendant l'embryogenèse. À l'état homozygote, nous avons noté que les femelles *Gw* deviennent obèses et sous-fertiles, rappelant le sous-type métabolique du syndrome des ovaires polykystiques (SOPK). Cette observation nous a motivé à mieux caractériser le phénotype des femelles *Gw*, dans l'espoir que ceci aiderait à expliquer le lien entre le gène *GATA4* et le SOPK dans les études génétiques humaines. Ces caractéristiques incluent l'obésité, la sous-fécondité et l'hyperandrogénie. Notre travail a confirmé des anomalies dans les niveaux plasmatiques de l'hormone d'œstrogène, testostérone et de l'hormone lutéinisante chez les souris *Gw*. On a également détecté des anomalies de fertilité chez les souris *Gw*, notamment un faible nombre des bébés, des anomalies du cycle œstral et une faible production d'ovocytes, en réponse à l'induction de l'ovulation, avec un grand pourcentage d'ovocytes non viables et non fécondables. Les ovaires des souris *Gw* montrent aussi un grand nombre de kystes, et des follicules ovariens atrétiques, plus, un faible nombre des follicules en croissance et des corps jaunes. La caractérisation métabolique a aussi montré une obésité significative, une résistance à l'insuline, de l'hyperinsulinémie, et de l'intolérance au glucose, chez certaines des souris *Gw*. On a aussi détecté une sous-expression des récepteurs des hormones de reproduction dans l'hypothalamus des souris *Gw*. Nos résultats suggèrent que ces anomalies sont attribuées à la partie Gata4 du transgène utilisé pour générer ce modèle. Alors, nos données soutiennent l'hypothèse d'une " résistance hypothalamique aux signaux de rétroaction hormonaux " comme une explication de l'origine de ce syndrome. Nous avons également détecté une sous-expression des neuropeptides métaboliques dans l'hypothalamus des souris *Gw*. Enfin, nous avons détecté des niveaux élevés de stress du réticulum endoplasmique dans les ovaires des souris *Gw*, et on les identifie comme une cible thérapeutique potentielle, en utilisant le TUDCA +/- le Metformin pour sauver la production, et la fécondabilité de ses ovocytes.

Mots clés : Fécondation *in vitro*, modèles animaux, stress du réticulum endoplasmique, TUDCA.

ABSTRACT

Polycystic ovary syndrome (PCOS) is one of the most common causes of female infertility worldwide. The most used diagnostic criteria are the Rotterdam criteria which require two of the following three key features: multiple cysts in the ovaries, hyperandrogenism, and oligo or anovulation. *Greywick* (*Gw*) is a transgenic mouse line bearing a *Gata4* promoter-driven fluorescent reporter, notably serving to label neural crest cells during embryogenesis. In the homozygous state, we noted that *Gw* females become obese and subfertile during adulthood, reminiscent of the metabolic subtype of polycystic ovary syndrome (PCOS). This observation prompted us to further characterize the phenotype of *Gw* females, hoping that this would help to explain the known association between *GATA4* and PCOS in human genetic studies. These similarities included obesity, subfertility and hyperandrogenism. Further testing for polycystic ovary syndrome key features in *Gw* mice confirmed anomalies in the plasma levels of estrogen, testosterone, and luteinizing hormone. Also, fertility abnormalities were detected in *Gw* mice in the form of low numbers of pups, estrous cycles, and low numbers of oocytes, in response to induction of ovulation, with a high percentage of non-viable and non-fertilizable oocytes. *Gw* mice ovaries also mimicked the polycystic ovary syndrome picture known in humans with many cysts, and atretic follicles, besides a low number of growing follicles and corpora lutea. The metabolic profile of *Gw* mice further validated polycystic ovary syndrome features in our model with significant obesity, insulin resistance, hyperinsulinemia, high leptin levels, and impaired glucose tolerance, in some of the *Gw* mice. In our pursuit of the origin of this syndrome, we detected hypothalamic reproductive hormone receptors under expression in *Gw* mice, including those of estrogen, progesterone, follicle-stimulating hormone, luteinizing hormone, testosterone, and gonadotropin-releasing hormone. Results further suggest that these receptor anomalies are attributed to the Gata4 part of the transgene used to generate the *Gw* model. Our data support the hypothesis of 'hypothalamic resistance to hormonal feedback signals' as the origin of this syndrome. We also detected metabolic neuropeptides under expression in *Gw* mice hypothalamus including pro-opiomela-nocortin, agouti-related peptide, and neuropeptide Y. Finally, we identified high endoplasmic reticulum stress levels in *Gw* mice ovaries as a potential therapeutic target, by treating *Gw* mice with TUDCA +/- Metformin and rescuing oocytes production, and fertility.
Keywords: Animal models, endoplasmic reticulum stress, *in vitro* fertilization, TUDCA.

CHAPTER I: REVIEW OF THE LITERATURE

1.1 Female reproductive system

1.1.1 Anatomy

Mice have long been used to study human diseases due to their genetic and physiological similarities to humans, and for being economic and easy to handle (Waterston, Lindblad-Toh et al. 2002, Foster, Small et al. 2014, Perlman 2016). Though, mice have adapted and evolved differently in some systems. These systems differences explain the failure of some medications that work perfectly in mice when tested in humans, particularly cancer medications (Adams 2012). A common cause of medication failure for tested drugs in genetically induced mice is the low phenotypic similarity to the human disease (Elsea and Lucas 2002). So, for a medication that perfectly works in mice to be efficient in humans, a high level of phenotypic similarity is crucial.

The female reproductive system is very similar and conserved among humans and mice (Figure 1.1, 1.2, humans, mice, respectively), and almost the same physiological mechanisms control its functions. The female reproductive system is divided into reproductive organs and a neuroendocrine regulatory system. The reproductive organs include the vagina (the birth canal), the uterus (the site for embryo fertilization, implantation, and growth), and the ovaries, which constitute the oocytes reserve and

maturation site. The vagina is a muscular organ with a mucosal lining that acts as a reservoir for male gametes (spermatozoa) until they migrate through the cervix to the uterus to meet the mature oocyte/s in the ampulla of the fallopian tube where fertilization occurs. The uterus has three layers, being found from the inside out the endometrium, the myometrium, and the perimetrium. The perimetrium is the outer connective tissue support of the uterus. The myometrium is the muscular layer of the uterus and is crucial for delivering the fetus by labour contractions, and for homeostasis thereafter. Lastly, the endometrium is the innermost layer of the uterus, and it is the implantation site of the embryo. It also works as the attachment bed for the placenta through which the fetus exchanges gases and nutrients with the mother. Endometrial growth is cyclic and synchronized with the ovulation cycle, as will be explained in the physiology section. A healthy and functional endometrium is vital for the success of implantation and the maintenance of pregnancy. In humans, the fallopian tubes have four main parts, from medial to lateral: the isthmus, ampulla, infundibulum, and the most distal proportion, the fimbria (Figure 1.1). The fallopian tubes act to pick up the luteinized oocytes from the adjacent ovary, through the fimbria and keep them in the ampulla where fertilization happens. The anatomical proximity of the fimbria of the fallopian tubes to the ovaries allows this process to occur (OpenStax 2013).

Anatomical differences exist between the female reproductive organs in mice and humans. Oviducts in mice are anatomically equivalent to human fallopian tubes (both having infundibulum and ampulla) but are relatively smaller and more tortuous than their human counterpart. The uterus also shows some anatomical differences. In mice, two uterine horns are lined with endometrium, have a muscular wall and serve as the implantation and maturation site for embryos: a small connecting body links them to the vagina (Figure 1.2) (Jackson_Laboratory 1966). In humans, on the other hand, there are no uterine horns, and the uterus body is the main site for the implantation and maturation of embryos.

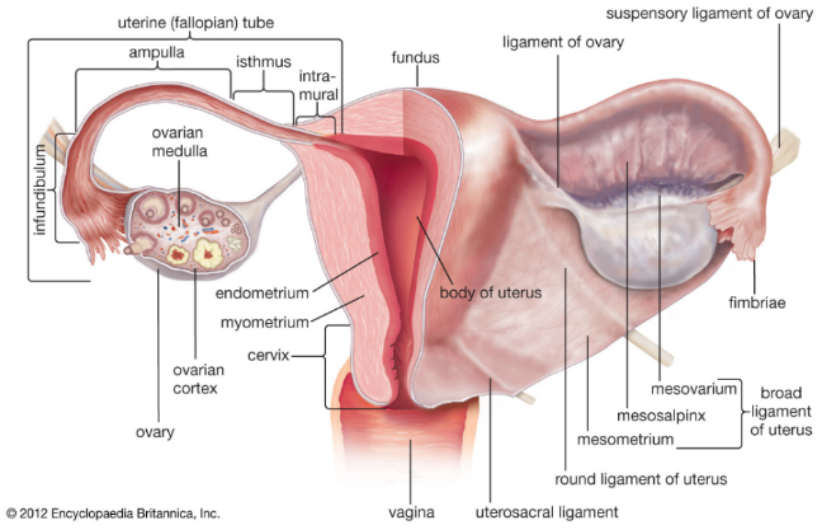

1.1 Human female reproductive organ anatomy.

The illustration represents female reproductive organs including, the vagina, the uterus, and fallopian tubes. The image demonstrates the proximity of the ovary to the fimbria of the fallopian tubes, where it picks up ovulated oocyte. The photo was adapted from Encyclopedia Britannica, Inc (2019), *Uterus anatomy,* https://www.britannica.com/science/uterus.

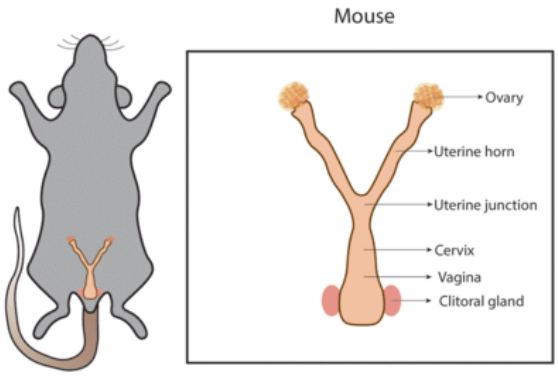

1.2 Mouse female reproductive organ anatomy.

The diagram shows the closeness of mice's oviducts and their ovaries. Different from humans, a mouse uterus has two uterine horns, a body, and a cervix. The photo was adapted from (Chumduri and Turco 2021), *Organoids of the female reproductive tract* Journal of Molecular Medicine.

The ovaries are the reservoir of oocytes and are a vital component of female fertility. Ovaries in humans and mice share the same anatomical and functional structure. In humans, a female is born with a fixed number of oocytes (stock) in each ovary and usually starts cycling using a cohort of oocytes, among which one or more oocytes reach maturity monthly. In some women, two or more oocytes can reach maturity simultaneously, which causes multiple non-conjoined pregnancies. In mice**,** the oocyte cohort that starts maturation is relatively more prominent than in humans, ending up with a higher number of ovulated oocytes in each cycle. An outer capsule surrounds the ovarian tissue and is composed of ovarian stroma to which the blood supply passes from the ovarian suspensory ligament. Ovarian stroma represents the ovarian medulla, surrounded by a cortex where the primordial follicles' stock resides. The primordial follicles start to grow at each cycle, and therefore the cortex also contains different stages of follicular growth as explained in detail in section 1.1.2 (Figure 1.5 humans, Figure 1.6 mice). As the growing follicles reach maturity, they erupt through the ovarian capsule and are picked up by the close fimbria of the fallopian tube/oviducts, in humans, and mice, respectively. Ovulation leaves a corpus luteum (CL) or corpus albicans in the ovarian cortex. The mature oocyte produced by the ovary stays in the ampulla of the fallopian tubes/oviducts, where it usually meets the spermatozoon and gets fertilized. The fertilized zygote is then pushed towards the uterine lumen/horns (humans, mice, respectively) by the villi of the fallopian tubes/oviducts for implantation in the endometrium. The uterus then expands, allowing embryo growth under the effect of progesterone (P4) from the CL at the start and the placenta afterwards (Zakar and Mesiano 2011). After fertilization, the cervix of the uterus becomes closed, and cervical mucus thickens to prevent the passage of more spermatozoa and various organisms (bacteria, viruses, and parasites) to the embryo.

1.1.2 Physiology

1.1.2.1 Hypothalamus-Pituitary-Gonadal (Ovary) Axis

The hypothalamic-hypophyseal-ovarian axis, also known as the hypothalamus-pituitary-gonadal axis is a tight neuroendocrine system that orchestrates the function of reproductive organs and assures fertility (Figure 1.3). This system starts in the hypothalamus, particularly in the preoptic area (POA) and arcuate nucleus (ARC) of the hypothalamus. In the ARC, axons from a subgroup of POA-located neurons secrete the gonadotropin-releasing hormone (GnRH), which is delivered by portal circulation to the anterior half of the pituitary gland to regulate the production of a follicle-stimulating hormone (FSH) and luteinizing hormone (LH) (Plant 2015).

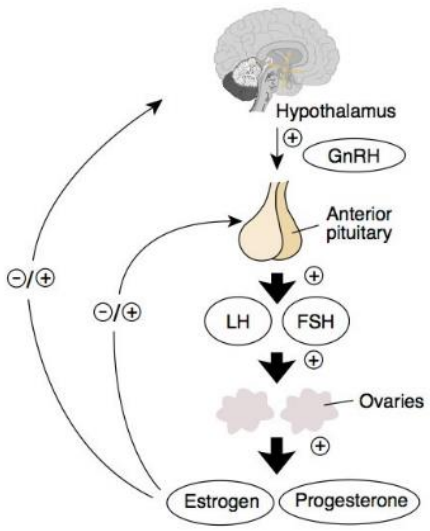

1.3 Hypothalamus-pituitary-gonadal (Ovary) axis.

The diagram summarizes the neuroendocrine axis controlling the female reproductive cycle and the regulatory feedback signals involved in synchronizing hormone production and release. Estrogen and P4 from ovaries have a complex feedback effect on both the pituitary and the hypothalamus as they change GnRH pulse frequency, turning FSH and LH up and down depending on where in the cycle the female is. Diagram acquired from (Kong, Tang et al. 2014), *Schematic representation of the hypothalamic—pituitary—gonadal (HPG) axes,* Int. J. Mol. Sci. 2014, 15, 21253-21269; Doi: 10.3390/ijms151121253.

GnRH is released in low or high pulse frequencies to regulate the ratio between FSH and LH production (Thompson and Kaiser 2014). Low GnRH pulse frequency favors FSH production over LH, which happens during the first half of the ovarian cycle (follicular phase). On the other hand, high GnRH pulse frequency favors LH over FSH to induce ovulation in the second half of the ovarian cycle (luteal phase). The uterine endometrial cycle is divided into a proliferative and a secretory phase, corresponding to the follicular and the luteal phases of the ovarian cycle, respectively, under the effect of ovarian hormones. Ovarian and uterine cycles are explained in detail in sections 1.1.2.3 and 1.1.2.4, respectively.

The hypothalamus and the pituitary both regulate the amplitude of LH pulses. LH pulse frequency is mainly controlled by the upstream GnRH pulse frequency handled by the interplay between different neurons in the neuroendocrine circuit regulating GnRH neurons, known as the "GnRH pulse generator" (Clarkson, Han et al. 2017). Among the most important neurons in this neuroendocrine circuit are gamma-aminobutyric acid (GABA) and kisspeptin neurons (Gottsch, Cunningham et al. 2004, Moore, Prescott et al. 2015). Both neurons are stimulatory for GnRH neurons, and their signals regulate GnRH production, pulse frequency, and amplitude, alongside kisspeptin neurons' inhibitory signals mediated through its dynorphin peptide. These upstream regulatory neurons (Kisspeptin and GABA) are responsive to feedback signals from steroid hormones, including estrogen (E2), P4 and androgen produced in the ovaries. This regulatory mechanism synchronizes the ovarian cycle and its follicular maturation with the hypothalamus-pituitary axis. These neurons detect the growth of a Graafian follicle among other follicles through the levels of E2 production, to switch GnRH pulse frequency from low to high, which favors LH production over FSH. A relatively low FSH level is not enough for the cohort of growing follicles, which eventually causes them to atrophy, except for the selected mature Graafian follicle. High LH acts on the mature Graafian follicle to induce ovulation and form a CL that produces P4.

P4, in turn, switches GnRH neurons again back to a low pulse frequency to favor FSH over LH and start a new cycle if pregnancy did not occur. Therefore, Kisspeptin and GABA neurons (and indirectly, GnRH neurons) are thought to detect GnRH regulating feedback signals through their steroid hormone receptors.

Kisspeptin is a 54-amino-acid protein hormone synthesized in the hypothalamus that exerts its action through a transmembrane Kiss1R receptor (Gottsch, Clifton et al. 2006). ARC-located kisspeptin neurons are also known as kisspeptin, Neurokinin B (NKB), and dynorphin neurons (KNDy), as they co-express NKB and Dynorphin (Dyn) (Goodman, Lehman et al. 2007). Both NKB and Dyn play a crucial role in regulating kisspeptin neuron activity and, therefore, GnRH and LH levels downstream (Navarro, Gottsch et al. 2009). Terasawa et al. reported that Neurokinin 3 and signalling through its receptor 'Neurokinin 3 receptor' signalling increase the release of GnRH, which is like the effect of kisspeptin (Terasawa, Garcia et al. 2018). Mutations in genes that encode either tachykinin 3 (*TAC3)* or its receptor (*TACR3)* genes in humans (encoding Neurokinin 3 and Neurokinin 3 receptors, respectively) (Navarro 2013)) are associated with hypogonadotropic hypogonadism (Topaloglu, Reimann et al. 2009). *Tachykinin 2* (*Tac2)* gene and *Tacr3* are the corresponding genes in rodents (Navarro 2013). Dyn, on the other hand, decreases LH secretion through its action on kappa opioid receptors. These receptors are thought to be inhibitory to KNDy neurons (Weems, Witty et al. 2016). Furthermore, Dyn also has an autocrine regulatory effect on the same neurons (Weems, Coolen et al. 2018). As mentioned before, ARC KNDy neurons are sensitive to negative feedback regulatory signals of sex hormones through androgen and E2 receptors (Smith, Cunningham et al. 2005, Kauffman, Gottsch et al. 2007). In contrast, anteroventral periventricular nucleus/PeN kisspeptin neurons are sensitive to positive feedback regulatory signals from estradiol (E2) and P4 (Kauffman, Gottsch et al. 2007, Stephens, Tolson et al. 2015). Dysfunctions of this neuron circuit lead to fertility problems, as will be discussed below in section 1.3. The interplay between different

KNDy neuron neuropeptides (in the ARC) and their role in regulating GnRH neurons (in the POA) is summarized in Figure 1.4.

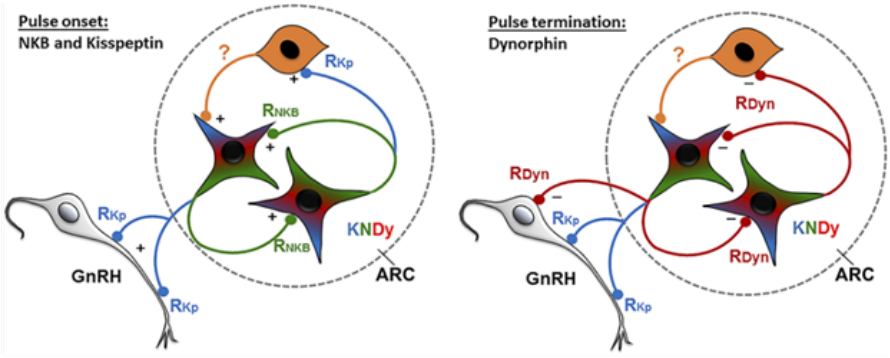

1.4 The interplay between KNDy neuron neuropeptides and GnRH neurons.

The diagram summarizes the Neurokinin B, kisspeptin, and dynorphin (of the KNDy neurons) sequential actions and their role in regulating GnRH neurons. Diagram adapted from (Moore, Coolen et al. 2018), PubMed Review, *Endocrinology*, DOI: 10.1210/en.2018-00389.

1.1.2.2 *Gnrh* Gene Expression

In mice, *Gnrh* gene expression is intermittent and controlled by a promoter region known as the neuron-specific enhancer (NSE) (Vazquez-Martinez, Leclerc et al. 2002). The *Gnrh* NSE promoter has been extensively characterized and different binding motifs for various transcription factors were identified in it (Clark and Mellon 1995, Lawson, Whyte et al. 1996, Belsham and Mellon 2000, Kelley, Givens et al. 2002, Givens, Kurotani et al. 2004, Rave-Harel, Givens et al. 2004, Givens, Rave-Harel et al. 2005). Among the well-characterized motifs are binding sites for, Pit-Oct-Unc (POU) transcription factor and octamer transcription factor 1 site (Oct-1) (Leclerc and Boockfor 2005). Three Oct-1 sites are present in the *Gnrh* NSE promoter (Leclerc and Boockfor 2005). Two of these sites are critical for *Gnrh* gene pulse expression (Leclerc and Boockfor 2005). Two GATA-binding motifs are also present in the *Gnrh* NSE

promoter, GATA-A (1753–1734) and GATA-B (1730–1706), with a common core deoxyribonucleic acid (DNA) motif: 5’ -(A/T) GATA (A/G) (Lawson, Whyte et al. 1995, Lawson, Whyte et al. 1996). Interestingly, the Oct transcription factors are sensitive to oxidative and metabolic stress (Tantin, Schild-Poulter et al. 2005).

1.1.2.3 GATA Transcription Factors Family

Analysis of various vertebrate cells and tissue proteins has led to the identification of six GATA transcription factors that recognize the common “GATA” DNA-binding site. GATA factors contain two zinc finger domains that bind to the GATA sequence motif and allow protein-protein interaction with other transcription factors (Molkentin 2000). GATA factors can be subdivided into two groups based on their function and tissue expression patterns. The first group includes GATA1, GATA2, and GATA3, which play a role in expressing genes involved in hematopoietic stem cell differentiation (Patient and McGhee 2002). GATA2 and GATA3 are also involved in the differentiation of some cell types in the mammalian pituitary gland and placenta (Ng, George et al. 1994, Dasen, O'Connell et al. 1999, Suh, Gage et al. 2002). The second group includes GATA4, GATA5, and GATA6, which are expressed in different organs including the heart, liver, lung, gut, and gonads, where they play a key role in regulating gene expression (Arceci, King et al. 1993, Kelley, Blumberg et al. 1993, Laverriere, MacNeill et al. 1994, Morrisey, Ip et al. 1996, Suzuki, Evans et al. 1996). Growing evidence in the literature suggests that some of these GATA transcription factors are implicated in gene expression in GnRH neurons. A study in 1996 showed evidence of the expression of GATA2 and GATA4 factors in GT1-7 cells, an immortalized cell line derived from mature GnRH neurons (Lawson, Whyte et al. 1996). GATA4 was the only transcription factor found in a complex binding to the GATA-B motif in the GnRH NSE promoter region (Lawson, Whyte et al. 1996). This finding strongly suggests a role for the GATA4 transcription factor in GnRH pulse regulation. Interestingly, in mice, some studies revealed that GATA4 expression in GnRH neurons is higher during

embryonal migration (embryonic age 13.5 days [e.13.5]) when compared to mature neurons (Lawson and Mellon 1998). Because of the conserved DNA-binding domain between GATA transcription factors, other GATA family members could also regulate *Gnrh* gene expression in mature GnRH neurons. Another study confirmed *GATA5* and *GATA6* expression in hypothalamic GT1-7 cells by reverse transcription-polymerase chain reaction (RT-PCR) and western blot (Leclerc, Bose et al. 2008). The binding of GATA5 to the GATA-A motif in the *Gnrh* NSE promoter region was also detected in the same study. Together, these findings suggest that multiple factors may regulate *Gnrh* gene expression pulses simultaneously. Elimination of both GATA4 and GATA5 completely disrupts *Gnrh* gene expression pulses (Leclerc, Bose et al. 2008). Also, combined mutations in GATA-A and GATA-B binding motifs within the *Gnrh* NSE promoter region completely disrupts *Gnrh* gene expression pulses, whereas modification of only one of the two sites partially alters them (Leclerc, Bose et al. 2008).

1.1.2.4 Ovarian Cycle

The ovarian cycle is divided into two phases, the follicular phase under the effect of FSH, and the luteal phase under the effect of LH. Ovulation occurs early in the luteal phase under the effect of the LH surge (Treloar, Boynton et al. 1967). Follicular growth starts under the effect of FSH, and the ovary begins using its primordial follicle stock to produce a cohort of growing oocytes, known as primary follicles (Figure 1.5). Most of the primary follicles stop growing and just contribute to the hormonal output, then, usually, one continues to grow into the Graafian follicle in humans (Durlinger, Kramer et al. 1999). In mice, a larger number of follicles continue growing into mature Graafian follicles. The different stages of follicular growth are similar between mice and humans (Figure 1.6). The cohort of growing follicles produces an increasing amount of E2 (through their granulosa cells) and inhibin as they mature, which signalizes the pituitary to decrease FSH production through negative feedback (Sawetawan, Carr et al. 1996, Welt, Martin et al. 1997). At this point, one oocyte is selected and becomes the

dominant follicle. It grows to become the Graafian follicle and is then ready for ovulation (Feingold KR 2018). Ovarian E2 also influences the hypothalamus to switch GnRH pulse frequency from low to high, to start the second half of the cycle (luteal phase) where LH levels become higher than FSH (Welt, Pagan et al. 2003). As FSH drops, the remaining primary follicles in the growing cohort, the non-dominant ones, do not have sufficient FSH to continue growing and therefore they atrophy. Persistently high E2 levels generate a fast rise in LH level, which is known as the LH surge. The LH surge is the signal for the mature Graafian follicle to luteinize and liberate the mature oocyte (ovulation) (Hoff, Quigley et al. 1983).

Graafian follicles ovulate and give rise to mature oocytes ready for the fallopian tube fimbria to pick them up for fertilization. The rest of the Graafian follicle becomes the CL and starts producing P4 to maintain pregnancy if fertilization of the oocyte occurred (Figure 1.5). At this moment, it becomes the CL and starts producing P4 to maintain pregnancy. Later, as the placenta develops, it takes over the role of the CL in P4 production, for the remaining of the pregnancy. High P4 levels have a negative feedback effect on the pituitary and the hypothalamus preventing them from starting a new ovarian cycle during pregnancy. Without oocyte fertilization, the CL atrophies and becomes corpus albicans, and P4 and inhibin levels drop, allowing for a new cycle to start (Groome, Illingworth et al. 1996).

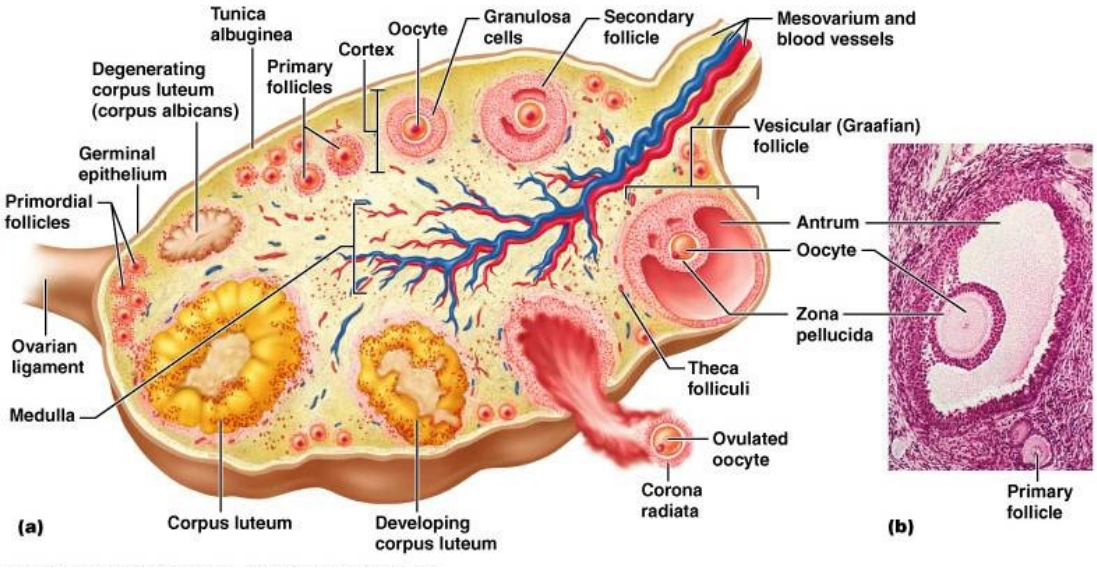

1.5 Different stages of ovarian follicular growth in humans.

(a) A diagram that shows different stages of follicular growth starting from the stock of primordial follicles to primary follicles, where the number of GCs (oocytes' supporting cells) grows. As the number of GCs increases, one follicle is selected and becomes dominant which later progresses to become the mature Graafian follicle. (b) The Graafian follicle containing the mature oocyte and well-differentiated granulosa and theca cells is further characterized by the presence of a fluid-filled antrum. After ovulation, the remaining granulosa and theca cells become the CL (yellow body). Photo adapted from (Marieb 2001), Human anatomy and physiology, 5th ed, Chapter 28, *The Reproductive System*, Pearson.

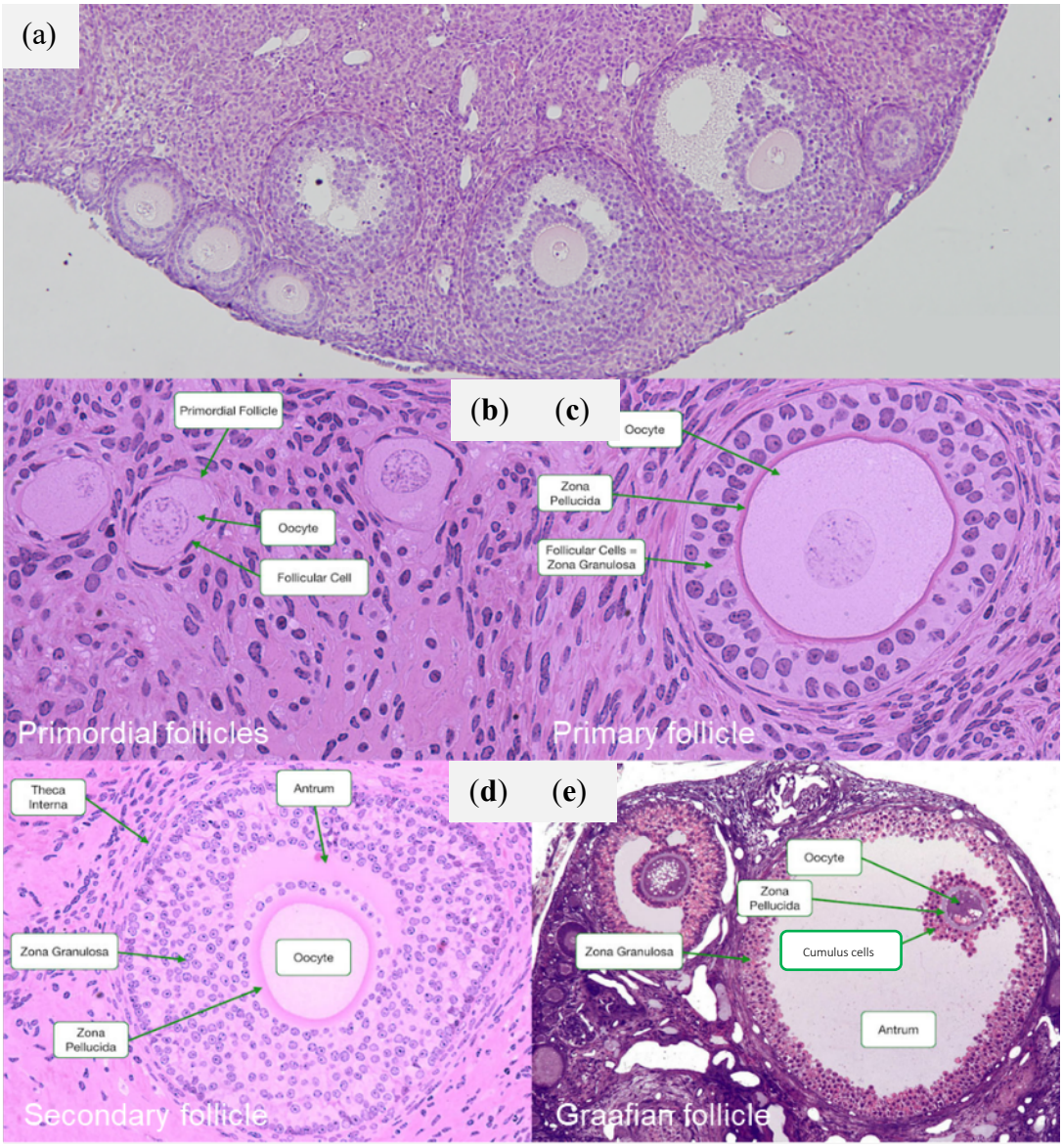

1.6 Mouse ovary histology.

(a) Hematoxylin and eosin sections show different stages of follicular growth in mice ovaries. The lower four panels (b-e) show various cell layers in growing follicles: primordial, primary, secondary, and Graafian follicles. Mouse follicles go through the same stages of growth and cellular differentiation as human follicles. Photos were adapted and modified from Histology @ Yale, *Female Reproductive System Lab*, http://medcell.med.yale.edu/histology/female_reproductive_system_lab.php.

Growing follicles in the ovary play an essential role in regulating the hypothalamic-pituitary-gonadal axis (HPG) axis through the production of steroid hormones, principally E2 and P4. Figures 1.5 and 1.6 show that growing follicles have an increasing number of granulosa cells (GCs) around the oocyte. GCs are the primary source of E2 in the ovary, and they are particularly responsive to FSH since they exclusively express FSH receptors (Feingold KR 2018). The increase in the number of GCs in the growing cohort of oocytes leads to a proportionate increase in their FSH receptors, making them more sensitive to FSH, and increasing E2 production in return (Feingold KR 2018). Rising E2 increases E2 receptors on the surface of GCs (Nimrod, Erickson et al. 1976). FSH in the presence of E2 stimulates GCs to express LH receptors in the preparation of the Graafian follicle for ovulation (Feingold KR 2018). At a certain level, rising E2 signalizes the hypothalamus to switch the GnRH production to high pulse frequency favouring LH production over FSH.

The outer layer of growing follicles contains theca cells, which are more elliptical than the rounded GCs. Theca cells express the LH receptor throughout the cycle in contrast to GCs. LH working on theca cells stimulates the production of androstenedione, and to some extent, testosterone (T). Androstenedione then moves to GC, where it is converted by aromatase (induced by FSH) to estrone then to E2 by 17-β-hydroxysteroid dehydrogenase type I (Zeleznik, Midgley et al. 1974, Feingold KR 2018). The interaction between the granulosa and theca cells to regulate E2 production is known as the two-cell, two-gonadotropin hypothesis (Figure 1.7) (Liu and Hsueh 1986).

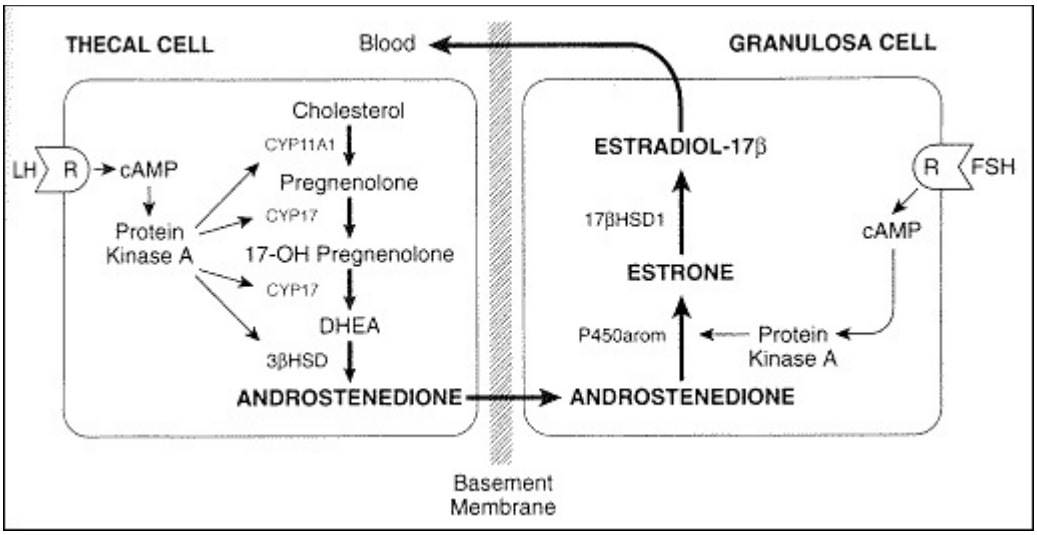

1.7 The interplay between granulosa and theca cells according to the two-cell, two-gonadotropin hypothesis for E2 production regulation.

In response to FSH, GCs convert androstenedione (delivered by theca cells) into estrone, then E2, which diffuses to the circulation. Theca cells react to LH by converting cholesterol to androstenedione. The latter diffuses through the basement membrane to GCs to be used for E2 production. Photo adapted from (Feingold KR 2018), *William's Textbook of Endocrinology 9th edition*, WB Saunders, Philadelphia, p.751-817, Endotext.

1.1.2.5 Uterine Cycle

E2 and P4 produced during the first and the second half of the ovarian cycle, respectively, regulate the uterine endometrial cycle generating proliferative and secretory phases. In this way, the ovary, through its endocrine function, prepares the uterus for implantation and pregnancy afterwards. The synchronization and harmony between the ovarian and the uterine cycles are crucial for the maintenance of fertility. As E2 levels build up in the follicular phase, the uterine endometrial glands proliferate and adopt a narrow tubular form with pseudo-stratification. After ovulation, which occurs on day 14 in a typical 28-day human cycle, E2 levels start to drop, and P4 starts to rise (luteal phase) to initiate the uterine secretory phase. In the secretory phase, the

proliferated endometrium suffers secretory changes where glands become more pseudostratified and accumulate glycogen. These endometrial changes confirm P4 production in the ovary by CL and therefore, ovulation. If fertilization of the oocytes occurs and pregnancy starts, the produced P4 keeps the endometrium in the secretory phase to allow the implantation of the embryo and placental attachment. P4 plays multiple critical roles in maintaining pregnancy besides endometrial changes, like inducing uterine relaxation. If fertilization of the oocyte does not occur, the CL degrades into corpus albicans as explained above, and P4 levels fall, leading to loss of the hormonal support for the endometrium. Secondary to P4 loss, the spiral arterioles that typically supply the endometrium with blood get coiled and constricted, and this cuts the blood supply from the endometrium leading to endometrial glands' death shedding (menstrual bleeding). Figure 1.8 simplifies the hormonal interaction and the crosstalk between reproductive organs at different phases of the reproductive cycle (Figure 1.8) (Feingold KR 2018).

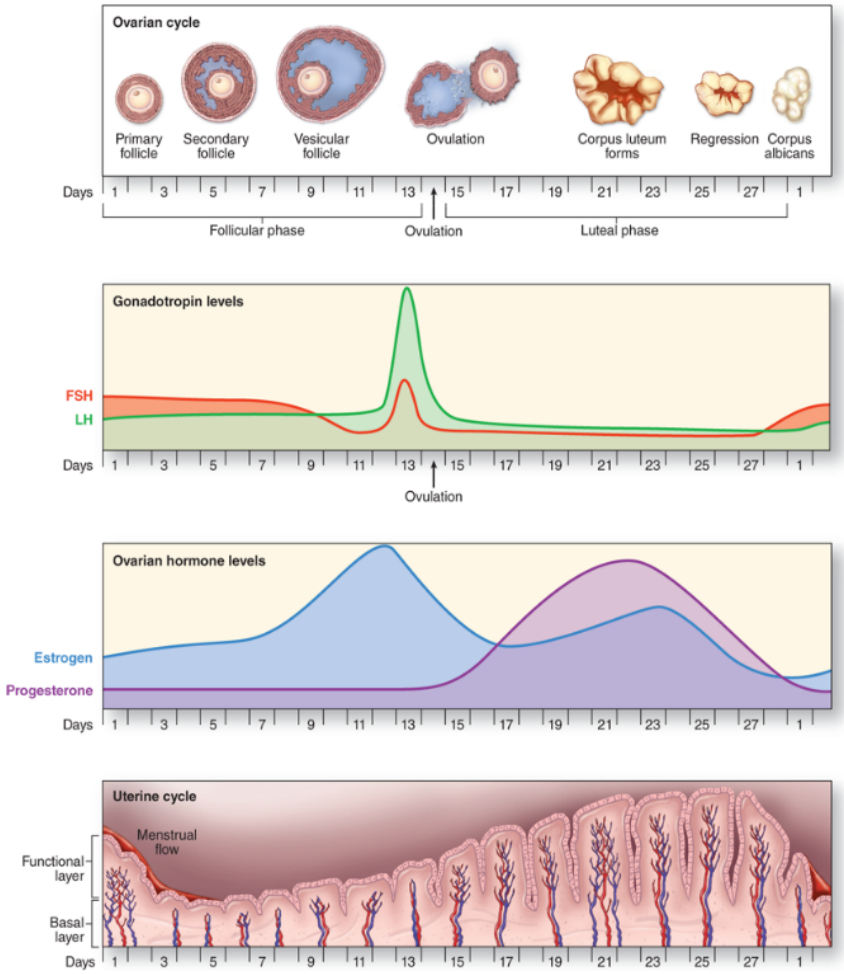

1.8 Hypothalamic-hypophysial ovarian-uterine harmony during the female cycle.

The female reproductive cycle can be viewed as a symphony orchestrated by the hypothalamic GnRH, leading to pituitary FSH and LH production and, therefore, ovarian response with E2 and P4 in a perfectly synchronized manner. As the oocytes mature, the ovary (through its endocrine function) prepares the endometrium for implantation and pregnancy. Simultaneously, ovarian hormones crosstalk with the pituitary and the hypothalamus to inform them of where the oocytes are regarding their growth. The CL also communicates with the pituitary and the hypothalamus to signal pregnancy or the start of a new cycle. Photo adapted from Anthony L. Mescher: Junqueira's basic histology, 14th edition, *Chapter 22: The Female Reproductive System*. Https://accessmedicine.mhmedical.com/book.aspx?bookid=1687.

In mice, the equivalent cycle, known as the estrous cycle, resembles the human menstrual cycle, although with some key differences. The estrous cycle is 4–5 days long, and it contains 4 phases, proestrus, estrus, metestrus, and diestrus (Miller and Takahashi 2013). Usually, the proestrus and metestrus phases take one day in mice, and up to 2 days in the estrus and diestrus phases (Caligioni 2009). Metestrus and diestrus show a slow, gradual increase in E2 and P4 that reaches a fast acceleration in the proestrus phase when oocyte maturation reaches its maximum. High levels of E2 switch GnRH pulse frequencies from low to high, increasing LH hormone levels and concomitantly decreasing FSH levels. Like the human cycle, the continuously rising E2 causes a sudden rise in LH levels (LH surge), and ovulation occurs in the late proestrus phase. During the estrus phase, all hormone levels start to decrease, then gradually build up again for the next cycle in the metestrus phase. The hormonal interplay between the hypothalamus and the ovary is very similar in mice and humans (Figure 1.9) (Caligioni 2009).

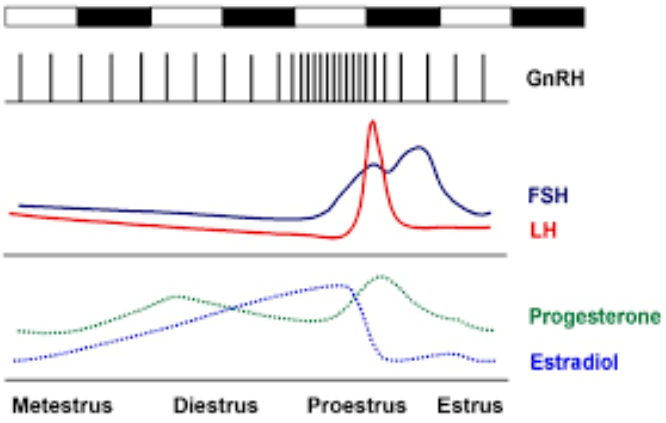

1.9 Different stages of the mouse estrous cycle and the hormonal interplay during them. The main difference between the human and mouse cycles is that the latter lasts for 4–5 days instead of 28 days in humans. The phases of mice's hormonal cycles are like those of humans (the proestrus corresponds to the follicular phase in humans, and the estrus to the luteal phase). The photo is adapted from (Miller and Takahashi 2013).

As in humans, the hormonal cycle affects the mouse uterine endometrium. The various phases of the mouse estrous cycle can be detected by following changes in the mouse vaginal epithelium, in response to the hormonal cycle (an in-detail explanation of the estrous cycle analysis using vaginal lavage and crystal violet stain is provided in the materials and methods chapter to come). Figure 1.10 shows the different types of cells in each phase of the estrous cycle. In the proestrus phase, the vaginal epithelium is well developed, and the vaginal cells have an apparent nucleus (as hormones peak). The hormone levels start to drop in the estrus phase, and the endometrium and vaginal epithelium lose their hormonal support. Here, the vaginal epithelial cells become keratinized cells, and the nucleus is no longer visible. At the metestrus phase, inflammatory cells start to appear to clear the dead keratinized cells from the previous phase. During the diestrus phase, the clearance process is advanced enough to eliminate most of the dead cells, and the vaginal lavage shows mainly inflammatory cells (dark purple small cells) (Figure 1.10) (Caligioni 2009, Byers, Wiles et al. 2012).

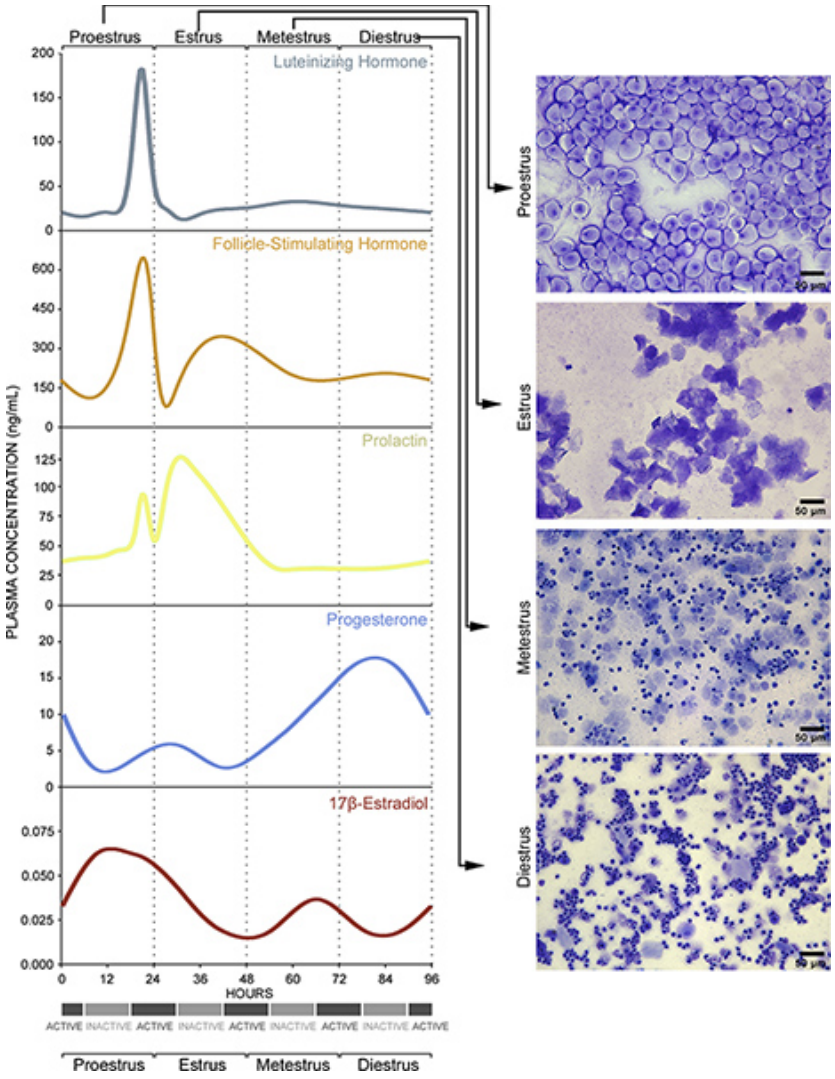

1.10 Different types of cells in mouse vaginal lavage and corresponding hormonal changes during an estrous cycle.

The right first panel shows mature epithelial cells with an apparent nucleus corresponding to the proestrus phase. Epithelial cells then die and become keratinized in the estrus phase, the second panel. Inflammatory cells (small dark cells) appear later in the metestrus phase and dominate in the diestrus phase, third and fourth panels, respectively. Photo adapted from the Journal of Visualized Experiments, *the protocol of vaginal lavage* (Au - McLean, Au - Valenzuela et al. 2012), https://www.jove.com/t/4389/performing-vaginal-lavage-crystal-violet-staining-vaginal-cytological.

1.1.3 Infertility

The most recently adopted definition of human infertility by the World Health Organization (WHO) is the inability to achieve conception despite regular unprotected sexual intercourse for at least 12 months (Zegers-Hochschild, Adamson et al. 2009). Infertility has significant psychological, economic, and health ramifications (Hanson, Johnstone et al. 2017). The prevalence of infertility in Canada is around 11.5-15.7% for couples of reproductive ages (Bushnik, Cook et al. 2012). In the United States prevalence of infertility ranges from 9 to 18% (Aghajanova, Hoffman et al. 2017).

Infertility could be primary, for which the couple has never been able to conceive, or secondary, for which the couple may have been previously able to conceive but cannot thereafter. Public Health Canada classifies causes of infertility into male, female, both male and female and infertility of unknown reasons. In North America, male factors represent 20–30% of all causes, while female factors contribute to around 50%. The remaining 20–30% is due to simultaneous male and female aspects or unknown reasons (Agarwal, Mulgund et al. 2015). In Europe and the United Kingdom, female factors alone represent 35%, male factors 30%, the combination of male and female factors is 20%, and the remaining 15% are of unexplained origin (Leaver 2016). A study by the WHO in developed countries (8500 infertile couples) showed slightly different statistics, where female factors of infertility represented 37% of all cases, male factors represented 8%, and male and female factors were 35%. The remaining percentage of participants had infertility of unknown etiology or became pregnant during the study (WHO 1992).

The principal cause of male infertility is low semen quality. Semen is the fluid that contains the spermatozoa (sperm) ejaculated during intercourse. Semen is composed of both sperm and seminal fluid. Low-quality semen could be due to a low sperm number (oligozoospermia), absence of sperm (azoospermia), sperm morphological

abnormalities (double-headed, bifid tail), or sperm functional abnormalities like weak or immotile sperm. Sperm production and maturation are testosterone-dependent, and therefore, hypogonadism in males (low level of T) leads to non-viable immature sperm. Hypogonadism could be due to different medical conditions, including cryptorchidism (hidden testes), Klinefelter syndrome, undescended testes, testicular cancer, and some medications (spironolactone, sulfasalazine, anabolic steroids, chemotherapy, marijuana and cocaine) (Leaver 2016). Besides the causes mentioned above, medical problems could also drastically affect male fertility. This includes diabetes, obesity, kidney diseases, hepatic disease, and varicocele (Leaver 2016). On the other hand, female infertility factors are more variable and complex and have different classification systems.

According to a 1992 WHO study (WHO 1992), the most common causes of female infertility are ovulatory disorders (25–40 %, including PCOS), endometriosis (15%), pelvic adhesions (12%), tubal factors (22%), and hyperprolactinemia (7%), based on the most used classification of female infertility as of May 2019 (Wendy Kuohung 2019). Ovulatory problems represent the most common causes of all female infertility cases. The low number of ovulatory cycles in 12 months (oligoovulation) and the absence of ovulatory cycles (anovulation) are direct causes of infertility in this category. Ovulatory dysfunction can be a result of various primary hypothalamic-pituitary dysfunctions. Among these defects are the immaturity at menarche, perimenopausal hormonal dysfunction, excessive exercise, eating disorders, stress, idiopathic hypogonadotropic hypogonadism, hyperprolactinemia, lactation, pituitary adenoma, and Kallmann's syndrome. Central defects can also be caused by physical damage to the hypothalamic or the pituitary region by malignant growth or trauma. Finally, Sheehan's syndrome and Empty Sella syndrome are two rare causes of central infertility. Hormonal causes of infertility include hormone-producing tumours (adrenal, ovarian, and thyroid), chronic liver or renal failure, Cushing's syndrome, and androgen

insensitivity syndrome. Infertility can also be attributed to mixed causes, including polycystic ovary syndrome (PCOS), which represents 85% of all ovarian causes, premature ovarian failure (autoimmune, genetic, surgical, idiopathic), and Turner syndrome. Interestingly, some medications such as various contraceptive methods, antidepressants, antipsychotics, corticosteroids, and chemotherapeutic agents can also contribute to infertility. Metabolically, obesity has been linked to infertility in various studies (Rogers and Mitchell 1952, Hartz, Barboriak et al. 1979), with evolving explanatory theories being discovered every day (Jungheim, Travieso et al. 2012). A comprehensive review of obesity and its contribution to female infertility is presented in the next section, 1.2.

Uterine anomalies (either tubal, muscular, or endometrial) are also one of the most significant contributing factors to infertility. Tubal dysfunction usually occurs secondary to pelvic inflammation or infection which leads to adhesions and collagen contractions. These contractions disrupt the naturally occurring proximity of the fallopian tube's opening to the nearby ovary, affecting, thereafter, the oocyte picking mechanism. Structural anomalies of the uterus affect embryo transfer to the uterine lumen and its growth. Benign tumours of the uterus muscular layer (leiomyoma/fibroid) can prevent the implantation of fertilized zygotes, causing recurrent miscarriage and infertility. Endometriosis (abnormally located endometrial tissues) can also contribute to infertility by causing pelvic inflammation and adhesions. Cervical mucus viscosity and the power of hydrogen could also jeopardize the capacity of sperm to transfer through it towards the uterus, causing infertility. Genetic causes like Turner, Kallmann, and fragile X syndromes also affect fertility on multiple levels, including the hormonal level. Besides the factors mentioned above, lifestyle and social circumstances can affect males' and females' fertility. With the rising rates of infertility, the demands for assisted reproductive technologies (ART) rise, increasing the health system's burden and the cost on the patients (Bushnik, Cook et al. 2012). Usually, multiple cycles of *in*

vitro fertilization (IVF) are needed to achieve conception, which could be secondary to numerous factors. The viability of the oocytes produced by the induction of ovulation (IO) is one of the leading causes of failure of IVF cycles.

1.2 Obesity

The Center for Disease Control in the United States defines obesity as a body mass index (BMI) above 30 (Division of Nutrition 2017). BMI is widely used as an indicator of obesity and the state of overweight and is strongly correlated to obesity-associated medical problems (Willett, Jiang et al. 2006, Flegal and Graubard 2009, Freedman, Ogden et al. 2015). BMI is a weight in kilograms divided by the square of height in metres. The normal range of BMI is between 18.5-25. At a BMI of 25–30 (20% excessive weight gain), the person is considered overweight. BMI values above previous numbers are considered obesity. According to BMI, the Center for Disease Control further classifies the severity of obesity into I, II, and III, where BMI is up to 35 (35% more weight gain), 40, and more than 40, respectively (Division of Nutrition 2017). The prevalence of obesity in Canada is around 26%, representing a significant burden on the public health system and the patients themselves (Janssen 2013). Worth mentioning here that these BMI and obesity data are mainly representative of North America and could differ in other parts of the world.

Obesity is associated with a wide range of health problems, ranging from ischemic heart diseases, strokes, peripheral vascular diseases, type II diabetes (T2D), and infertility. Obesity occurs due to excessive free fatty acids (FFA) deposition in adipose tissue with hypertrophy plus or minus hyperplasia of adipocytes (Jo, Gavrilova et al. 2009). Obesity is a multifactorial disease that occurs secondary to different pathological defects. Inducing factors could be central or peripheral, with some genetic and environmental, as well as behavioural predisposing factors (Hruby and Hu 2015).

Peripheral causes include inborn errors of metabolism and phenylketonuria, medium-chain acyl CoA dehydrogenase deficiency, and glutaric acidemia type I (Rice and Steiner 2016). Central causes include psychological (e.g., bulimia nervosa, depression), hypothalamic dysregulation, leptin resistance, and satiety center dysfunction. The satiety center is composed of different regulatory neurons and neuropeptides, including proopiomelanocortin (POMC), neuropeptide Y (NPY), and agouti-related peptide (AgRP) (Ahima and Antwi 2008). POMC-secreting neurons are present mainly in the hypothalamic ARC nucleus and the nucleus solitarius of the brainstem (Millington 2007). POMC is a precursor that transforms enzymatically into various hormones and neuropeptides in a tissue-specific manner. These include melanocyte-stimulating hormones, adrenocorticotropic hormones, and β-endorphin (Cawley, Li et al. 2016, Harno, Gali Ramamoorthy et al. 2018). POMC neurons (in the ARC) play a vital role in the activation of the satiety center and energy expenditure and suppression of the feeding center in the lateral hypothalamus. On the other hand, POMC's neurons in the nucleus solitarius involve regulating aspects of sexual behaviour and the reproductive cycle (Millington 2007). Therefore, POMC is a central neuropeptide in the metabolic-reproductive crosstalk. Mice that are KO for *Pomc* develop obesity with high leptin levels (Yaswen, Diehl et al. 1999, Millington 2007). NPY and AgRP are the counter-regulatory neuropeptides of POMC, stimulating the feeding center and suppressing energy expenditure (Ahima and Antwi 2008). Leptin exerts its anorexigenic effect by exciting POMC neurons and inducing *POMC* expression, and by inhibiting NPY and AgRP neurons' expression of *AGRP* (Ahima and Antwi 2008, Timper and Brüning 2017).

Most of the pathological effects of obesity occur secondary to the excessive deposition of FFAs in different tissues after adipose tissues become saturated. FFAs are toxic to various tissues and cause hepatic steatosis, cirrhosis, vascular endothelial inflammation, plaques formation, ovarian inflammation, and ovarian fibrosis (Sarwar, Pierce et al.

2018, Snider and Wood 2019). FFAs deposition in the pancreas reduces the beta-cell mass and causes insulin resistance (impaired response to endogenous insulin) and T2D through the induction of endoplasmic reticulum (ER) stress and apoptosis (Cui, Ma et al. 2013, Saisho 2016). Ovaries are affected in the same way, where ER stress had been found high in the peri-follicular cells (cumulus cells) of obese women and overfeeding induced obesity animal models (Wu, Dunning et al. 2010, Garfinkel and Hotamisligil 2017, Snider and Wood 2019). High levels of ER stress decrease mitochondrial membrane potential, which leads to the leakage of oxygen free radicals from the inner mitochondrial membrane to the cell cytoplasm, in humans and mice (Gupta, Cuffe et al. 2010). The leak of oxygen free radicals through the inner mitochondrial membrane is an irreversible stage that induces programmed cell death (apoptosis). The death of cumulus cells affects the maturity and viability of oocytes. Free fat deposition in the peri-follicular area (in an obesity mouse model) also reduces mitochondrial deoxyribonucleic acid copy number, and this pathology is inheritable to offspring (Wu, Russell et al. 2015). Mitochondrial DNA copy number is a well-known factor that affects oocyte quality (and that of the embryo afterwards) (Desquiret-Dumas, Clement et al. 2017). Obesity, therefore, impairs ovarian follicular development, oocyte production both qualitatively and quantitatively, fertilization, embryo development, and implantation (Jungheim, Travieso et al. 2013). These mechanisms, among others, contribute to the overall fertility problems associated with obesity.

Other mechanisms by which obesity affects fertility include HPG axis dysregulation, adipose tissue-induced hormonal anomalies, endometrial anomalies, and ovarian inflammation and lipotoxicity, which reduces oocyte viability (Jungheim, Travieso et al. 2013). Adipocytes have an aromatase enzyme that converts androgens to E2. The excess adipose tissue in obese women causes their overall E2 production to be high. High E2 levels enforce a negative feedback effect on GnRH production by the hypothalamus. Low GnRH's output causes low FSH levels and follicular maturation

defects with significant disruption of the HPG axis ending up in irregular anovulatory cycles (Silvestris, de Pergola et al. 2018).

Adipocytes also secrete cytokines (adipokines), like leptin hormone and adiponectin. Anomalies in these adipokines' levels cause abnormal cell signalling and affect their metabolism and function (Jungheim, Travieso et al. 2012). The levels of adiponectin decrease with obesity. One of the key functions of adiponectin is to limit the accumulation of triglycerides in various tissues and therefore improve insulin sensitivity, among other functions. Triglycerides are synthesized by the liver and then shuttled by lipoproteins to be stored in adipose tissues. Tumour necrosis factor-alpha (TNF-α) levels increase with obesity mediating obesity-induced lipotoxicity in various tissues (Engin 2017), which causes insulin resistance and T2D (Kadowaki, Yamauchi et al. 2006). TNF-α is considered more of a cytokine rather than an adipokine as it is secreted by various other tissues. Insulin resistance and high insulin levels, increase the secretion of androgen from theca cells and free E2 and T levels by decreasing sex hormone binding globulins (SHBG), leading to high LH levels and anovulation (Sakumoto, Tokunaga et al. 2010). SHBG is a 93.4-kDa plasma transport glycoprotein that is produced by the liver and controls the bioavailability of sex steroid hormones (Deswal, Yadav et al. 2018). Obesity also increases leptin hormone levels in plasma and ovarian follicular fluid (Metwally, Li et al. 2007). Normally, leptin stimulates the HPG axis by increasing LH levels and pulse frequency promoting fertility and reproduction, (Odle, Akhter et al. 2018). Excessive leptin, on the other hand, overstimulates the HPG axis by continuous signal, disrupting normal cyclicity and leading to anovulation. In an overfeeding-induced obesity mouse model, a 60% reduction of spontaneous pregnancies occurs in mice with high leptin levels (Tortoriello, McMinn et al. 2004). Leptin also inhibits ovarian steroidogenesis in theca and GCs and affects embryo early development (Dağ and Dilbaz 2015). Table 1.1 summarizes adipokine molecule status in obesity and its effect on fertility.

1.1 Adipokines levels in obese females and their effects on reproduction

The table is adapted from (Dağ and Dilbaz 2015).

Adipokines	**Serum levels with obesity**	**Effects on reproduction with obesity**
Leptin	Increases (leptin resistance occurs with obesity)	Inhibits insulin-induced ovarian steroidogenesis
		Inhibits LH* -stimulated E2 production by the GCs
Adiponectin	Decreases	Plasma insulin levels increase
Resistin	Increases	Causes insulin resistance
Visfatin	Increases	Increased insulin sensitivity
Omentin	Decreases	Increased insulin sensitivity
Chemerin	Increases	Negatively regulates FSH-induced follicular steroidogenesis

Obesity is also widely known to increase the prevalence of miscarriages both in normal pregnancies and in ART patients (Fedorcsak, Dale et al. 2004, Lashen, Fear et al. 2004, Metwally, Tuckerman et al. 2007). Metwally, Tuckerman et al. attributed the higher rates of miscarriage in obese patients to endometrial plus or minus embryo malfunction. Endometrial malfunction leads to impaired implantation and, therefore, miscarriage. Chromosomopathy, which is usually associated with embryonal malformation, was not exceptionally high in obese women as has been reported in relatively more recent studies (Landres, Milki et al. 2010, Bellver, Cruz et al. 2011). Even with ART, obese patients still have more difficulties achieving conception (Rittenberg, Seshadri et al. 2011). Metwally et al. attributed this to low embryo viability in obese women (Metwally, Cutting et al. 2007). Bellver et al., on the other hand, showed also lower ART success rates in obese women even without impaired embryo quality (Bellver, Ayllon et al. 2010). Embryo quality in ART and IVF is assessed using the Gardner and Schoolcraft grading system which considers the numbers, fragmentation and uniformity of blastomeres at days 3 and 4, and blastocyst growth and inner cell mass development at days 5 and 6 (Hardarson, Van Landuyt et al. 2012, Wang, Cai et al. 2020). Obese ART patients also suffer from deficient oocyte retrieval, besides the low quality of the retrieved oocytes themselves (Dağ and Dilbaz 2015). They also show a low embryo transfer success and multiple implantation failures even when the oocytes came from a healthy mother and were transferred into an obese recipient (Bellver, Melo et al. 2007). Overall, the role of obesity in impairing ART success is evident, though the mechanisms involved are still not fully explored.

In summary, the association between obesity and infertility has been well established (Gesink Law, Maclehose et al. 2007, Wise, Rothman et al. 2010) for a long time (Zaadstra, Seidell et al. 1993, Crosignani, Ragni et al. 1994, Rich-Edwards, Goldman et al. 1994). However, this effect happens through various complex mechanisms that are not fully deciphered by scientific societies yet. Moreover, obesity-related

pathologies are evident in multiple complex infertility diseases, such as PCOS, where patients usually present with some degree of excess weight or even obesity. PCOS patients can also be of average weight.

1.3 Polycystic ovary syndrome

PCOS was first described in 1935 by Dr. Stein and Dr. Leventhal, being named Stein-Leventhal syndrome. Later, the syndrome received a more descriptive name, related to its most prominent pathological feature, the presence of multiple cysts in the ovaries. PCOS is a multisystem disease involving anomalies in the central nervous system, endocrine system, hormonal balance, ovarian cycle, follicular maturation, and metabolic profile. Due to the complex nature of PCOS and its multisystem involvement, it exhibits a broad spectrum of medical and psychological effects, including infertility, hyperandrogenism, hirsutism, insulin resistance, impaired glucose tolerance, T2D, cardiovascular diseases, anxiety, and depression (Teede, Deeks et al. 2010). The predominance of each of these PCOS symptoms varies from one patient to another, which gives the disease its heterogeneous nature.

1.3.1 Definition and diagnosis

PCOS is defined in various ways depending on the criteria used. Due to its heterogeneous nature, multiple diagnostic criteria for PCOS have been developed. The most famous and commonly used criteria for PCOS diagnosis are those of the European Society of Human Reproduction and Embryology and the American Society for Reproductive Medicine (known as the Rotterdam criteria) which were put together in 2003 (Boyle and Teede 2012). Rotterdam criteria require the presence of at least two of the following three criteria to make the diagnosis: oligo or anovulation, hyperandrogenism (clinical or biochemical), and multiple cysts in the ovaries upon ultrasound (US) examination (Boyle and Teede 2012). Considering that humans

usually produce one oocyte per month in each cycle, oligo-ovulation is defined as the presence of 8 or fewer ovulatory cycles during 12 months in females of reproductive age. Mice usually produce multiple oocytes in each cycle, therefore, the production of a lower number of oocytes compared to the average of their mates from the same background is considered oligo-ovulation. Anovulation in mice is still defined as the complete absence of oocytes. Clinical hyperandrogenism manifests with hirsutism, which is excessive body hair that is sometimes difficult to diagnose. On the other hand, biochemical hyperandrogenism represents high plasma levels of T (Boyle and Teede 2012). The presence of multiple cysts in the ovaries, upon ultrasound scan examination, is suggestive of PCOS. In humans, there are normally ten to fifteen small antral follicles in both ovaries, and sometimes, in a single ovary (Boyle and Teede 2012).

Multiple trials have been conducted by different societies to establish more inclusive and accurate diagnostic criteria to avoid misdiagnosing PCOS patients. Among those trials are found the National Institutes of Health (NIH) criteria and the Androgen Excess Society criteria. NIH criteria were defined in 1990 and require the presence of clinical or biochemical hyperandrogenism plus chronic anovulation to diagnose PCOS (Zawadzki and Dunaif 1992). The Androgen Excess Society requires the presence of hyperandrogenism, plus polycystic ovarian morphology (PCOM), or oligo/ovulation, to achieve the diagnosis of PCOS (Azziz, Carmina et al. 2006). NIH 2012/International PCOS guidelines assembled the most recent criteria in 2018 and have adapted the same two out of three features of the Rotterdam criteria to diagnose PCOS (Guidelines 2018, Wolf, Wattick et al. 2018).

In humans, PCOM is defined as the presence of $\geqslant$ 12 follicles per ovary and/or the increase of ovarian size by >10 cubic centimetres (Reid, Kao et al. 2017). PCOM is a key diagnostic feature for PCOS in the Rotterdam criteria, though the detection of ovarian cysts is widely variable depending largely on the sensitivity of the ultrasound

(US) scanner and the expertise of its operator. Advanced ultrasound scanner equipment can better detect antral follicles, even small ones. As sensitive scanners and appropriate expertise are not always available, there is a paramount need for an indirect indicator of the numbers of antral follicles. In this context, the Anti-Mullerian hormone (AMH) is produced exclusively by the GCs of pre-antral and antral ovarian follicles (Jeppesen, Anderson et al. 2013). AMH is a member of the transforming growth factor-beta family, which plays a crucial role in regulating early follicular development (Sahmay, Aydin et al. 2014). A direct link between the number of 'pre-antral and antral follicles and their growth levels from one side, and serum levels of AMH, from another side, has been well established (Pigny, Merlen et al. 2003, Weenen, Laven et al. 2004). Circulating and follicular AMH levels follow a pattern reflecting the number and size of growing follicles. AMH levels increase with the increase of the size of the follicle, and these levels reach their peak when follicles are around the size of 5-8 millimetres (mm). As follicles grow further, their production of AMH (in peri-follicular fluid) decreases gradually, which in turn is reflected in the serum AMH levels (Jeppesen, Anderson et al. 2013). Based on several studies including those mentioned above, a new diagnostic approach has appeared, which aims toward the use of the serum level of AMH as a replacement for the antral follicles count (and PCOM) in the diagnosis of PCOS (Pigny, Jonard et al. 2006). This trend never reached the guideline levels and never became a diagnostic criterion of PCOS due to many factors. Among these factors, the absence of standard AMH serum level value is an obstacle preventing its use as a biomarker to detect the abnormal number of pre-antral and antral follicles (Sahmay, Aydin et al. 2014).

More studies are emerging every day, confirming the direct correlation between AMH and PCOM in PCOS. Sezai et al. in 2014 showed 83 % sensitivity and 100 % diagnostic specificity for PCOS when they used serum levels of AMH combined with oligo-anovulation and hyperandrogenism for the diagnosis (Sahmay, Aydin et al. 2014).

These results showed great potential for serum AMH levels to replace the need for PCOM criteria to diagnose PCOS. Therefore, physicians can resolve the technical difficulties they face to detect PCOM by using serum AMH levels instead. Besides the three main criteria discussed above, PCOS also has a wide range of critical metabolic anomalies.

Being overweight and obesity are the most common metabolic anomalies associated with PCOS. The prevalence of excess weight and obesity among PCOS patients in the United States reaches as high as 80% (Sam 2007). This prevalence varies from one country to another and from one diagnostic criterion to another (Sam 2007). The difference in overweight and obesity prevalence among PCOS patients in different countries is mainly due to lifestyle differences. Though the consistent presence of obesity among those patients strongly suggests a biological link for both pathologies. Moreover, obesity is widely known to affect the reproductive system regardless of PCOS, as explained above.

1.3.2 Insulin resistance

Insulin exerts its effect through multiple mechanisms, including activation of glucose transporter proteins (GLUT), activation of key enzymes in metabolism, and gene expression regulation in the long term (Gribble 2005). Three primary tissues handle body glucose regulation and energy expenditure under the influence of insulin: muscles, liver, and adipose tissues. Insulin mediates glucose absorption from the digestive system, and its uptake by muscles and adipose tissues. Glucose is then converted into glycogen and triglycerides. In the liver, insulin also inhibits the synthesis of new glucose by inhibiting gluconeogenesis, glycogenolysis and ketogenesis and promotes protein synthesis in muscles. In PCOS patients, insulin resistance is not always associated with obesity. Rather, insulin resistance is highly abundant among those patients regardless of their weight (Sam 2007, Polak, Czyzyk et al. 2017). However,

insulin resistance worsens in obese patients. Insulin resistance, also known as impaired inulin tolerance, is the body's inability to reduce blood sugar in response to endogenous insulin (Lebovitz 2001). A 1999 study showed that glucose utilization in skeletal muscles of PCOS patients is 35-40% lower compared to similar weight women without PCOS, despite hyperinsulinemia (Dunaif 1999, Sam 2007), which was mainly attributed to muscular insulin resistance. The same study showed that this phenomenon does not happen in liver tissues except in obese women regardless of their PCOS status.

On a structural level, insulin is a polypeptide composed of two chains, A and B, formed of 21 and 30 amino acids, respectively and connected by disulphide bridges (de Luca and Olefsky 2008). Beta cells of the islets of Langerhans in the pancreas are the source of insulin. Insulin receptors are membranous glycoproteins that have two α-subunits (135 kilodaltons (kDa) each) and two β-subunits (95 kDa each). The α-subunits (extracellular part of the receptor) contain insulin binding sites and connect with the β-subunits through disulphide bridges. Each β-subunit has an extracellular region, a transmembrane region, and an intracellular tyrosine kinase domain (Hubbard 2013).

On molecular and functional levels, the binding of insulin to the α-subunit of the insulin receptor triggers conformational changes that induce a catalytic activation of the receptor and β-subunit autophosphorylation, at multiple tyrosine (Tyr) residues (Hubbard 2013). Phosphorylated residues on the insulin receptor β-subunit interact with different adaptor proteins, among which is the insulin receptor substrate (IRS). IRS-1 and IRS-2 are the main adaptor proteins involved in the insulin signalling pathway by forming complexes initiating the intracellular signalling cascade (Jensen and De Meyts 2009). Insulin receptor activates two main downstream pathways, the phosphatidylinositol-3-kinase (PI3K) pathway and the mitogen-activated protein kinases (MAPK) pathway (White 2003). Insulin receptor activity depends on phosphotyrosine phosphatase activity, which dephosphorylates Tyr-residues on the

active receptor β-subunit, reducing its activity. Phosphotyrosine phosphatase 1 B is a well-known regulator of insulin receptor activity (Boucher, Kleinridders et al. 2014). Phosphotyrosine phosphatase 1 B knockout mice are more sensitive to insulin and more resistant to obesity, even with a high-fat diet (Elchebly, Payette et al. 1999). Another mechanism of insulin receptor function regulation is through the phosphorylation of the receptor's β-subunit serine/threonine (Ser/Thr) residues, which reduces the receptor kinase activity (Youngren 2007) and can therefore contribute to insulin resistance in PCOS.

IRS has around 230 Ser/Thr residues, among which more than 70 are phosphorylation sites. Different kinases target these phosphorylation sites, including c-Jun N-terminal kinase (JNK), mammalian target of rapamycin, extracellular signal-regulated kinases, and protein kinase C (PKC) (Copps and White 2012). Phosphorylation of IRS Ser/Thr residues is an important pathway for attenuating insulin receptor activity by reducing its PI3K activity and promoting its degradation (Copps and White 2012). Furthermore, multiple adapting proteins interact with insulin receptors and IRS decreasing their activities. Among these adapting proteins, suppressors of cytokine signalling (SOCS) proteins, particularly SOCS-1 and SOCS-3, are potent inhibitors of the insulin signalling pathway (Lebrun and Van Obberghen 2008).

Interestingly, insulin itself mediates these adapting proteins expression in different tissues (Lebrun and Van Obberghen 2008). Another essential cytoplasmic adapting protein is the growth factor receptor-bound protein. The growth factor receptor-bound protein 10 and growth factor receptor-bound protein 14 both bind directly to insulin receptor phosphotyrosine residues decreasing their catalytic activity and preventing the receptor interaction with IRS. The overexpression of these proteins from adipose and muscular tissues of obese people is associated with reduced insulin sensitivity (Desbuquois, Carre et al. 2013).

Insulin receptor gene expression level is another mechanism regulating the overall activity of insulin. In the presence of insulin, PI3K phosphorylates the Forkhead box O1 (FOXO1) transcription factor, which enhances FOXO1 interaction with protein 14-3-3 (Tzivion, Dobson et al. 2011). FOXO1 plays a role in the expression of the insulin receptor gene, and when it interacts with protein 14-3-3, it gets degraded, lowering any further expression of insulin receptors. This elimination happens by excluding FOXO1 from the nucleus, which then undergoes ubiquitination-dependent proteasomal degradation (Gutierrez-Rodelo, Roura-Guiberna et al. 2017). On the other hand, in the absence of insulin, FOXO1 binds to the insulin receptor gene promoter and initiates its transcription (Gutierrez-Rodelo, Roura-Guiberna et al. 2017). PI3K also generates an important effector protein, phosphatidylinositol- 3,4,5-triphosphate, from diphosphate by phosphorylation, which is a key protein in the insulin receptor downstream signal. Phosphatidylinositol triphosphate has a negative feedback regulatory effect on PI3K transcription preventing its overactivity through phosphoinositide-dependent kinase 1 effector protein (Dieterle, Böhler et al. 2014). Lipid Phosphatase, tensin homolog, and SH2 domain-containing inositol 5-phosphatase are essential factors regulating phosphatidylinositol-3,4,5-trisphosphate phosphorylation levels and therefore insulin receptor signalling (Dyson, Fedele et al. 2012).

The most common mechanisms by which insulin resistance occurs are the downregulation of insulin receptor gene expression, the decrease of the receptor catalytic activity, the increase of Ser/Thr residues phosphorylation in insulin receptors and IRS, the increase of Tyr phosphatase activity (particularly phosphotyrosine phosphatase 1 B) leading to dephosphorylation of the receptor and IRS, the decrease of PI3Ks and protein kinase B (also known as Akt kinases) activities, and the downregulation of GLUT-4 transporter protein expression or function (Gutierrez-Rodelo, Roura-Guiberna et al. 2017). Chronic inflammation, ER stress, mitochondrial

dysfunction, and alterations in adipokines and fatty acids levels are all found to contribute to insulin resistance (Gutierrez-Rodelo, Roura-Guiberna et al. 2017).

1.3.3 Chronic inflammation and ER stress

Chronic inflammation caused in part by the action of inflammatory mediators like toll-like receptors 4 alters IRS phosphorylation patterns at Ser/Thr residues through JNK, NF-κ-inhibitor kinase, "inhibitory-κB kinase" and MAPK activation, leading to insulin resistance (Johnson and Olefsky 2013). Inflammatory cytokines such as TNF-α, IL-6 and interleukin one beta, also contribute to insulin resistance through Ser/Thr kinases activation, decrease IRS-1, GLUT-4 and peroxisome proliferator-activated receptor-gamma expression and SOCS-3 expression and activation (Senn, Klover et al. 2003, Kwon and Pessin 2013). Chronic low-grade inflammation is a consistent feature of PCOS (Shorakae, Ranasinha et al. 2018). Furthermore, obesity contributes directly to chronic inflammation and insulin resistance in overweight patients (PCOS or not) through various mechanisms including adipocytes' death (Kuroda and Sakaue 2017).

ER stress happens when cells become unable to handle the increasing demands for protein synthesis and calcium transport, among other functions, leading to imperfect protein formation (misfolded proteins) (Banhegyi, Baumeister et al. 2007, Guerrero-Hernandez, Leon-Aparicio et al. 2014). As a response to excessive misfolded proteins, cells activate the unfolding protein response (UPR) to try to restore ER homeostasis by decreasing protein synthesis and enhancing protein folding through chaperones, for example, BiP/glucose-regulated protein 78 (GRP78) (Yalcin and Hotamisligil 2013). Chaperones are defined as small molecular weight compounds that enhance ER folding capacity and improve, therefore, protein conformation. Chaperones could be pharmacological (chemical compounds) or molecular (proteins) (Welch and Brown 1996, Ozcan, Yilmaz et al. 2006). When cells are not under stress, GRP78 binds to ER stress sensors (protein kinase R-like endoplasmic reticulum kinase (PERK), inositol-

requiring kinase/endoribonuclease 1 (IRE-1) and transcription factor 6 (ATF-6) and stabilizes them. Upon ER stress, the misfolded proteins in ER lumen cause dissociation of GRP78 from the ER stress sensors, activating them in the process. Following the GRP78 dissociation, PERK homodimerizes and trans-autophosphorylates at residue threonine 980, causing self-activation (Cawley, Deegan et al. 2011).

PERK activation promotes nuclear factor kappa-light-chain-enhancer of activated B cells (NF-κB) activation, which induces the expression of different genes involved in inflammation, for example, *Tnf-α*, interleukin one beta and interleukin 6 (Hu, Han et al. 2006). Inflammatory mediators activate serine/threonine kinases such as JNK (Hirosumi, Tuncman et al. 2002), an inhibitor of nuclear factor-kappa b kinase subunit beta (Yuan, Konstantopoulos et al. 2001) and PKC-θ (Perseghin, Petersen et al. 2003) which leads to phosphorylation of insulin receptor and IRS-1 on Ser/Thr residues rendering it inactive and causing insulin resistance (Gutierrez-Rodelo, Roura-Guiberna et al. 2017). Chaperons (GRP78) increase insulin sensitivity by reducing ER stress (Ozawa, Miyazaki et al. 2005, Kammoun, Chabanon et al. 2009). In obesity studies of mice, the administration of chemical (pharmacological) chaperones like 4-phenylbutyrate or tauroursodeoxycholic acid (TUDCA) can reverse obesity-induced hyperglycemia and insulin resistance through the reduction of PERK and IRE-1 (Ozawa, Miyazaki et al. 2005). These two components showed similar effects in obesity human trials as well (Kars, Yang et al. 2010, Xiao, Giacca et al. 2011). If these compensatory mechanisms fail to regain homeostasis, programmed cell death (apoptosis) happens (Fu, Watkins et al. 2012, Sommerweiss, Gorski et al. 2013). Figure 1.11 summarizes the impact of ER stress on insulin resistance.

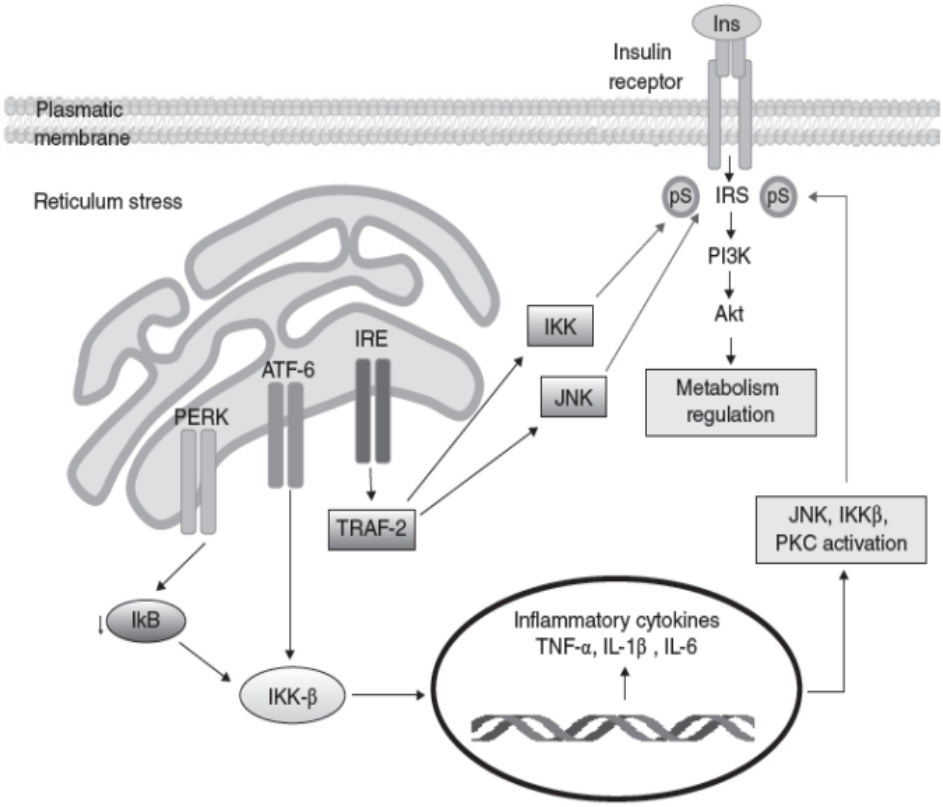

1.11 ER stress and its contribution to insulin resistance.

The accumulation of misfolded proteins activates three stress-sensor kinases, PERK, IRE-1, and ATF-6, which induce inflammatory cytokines and trigger the UPR. PERK releases nuclear factor kappa-light-chain-enhancer of activated B cells from its inhibitor IκB (activating it), causing it to translocate to the nucleus, which in turn activates the synthesis of inflammatory cytokines, TNF-α, interleukin one beta and IL-6. As a result, multiple Ser kinases become active, including JNK and PKC-θ, which induces IRS-1 phosphorylation rendering them less interactive with their downstream substrates (PI3K/Akt and MAP kinases) and causing insulin resistance. The IRE-1 kinase activates JNK, which again phosphorylates IRS-1. The ATF-6 pathway, by contrast, directly activates nuclear factor kappa-light-chain-enhancer of activated B cells inducing pro-inflammatory cytokines as above. Gray arrows indicate inhibitory signals. Figure adapted from, Gaceta Médica de México 153(2):214-228, *Molecular Mechanisms of Insulin Resistance, An Update* (Gutierrez-Rodelo, Roura-Guiberna et al. 2017). https://anmm.org.mx/GMM.

Multiple ongoing studies are trying to determine the causality of insulin resistance secondary to mitochondrial dysfunction (Pagel-Langenickel, Bao et al. 2010) versus mitochondrial dysfunction because of insulin resistance (Morino, Petersen et al. 2005). A vicious cycle of events is involved: a decrease in glucose uptake by the cells, leading to reduced mitochondrial functions and even their overall numbers. These reductions make cells more and more deprived of energy, and they become less able to transport glucose actively and, therefore, more resistant to insulin (Montgomery and Turner 2015). Genetically induced mouse models of insulin resistance also show lower numbers of mitochondria and lower expression levels of the genes responsible for mitochondrial function plus alterations in the levels of oxidative phosphorylation and Adenosine triphosphate (ATP) production (Long, Cheng et al. 2011). In contrast, FFAs excess in obesity induces mitochondrial over-activation through an increase in β-oxidation, which leads to the generation of large amounts of ATP from fatty acids metabolism. Excess ATP generates a negative feedback effect to control substrate-induced mitochondrial function. In this way, extra ATP inhibits adenosine monophosphate-activated protein kinase (AMPK), reducing, in turn, insulin-mediated glucose uptake, leading to insulin resistance (Ruderman, Carling et al. 2013).

AMPK works as a cellular energy status sensor, that gets activated when the ratio of adenosine monophosphate to ATP increases, indicating low levels of energy. Activated AMPK regulates cellular metabolism (in skeletal muscle, liver, and adipose tissues) by stimulating glucose uptake and lipid oxidation to produce energy. AMPK is also involved in various other functions, including cellular growth, mitochondrial function, inflammation, and ER stress, that are directly related to insulin resistance (Ruderman, Carling et al. 2013).

In this context, insulin resistance is a cell-protecting mechanism aiming at controlling ATP-induced stress, in muscles, liver, and adipose tissues. Insulin sensitizers were

developed to inhibit mitochondrial β-oxidation to successfully reverse insulin resistance in humans (Ye 2013). Mitochondrial dysfunction leads to the leak of reactive oxygen species (ROS) from the inner mitochondrial membrane to the cytoplasm. These ROS cause further damage to mitochondrial DNA, oxidative injury, protein aggregation and lipid peroxidation. These insults lead to mitophagy (elimination of damaged mitochondria) and eventually apoptosis if the cell fails to achieve homeostasis. ROS accumulation also causes Ser/Thr kinases activation, including inhibitor of nuclear factor-kappa b kinase subunit beta, JNK and PKC, which increases IRS protein phosphorylation on Ser residues, leading eventually to insulin resistance (Montgomery and Turner 2015). Figure 1.12 summarizes the effect of mitochondrial dysfunction on insulin resistance.

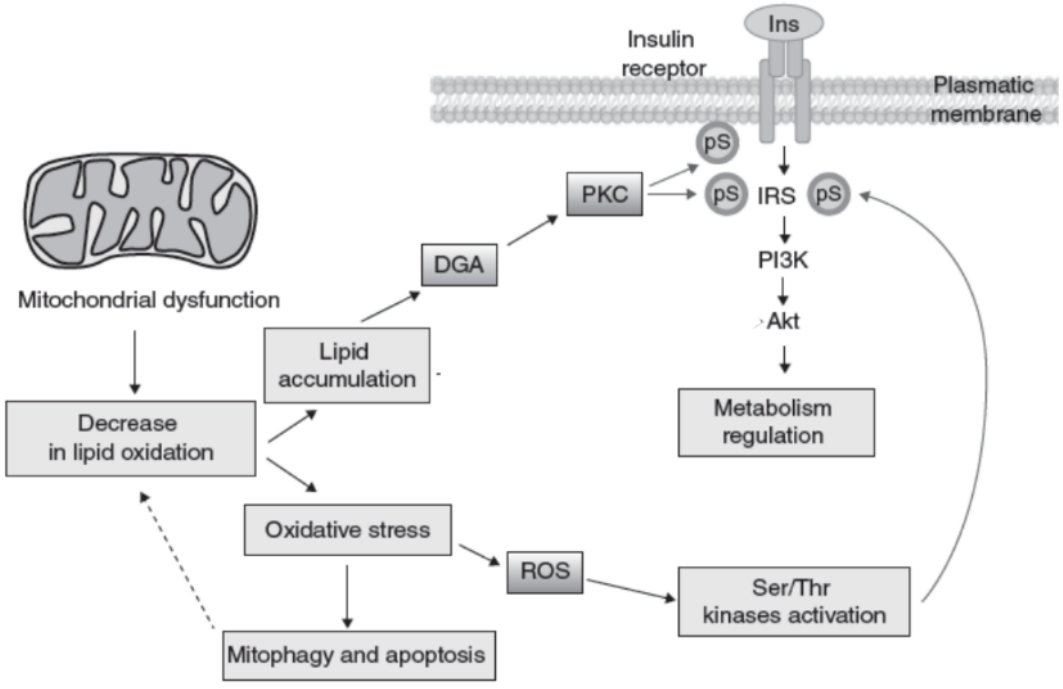

1.12 Mitochondrial dysfunction inducing insulin resistance.

Mitochondrial dysfunction reduces overall levels of oxidative phosphorylation, leading to decrease lipid oxidation. Consequently, FFAs and lipids start to accumulate contributing to the development of insulin resistance. Diglycerides enhance PKC activation, which in turn phosphorylates and inhibits signalling through insulin receptors. The accumulation of non-oxidized lipids leads to ROS generation, inducing oxidative stress that damages mitochondria and other organelles, leading eventually to mitophagy (mitochondrial death and autophagy), and apoptosis. Mitophagy reduces the overall numbers of mitochondria which causes a further reduction in lipids and FFAs oxidation, in a vicious cycle. ROS also causes activation of inhibitor of nuclear factor-kappa b kinase subunit beta, JNK and PKC, kinases, which increase IRS phosphorylation on Ser residues, which subsequently induces insulin resistance. Figure adapted from, Gaceta Médica de México 153(2):214-228, *Molecular Mechanisms of Insulin Resistance, An Update* (Gutierrez-Rodelo, Roura-Guiberna et al. 2017). https://anmm.org.mx/GMM.

The body tries to compensate for insulin resistance by increasing insulin secretion, to a point, until β-cells dysfunction eventually develops (Malin, Kirwan et al. 2015). This increased insulin secretion causes prominent hyperinsulinemia, consistent in PCOS patients regardless of their weight (Dunaif, Segal et al. 1989). The roles that insulin resistance or hyperinsulinemia play in PCOS sub-, or infertility and metabolic anomalies are complex and are currently the subject of many studies. These roles are reviewed in section 1.3.5.

1.3.4 Prevalence and demography of PCOS

PCOS is the most common cause of female anovulatory infertility representing around 75% of all anovulatory cases (Homburg 2004). The percentage that PCOS occupies among other female infertility causes varies little from one study to another. Figure 1.13 demonstrates the significant proportion of PCOS among causes of female infertility.

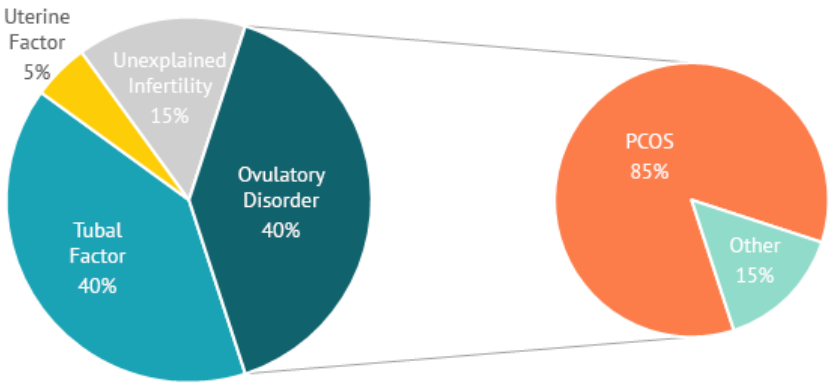

1.13 The prevalence of PCOS among all other causes of female infertility.

Figure adapted from Dr. Ila Gupta, *causes of infertility in women*, https://www.ilaguptaivf.com/news/causes-infertility-women/.

The prevalence of PCOS ranges from 8-13% amongst all women, depending on the diagnostic criteria used and the tested population (Costello, Misso et al. 2019). Earlier studies showed that the overall percentage of women affected by this syndrome ranges from 5-20% of all women in the childbearing period. This wide range depends on the diagnostic criteria used (Moran, Hutchison et al. 2011, Sirmans and Pate 2013). Initially, hyperandrogenism and anovulation were the hallmarks of PCOS diagnosis, later with the introduction of the US in its diagnosis, the spectrum of patients vastly widened. The number of cysts identified by the US to fulfill the PCOM needed for PCOS diagnosis also varies from one society to another. Furthermore, technology development led to more sophisticated US machines, which could detect even smaller cysts and widen the diagnosed population. However, sophisticated US machines are not always available, and the skilled enough radiologists to operate them are not also that available, as discussed before. These factors together cause a wide range of variability in PCOS prevalence. In Canada, the estimates are around 1.4 million Canadian women are affected by this syndrome.

1.3.5 Etiology and hypothesis of PCOS

The etiology of PCOS is complicated and is still unexplored at multiple levels. Most experts attribute its etiology to an interplay between genetic and environmental factors (Rosenfield and Ehrmann 2016). The most current hypothesis for PCOS development is based on the ‘two hits hypothesis for disease development. In this hypothesis, the patients have a genetic predisposition for the disease (first hit) and environmental factors then trigger anomalies (second hit) to produce the phenotype (Rosenfield and Ehrmann 2016). The first hit can be an inherited genetic anomaly or an acquired one during pregnancy due to intrauterine fetal exposure to maternal hormones or drugs. The

second hit is the insulin-resistance/hyperinsulinemia complex, which can also be genetically acquired or postnatally acquired due to obesity.

1.3.5.1 Genetic hypothesis of PCOS

The hereditability of PCOS has been well established, and in some studies, it has reached levels as high as 70% (Dumesic, Oberfield et al. 2015). The fact that environmental factors trigger existing genetic anomalies explains, to some extent, the heterogenicity of the disease. PCOM, a variant of ovarian cysts seen in PCOS patients, is also inherited by daughters from PCOS mothers, mostly in an autosomal dominant manner (Maliqueo, Sir-Petermann et al. 2009). Defective insulin secretion and insulin resistance also have considerable evidence of inheritance in PCOS patients (Legro, Driscoll et al. 1998, Rosenfield and Ehrmann 2016). Metabolic syndrome has a high prevalence among first-degree relatives of PCOS patients, further supporting its genetic origin (Vink, Sadrzadeh et al. 2006, Rosenfield and Ehrmann 2016). Overweight or obesity is present in 94% of fathers and 66% of mothers of PCOS patients (Vink, Sadrzadeh et al. 2006). Impaired glucose tolerance is also evident in 49% of PCOS patients' mothers and 84% of their fathers. Differential expression and polymorphisms of genes are well established in steroidogenic enzyme genes and genes encoding sex hormone-binding globulins, androgen receptor (*AR*), transcription factors, and gonadotropins' receptors, as well as insulin production and sensibility, obesity, and congenital adrenal hyperplasia. This variation in gene expression is one of the main reasons for the variability of PCOS symptoms and their severity.

Studies are ongoing to identify persistent gene loci among PCOS patients to pinpoint genes that eventually generate PCOS pathologies. Early genome-wide association studies (GWAS) conducted in Chinese Han patients identified two loci on chromosome 2 (Chr2) and a third locus on chromosome 9 (Chr9) that are significantly related to PCOS. (Chen, Zhao et al. 2011). The locus on chromosome 2p16.3 codes for the

luteinizing hormone/choriogonadotropin receptor (*LHCGR*), a logical participating gene in the PCOS phenotype. The two other loci, 2p21 and 9p33.3, have multiple single-nucleotide polymorphisms (SNPs) strongly associated with PCOS (Simonis-Bik, Nijpels et al. 2010). GWAS has further identified PCOS-associated SNPs near various reproduction-related genes, including, follicle-stimulating hormone receptor (*FSHR*), *LHCGR, GATA4*, *DENND1A*, and follicle-stimulating hormone subunit beta (*FSHB*), (McAllister, Legro et al. 2015, Azziz 2016). Three loci were found by GWAS to have a genome-wide significance; 8p32.1, 11p14.1 and 9q22.32 which were previously identified by GWAS in Chinese women with PCOS (Hayes, Urbanek et al. 2015).

GATA4 is one of the important genes, located near the 8p32.1 locus and encodes for the GATA4 transcription factor, a key factor in development and reproduction as discussed before. At the 11p14.1 locus is found the *FSHB* gene, which codes follicle-stimulating hormone (FSH). This locus is significantly associated with a high LH/FSH ratio. Near the 9q22.32 locus, GWAS identified six new loci that have reached genome-wide significance for PCOS (Day, Hinds et al. 2015). Among the most exciting discoveries of GWAS was the identification of 'differentially expressed in normal and neoplastic development isoform 1A' (*DENND1A*) as a significant locus linked to PCOS (Almawi, Gammoh et al. 2016, Li, Zhang et al. 2016, Liu, Huang et al. 2016). The importance of this locus lies in the fact that *DENND1A.V2* (differentially expressed in normal and neoplastic development isoform 1A, variant 2) codes for a steroidogenesis stimulating protein that is overexpressed in theca cells of PCOS patients. (Ding, Zhuo et al. 2016, Mykhalchenko, Lizneva et al. 2017). To this point, 16 loci had been identified in Chinese and European women to be strongly associated with PCOS (Chen, Zhao et al. 2010, Shi, Zhao et al. 2012, Day, Hinds et al. 2015, Hayes, Urbanek et al. 2015).

In 2018, a large meta-analysis confirmed 11 previously identified loci that were linked to metabolic and steroidogenic anomalies plus three new loci near "plasminogen receptor with a c-terminal lysine", zinc finger and *BTB* domain-containing 16 and microtubule-associated protein *RP/EB* family member 1 with potential endocrine relation (Day, Karaderi et al. 2018). Zinc Finger and BTB Domain Containing 16 (also known as promyelocytic leukemia zinc finger (*ZBTB16/PLZF*)) plays a key role in *GATA4* gene transcription and cardiac hypertrophic stimulation in response to angiotensin II receptor two signals (Wang, Frank et al. 2012). *PLZF* expression is upregulated during adipocyte differentiation (Ambele, Dessels et al. 2016). Also, it plays a role in the early stages of spermatogenesis (Lovelace, Gao et al. 2016) besides a role in endometrial stromal cell decidualization (Kommagani, Szwarc et al. 2016). The third locus codes for a metabolic candidate gene; *MAPRE1* that is known to interact with the low-density lipoprotein receptor-related protein 1, which plays a crucial role in adipogenesis (Masson, Chavey et al. 2009); additionally, it participates in follicular development and angiogenesis (Greenaway, Lawler et al. 2007). Deletion of the *GATA4* locus in mice results in infertility and impaired responses to exogenous gonadotropins (Efimenko, Padua et al. 2013). The *GATA4/NEIL2* locus also encodes the promoter for *FDFT1*, which is the first enzyme in cholesterol biosynthesis, and the main substrate for T synthesis (Do, Kiss et al. 2009, Chalasani, Guo et al. 2010). The 11 confirmed loci plus the three newly identified ones are presented in Figure 1.14, adapted from this meta-analysis article (Day, Karaderi et al. 2018).

PLOS GENETICS

PCOS genetics meta-analysis

Table 2. The 14 genome-wide significant variants associated with PCOS in the meta-analysis.

Chr:Position[1]	rsID	Alleles[2]	EAF[3]	Beta	Odds Ratio (95% CI)[4]	Std. Error	Nearest Gene	P-value	Effective N[5]	Ref[6]
2:43561780	rs7563201	A/[G]	0.4507	-0.1081	0.90 (0.87–0.93)	0.0172	*THADA*	3.678e-10	17192	
2:213391766	rs2178575	G/[A]	0.1512	0.1663	1.18 (1.13–1.23)	0.0219	*ERBB4*	3.344e-14	17192	17
5:131813204	rs13164856	[T]/C	0.7291	0.1235	1.13 (1.09–1.18)	0.0193	*IRF1/RAD50*	1.453e-10	17192	17
8:11623889	rs804279	A/[T]	0.2616	0.1276	1.14 (1.10–1.18)	0.0184	*GATA4/NEIL2*	3.761e-12	16895	16
9:5440589	**rs10739076**	**C/[A]**	**0.3078**	**0.1097**	**1.12 (1.07–1.16)**	**0.0197**	***PLGRKT***	**2.510e-08**	**17192**	
9:97723266	rs7864171	G/[A]	0.4284	-0.0933	0.91 (0.88–0.94)	0.0168	*FANCC*	2.946e-08	17192	16
9:126619233	rs9696009	G/[A]	0.0679	0.202	1.22 (1.15–1.30)	0.0311	*DENND1A*	7.958e-11	17192	
11:30226356	rs11031005	[T]/C	0.8537	-0.1593	0.85 (0.82–0.89)	0.0223	*ARL14EP/FSHB*	8.664e-13	17192	16,17
11:102043240	rs11225154	G/[A]	0.0941	0.1787	1.20 (1.13–1.26)	0.0272	*YAP1*	5.438e-11	17192	17
11:113949232	**rs1784692**	**[A]/G**	**0.8237**	**0.1438**	**1.15 (1.10–1.14)**	**0.0226**	***ZBTB16***	**1.876e-10**	**17192**	
12:56477694	rs2271194	A/[T]	0.416	0.0971	1.10 (1.07–1.14)	0.0166	*ERBB3/RAB5B*	4.568e-09	17192	17
12:75941042	rs1795379	C/[T]	0.2398	-0.1174	0.89 (0.86–0.92	0.0195	*KRR1*	1.808e-09	17192	17
16:52375777	rs8043701	[A]/T	0.815	-0.1273	0.88 (0.85–0.92)	0.0208	*TOX3*	9.610e-10	17192	
20:31420757	**rs853854**	**A/[T]**	**.4989**	**-.0975**	**0.91 (0.88–0.94)**	**0.0163**	***MAPRE1***	**2.358e-09**	**17192**	

[1]Chr—Chromosome:Position (bp) in hg19;

[2]Alleles are shown as Major/Minor by allele frequency in 1000G EUR cohort, with the effect allele shown within [];

[3]Effect allele frequency;

[4]95% Confidence Interval of the Odds Ratio;

[5]Effective N—effective sample size;

[6]Ref = Reference.

Loci previously identified in GWAS studies of European ancestry are referenced. Novel associations with PCOS not previously reported are shown in bold. EAF = Effect Allele Frequency.

https://doi.org/10.1371/journal.pgen.1007813.t002

1.14 The 14 identified genetic loci that are frequently associated with PCOS. Photo adapted from https://doIOrg/10.1371/journal.pgen.1007813.t002.

Furthermore, using the “linkage disequilibrium score-regression analysis” technique, direct genetic correlations between discovered loci and different PCOS traits have been identified, including hyperandrogenism, ovulatory dysfunction, PCOM, T, FSH and LH levels, obesity, fasting insulin levels, and T2D. Four variants associated with hyperandrogenism, nine with ovulatory dysfunction, and eight with PCOM have been revealed. Interestingly, seven of the PCOM-associated loci are also associated with ovulatory dysfunction. Furthermore, three of the four loci associated with hyperandrogenism are also related to ovulatory dysfunction. Two new additional loci are associated solely with ovulatory dysfunction, one of them near *FSHB*. This last locus is also associated with LH and FSH levels. Lastly, one more locus was identified near the interferon regulatory factor 1/DNA repair protein RAD50 gene and is associated with T levels. Identified loci and their association are in Figure 1.15, which we also adopted from the same article (Day, Karaderi et al. 2018).

PLOS | GENETICS

PCOS genetics meta-analysis

Table 3. Association of PCOS GWAS meta-analysis susceptibility variants and PCOS related traits.

Chr:Position	rsID	Gene	Ref. allele	Other allele	Hyperandrogenism			PCOM		OD	
					EAF	Beta	P-value	Beta	P-value	Beta	P-value
2:213391766	rs2178575	*ERBB4*[*]	G	A	0.83	-0.126	4.3E-03	**-0.24**	**1.4E-05**	**-0.23**	**1.2E-11**
2:43561780	rs7563201	*THADA*[*†]	G	A	0.56	0.061	8.0E-02	**0.16**	**3.7E-04**	0.08	1.5E-03
5:131813204	rs13164856	*IRF1/RAD50*[*]	T	C	0.73	0.092	1.8E-02	0.16	1.4E-03	0.08	5.6E-03
8:11623889	rs804279	*GATA4/NEIL2*[*]	A	T	0.27	0.126	8.7E-04	**0.22**	**1.5E-06**	**0.16**	**9.9E-09**
9:126619233	rs9696009	*DENND1A*[†]	G	A	0.94	**-0.330**	**2.9E-07**	**-0.32**	**4.0E-05**	**-0.36**	**4.4E-15**
9:5440589	rs10739076	*PLGRKT*	A	C	0.30	0.026	5.3E-01	0.10	5.9E-02	0.00	8.9E-01
9:97723266	rs7864171	*C9orf3*[*†]	G	A	0.60	**0.124**	**3.8E-04**	**0.19**	**1.3E-05**	**0.10**	**2.3E-04**
11:30226356	rs11031005	*ARL14EP/FSHB*[*]	T	C	0.85	-0.079	8.2E-02	-0.18	1.3E-03	**-0.13**	**2.8E-04**
11:102043240	rs11225154	*YAP1*[*†]	G	A	0.91	-0.144	1.4E-02	**-0.24**	**3.5E-04**	-0.23	5.7E-08
11:113949232	rs1784692	*ZBTB16*	T	C	0.85	0.146	4.6E-03	**0.30**	**2.8E-06**	**0.21**	**6.6E-09**
12:75941042	rs1795379	*KRR1*[*]	T	C	0.24	-0.104	8.0E-02	-0.16	1.5E-03	**-0.11**	**1.8E-04**
12:56477694	rs2271194	*ERBB3/RAB5B*[†]	A	T	0.42	**0.126**	**2.7E-04**	**0.17**	**7.9E-05**	**0.13**	**1.4E-06**
16:52375777	rs8043701	*TOX3*[†]	A	T	0.82	**-0.166**	**1.4E-04**	-0.17	1.5E-03	-0.08	9.2E-03
20:31420757	rs853854	*MAPRE1*	T	A	0.50	0.111	9.8E-04	0.10	2.1E-02	0.05	3.8E-02

Significant associations are highlighted in bold. Variant previously reported as a PCOS risk variant in

[*]European or

[†]Han Chinese populations.

https://doi.org/10.1371/journal.pgen.1007813.t003

1.15 The 14 susceptibility loci among PCOS patients and their association with different PCOS traits.

In bold are the newly identified loci in this study, and in regular font are the 11 previously confirmed loci; photo adapted from https://doi.org/10.1371/journal.pgen.1007813.t003

In summary, GWAS confirmed once more a shared genetic architecture between PCOS patients with similar traits albeit with small variations that are thought to be related to the severity of their symptoms and the differences in their phenotypes.

1.3.5.2 Gonadotropin secretion and action in PCOS

GnRH is the primary regulator of the LH/FSH ratio through its pulse frequency, as previously explained. LH levels are higher in PCOS patients than in normal controls (Rebar, Judd et al. 1976, Balen 1993). LH is high in both its overall plasma level and its pulse frequency as well, in PCOS patients (Waldstreicher, Santoro et al. 1988). However, LH levels are lower in obese PCOS patients than in non-obese counterparts (Taylor, McCourt et al. 1997). LH action is further enhanced in PCOS patients by the overexpression of its receptors in theca and GCs from polycystic ovaries (Jakimiuk, Weitsman et al. 2001).

Genetic variants of the *LH* beta-subunit and *FSHR*, *LHCGR*, and *FSHB* loci exist in PCOS patients, as shown in various GWAS (Taylor, McCourt et al. 1997, Nilsson, Jiang et al. 1998, Azziz 2016). The high LH/FSH ratio increases androgen secretion from the theca cells of ovarian follicles. This excess androgen impairs follicular development leading to defective E2 and P4 production. Defective P4 production (in the second half of the cycle) reduces its negative feedback effect on hypothalamic GnRH release, enhancing high overall GnRH pulse frequency. This high GnRH pulse frequency leads again to a high LH/FSH ratio in a vicious cycle and further develops PCOS morphology (Burt Solorzano, McCartney et al. 2010). Besides, there is emerging evidence of follicular resistance to FSH in the ovaries of PCOS patients, probably secondary to an excess of AMH production in them (Broekmans, Visser et al. 2008). An important point to highlight here is that LH is not the only mechanism for hyperandrogenism in PCOS patients. In a study done on 45 women with the same levels of LH, those who had abundant PCOM by US examination (n=21) had higher androgen

levels compared to the rest of the study members who had normal ovarian morphology (n=24) (Adams, Taylor et al. 2004).

1.3.5.3 Ovarian dysfunction in PCOS

During the ovarian cycle of healthy women, one follicle among the cohort of growing follicles, at the beginning of each cycle, is selected to continue to grow and dominate, which further forms the mature Graafian follicle. The rest of the follicles become atrophic. In PCOS, this selection process is defective because of insufficient FSH production and the local resistance to FSH action caused by high AMH levels besides other intraovarian factors (Fauser and Van Heusden 1997). Theca cells of PCOS patients were found, by immunostaining studies, to overexpress DENND1A. The presence of DENND1A protein in the cytoplasm and nuclei of theca cells suggests a possible role for this protein in gene regulation (McAllister, Modi et al. 2014). Furthermore, DENND1A variant 2 (DENND1A.V2) protein and mRNA levels are higher in PCOS theca cells than in non-PCOS theca cells. GWAS studies have persistently identified SNPs close to the *DENND1A* gene as candidate PCOS loci (Azziz 2016). These findings suggest potential hypersensitivity of theca cells to LH, besides its resistance to FSH as another mechanism for PCOS development.

1.3.5.4 Insulin secretion and action in PCOS

As discussed before insulin resistance and compensatory hyperinsulinemia are well-established findings in PCOS patients for a long time (Dunaif 1997, Legro, Finegood et al. 1998, DeUgarte, Bartolucci et al. 2005). The mechanism by which insulin resistance happens remains unclear. Though, downstream of the insulin receptor, a signalling pathway defect has been suggested in PCOS patients (Diamanti-Kandarakis and Dunaif 2012). Epigenetic modifications are also widely thought to play a role in insulin resistance among PCOS patients (Chen, Heneidi et al. 2013). Genome-wide

analysis of DNA samples from PCOS patients showed significant hypermethylation in the CpG island just outside the promoter region of 342 genes, compared to healthy women (Yu, Sun et al. 2015). These genes were involved in various molecular functions, including hormone activity, and transcription regulation (Yu, Sun et al. 2015). The same finding was detected in prenatally androgenized PCOS rat models (Zhang, Cong et al. 2014). The administration of insulin-sensitizing agents, like Metformin and thiazolidinediones, has been known to improve insulin resistance and overall fertility of PCOS patients (Azziz, Ehrmann et al. 2001, Lord, Flight et al. 2003). High insulin levels, in PCOS patients, are directly linked to high levels of androgen, which is a key pathology in PCOS development (Nestler, Powers et al. 1991, Nestler, Jakubowicz et al. 1998). The pathological effects of insulin resistance and hyperinsulinemia are further discussed in section 1.3.6.3.

1.3.5.5 Weight and energy regulation in PCOS

There is a close link observed between the degree of obesity, insulin resistance, and hyperinsulinemia, on the one hand, and the severity of ovulatory dysfunction and infertility after that in PCOS, on the other (Legro, Kunselman et al. 1999, Barber, McCarthy et al. 2006, Boomsma, Eijkemans et al. 2006, Dokras, Jagasia et al. 2006, Ehrmann, Liljenquist et al. 2006). These factors also determine the degree of metabolic syndrome and the prevalence of cardiovascular diseases among PCOS patients. These links enforce the hypothesis of weight and energy dysregulation as a key player in PCOS pathology development (as explained in the obesity section above). However, this is still not the only factor initiating all PCOS pathologies. In a study done in the United States in 2004, 60% of PCOS patients were obese, twice the percentage that is seen in healthy women of the same age (Azziz, Sanchez et al. 2004). The variation in the percentage of obesity among PCOS patients is attributed mainly to social and environmental factors, like lifestyle, high-caloric intake and the lack of exercise (Asuncion, Calvo et al. 2000).

1.3.5.6 Androgen biosynthesis and action in PCOS

Hyperandrogenism has always been a critical feature of PCOS in almost all diagnostic criteria. Excessive androgen production occurs mainly in ovarian stroma under the influence of LH and the adrenal glands (Kumar, Woods et al. 2005). High LH comes from the loss of the negative feedback regulatory effect of P4 on GnRH pulse frequency, which also increases. Hyperandrogenism has also been attributed to hyperinsulinemia (Korhonen, Hippelainen et al. 2001). Multiple variations in steroidogenesis genes have been identified in PCOS patients, including variants in DENND1A, as described above. These consistent genetic variants suggest that a genetic predisposition for hyperandrogenism must be there.

1.3.5.7 Environmental factors contributing to PCOS development

The most critical environmental factor affecting PCOS development is a diet enriched in saturated fatty acids and monosaccharide sugars and its associated obesity. Other potential environmental factors include environmental toxins that mimic androgen function (Kandaraki, Chatzigeorgiou et al. 2011, Vagi, Azziz-Baumgartner et al. 2014).

1.3.5.8 Hypothalamic resistance hypothesis in PCOS

The hypothalamic dysfunction hypothesis is a relatively new emerging theory aiming at explaining the origin of PCOS. The hypothalamic-hypophyseal gonadal axis's role in regulating sexual maturation, puberty, and fertility makes it worth a closer look to identify the origin of PCOS. The physiology of this axis was discussed in section 1.1.2.1 and its pathological effects in PCOS patients are discussed here. This section discusses the axis main dysregulations in PCOS patients to clarify the origin of the hypothalamic resistance hypothesis.

Hyperandrogenism is a crucial pathology in PCOS patients that causes impairment of follicular maturation and dysregulation of menstrual cycles (Rosenfield and Ehrmann 2016). Hyperandrogenism is caused by ovarian theca cells' response to high LH levels, in PCOS (Rosenfield and Ehrmann 2016). PCOS patients (and animal models) are known to have a high LH/FSH ratio secondary to high GnRH pulse frequency (Coutinho and Kauffman 2019). These high LH levels are formed of two components: increased LH pulse frequency and amplitude. Multiple irregularities involving the GnRH pulse generator were identified among PCOS animal models (Coutinho and Kauffman 2019) (Figure 1.16).

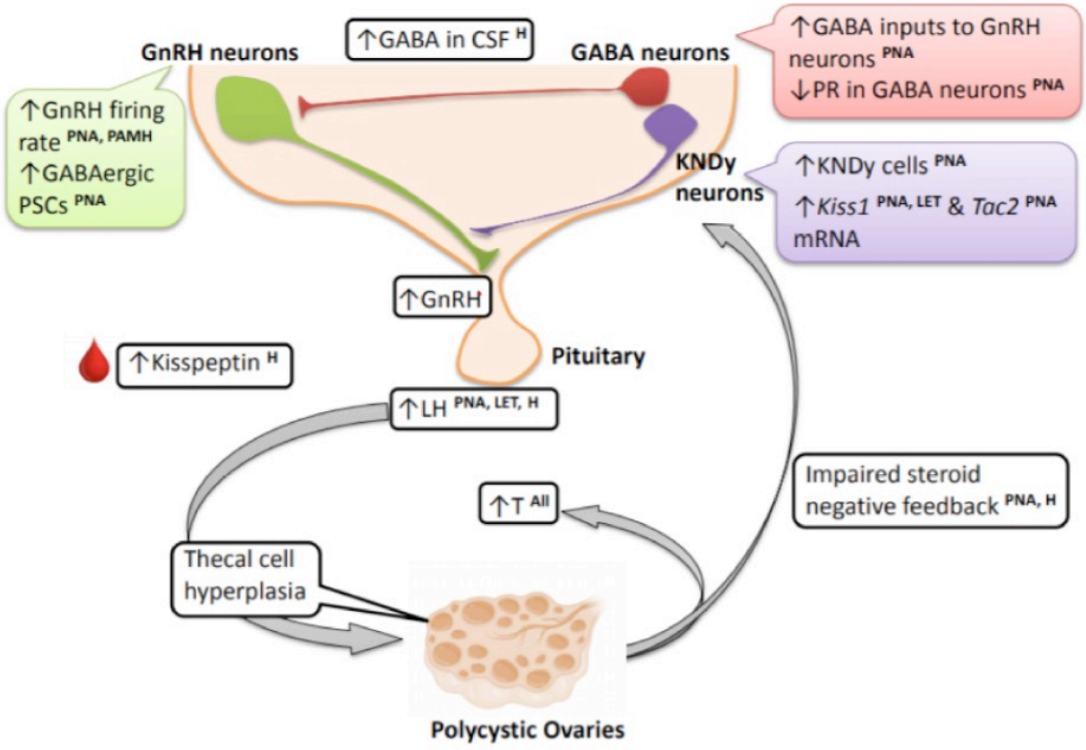

1.16 Hypothalamic dysregulation in PCOS patients and animal models

High LH levels and pulse frequencies observed in PCOS patients and animal models are due to upstream high GnRH pulse frequency. Prenatally androgenized (PNA) mice and women with PCOS show an increase in GABAergic postsynaptic currents, a potent stimulant of GnRH neurons, plus, an impairment of the negative feedback signal of sex hormones (particularly P4) to GABAergic neurons. The impaired negative feedback signal is probably due to the progesterone receptor (PR) under-expression in ARC GABA neurons in PNA mice and the mediobasal hypothalamus of LET mice. Besides the increased GABAergic signals, there was also an increase in mRNA levels of ARC KNDy cells and ARC Kiss1 (another potent stimulant of GnRH neurons) and Tac2 in PNA and LET-induced animal models. These findings are suggesting an increase in the overall stimulatory signals to GnRH neurons. PNA = (prenatally androgenized), PAMH (prenatally treated with AMH), LET = (letrozole) animal models, H = human. Figure adapted from (Coutinho and Kauffman 2019), *Medical Sciences Journals, volume 7, issue 8, 10.3390/medsci7080084,* https://doi.org/10.3390/medsci7080084.

GnRH neurons have an increased firing activity in prenatally androgenized (PNA) female mice compared to wild-type mice (Roland and Moenter 2011). Furthermore, Roland et al. detected an increase in the frequency of the GABAergic signals to GnRH neurons, and their size as well, in the PNA female mice. Their findings strongly suggest an increase in the overall GABAergic 'excitatory' input to GnRH neurons. Worth mentioning here that, GABA neurons are generally inhibitory in most brain centers, except for the GnRH neuroendocrine circuit, where they are excitatory (DeFazio, Heger et al. 2002). This enhanced GABAergic input to GnRH neurons has been also evident in other studies, using PNA, and AMH-treated, mouse models (Moore, Prescott et al. 2015, Tata, Mimouni et al. 2018). In humans, cerebrospinal fluid samples from PCOS patients show higher levels of GABA when compared to normal women (Kawwass, Sanders et al. 2017), which also suggests a role for GABA in the observed high GnRH levels in these patients.

Studies have also shown an impairment of steroids regulatory feedback signals to GnRH neurons in PNA mouse models of PCOS (Moore, Prescott et al. 2013, Moore, Prescott et al. 2015). Era and AR are the usual receptors involved in the negative feedback signals of various steroid hormones to the hypothalamus and the pituitary. GnRH neurons express E2 receptor beta (ERβ) only (Hrabovszky, Steinhauser et al. 2001), but not E2 receptor alpha (Era) (Herbison, Skynner et al. 2001), nor AR (Huang and Harlan 1993). The absence of these receptors in GnRH neurons suggests the involvement of the neuroendocrine circuit's neurons in the regulatory feedback pathway. In PNA female mice, ARC GABA neurons under-express progesterone receptor (PR), which could contribute to the resistance to negative feedback signals identified in these mice (Moore, Prescott et al. 2013, Moore, Prescott et al. 2015). Similar resistance has been identified in some women with PCOS, as these patients generally needed higher doses of P4 to suppress their LH compared to healthy women (Pastor, Griffin-Korf et al. 1998, Chhabra, McCartney et al. 2005). A similar form of

resistance to P4 also exists in LET-induced mouse models of PCOS as studies have identified lower PR mRNA expression levels in the ARC region of these mice compared to control mice (Kauffman, Thackray et al. 2015). Thus, ARC GABA neurons are possibly the cornerstone in P4-mediated regulatory feedback signals to GnRH neurons in PCOS patients. Further studies are needed on GABA neurons to better understand their complex role in PCOS patients.

ARC kisspeptin- and NKB positive cells are more abundant in females of PNA rat models of PCOS than wild-type rats (Osuka, Iwase et al. 2016). These PNA rats also show higher mRNA expression levels of *Kiss1* and *Tac2* (the gene coding for NKB) in the ARC (Yan, Yuan et al. 2014). The number of kisspeptin cells and the levels of *Kiss1* and *Tac2* mRNA in the ARC of PCOS animal models positively correlate with their LH levels. Furthermore, data from *Kiss1* and *Kiss1R* knockout (KO) mice make compelling evidence for the role of kisspeptin and its receptors in GnRH neuron regulation and, therefore, LH levels (d'Anglemont de Tassigny, Fagg et al. 2007, Lapatto, Pallais et al. 2007). PCOS patients have high plasma levels of kisspeptin with a strong positive correlation with LH plasma levels (Katulski, Podfigurna et al. 2018). This positive correlation is identified in multiple studies, though the source of the high levels of kisspeptin in PCOS patients is still unknown (Wang, Han et al. 2019). A recent clinical trial on PCOS patients treating them with a Neurokinin 3 receptor antagonist showed a significant reduction in LH pulse frequency and serum T levels (George, Kakkar et al. 2016). These findings make kisspeptin, GABA and GnRH neurons and their receptors important study targets for understanding the neuroendocrine circuit of PCOS and its role in PCOS pathology.

A global *Era* gene KO mouse was generated and observed for fertility anomalies to understand the effect of E2 on PCOS phenotype development. Era-KO mice showed elevated serum levels of E2 (E2), T, and LH, indicating a hypothalamic-hypophyseal

gonadal axis dysregulation (Couse, Yates et al. 2003). Pituitary-specific Era-KO mouse models have variable PCOS phenotypes depending on the study (Herbison 2008, Singh, Wolfe et al. 2009, Cheong, Porteous et al. 2014). Two different studies using the same mouse model of *Era* pituitary-specific KO showed that the females were infertile or subfertile with a cystic formation in the ovaries. However, one study reported high LH levels, and the other one reported normal LH levels, with variation in the severity of the ovarian cystic morphology between both (Gieske, Kim et al. 2008, Singh, Wolfe et al. 2009). In more recent work, Areo et al. used a different approach; they reintroduced pituitary specific *Era* gene in a complete E2 receptor-alpha knock-out mouse (PitERtgKO) to evaluate its role in PCOS phenotype (Arao, Hamilton et al. 2019). Interestingly, serum levels of E2 and LH went back to normal in the PitERtgKO mice, suggesting a pivotal role for E2 feedback signals, to the pituitary, in the hormonal axis regulation. PitERtgKO mice showed hemorrhagic cysts in their ovaries that were more severe compared to the Era-KO mice (Couse, Yates et al. 2003)). These cysts are probably due to the absence of E2 regulatory feedback signals on the hypothalamus leading to sporadic high LH secretion (Arao, Hamilton et al. 2019). This was confirmed by measuring mRNA expression levels of LH early response genes (*Ptgs2, Btc, Areg, and Cebpb*) in PitERtgKO adult female mice, which were higher than their levels in ERaKO and wild-type mice ovaries.

Androgens affect follicular maturation not only through their known direct effect on the ovaries but also through the neuroendocrine circuit (Caldwell, Edwards et al. 2017). In their study, Caldwell et al. removed AR globally one time, and in specific neurons another time, from dihydrotestosterone (DHT) induced mouse models of PCOS. DHT is a more potent form of testosterone, which is produced endogenously by the reduction of testosterone through the 5α-reductase enzyme in certain organs including the prostate, epididymis, and seminal vesicles (Swerdloff, Dudley et al. 2017). They detected the effect of androgens receptors on PCOS phenotype by rescuing the

phenotype upon AR loss. Global loss of the AR showed a complete reversal of the PCOS phenotype induced by DHT, confirming that androgens contribute to all DHT-induced PCOS features. Neuron-specific AR loss rescued only DHT-induced dysfunctional ovulation, PCOM, and metabolic traits like obesity and dyslipidemia, but not high LH (Caldwell, Edwards et al. 2017). Additionally, the authors of the Caldwell study tested ovariectomized global AR KO mice transplanted with wild-type ovaries and then exposed to DHT; under these conditions, estrous cycles, and corpora lutea went back to normal despite DHT treatment. These results again strongly support an extra-ovarian role for androgen in PCOS morphology (Caldwell et al., 2017).

The role of androgen in PCOS etiology is also abundant in humans, where studies showed that the use of flutamide (anti-androgen) makes PCOS patients more responsive to E2 or P4 treatment. The successful suppression of LH levels to a similar degree to that of non-PCOS patients confirmed this role (Eagleson, Gingrich et al. 2000). This suppression was not achievable in non-flutamide E2 and P4 treated PCOS patients (Pastor, Griffin-Korf et al. 1998). These results strongly suggest that androgens block E2 and P4 feedback signals to the hypothalamus and pituitary. In a study by Prescott et al. on a PNA PCOS mouse model, the effect of treatment with flutamide was more prominent. In that study, they were able to show a reversal of the abnormal GnRH neuron morphology usually detected in these mice plus a decrease in serum T levels and restoration of normal estrous cyclicity in flutamide-treated PNA mice (Silva, Prescott et al. 2018).

Putting these findings together with the known hypothalamic resistance to leptin (Chakrabarti 2013, Lian, Zhao et al. 2016), and the resistance of the peripheral tissues to insulin in PCOS patients (Sakumoto, Tokunaga et al. 2010, Rojas, Chávez et al. 2014, Cree-Green, Rahat et al. 2017), support a hypothesis of multi-receptor resistance or failure as the origin of PCOS. This multi-receptor resistance or failure could still be of

genetic origin, caused by either multiple gene defects or a defect in one key gene that codes for vital transcription factor affecting various genes related to fertility, such as the *GATA4*/*Gata4* genes.

1.3.6 Pathophysiology of PCOS

PCOS features are manifested at variable degrees among patients, making the presentation of every patient unique. Approximately 90% of PCOS patients manifest with certain degrees of ovarian androgen dysregulation (hyperandrogenism) (Rosenfield and Ehrmann 2016). One-half of PCOS patients have some degree of insulin resistance, obesity, and high LH levels in their plasma (Legro, Driscoll et al. 1998), suggesting that PCOS pathologies are mainly due to ovarian hyperandrogenism, with variable degrees of insulin resistance and associated hyperinsulinemia. The latter appears to be a non-essential feature but rather a common aggravating factor. Obesity and high levels of LH, on the other hand, seem to be secondary to hyperandrogenism and hyperinsulinemia. A simplified model of PCOS pathophysiology is presented in Figure 1.17.

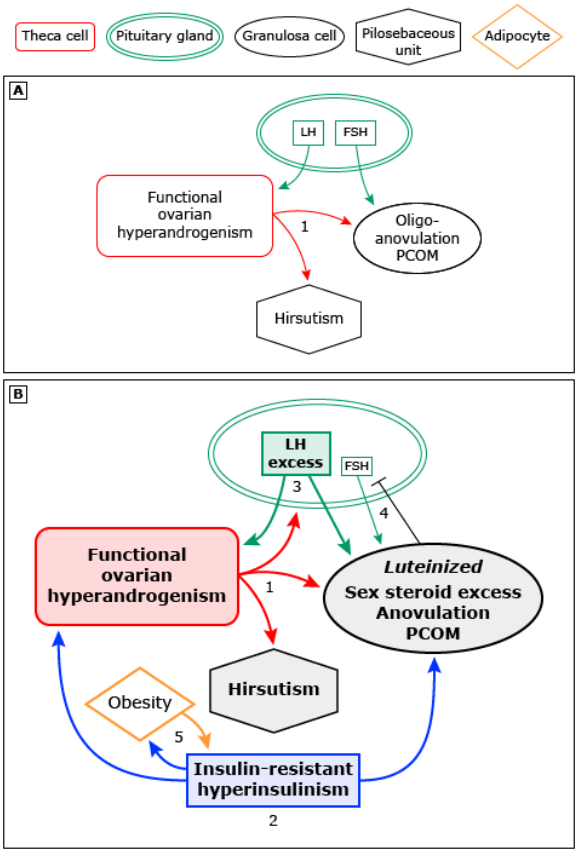

1.17 A simplified representation of PCOS pathophysiology

Panel A represents functional ovarian hyperandrogenism (FOH) in around 90% of PCOS patients. Panel B represents 50% of PCOS patients with insulin-resistant and hyperinsulinism. Hyperinsulinism aggravates the production of androgen by theca cells and enhances premature androgen luteinization of GCs. Hyperandrogenaemia works on the pituitary to increase LH production, which in turn acts on both the theca and the luteinized GCs to induce more hyperandrogenism in a vicious cycle (step 3). Excess LH also stimulates the luteinized GCs to produce more E2 (step 4), suppressing pituitary FSH secretion in a negative feedback loop. Hyperinsulinism-induced pathophysiological changes in GCs aggravate PCOM and anovulation. Obesity is a critical factor in exaggerating insulin resistance and causing hyperinsulinism and hyperandrogenism (step 5). Effects and pathways in bold underline a more significant impact. Figure adapted and modified from Rosenfield RL, Ehrmann DA, (Rosenfield and Ehrmann 2016). Endocrine Reviews, Volume 37, Issue 5, 1 October 2016, Pages 467–520. *The Hypothesis of PCOS as Functional Ovarian Hyperandrogenism Revisited*, https://doi.org/10.1210/er.2015-1104.

1.3.6.1 Functional ovarian hyperandrogenism (FOH) in PCOS

FOH is a hyperandrogenic status secondary to generalized ovarian steroidogenic hyperactivity, particularly that of the 17-hydroxyprogesterone enzyme, which indicates dysregulation of cytochrome P450c17 (Rosenfield and Ehrmann 2016). FOH is the most predominant pathology in PCOS patients (90%), and it accounts for the three main clinical features of PCOS: hirsutism (clinical hyperandrogenism), oligo-anovulation, and polycystic ovaries. In a small proportion of PCOS cases, hyperandrogenism is extrinsic in origin, from adrenal or peripheral sources, rather than intrinsic from the ovaries. Androgen excess works on the skin's pilosebaceous glands to induce the disease's cutaneous manifestation, hirsutism. Hyperandrogenism causes GCs dysfunction on the ovary level, which eventually leads to oligo-anovulation and, therefore, PCOM.

Cytochrome P450c17 processes 17-hydroxylase and 17,20 lyase enzyme activities; the latter is the rate-limiting step for androgen synthesis. Androgen is the substrate for E2 synthesis in the ovaries and adipose tissue and therefore is necessary for efficient fertility (Kosidou, Dalman et al. 2016). Under the influence of LH, thecal cell production of androgen is coordinated with GCs E2 production through a direct intraovarian cellular interaction rather than a hormonal negative feedback loop. This cellular interaction occurs by the same mechanism as illustrated in Figure 1.7. On the ovarian level, the activity of P450c17 in theca cells is under the influence of LH. High LH levels lead to the downregulation of LH receptors, a phenomenon known as "homologous desensitization", to reduce androgen production. Androgen production is also downregulated by high levels of E2 and androgen itself through granulosa-theca cells interplay.

On the other hand, androgen production is upregulated by GCs factors that increase P450c17 activities like insulin-like growth factors, inhibin, and inflammatory cytokines

(Mesiano, Katz et al. 1997). A delicate balance between up-regulators and down-regulators controls the overall ovarian androgen production under physiological conditions. In PCOS, ovaries are particularly hypersensitive to LH stimulation (Foecking, Szabo et al. 2005), strongly suggesting that PCOS steroidogenesis dysregulation is an intrinsic defect. *In vivo* studies confirmed ovarian steroidogenic hypersensitivity to gonadotropins in PCOS patients (Mesiano, Katz et al. 1997). *In vitro,* thecal cell cultures from PCOS patients have shown abnormal steroidogenic patterns that have been preserved even after multiple cell passages. This latter finding strongly suggests an intrinsic genetic origin for this phenotype. Lastly, GWAS was used to show a genetic linkage of PCOS to the *DENND1A.V2* gene and its protein product, which could regenerate the same theca cell phenotype seen in PCOS patients when used in cultured cells *in vitro* (Ding, Zhuo et al. 2016, Mykhalchenko, Lizneva et al. 2017).

1.3.6.2 Granulosa cell dysfunction in PCOS

GCs are the supporting cells that maintain oocyte maturation by producing different growth factors and hormones, including E2 (Homburg, Gudi et al. 2017). GCs require androgen hormone input to regulate their response to gonadotropins (Kosidou, Dalman et al. 2016). Androgen also induces the transformation of primordial follicles into primary follicles to form a growing cohort of oocytes that later develop into small antral follicles (Ibanez, Potau et al. 1998). Thecal androgen induces LH receptor expression in GCs with the help of FSH. In response to LH, GCs produce P4 in preparation for the luteinization of a mature Graafian follicle. In PCOS, hyperandrogenaemia induces GCs dysfunction leading to anovulation and eventually PCOM (Rosenfield and Ehrmann 2016). Hyperandrogenaemia also causes an abnormally high number of small follicles to join the cohort of growing follicles each cycle. Furthermore, it induces premature follicular luteinization in the mid-follicular phase causing a maturation arrest. This arrest stops the process of natural selection of a dominant follicle to grow into a mature Graafian follicle, ending eventually into oligo-anovulation. The large cohort of small

growing follicles and their maturation arrest induced by hyperandrogenaemia are the main pathologies behind PCOM and oligo-anovulation. Hyperproliferating GCs (under the influence of hyperandrogenism) cause high serum levels of AMH in PCOS (Rosenfield and Ehrmann 2016). On the other hand, high levels of FSH-dependent inhibin-B from GCs (which have an androgen stimulatory effect) could reflect an intrinsic dysfunction of folliculogenesis, leading to GCs dysfunction in PCOS.

1.3.6.3 Hyperinsulinism and obesity in PCOS

Hyperinsulinemia sensitizes ovarian theca cells to LH, leading to an increase in their production of androgen and the premature luteinization of GCs. This luteinization, in turn, leads to an aggravation of hyperandrogenism and the development of polycystic ovaries and oligo- or anovulation afterwards. Hyperinsulinemia secondary to insulin resistance also enhances adipocyte proliferation, which further aggravates the existing insulin resistance in a vicious cycle. This phenomenon makes insulin resistance relatively proportionate to obesity and BMI (Fulghesu, Manca et al. 2015). Despite this clear link between insulin resistance and obesity, non-obese PCOS patients still have some degree of insulin resistance and hyperinsulinism in multiple studies (Shi, Zhao et al. 2010, Messer, Boston et al. 2012, Rojas, Chávez et al. 2014). The intrinsically dysregulated theca cells significantly aggravate FOH by reversing the natural LH-induced downregulation of LH receptors. Insulin also induces hyperandrogenism by upregulating 17ß-hydroxysteroid dehydrogenase (type 5) through adipogenesis influencing transcription factors (Robinson, Kiddy et al. 1993). Insulin, androgen and FSH have a synergistic effect on upregulating GC's LH receptors, rendering them more responsive to LH, which causes GCs premature luteinization and follicular growth arrest (Barnes, Rosenfield et al. 1994, Rosenfield and Ehrmann 2016). These findings were the cornerstone for treating PCOS with insulin-lowering drugs like Metformin, which subsequently reduces androgen levels in PCOS patients to some extent.

Obesity is predominant in around 50% of PCOS patients, with a particular increase in intra-abdominal (visceral) fat (Hirshfeld-Cytron, Barnes et al. 2009, Rosenfield and Ehrmann 2016). Insulin signals are particularly essential for transforming pre-adipocytes into adipocytes (adipogenesis) and for lipogenesis in adipose tissues (Ehrmann, Barnes et al. 1995, Sen and Hammes 2010, Hsueh, Kawamura et al. 2015). Insulin resistance is attributed mainly to the lipotoxic effect of excess FFAs on hepatocytes in liver tissues. On a molecular level, adipose tissues induce insulin resistance through the production of inflammatory cytokines such as TNF-α from mononuclear cells (Du, Rosenfield et al. 2009).

1.3.6.4 LH excess in FOH

FOH disturbs ovarian hormone syntheses, which in turn dysregulates their negative feedback effect on the pituitary and the hypothalamus ultimately leading to high LH production (Rosenfield and Ehrmann 2016). Increased LH levels in PCOS further aggravate follicular maturation and luteinization defects leading to more and more ovarian dysfunction in a second vicious cycle. There is a constant inverse relation between the levels of LH and FSH in plasma, which makes high LH levels in PCOS associated with low FSH levels. Abnormally low FSH levels interrupt follicular maturation in PCOS and induce, therefore, PCOM. LH levels in PCOS are less responsive to the natural negative feedback regulatory signals of E2 and P4 (Hewlett, Chow et al. 2017), which is probably due to resistance at the pituitary and hypothalamus levels to these signals. Antiandrogen treatment has been shown to alleviate some LH resistance to negative feedback (Rutkowska and Diamanti-Kandarakis 2016), which suggests that a high LH level in PCOS is a result of FOH and not a cause for it.

1.3.6.5 ER stress in PCOS

High ER stress levels are evident in the GCs of antral follicles in PCOS through the upregulation of unfolded protein response (*Upr*) genes (Takahashi, Harada et al. 2017, Azhary, Harada et al. 2019). In a study by Azhary et al., T induced ER stress in human granulosa-lutein cells (GLCs), *in vitro*, which led to apoptosis through the induction of the UPR transcription factor CCAAT enhancer-binding proteins homologous protein (CHOP) and the subsequent activation of death receptor 5 (DR5) (Azhary, Harada et al. 2019). The knockdown of *Chop* blocked the effect of T on DR5 activation and apoptosis thereafter. Furthermore, the knockdown of *Dr5* blocked the apoptotic effect of T on these cells. Pre-treating human GLCs, *in vitro*, with ER stress inhibitor TUDCA successfully prevented the previously observed lethal impact of T on them. Similar results also occurred when GLCs were pre-treated with flutamide, with a significant reduction of *Dr5* and *Chop* expression levels in response to T. Similarly, *in vivo*, high expression levels of *DR5/ Dr5* and *CHOP/ Chop* genes exist in GLCs obtained from PCOS patients and dehydroepiandrosterone induced PCOS mice.

Furthermore, PCOS mouse models treated with TUDCA showed reduced *Dr5* and *Chop* expression levels and subsequently reduced apoptosis in their antral follicle GCs (Azhary, Harada et al. 2019). The above findings provide strong evidence that hyperandrogenism in PCOS exerts its pathological effects through ER stress induction. These findings make ER stress an important therapeutic target for PCOS.

1.3.7 Clinical management of PCOS

The current PCOS management strategies involve medical therapeutics or surgical procedures, plus some lifestyle modifications. Life-style modifications aim mainly to reduce weight through diet and exercise. Weight reduction reverses obesity, and hyperinsulinemia, restoring ovulatory cycles and fertility and improving

hyperandrogenic features in women with PCOS. The American College of Obstetricians and Gynecologists and the Society of Obstetricians and Gynecologists of Canada recommend lifestyle modification as the first line of PCOS management.

Medical treatment of PCOS aims mainly to correct metabolic anomalies, anovulation, hyperandrogenaemia (hirsutism), and menstrual irregularity. Combined oral contraceptive pills (COC) are the first medical line of management as it improves ovulation and correct hyperandrogenaemia (McCartney and Marshall 2016, Ibanez, Oberfield et al. 2017). COCs contain both E2 and P4 and can suppress the hypothalamic-hypophysial-gonadal axis resolving the excess LH, GnRH, and T in PCOS patients. P4-only pills, such as medroxyprogesterone acetate, also have the same effect and are used when COCs are contra-indicated (Bagis, Gokcel et al. 2002). COCs and P4-only pills sometimes fail to achieve symptom resolution in some PCOS patients, potentially due to a higher degree of hypothalamic resistance to the feedback of E2 and P4, as explained before. This failure is probably because of significantly high androgen levels in those patients, which blocks the feedback input; here, the flutamide (anti-androgen) treatment is effective. Flutamide is also useful when COCs or P4-only pills and cosmetic measures do not control hirsutism. Insulin sensitizers like Metformin are most valuable when metabolic anomalies are abundant and have failed to be corrected by lifestyle modifications (McCartney and Marshall 2016). The molecular mechanism of Metformin action involves inhibiting mitochondrial complex I ATP generation, which interferes with glucagon signalling and gluconeogenesis, enhancing effective glucose utilization (Gardner, Trepanowski et al. 2018). Metformin exerts its effect on improving fertility by reducing ovarian steroidogenesis (androgen production) (Ladson, Dodson et al. 2011) and insulin levels (Rena, Pearson et al. 2013). Interestingly, patient response to Metformin is genetic dependent as results were variable among patients with different genetic polymorphisms (Rice, Elia et al. 2013, Buse, DeFronzo et al. 2016). Thiazolidinediones are another family of insulin sensitizers that works by

enhancing lipid mobilization from the blood through the activation of peroxisome-proliferator-related receptors (Cosma, Swiglo et al. 2008). Surgical management of PCOS is centred mainly around laparoscopic drilling of the ovaries to make micro-burns in the ovarian stroma where androgen is produced (Mitra, Nayak et al. 2015). Drilling is usually successful in reducing androgen levels and improving PCOS patient responsiveness to the IO by clomiphene citrate (CC) (Mitra, Nayak et al. 2015, Eftekhar, Deghani Firoozabadi et al. 2016).

ART includes IO followed by IVF or intracytoplasmic sperm injection. Physicians achieve IO in PCOS patients with CC, an anti-E2 that competes with E2 in the hypothalamus (Yagel, Ben-Chetrit et al. 1992). Recently a new drug Letrozole (LET) started to be introduced for the same purpose. Letrozole (LET) is an aromatase inhibitor that reduces E2 production (Franik, Eltrop et al. 2018). LET has been able to reduce E2 levels in PCOS patients to a great extent, reaching in some cases up to 97% reduction (Pavone and Bulun 2013). Interestingly, most clinical trials and meta-analyses showed that LET is superior to the traditional way of IO in PCOS patients using CC in achieving a successful pregnancy (Roque, Tostes et al. 2015, Amer, Smith et al. 2017). In summary, successful management of PCOS usually requires lifestyle modification plus IO and IVF. If obesity and metabolic anomalies are abundant, Metformin is also useful besides the lines mentioned above.

1.4 Mouse models of PCOS

Various animal models are available to study PCOS. These models are either hormonally induced (prenatal or post-natal), or genetically induced (transgene insertion or gene KO). Each model has a degree of representation of the human phenotype of the syndrome. To my knowledge, there is no animal model, currently available, representing the whole spectrum of the human PCOS phenotype with its metabolic and infertility components.

1.4.1 Hormonally induced PCOS models

Animal models of PCOS induced by hormones include mammals and rodents, prenatally or postnatally treated with androgen, E2, or anti-progestins. Prenatally treated rhesus monkeys and sheep with androgen or its equivalents (like DHT) display many reproductive and metabolic features of PCOS (Abbott, Tarantal et al. 2009, Padmanabhan and Veiga-Lopez 2013). Because of ethical or economic considerations, the use of these models is limited, and rodents are generally used. Postnatally (before puberty to adult age) treated female rats and mice with DHT develop a broad spectrum of PCOS phenotypes, including anovulation, high insulin levels and obesity and metabolic anomalies in some cases (Manneras, Cajander et al. 2007, van Houten, Kramer et al. 2012). These models display average ovarian weight and normal or even reduced plasma LH, T, and E2 levels, which renders them non representative of the complete PCOS phenotype. Prenatally DHT-treated mice also lack some of the critical features of the PCOS phenotype, particularly metabolic (insulin resistance and impaired glucose tolerance) and ovarian elements (Sullivan and Moenter 2004, Roland, Nunemaker et al. 2010, Roland and Moenter 2011, Witham, Meadows et al. 2012, Moore, Prescott et al. 2013). Recently, a new rat model of PCOS was generated using the nonsteroidal aromatase inhibitor LET, which has become one of the most

representative models currently available for this syndrome (Maliqueo, Sun et al. 2013). The LET rat model recapitulates some metabolic and hormonal anomalies of PCOS. Postnatally LET-treated female rats show estrous cycle abnormalities, anovulation, ovarian cysts formation, and increased atretic follicles (Maliqueo, Sun et al. 2013). These rats also show higher levels of T and LH compared to non-treated rats. Metabolically, they also show significant weight gain and insulin resistance compared to non-treated mice (Maliqueo, Sun et al. 2013). These phenotypes usually appear within five weeks of LET treatment. However, these results have not been reproducible in mice. LET-treated mice initially did not show any of the previously reported phenotypes (Caldwell, Middleton et al. 2014). A more recent LET mouse trial generated a more convincing PCOS phenotype. Kauffman et al. treated female C57BL/6N mice with LET for 5 weeks at puberty (6-8 weeks of age). LET-treated C57BL/6N female mice showed higher serum T and LH levels, lower serum FSH levels, acyclicity, more ovarian cysts, and a lower CL than non-treated mice (Kauffman, Thackray et al. 2015). Metabolically, LET-treated C57BL/6N female mice showed more weight gain, higher abdominal adiposity and adipocyte size, and impaired glucose tolerance than control mice (Kauffman, Thackray et al. 2015).

Furthermore, LET-treated mice showed higher kisspeptin receptor mRNA levels than controls, in the hypothalamus, making GnRH neurons more sensitive to kisspeptin's stimulatory effect. In addition, they showed lower PR mRNA levels compared to controls, making their GnRH neurons resistant to P4 negative feedback signals (Kauffman, Thackray et al. 2015). LET-treated mice did not share a consistent phenotype among different studies. Also, hyperandrogenism in this model is artificial and is secondary to aromatase inhibition, making tracing the origin of this syndrome almost impossible. LET is used to treat PCOS in humans, as previously described, making the use of it to generate a truly representative PCOS animal model questionable.

1.4.2 Transgenic mouse models for PCOS

Researchers have generally created genetic mouse models of PCOS by overexpressing different genes such as beta-human chorionic gonadotropin (*βhcg)*, ovarian nerve growth factor (*Ngf*), human plasminogen activator inhibitor-1 (*Pai-1*) and *βlh* (Risma, Clay et al. 1995, Kumar, Palapattu et al. 1999, Rulli, Kuorelahti et al. 2002, Matzuk, DeMayo et al. 2003, Meehan, Harmon et al. 2005). Most of these genetic models induce hemorrhagic cysts instead of regular PCOS cysts, which is not typical for human PCOS patients. These mice also express higher levels of T and LH compared to their wild-type controls, characterized by a 5 to 1000-fold increase in some models based on the promoter used to overexpress βLH or βhCG. These high levels may be responsible for the development of hemorrhagic cysts. Women with PCOS have, on average, only three-fold increases in LH levels (Group 2004).

Interestingly, *βhcg* overexpressing mice with low transgene copy numbers do not have the ovarian morphology characteristic of PCOS and therefore, they develop infertility later in life (6-7 months old) (Matzuk, DeMayo et al. 2003). *βlh* overexpressing mice also show significant obesity and increased white adipose tissue mass besides increased leptin and insulin levels. Surprisingly, insulin resistance does not develop in these mice (Kero, Savontaus et al. 2003). The *Pai-1* mouse model overexpresses this gene under the control of murine pre-pro-endothelin one promoter, specific for vasculature and epithelial cells (Devin, Johnson et al. 2007). These mice develop ovarian cysts, ovulatory abnormalities, and high levels of T. In women affected by PCOS, high PAI-1 levels have been reported, mainly in obese individuals, suggesting a role of PAI-1 in the associated metabolic anomalies (Gonzalez, Kirwan et al. 2013). Ovarian NGF is also involved in ovarian PCOS-related pathologies through sympathetic overactivity (Lansdown and Rees 2012). The NGF is an indicator of sympathetic nerve activity, and its levels are high in follicular fluid and GCs culture of PCOS patients (Dissen, Garcia-Rudaz et al. 2009). Overexpression of *Ngf* under the control of the Cyp17 promoter in

the previous mouse model caused hyperandrogenemia, follicular growth arrest, and infertility, although LH levels are normal, and no follicular cysts develop in the ovaries of affected female mice.

1.4.3 Knock-out mouse models for PCOS

Knock-out mouse models for PCOS are mainly generated by targeting aromatase (*Cyp19*), insulin and leptin receptors in pro-opiomelanocortin neurons (*Ir*/*Lep*RPOMC) or E2 receptor α (αERKO mouse) genes. Mice lacking *Era* or *Cyp19* genes had high LH levels secondary to the loss of E2 negative feedback effect on the hypothalamic-pituitary-gonadal axis (Couse, Bunch et al. 1999, Britt, Drummond et al. 2000). Like the *βhcg* and *Lhb* overexpressing mice, *Esr1* and *Cyp19* KO mice also show hemorrhagic cysts. Additionally, these mice also develop pathologies that are not among PCOS features, such as pituitary adenomas, mammary gland tumours and ovarian teratomas (Rulli, Kuorelahti et al. 2002, Huhtaniemi, Rulli et al. 2005). A mouse model with leptin and insulin receptors KO selectively in pro-opiomela-nocortin (POMC) neurons of the hypothalamus (*Ir*/*Lep*RPOMC) developed a wide range of the metabolic features of PCOS, including increased basal insulin levels, glucose intolerance, insulin resistance, and obesity (Hill, Elias et al. 2010, Marino, Iler et al. 2012). At the age of 4 months, 45% of these mice develop ovarian cysts and some degree of anovulation, with incomplete penetrance (Marino, Iler et al. 2012). They also showed at least a two-fold increase in T and LH levels. Furthermore, POMC neurons have an afferent neuronal input to GnRH neurons (Xu, Faulkner et al. 2011). Most transgenic, KO, and, to a less extent, hormonal PCOS mouse models have an incomplete representation of the PCOS phenotype. Therefore, there is a definite need for a more representative PCOS model, preferable if it is a genetic model considering the rising evidence of genetic origin for this syndrome.

1.5 Hypothesis and objectives

1.5.1 Hypothesis

I hypothesize that the *Gw* mouse model is a new, highly representative, transgenic model for PCOS, particularly the metabolic subtype of the syndrome. I also hypothesize that obesity is not the leading cause of *Gw* mice sub-fertility or infertility but rather, an essential aggravating factor. I predict that the syndrome pathology is attributed, at least in part, to multi-receptor resistance or failure. I also predict that the *Gata4* gene plays a crucial role in the development of PCOS phenotype in *Gw* mice through the inserted transgene sequence plus or minus insertion-site-specific effect. Finally, the *Gw* mouse model provides a great opportunity to further study origins of PCOS and identify critical pathologies and potential therapeutic targets for this syndrome.

1.5.2 Objectives

The first objective of this work was to do a genetic and phenotypic characterization of *Gw* mice and validate it as a mouse model for PCOS. The second objective was to evaluate the impact of obesity on *Gw* mice sub-fertility or infertility phenotype. The next objective was to identify some supporting evidence for the multi-receptor resistance or failure hypothesis, as the origin of PCOS in *Gw* mice. I also aimed to detect *Gata4* gene expression anomalies in the *Gw* mouse model. Finally, I measured *Gw* mice ER stress levels (a fundamental pathology in PCOS) and tested ER stress inhibitor (TUDCA) potentials in improving *Gw* sub-fertility and infertility.

CHAPTER II: MATERIALS AND METHODS

2.1 Origin and genetic analysis of the *Gw* mouse model

2.1.1 *Gw* mouse model

The generation of the *Gw* transgenic mouse line (*Gata4p[5kb]-RFP* line #2) has been previously described (Methot, Reudelhuber et al. 1995). Briefly, one-cell FVB/N embryos received a linearized rat *Gata4* promoter [5kb] - dsRed2 fluorescent protein construct using standard pronuclear microinjection methods (Nagy A. 2003). To aid in the visual identification of transgenic animals by pigmentation rescue of the FVB/N albino background (Methot, Reudelhuber et al. 1995), a previously described *Tyrosinase* mini-gene construct (Bergeron, Nguyen et al. 2016) was co-injected. All animal experiments were approved by the 'Comité institutionnel de protection des Animaux' at the University of Quebec at Montreal, reference # 931, and were executed following the regulations of the Canadian Council on Animal Care.

2.1.2 RNA and DNA extraction, RT reaction, and whole-genome sequencing

Highly purified DNA samples (from the spleen) were sent to Genome Quebec for whole-genome sequencing analysis using the Illumina TruSeq LT technique. Due to the high sequence similarity between the region of interest (*Gm10800*, on chromosome 2) and other loci in the genome, the use of standard whole-genome sequencing and

mapping techniques made it challenging to identify the insertion site. Sequencing was therefore repeated using the "10X linked reads" approach (Sun, Rowan et al. 2019).

High-quality DNA extraction (from various organs), agarose gel DNA extraction and plasmid extraction were done using the EZ-10 Spin Column Plasmid DNA Miniprep Kit (Thermo Fisher Scientific, #BS413) following their standard protocol. Routine DNA extractions from mouse tissues or cells were carried out using the standard phenol: chloroform: isoamyl alcohol (25:24:1) DNA extraction procedure. In brief, 30 mg of tissues were homogenized in DNA extraction buffer using a tissue homogenizer, followed by 10 seconds of vortex mixing. Homogenized tissues were then incubated with 1 ml of proteinase-K digestion buffer supplemented with proteinase enzyme (1 mg/ml) overnight at 55^{o}C in a water bath. Next, 500 µl of phenol: chloroform: isoamyl alcohol (25:24:1) was added to the mix and vortexed for 30 seconds.

RNA was extracted from mouse tissues or cells, using the RNeasy Plus Mini Kit (Qiagen, #74134) according to the manufacturer's protocol. RNA was reverse transcribed using the SuperScript™ II Reverse Transcriptase enzyme, (Invitrogen, #18064014). In brief, tube one contained the following mixture: 1 µl of oligo dT (500 µg/ml), 2 µg of RNA (x µl), 1 µl of 10 mM dNTP mix, and completed to a total volume of 12 µl by sterile distilled water, for each sample to be reverse transcribed. The mixture was heated to 65^{o}C for 5 minutes, quickly chilled on ice, and then centrifuged to collect the mix. Tube two was formed by mixing 4 µl of standard 5X First-Strand buffer, 2 µl of 0.1 M DTT, 1 µl of RNaseOut (40 units/µl) and 1 µl of SuperScript II-RT enzyme, for each sample. Contents from tube two were then gently mixed by pipetting up and down. 8 µl of the mix of tube two was then added to each of the 12 µl of tube one and mixed gently. Next, the tubes were incubated at 42^{o}C for 50 minutes, followed by enzyme inactivation by heating at 70^{o}C for 15 minutes. Complementary deoxyribonucleic acid samples were stored at -80^{o}C until further testing.

2.1.3 Polymerase chain reaction

Primers used for the polymerase chain reaction (PCR), qPCR, rapid amplification of cDNA ends (RACE), as well as "clustered regularly interspaced short palindromic repeats" (CRISPR) guides, are listed in Table 2.1. DNA samples were analyzed using a 2% agarose gel with a 200 bp or 1kb ladder and a standard loading buffer from Invitrogen. PCR reactions were run using SimpliAmp™ Thermal Cycler from Thermo Fisher Scientific using the standard PCR protocol of Taq DNA polymerase (Invitrogen, #10342053). Briefly, 2.5 µl of 10X PCR buffer was mixed with 2 µl of band sharpener, 0.5 µl of 10 mM dNTP mix, 1 µl of each primer (500 nM), 0.125 µl of Taq DNA polymerase, 2 µl of cDNA and finally sterile DNA-free water to complete the reaction volume to 25 µl. The mix was then run in the thermocycler at 95°C for 5 minutes (denaturation), 25-35 cycles at 95°C for 45 seconds and 55-60°C depending on the Tm of the primers (annealing), and finally 72°C for 1-5 minutes depending on the target fragment size (elongation). Lastly, samples were incubated for another 10 minutes at 72°C for a final extension. Samples were kept at 4°C until collected.

2.1.4 Q-PCR

All qPCR reactions were performed using the SensiFAST SYBR green Mix (Bioline, #BIO-98005). First-strand cDNA was synthesized from 500 ng RNA, as described before in the RT reaction. A mixture of 2 µl cDNA, 1 µl of each primer (500 nM), 10 µl of SYBR green mix, and 5 µl of RNAse-free water was prepared for each tested sample in 96-well plates. All qPCR samples were tested in triplicates. QPCR plates were run in a Roche thermocycler (LightCycler® 480) at 95°C for 2 min, followed by 40 cycles of 95°C for 5 seconds, 60-65°C for 10 seconds, and 72°C for 5-20 seconds. The cycle threshold (Ct) was normalized for each sample against the housekeeping gene (Hypoxanthine Phosphoribosyltransferase 1, HPRT1) of the same mouse to calculate the $^{\Delta}$Ct and then against the average of the $^{\Delta}$Ct for the gene of interest from three control mice (FVB) to obtain the $^{\Delta\Delta}$Ct.

2.1.5 RACE

The RNA Ligase-Mediated (RLM)-Rapid Amplification of cDNA Ends (RLM-RACE) kit (Thermo fisher scientific, #AM1700M) was used to identify the putative 5’ and the 3’ ends of the *Gm10800* ORF. Adaptors, primers, and gene-specific primers used during this experiment are listed in Table 2.1. Briefly, for the 5’ end of the RACE protocol, RNA was treated with calf intestinal phosphatase to remove the 5'-phosphate from all nucleotides that contain a free phosphate group at their 5' end, sparing the 5'-capped mRNAs. Samples were then treated with tobacco acid pyrophosphatase to de-cap full-length mRNAs (exposing their 5'-end phosphate), followed by T4 RNA ligase to join an RNA oligonucleotide adaptor to the newly exposed 5'-phosphate group. Finally, an RT reaction was performed using random hexamer primers, followed by a PCR reaction to amplify the 5’ end of the putative open reading frame (ORF) using a primer within the 5’ adaptor (provided with the kit) and a gene-specific reverse primer for the *Gm10800*.

For the 3’-end of the RACE protocol, a 3’ RACE adaptor (provided with the kit) that complements the poly-A tail of the full-length mRNA was used for the RT reaction. A PCR reaction was done next using a forward primer in the 3’ adaptor and a reverse gene-specific primer for the *Gm10800*. Gene-specific primers, for the 5’- and the 3’-ends of the RACE reaction, were designed to allow the amplification of overlapping fragments from PCR reactions that can be later used to identify the complete ORF. The complete ORF was then sequenced and subcloned in an expression vector to study the *Gm10800’s* hypothetical protein subcellular localization and its potential interactants.

2.1.6 CRISPR

CRISPR technology was used to knock out the *Gm10800* gene in an FVB mouse. CRISPR guides were designed within the 200 base pairs directly upstream and downstream of *Gm10800* using the Zhang lab guides designing tool (Zhang_Lab) and

were verified for off-target cuts using the platform of Integrated DNA Technologies. Each guide was ordered as two complementary strands with a Bbsi restriction site upstream to facilitate the subcloning of each hybridized guide into a Cas9 endonuclease expressing vector. The Cas9 expressing vector used in this work was the px330-u6-chimeric_bb-cbh-hspcas9 (Addgene, Plasmid #42230). Two vectors were transfected or microinjected together to achieve a DNA cut on both sides of the *Gm10800* gene to ensure a complete KO. Guides were first tested *in vitro* (in mouse neuroblastoma cells (N2a)) to confirm successful on-target cuts and the absence of off-target cuts, using standard transfection protocol, as will be discussed below. The microinjection platform of the University of Quebec at Montreal was used to inject successful guides into the pronucleus of FVB mouse embryos *in vivo*. Embryos were then transferred into pseudo pregnant female FVB mice and their offspring were genotyped by PCR using primers that flanked the targeted region.

2.1 List of primers, adaptors, and guides used for CRISPR experiments.

	Name	**Sequence**	**Notes**
CRISPR guides	CRISPR guide 1F	5'->3': CACCGGAAGGGGAATTTTGGTGGCA	Including a BBSI site, underlined, for cloning.
	CRISPR guide 1R	5'->3': AAACTGCCACCAAAATTCCCCTTCC	
	CRISPR guide 2F	5'->3': CACCGCATGTTCAAAAGGGGCCCGA	

	CRISPR guide 2R	5'->3': AAACTCGGGCCCCTTTTGAACATGC	
CRISPR genotyping primers	Cr-F	ATTCATTCATAAGTGGATAGTGGC	
	Cr-R1	TAACTCCTGGGCTCAAGCAGTC	
	Cr-R2	TGACGAAATCATCTGTTTCCAAAG	
Transition events primers	Chr2-F	GCACACTGAAGGACCTGGAATATG	
	Rfp-R	CCTAATATTCTAATAGCAGCCATAAAATACTCC	
	Tyro-F	GCTGTTTGGCTTTTTTTCAGACCC	
	Chr2-R	CATATTCCAGGTCCTTCAGTGTGC	
Q-PCR primers	*Agrp*-F	CGGAGGTGCTAGATCCACAGA	
	Agrp-R	AGGACTCGTGCAGCCTTACAC	
	Npy-F	CTCCGCTCTGCGACACTACA	
	Npy-R	AATCAGTGTCTCAGGGCTGGA	
	Pomc-F	ATGCCGAGATTCTGCTACAGT	
	Pomc-R	TCCAGCGAGAGGTCGAGTTT	
Q-PCR primers	*Gnrhr*-F	GCCCCTTGCTGTACAAAGC	
	Gnrhr-R	CCGTCTGCTAGGTAGATCATCC	
	Fshr-F	GTGCATTCAACGGAACCCAG	
	Fshr-R	TCTAAGCCATGGTTGGGCAG	
	Lhr-F	GCCATGCATTCAATGGGACG	
	Lhr-R	GGCCTGCAATTTGGTGGAAG	
	Pgr-F	CATACCTTAACTACCTGAGG	
	Pgr-R	GATTAAGCAGATCTTCTGAGG	
	Esr-F	AGGACCACATCCACCGTGTC	

	Esr-R	GGGATTCTCAGAACCTTTCGG	
	Gata4-F	CTCTGGAGGCGAGATGGGAC	
	Gata4-R	CGCATTGCAAGAGGCCTGGG	
Housekeeping gene primers	*Hprt1*-F	TCAGTCAACGGGGGACATAAA	
	Hprt1-R	GGGGCTGTACTGCTTAACCAG	
RACE adaptors and primers	5’ adaptor	5'GCUGAUGGCGAUGAAUGAACACUGCGUUUGCUGGCUUUGAUGAAA-3'	Including a BamHI site, underlined, for cloning.
	5’ adaptor primer	5'CGCGGATCCGAACACTGCGTTTGCTGGCTTTGATG-3'	
	3’ adaptor	5'GCGAGCACAGAATTAATACGACTCACTATAGGT12VN-3'	
	3’ adaptor primer	5'CGCGGATCCGAATTAATACGACTCACTATAGG-3'	Including a BamHI site, underlined, for cloning.
	5’ Gene-specific primer	CAGCAGTTCACCTACAAAGAGT	
	3’ Gene-specific primer	TCCTCGCCGTATTTCACGTCC	

	ORF forward primer	CTCGAGATGTTTCTCATTTTCCATGATTTTCAGTTTTC	Including an XhoI site, underlined, for cloning.
	ORF reverse primer	GGATCCTCATTGTAACTCATTGATATACACTGTTCTAC	Including a BamHI site, underlined, for cloning.
F = forward, R = reverse.			

2.1.7 DNA cloning

Standard digestion and ligation protocols were used for DNA cloning using EcoRI and BamHI restriction enzymes and T4 DNA ligase enzyme (Thermo Fisher Scientific, #ER0271, ER0051, and EL0012 respectively) following manufacturer protocols. A ligation ratio of 3:1 (insert: vector) was used (NEBioCalculator) for all ligation reactions. A PGEM-T-easy vector (Promega, #A1360) was used for the amplification and sequencing of various DNA fragments through the transformation of competent Escherichia coli bacteria using heat shock. Plasmids were then purified from bacterial cultures using mini- or maxi-prep plasmid extraction kits (Thermo Fisher Scientific, #K0502, and K0491 respectively). The vector used had a backbone of the pIRES2-EGFP plasmid (Addgene, Plasmid #12283), which co-express a green fluorescent protein (GFP), and was modified to include a *Myc*-tag to expressed protein.

2.2 Cell culture and transfection

Albino mouse neuroblastoma (N2a), and African green monkey kidney fibroblast-like (Cos7) cell lines were used, in standard culture conditions, to study the predicted protein product of the *Gm10800* gene. GeneJuice transfection agent (Millipore #70967-4) was used for all transfection reactions following the manufacturer's protocol. In brief, cells were seeded in a 6-well plate at a density of 1-3 $X10^5$cells per well with 2 ml of growth medium (Dulbecco's Modified Eagle's – Medium (DMEM) + 10% Fetal Bovine Serum (FBS) + 1% antibiotic + 1% antifungal). A transfection mix was prepared using 100 µl of serum-free medium plus 3 µl of GeneJuice and 1 µg of the plasmid for each well. For the 10 cm cell culture plates, cell density was 15-25 $X10^5$ and the volume of the growth medium used was 10 ml. The serum-free medium volume used in the transfection mix for the 10 cm plates was 500 µl, the GeneJuice was 21 µl, and the DNA was 7 µg. The transfection mix was added to the cultured cells 16 hours after their seeding in a plate or a well, and cells were incubated at 37^o C with 5% CO_2 in a humidified incubator for 48 hours. After the incubation period, the culture medium was removed, and cells were washed twice using Phosphate-buffered saline (PBS) 1 ml each. Cells were then detached from plates or wells using Trypsin-EDTA (0.25%) (Thermo Fisher Scientific, #25200056) 1 ml per plate or 200 µl per well. Cells were incubated with Trypsin for 2-5 minutes under the same incubation conditions as before. After incubation, the trypsin enzyme was deactivated by adding 9 ml of the growth medium with 10% FBS to each 10 ml plate or 2 ml to each well. Detached cells were collected in an Eppendorf tube and centrifuged at a rate of 1200 g for 2 min. Cells were then washed using PBS and centrifuged two more times. Green fluorescent protein (GFP) expressing cells were separated from cultured cells using a fluorescence-activated cell sorting service (FACS) to purify successfully transfected cells (GFP positive) for further analysis.

2.3 Estrous cycle analysis

Estrous cycle phases were determined by daily vaginal lavage of mice, over 16 days, as McLean et al. previously described (McLean, Valenzuela et al. 2012). In brief, vaginal epithelial cells were collected by gently pipetting 30 µl of sterile normal saline, using a 200 µl pipette tip, in and out of the mouse vagina three times. Collected cells were spread on a glass slide and left to dry at room temperature. Vaginal smears were then stained with crystal violet stain (0.1% solution) for 1 minute, washed with PBS twice (1 minute each), and then left to dry at room temperature. Slides were then examined under a Leica DM2000 microscope to assess the relative number of nucleated epithelial cells, cornified squamous epithelial cells, and leukocytes, to determine the stage of the mouse cycle. The proestrus phase was identified by the predominance of nucleated epithelial cells in the smear. The estrus phase, on the other hand, was identified by the predominance of cornified epithelial cells. The diestrus phase was characterized by the presence of many leucocytes in the smear, and the metestrus phase was by the presence of a mixture of nucleated cells, cornified cells, and leucocytes.

2.4 Mating and counting pups

To examine fertility, a fertile FVB male mouse was mated overnight with a female FVB or *Gw* mouse. Vaginal plugs were checked every morning. Successful pregnancies were determined by the delivery of a litter of pups, 18-20 days after the detection of a plug. Data were collected by counting the number of vaginal plugs that ended up with a successful pregnancy, versus those that failed. In addition, the number of pups was also counted.

2.5 Induction of ovulation and *in vitro* fertilization

To induce superovulation, a mouse was first injected intraperitoneal (IP) with 5 IU of pregnant mare's serum gonadotropin hormone (Sigma, #G4877). This was then followed by a second IP injection of 5 IU of hCG hormone (Sigma, #CG10), 48 hours later. Fourteen hours following the second injection, mice were sacrificed, using isoflurane sedation and CO_2 euthanasia, and oocytes were collected from their oviducts. Thawed spermatozoa from a two-month-old fertile FVB mouse were first incubated in a capacitation medium for 30 minutes (at 37° C). Capacitated spermatozoa (10 µl) were used to inseminate collected oocytes in IVF medium (Sigma, #MR-070-D), and IVF plates were incubated at 37° C with 5% CO_2 for 6 hours. Oocytes were then washed three times, in an IVF medium, and further incubated for five days. Oocyte fertilization and zygote development were observed daily using a Leica microscope. Protocols used for sperm cryopreservation and IVF were adapted from "IVF protocol using freshly harvested and frozen sperm (MBCD+GSH) (Sep 2018)", and "IVF protocol for sperm samples frozen in vials and MTG straws (Sep 2018)" by infrafrontier (infrafrontier 2018).

2.6 Histology

Dissected organs (ovaries and adipose tissue) were fixed in paraformaldehyde 4% at 4° C overnight and then washed twice in PBS for 10 minutes each. Tissues were then subjected to gradual dehydration by serial incubations, starting with saline 0.85% for 30 minutes, followed by ethanol 50%/saline 0.42% solution for another 30 minutes. The subsequent incubations set were done in ethanol 70%, 95%, and 100% in three consecutive incubations, each lasting for 30 minutes. A toluene 50%/ethanol 50% solution was then used for another 30 minutes, followed by toluene 100% twice, for 30

minutes incubation each. Tissues were then incubated for 24 hours in a paraffin bath at 45° C, followed by a second clean paraffin bath for another 24 hours. Tissues were then embedded in paraffin blocks and kept overnight at 4° C. Histology sections were cut using a microtome at a thickness of 10 µm and incubated on slides at 37° C overnight. Histology slides were then deparaffinized and stained with hematoxylin and eosin, Masson's trichrome, or oil red O stain using standard histology protocols.

For collagen quantification, blue pixels (collagen) were counted against black pixels (nuclei) in each ovary, using ImageJ software. The identification of various stages of growing follicles, CL and cysts was based on morphological features following previously established protocols (Myers, Britt et al. 2004, Caldwell, Middleton et al. 2014). In brief, a primordial follicle had one layer of flattened granulosa cells surrounding the oocyte while a primary follicle had one or two layers of cuboidal granulosa cells. Secondary follicles were characterized by the presence of an oocyte surrounded by more than one layer of cuboidal granulosa cells and no antrum. The antral follicle, on the other hand, had a central oocyte surrounded by multiple layers of cuboidal granulosa cells and contained one or more antral spaces. Finally, atretic follicles were identified by their characteristic morphology of condensed dead oocytes, and the absence of surrounding cells. A total of three (n=3) mice were studied per genotype.

2.7 Immunofluorescence

Cells were seeded in a 6-well plate on a coverslip and then transfected as above and then directly fixed with 4% formaldehyde solution at 4° C overnight. Coverslips containing fixed cells were then washed three times with PBS under agitation and incubated with a blocking solution (PBS 1X, Triton X 0.1% and FBS 10%) for 1 hour at room temperature under agitation. Cells were then encircled on coverslips with a

hydrophobic layer of wax using a Pap-Pen (Abcam, #ab2601) to create a virtual well on the coverslip. 200 µl of the first antibody was added to the virtual well on the coverslip and incubated for 16 hours at 4° C. Cells were then washed with PBS three times and incubated with 200 µl of a fluorescent second antibody (concentration 1:500) for 2 hours at room temperature. Three more washes were done next to clear the excess of the second antibody, and cells were then incubated for 5 minutes with 4',6-diamidino-2-phenylindole (DAPI) to stain their DNA. After two more washes, a drop of glycerol 100% was added to processed cells and coverslips were inverted on a glass slide and sealed with nail polish. All incubations were done in a humidified chamber, away from light and under gentle rotatory agitation.

To study protein pattern and function of the Gm10800 gene, various cell lines were transfected with the ORF of the *Gm10800* gene and subcloned in an in-house modified expression vector. Considering that *Gm10800* is a gene model, there was no antibody available against its hypothetical protein, therefore, we used a *Myc*-tagged protein expressing vector to identify the predicted protein. This victor had the backbone of the pIRES2-EGFP plasmid (Addgene, Plasmid #12283), which co-express a green fluorescent protein (GFP), and was modified to include a *Myc*-tag to the N-terminal end of the ORF. The *Myc*-tag was added to detect the subcellular localization of the protein using a first antibody against the *Myc*-tag (homemade, at a concentration of 1:500) and a fluorescent second antibody (Alexa 647 or 488, Thermo Fisher, at a concentration of 1:1000). Another *Myc*-tagged protein expressing vector, pEYFP-N1, was also used to express the ORF of the *Gm10800* gene with the *Myc*-tag linked to the C-terminal end of the protein, to ensure that the tag is not affecting the expression of the protein. IF slides were examined using Leica confocal microscopy with laser wavelengths corresponding to secondary antibodies used.

IF studies of ovarian tissues were done by treating paraformaldehyde-fixed ovarian tissues, paraffinized and sliced as before, with anti-CHOP, ATF6, or IRE1 as the primary antibody (Abcam, #ab11419, #ab37149, and #ab48187 respectively) at a concentration of 1:500, and a fluorescent secondary antibody as before. ER stress levels were quantified by counting the number of positive granulosa and theca cells, within growing follicles, and dividing them by the overall number of growing follicles in each ovary.

2.8 Enzyme-linked immunosorbent assay

Insulin and leptin levels were measured from plasma samples of 6-hour fasted mice, using Enzyme-Linked Immunosorbent Assay (ELISA) kits, following manufacturer protocols (Crystal Chem, #90080 and #90030, respectively). E2, T and AMH plasma levels were measured from plasma samples taken during the met-estrus phase of the mouse cycle, using ELISA kits (Cayman Chemical, #582251, and #582701, and MyBioSource, #MBS268824, respectively). Met-estrous phase LH hormone levels were measured via a service provided by the lab of Dr Daniel Bernard using a highly sensitive ELISA technique they adapted from a protocol by Steyn et al. (Steyn, Wan et al. 2013). Plasma samples were collected by either tail bleeding or cardiac sampling according to the volume required for each test.

2.9 Weight gain

Mice, either *Gw* or FVB, males or females, were allowed regular standard food. The body weight of each mouse was measured bi-weekly. *Gw* mice with similar weights to the average weight of FVB mice were considered non-obese, and *Gw* mice with weights above the FVB average were considered obese.

2.10 Food consumption

Mice (4 in a cage) were allowed to nourish on the standard food used throughout this work and food weight was measured every four days for one month to calculate the average consumption of food per mouse per day. This experiment was repeated 3 times in total, on different mice (4 in a cage), for a total of n=12 in each group. The average food consumption of each mouse was then separately estimated.

2.11 Quantification of fat pocket size

Mice from each test group were anesthetized using isoflurane inhalation followed by CO_2 euthanasia. Abdominal skin and the peritoneal sac were opened longitudinally and fat depots (mesenteric, parametrial, para ovarian, sub-cutaneous and pericardial) were carefully dissected and weighed separately.

2.12 Glucose and insulin tolerance test

Fasting blood glucose was measured following six hours of fasting (8:00-14:00) for glucose tolerance tests, or four hours of fasting (8:00-12:00) for insulin tolerance tests. Next, glucose (1.0 mg/g of body weight) or insulin (0.5 mU/g of body weight) were injected intraperitoneally, and blood glucose levels were measured again at 30 minutes, 1 hour, and 2 hours after either injection. Blood samples were collected through a small cut at the tip of each mouse tail using a scalpel, and blood glucose was measured using an Accu-Check Aviva glucose meter (Roche).

2.13 Brain dissection

Whole brains of female adult *Gw* mice were collected after sacrificing them (using Isoflurane anesthesia followed by CO_2 euthanasia) at different age points. Whole brains were dissected without fixation (fresh) using a 1 mm sectioned, sagittal-oriented brain matrix (VWR, #100491-540). All dissections were done on ice to preserve RNA and DNA. The first blade was inserted in the midline groove and another blade in each of the immediate sidetracks on both sides (the distance between each track is 1 mm). The three blades were then removed together, and the outer blades were carefully separated from the midline one, aiming to have the 1mm thick brain slice on each of the two outer blades' inner surfaces.

Three cuts were made on each brain slice to dissect different hypothalamic nuclei, including arcuate, ventromedial, and dorsomedial hypothalamus (ARC, VMH, DMH, respectively). The first cut links the anterior border of the brain stem (A) to a point just below the thalamus's lower anterior part (B). The second cut links the last point (B) to another point just posterior to the optic chiasma (C). The third cut connects the points (A) and (C), making a triangle of the 3 points with a small slice of brain tissue inferior to this triangle, the ARC nucleus, Figure 2.1. Inside the triangle are the VMH and DMH nuclei. Similar hypothalamic nuclei from both sides of the same mouse were pooled together.

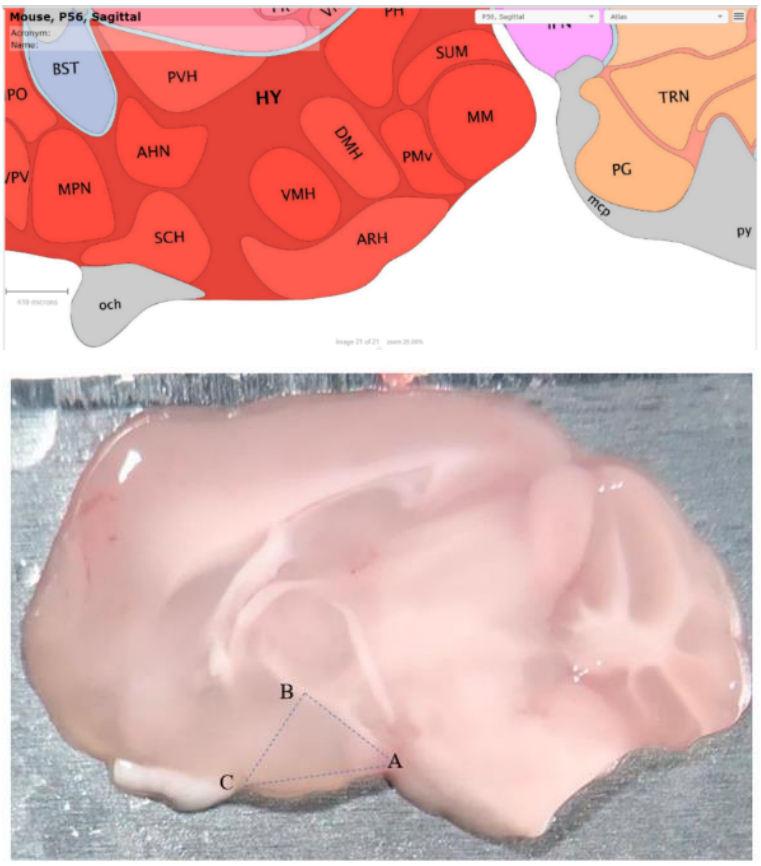

2.1 Hypothalamic nuclei dissection cut lines.

The upper panel is adapted from a mouse brain atlas showing the anatomy of the hypothalamus and its nuclei. The lower panel is a 1 mm mouse brain section dissected by a brain matrix, demonstrating the approximate locations of the three cut lines used to separate the Arc, VMH and DMH nuclei. Points A, B and C make a triangle that contains the VMH and DMH nuclei, while the ARC nucleus exists below the A-C line. Photo adapted from; Allen Institute Publications for Brain Science, https://mouse.brain-map.org/static/atlas

2.14 Medication protocols

Medications were delivered to mice in drinking water at a dose of 50 mg/100 g of the mouse body weight for TUDCA and 1.6 mg/100 g for Metformin (Sigma-Aldrich, #T0266-1G and #D150959-5G respectively). The same doses were used for the combined treatment experiment. These doses were adapted from previous studies that assessed the effects of TUDCA (Takahashi, Harada et al. 2017) and Metformin (Sabatini, Guo et al. 2011) on mice fertility. We calculated the average consumption of water per mouse to ensure the deliverance of the correct dose of each medication.

2.15 Statistical analysis

The data shown are means ± standard error of the mean. The student's t-test was used (two-tailed, unpaired) to compare every two sets of data separately. A p-value of ≤ 0.05 was considered statistically significant. For all reported data, an asterisk (*) marks a p-value of ≤ 0.05, and a double asterisk (**) denotes a p-value of ≤ 0.01.

CHAPTER III: RESULTS

3.1 The origin of the *Gw* transgenic mouse line

The *Gata4p[5kb]-Rfp* transgenic mouse line #2 (referred to as *Greywick* or *Gw,* considering the coat colour) was initially generated as a tool to fluorescently label pre-Sertoli and neural crest cell lineages during prenatal development (Mazaud Guittot, Tetu et al. 2007). This mouse line is of FVB/N albino background, bearing a *Tyrosinase* minigene co-injected to facilitate the identification of transgenic animals by pigmentation rescue (Methot, Reudelhuber et al. 1995). The co-occurrence of fluorescence and pigmentation for over 50 generations points to a single transgenic insertion site in the *Gw* genome, which is the norm with this strategy (Methot, Reudelhuber et al. 1995). *Gw* homozygotes were recovered from heterozygous intercrosses at the expected Mendelian frequency, without any sign of congenital anomaly, thereby allowing to maintain the line as homozygous. Yet, a subset of adult *Gw* female mice tended to develop subfertility concomitant with being overweight, recapitulating key features of PCOS. Interestingly, this phenotype was only observed in female *Gw* mice and not males. Furthermore, this phenotype was not observed in any of the other four *Gata4*-reporter lines generated using the same co-injection technique (*Gata4p[5kb]-Rfp* transgenic mouse line #5, and *Gata4p[5kb]-Gfp* transgenic mouse lines #1, 2 and 6a) (Pilon, Raiwet et al. 2008). This strongly suggests

that the phenotype is not linked to the transgene sequence alone but likely to its insertion site as well.

3.2 Genotypic characterization

The genotypic characterization of the *Gw* mouse model aimed mainly to identify the transgene insertion site and understand the role of the transgene in the observed phenotype. To identify the transgene insertion site, the whole-genome sequencing technique (Illumina HiSeq offered by Genome Quebec) was used to sequence the genomic deoxyribonucleic acid (gDNA) of *Gw* mice. Sequenced gDNA fragments were then mapped to the Mus musculus (house mouse) genome assembly GRCm38 (mm10) from Genome Reference Consortium [GCA_000001635.2 GCF_000001635.20]. The mapping data were then analyzed to identify breakpoints within the mapped gDNA fragments. These breakpoints would suggest possible transgene insertion sites. The most interesting gap was identified on chromosome two (Chr2) at location 'Chr2:98,648,316-98,703,256', Figure 3.1A. Surprisingly, the mapped fragment that led to the identification of this gap had both ends perfectly mapped to Chr9 as well as Chr2, due to sequence similarities between the two regions. Therefore, the breakpoint could not be confirmed using this technique.

The "10X linked reads" sequencing technique was next used to tag large gDNA fragments before breaking them into smaller ones, which were then sequenced and mapped. This technique allowed for small fragments, with the same tag, to be traced back to a larger piece of gDNA (10-40kb) which can then be mapped to a single location on a single chromosome. Using this technique, a specific location on Chr2 was identified as the site of the insertion of the transgene. The transgene insertion interrupted a gene model known as *Gm10800* in its 2nd and 3rd exons with the deletion of 81 nucleotides, Figure 3.1B. To further validate the identified insertion site, PCR

technology was used to amplify the transition events from the mouse gDNA into the transgene and back to gDNA again. Sequencing PCR products confirmed the transition from Chr2 to the RFP part of the transgene on one side, and from the *Tyrosinase* mini gene part of the transgene back to Chr2 again, at the exact breakpoint previously identified on Chr2, Figure 3.1C. Transition events sequences are listed in Table 3.1 below.

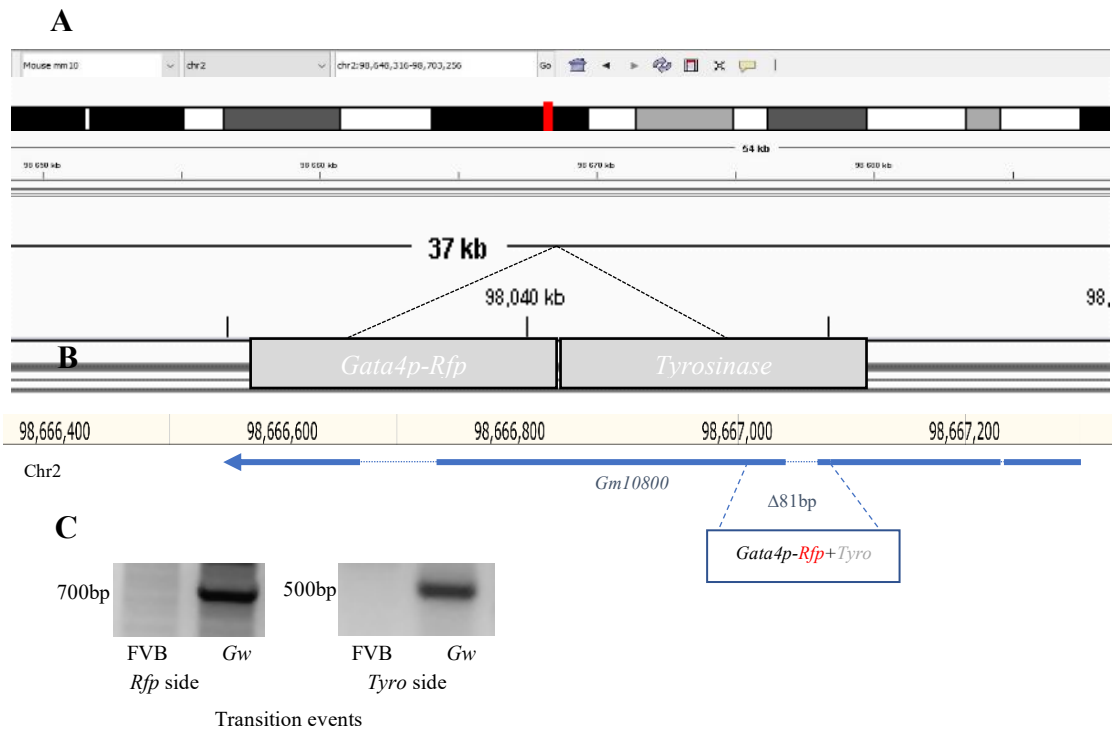

3.1 Genotypic characterization of the *Gw* mouse model.

A Representative photo for the breakpoint of the gDNA of *Gw* mouse, upon sequence mapping, at the insertion site of the transgene. **B** A diagram of the transgene insertion site, using Ensemble genome browser, disrupting the 2nd and 3rd exons of the *Gm10800* gene with a deletion of 81bp. **C** An agarose gel of the amplified transition events, using PCR, starting with *Gw* mouse gDNA (Chr2) fused to the *Rfp* segment of the transgene (700bp), and from the *Tyro* segment of the transgene back to Chr2 again (500bp).

3.2.1 Gm10800 characterization

Further analysis of the *Gm10800* gene was needed to understand its function and hence its contribution to the phenotype of *Gw* mice. The first step for characterizing the *Gm10800* gene was to identify possible ORF within *Gm10800*'s cDNA. The sequence of the *Gm10800* was extracted from Ensembl.org as a predicted gene composed of 2075 nucleotides with five exons and four introns, including a 660 nucleotides transcript. This sequence was further validated by PCR amplification, subcloning and sequencing of the intrinsic gene from an FVB mouse. The *Gm10800* gene sequence analysis predicted an ORF that codes for a hypothetical protein that is composed of 220 amino acids, using Bioinformatics.org. The analysis of the hypothetical protein, using Uniprot.org and SMART.org identified five 'transmembrane' domains within the protein sequence. The cDNA, ORF and the protein amino acid sequences of the *Gm10800* gene are listed in Table 3.1. Blasting the predicted protein amino acid sequence against protein libraries, SMARTBLAST, identified a 78% similarity to a 274 amino acid human protein known as Progranulin-induced receptor-like gene during osteoclastogenesis (PIRO) protein, (accession: BAQ19261.1), Table 3.1.

3.1 list of the *Gw* mouse genotyping sequences

Description	**Sequence**
Chr2-*Rfp* transition event sequence	GCACACTGAAGGACCTGGAATATGGCGAGAAAACGGAAAAT CACGGAAAATGAGAAATACACACTTTAGGACGTGAAATATGG CGAGGAAAACTGAAAAAGGTGGAAAAATTT*AAAGACTAAAAAA TAAAAGGACTGTCACAAGGAGTATTTTATGGCTGCTATTAGAATAT TAGG*

Tyro-Chr2 transition event sequence	*GCTGTTTGGCTTTTTTTCAGACCCATGTTTTTTCCTAAGTCCTAGTT TCTAAGAAATGACTGGGATTTGCTAAAATATATATATATATAAATAA TAACTTACTAATAGCTAAATAAAATTTCCTCTTACAACTAA*ATCCAC TTGACGACTTGAAAAATGACGAAATCACTAAAAAACGTGAAA AATGAAAAATGCACACTGAAGGACCTGGAATATG
Gm10800 DNA FASTA sequence	ATGTTTCTCATTTTCCATGATTTTCAGTTTTCTTGCCATATTTC ACGTCCTACAGTGGACATTTCTAAACCACCTTTTTCAGTTTTC CTCGCCATATTTCACGTCCTAAAGTGTGTATTTCTCATTTTCCG TGATTTTCAGTTTTCTCGCCATATTCCAGGTCCTTCAGTGTGCA TTTCTCATTTTTCACGTTTTTTAGTGATTTCGTCATTTTTCAAG AGTCAAGTGGATTTTTCTTTGATTTTCAGTTTTCTTGCCATACT CCACGTCCTACAGTGGACATTTCTAAATTTTCCACCTTTTTCA GTTTTCCTCGCCATATTTCACGTCCTAAAGTGTGTATTTCTCAT TTTCCGTGATTTTCAGGTTTCTCGCCATATTCCAGGTCCTTCAG TGTGCATTTCACATTTTTCACGTTTTTTAGTGATTTCGTCATTT TTCAAGTCGTCAAGTAGATGTTTCTCATTTTCCATGATTTTCAG TTTTCTTGCAATATTCCACGTCCTACAGTGGACATTTCTAAAT ATTCCACCTTTTTTCTCTCCATATTCCAGGTCCTTCAGTGTGCA TTTCTCATTTTTCACGTATTTTAGTGATTTCGTCATTTTTCAAG TCGTCAAGTGGATGTTTCTCATTTTCCATGATTTTCAGTTTTCT TTC

The 660bp ORF identified within the *Gm10800* gene	ATGTTTCTCATTTTCCATGATTTTCAGTTTTCTTGCCATATTTC ACGTCCTACAGTGGACATTTCTAAACCACCTTTTTCAGTTTTC CTCGCCATATTTCACGTCCTAAAGTGTGTATTTCTCATTTTCCG TGATTTTCAGTTTTCTCGCCATATTCCAGGTCCTTCAGTGTGCA TTTCTCATTTTTCACGTTTTTTAGTGATTTCGTCATTTTTCAAG AGTCAAGTGGATTTTTCTTTGATTTTCAGTTTTCTTGCCATACT CCACGTCCTACAGTGGACATTTCTAAATTTTCCACCTTTTTCA GTTTTCCTCGCCATATTTCACGTCCTAAAGTGTGTATTTCTCAT TTTCCGTGATTTTCAGGTTTCTCGCCATATTCCAGGTCCTTCAG TGTGCATTTCACATTTTTCACGTTTTTTAGTGATTTCGTCATTT TTCAAGTCGTCAAGTAGATGTTTCTCATTTTCCATGATTTTCAG TTTTCTTGCAATATTCCACGTCCTACAGTGGACATTTCTAAAT ATTCCACCTTTTTTCTCTCCATATTCCAGGTCCTTCAGTGTGCA TTTCTCATTTTTCACGTATTTTAGTGATTTCGTCATTTTTCAAG TCGTCAAGTGGATGTTTCTCATTTTCCATGATTTTCAGTTTTCT TTC
The amino acid sequence of the identified ORF	MFLIFHDFQFSCHISRPTVDISKPPFSVFLAIFHVLKCVFLIFRDFQF SRHIPGPSVCISHFSRFLVISSFFKSQVDFSLIFSFLAILHVLQWTFL NFPPFSVFLAIFHVLKCVFLIFRDFQVSRHIPGPSVCISHFSRFLVIS SFFKSSSRCFSFSMIFSFLAIFHVLQWTFLNIPPFFSPYSRSFSVHFS FFTYFSDFVIFQVVKWMFLIFHDFQFSF
The amino acid sequence of the human PIRO protein	MIFSFLAIFHVLQWTFLNFPPFSVFLAIFHVLKCVFLIFRDFQFSRH IPGPSVCISHFSRFLVISSFFKSSSGCFSFSMIFSFLAIFHVLQWTFL NFPPFSVFLAIFPVLKCVFLIFRDFQFSRHIPGPSVCISHFKRFLVIS TFFKSSSGCFSFSMIFSFLAIFHVLQWTFLNFPPFSVFLAIFHVLKC VFLIFRNFQFSRHIPGPSVCISHFSRFLVISSFFKVVKWMFLIFHDF QFSCHIPRPTVDISKFSTFFSFPRHISRPKVCISHFP

The sequence of the 618bp ORF identified within the RACE fragment	ATGTTTCTCATTTTCCATGATTTTCAGTTTTCTTTGATTTTCAGT TTTCTTGCCATACTCCACGTCCTACAGTGGACATTTCTAAATTT TCCACCTTTTTCAGTTTTCCTCGCCATATTTCACGTCCTAAAGT GTGTATTTCTCATTTTCCGTGATTTTCAGGTTTCTCGCCATATT CCAGGTCCTTCAGTGTGCATTTCACATTTTTCACGTTTTTTAGT GATTTCGTCATTTTTCAAGTCGTCAAGTAGATGTTTCTCATTTT CCATGATTTTCAGTTTTCTTGCAATATTCCACGTCCTACAGTG GACATTTCTAAATATTCCACCTTTTTCAGTTTTCCTCGCCATGC TTCACGTCCTAAAGTGTGTATTTCTCATTTTCCGTGATTTTCAG TTTTCTCTCCATATTCCAGGTCCTTCAGTGTGCACTTCTCATTT TTCACGTATTTTAGTGATTTCGTCATTTTTCAAGTCGTCAAGTG GATGTTTCTCATTTTCCATGATTTTCAGTTTTCTTTCCAAAGTA GGTACACACACAAAAAAAACACATACGTTGGAAACCGGCATT GTAGAACAGTGTATATCAATGAGTTACAATGAAAAACATGGA AAATGA

A review of the literature showed that the human PIRO protein (hPIRO) has a structural similarity to a superfamily of similar mouse PIRO proteins (mPIRO) coded on Chr2 (*Gm10800*) and Chr9, as confirmed by motifs preservation between these proteins (Oh, Kim et al. 2015). The diagram in Figure 3.2A showed this superfamily and was adapted from the same article (Oh, Kim et al. 2015). Extensive trials were done to express the ORF of the *Gm10800* gene, and to isolate its protein product, using various *Gw* and FVB mice's tissues, including the spleen, liver, testicles, and ovaries, with no success. The most likely representative cDNA band for the predicted protein was identified based on its expected size of 660 nucleotides. Expression patterns of the 660bp cDNA fragment were compared between *Gw* and FVB mice in various organs (using RT-PCR) to identify missing bands in *Gw* mice tissues caused by transgene insertion.

Surprisingly, the 660bp bands were not missing in some of the tissues of *Gw* mice (small and large intestine) while it was missing in other tissues (spleen and lungs), Fig. 3.2B. A similar-sized band from the *Piro* genes superfamily on Chr9 has most likely compensated for the missing band in *Gw* mice due to sequence similarity. A different technique was, therefore, needed to isolate the correct cDNA of the *Gm10800* gene. RACE protocol was used for this purpose in combination with the predicted cDNA sequence.

RACE primers were designed within the predicted cDNA, as specific as technically possible. Both the 5' and 3' ends of the message of the *Gm10800* gene (mRNA) were amplified from a full-length RNA extracted from FVB spleen tissues. RACE reactions generated two cDNA fragments that were sequenced and combined and a 618bp ORF was then identified within the final product of RACE, Table 3.1. Ovaries and testicle tissues did not give consistent results and, therefore, were not presented here. The 618bp ORF, previously detected by RACE, was subsequently cloned in an 'in-home modified' expression vector with a *Myc*-tag at the 5' end of the ORF plus the co-expression of a GFP. The expression of the protein from the *Gm10800* gene has been attempted in various cell lines including N2A and Cos7 cells, with the *Myc*-tag at the 5' end of the ORF, one time, and the 3' end, another time, without success (no *Myc*-tag signal), Fig. 3.2C and Fig. 3.2D**,** respectively. Protein expression control experiments have been successfully done using a homemade construct expressing a 5' end *Myc*-tagged family with sequence similarity 172 member A protein, data not shown here. The efficacy of the transfection process was validated by GFP expression.

A

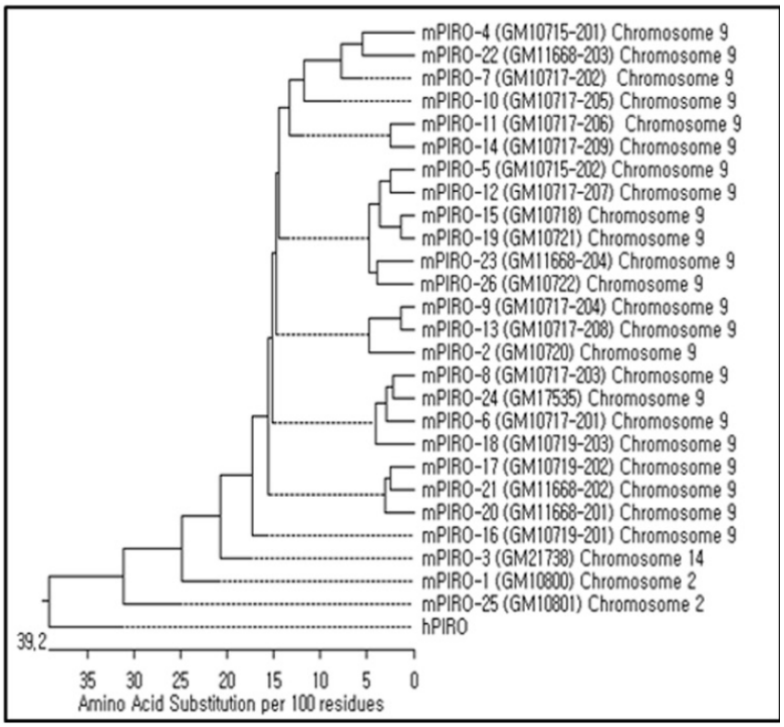
mPIRO-4 (GM10715-201) Chromosome 9
mPIRO-22 (GM11668-203) Chromosome 9
mPIRO-7 (GM10717-202) Chromosome 9
mPIRO-10 (GM10717-205) Chromosome 9
mPIRO-11 (GM10717-206) Chromosome 9
mPIRO-14 (GM10717-209) Chromosome 9
mPIRO-5 (GM10715-202) Chromosome 9
mPIRO-12 (GM10717-207) Chromosome 9
mPIRO-15 (GM10718) Chromosome 9
mPIRO-19 (GM10721) Chromosome 9
mPIRO-23 (GM11668-204) Chromosome 9
mPIRO-26 (GM10722) Chromosome 9
mPIRO-9 (GM10717-204) Chromosome 9
mPIRO-13 (GM10717-208) Chromosome 9
mPIRO-2 (GM10720) Chromosome 9
mPIRO-8 (GM10717-203) Chromosome 9
mPIRO-24 (GM17535) Chromosome 9
mPIRO-6 (GM10717-201) Chromosome 9
mPIRO-18 (GM10719-203) Chromosome 9
mPIRO-17 (GM10719-202) Chromosome 9
mPIRO-21 (GM11668-202) Chromosome 9
mPIRO-20 (GM11668-201) Chromosome 9
mPIRO-16 (GM10719-201) Chromosome 9
mPIRO-3 (GM21738) Chromosome 14
mPIRO-1 (GM10800) Chromosome 2
mPIRO-25 (GM10801) Chromosome 2
hPIRO
39,2
35 30 25 20 15 10 5 0
Amino Acid Substitution per 100 residues

B

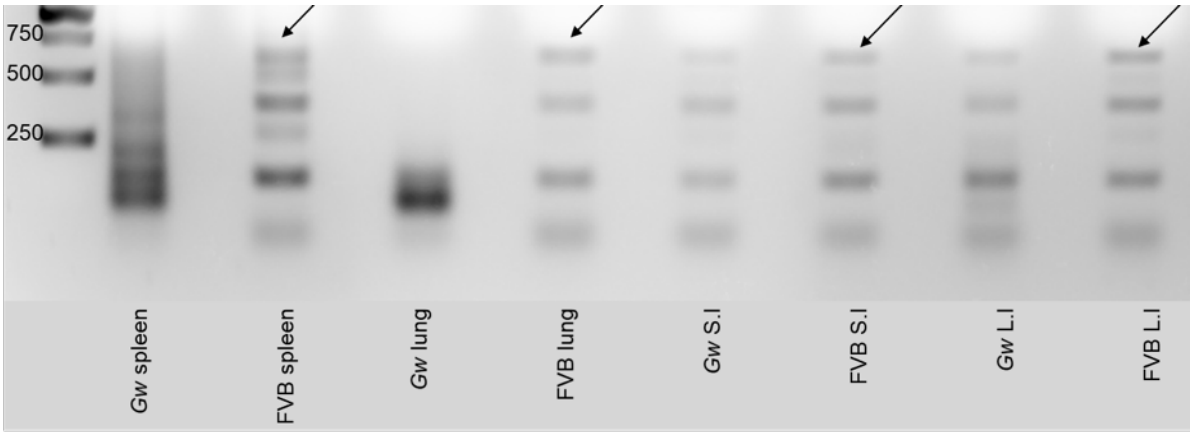
750
500
250
Gw spleen
FVB spleen
Gw lung
FVB lung
Gw S.I
FVB S.I
Gw L.I
FVB L.I

C

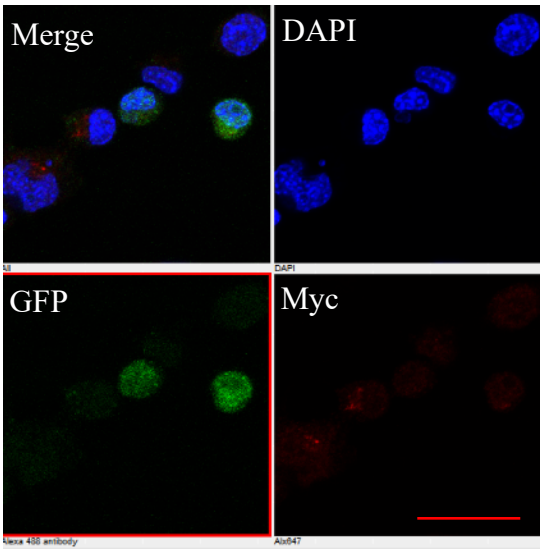

N2A

D

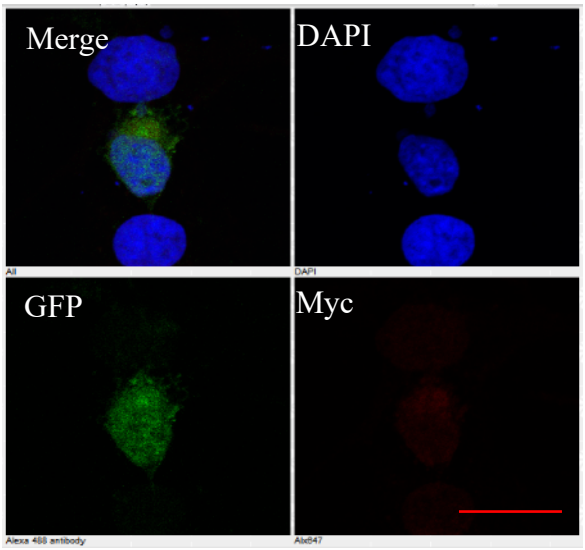

Cos7

3.2 The expression of the *Gm10800* gene ORF in N2A and Cos7 cells.

A Diagram of members of the PIRO protein superfamily, highlighting structural similarities between human and mouse versions of the protein, hPIRO and mPIRO, respectively. The diagram was adapted from an article by Kim et al. (Oh, Kim et al. 2015). **B.** An agarose gel representation of the 618bp ORF bands amplified from RNA extracts from *Gw* and FVB mice tissues including spleen, lung, small intestine (S.I) and large intestine (L.I). **C** and **D** IF images show the attempts to express the 618bp ORF of the *Gm10800* gene in N2A and Cos7 cells, respectively. DAPI was used as nucleic acid stain and GFP was co-transfected to identify successfully transfected cells. A 5' end *Myc*-tag expression vector was used in the presented images. Similar results were obtained using a 3' end *Myc*-tag expression vector, results are not shown here.

3.2.2 *Gm10800* knockout mouse

To evaluate the effect of the disruption of the *Gm10800* gene, by the insertion of the transgene, on the phenotype of *Gw* mice, a homozygous *Gm10800* KO mouse (*Gm10800*$^{KO/KO}$, on FVB/N background) was generated using CRISPR-Cas9 technology and was examined for the phenotype of *Gw* mice. Figure 3.3A shows the successful excision of the *Gm10800* gene (1.3kb guide to guide) from the gDNA of N2A cells, during *in vitro* validation of CRISPR guides. Sequences of successful guides are listed in Table 2.1. Genomic DNA of knockout mice was then sequenced using whole genome sequencing service to confirm the successful removal of the *Gm10800* gene. Interestingly, *Gm10800*$^{KO/KO}$ female mice showed neither the obesity nor the subfertility (reduced number of pups) phenotypes observed in *Gw* mice, Figure 3.3B and C respectively.

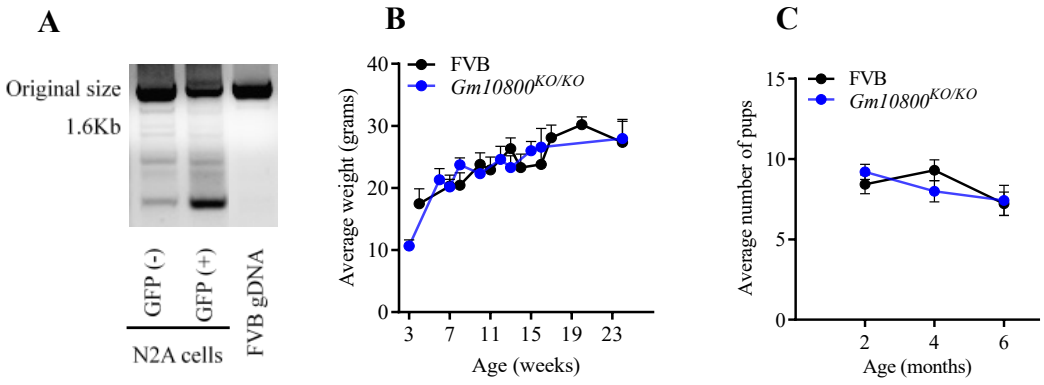

3.3 *Gm10800*$^{KO/KO}$ mice average weight and number of pups compared to FVB mice.

A An agarose gel photo represents the successful excision of a 1.3kb gDNA fragment from N2A cells to knockout the *Gm10800* gene, leaving a smaller fragment of 300bp between sequencing primers. N2A cells used for the *in vitro* validation of CRISPR guides were co-transfected with a GFP expressing vector alongside the CRISPR cassette expressing vector to enable a GFP guided cell sorting. **B** and **C** compare the average weight and number of pups of *Gm10800*$^{KO/KO}$ mice and FVB (background) mice, respectively.

3.3 Phenotypic characterization of *Gw* mouse model

3.3.1 Fertility and hormonal profile of *Gw* female mice

Gw female mice showed reduced numbers of pups when conceiving. A systematic characterization of the fertility of *Gw* female mice was, therefore, necessary alongside a comparison with FVB female mice. To normalize for the male factor during fertility assessment, previously confirmed fertile FVB males were used for all fertility experiments including, mating FVB males with *Gw* or FVB females, and IVF experiments using FVB sperms. FVB male mice were confirmed fertile by the successful impregnation of FVB female mice after natural mating. Multiple fertility parameters were assessed to delineate the extent of the fertility problem of *Gw* mice and to further understand its origin.

3.3.1.1 Estrous cycle anomalies in *Gw* mice and di-estrus arrest

In humans, oligo-ovulation and anovulation are prominent features of PCOS, and they occur secondary to disturbances in ovarian cycles attributed mainly to hypothalamic hormonal imbalances. These hormonal imbalances are also strongly reflected in the closely related uterine/menstrual cycles, generating various irregularities. PCOS patient suffers from oligo-/amenorrhea (Harris, Babic et al. 2018) in concomitance with oligo-/anovulation. Similarly, PCOS mice show reduced numbers of estrous cycles in response to their ovarian and hormonal cycles irregularities. *Gw* female mice were tested for their estrous cycle irregularities, particularly the reductions of the overall number of cycles in each period.

Different stages of the estrous cycle (Pro-estrous (P), Estrous (E), Met-estrous (M) and Di-estrous (D)) of a six-month-old subfertile *Gw* mouse are presented in Figure 3.4A. A sub-population of six-month-old *Gw* mice was subfertile compared to the rest of the

mice at the same age. Subfertile *Gw* mice showed a di-estrous phase of 5 days, from day 4 to day 8 (d4-d8), which is significantly prolonged compared to FVB mice's average di-estrous phase length of 2-3 days. The prolongation of the di-estrous phase in *Gw* mice as well as in other PCOS mouse models is known as di-estrous arrest (Kauffman, Thackray et al. 2015). Variable degrees of di-estrous phase prolongation/arrest were also observed in subpopulations of *Gw* mice at younger age points (2 and 4 months of age).

An example of estrous cycles follow-up tests for FVB mice versus *Gw* mice with regular cyclicity/ovulation and *Gw* mice with oligo-cyclicity/oligo-ovulation at the ages of 2, 4, and 6 months is presented in Figure 3.4B. With the di-estrous phase (D) highlighted in red and the estrous phase (E) in blue, the prolongation of the di-estrous phase and the relative shortening of the estrous phase can be easily visualized in the oligo-ovulatory *Gw* mice group. Five mice (n=5) were used in each group, mouse identification (ID) 1-5, and the overall number of cycles, over 16 days, were counted for each mouse at the end of each time point (2,4 and 6 months). Notably, the observed di-estrous prolongation (and the subsequent reduction in the number of cycles) were more evident with age. To identify the potential relation between the di-estrous phase prolongation and mouse weight, *Gw* mice were divided into obese (those with a weight above the average of that of same age FVB mice) and non-obese.

The overall number of cycles (in 16 days) for each mouse in each of the three groups (FVB, *Gw* non-obese and *Gw* obese) and the average of each group were presented in Figure 3.4C. The number of *Gw* mice with cycles below the average of FVB mice was increasing with age in each *Gw* mice sub-group. Interestingly, the difference between *Gw* mice cycles average compared to FVB average was higher among *Gw* obese mice (50%) compared to non-obese (35%) at 6 months of age with statistical significance. These findings suggest a progressive pathology in *Gw* mice with ageing and a direct

correlation to mouse weight. The fact that there were many non-obese *Gw* mice with their number of cycles below the FVB average strongly suggests that obesity is not the only cause of the di-estrous prolongation but rather an important aggravating factor. A direct correlation between the length of the di-estrous phase and the number of cycles (in 16 days) have been identified, Figure 3.4D. A detailed breakdown of the average time spent in various phases of the cycle is presented in Figure 3.4E with an obvious shortening of the estrous and pro-estrous phases of the cycle in concomitance with the prolongation of the di-estrous phase.

A

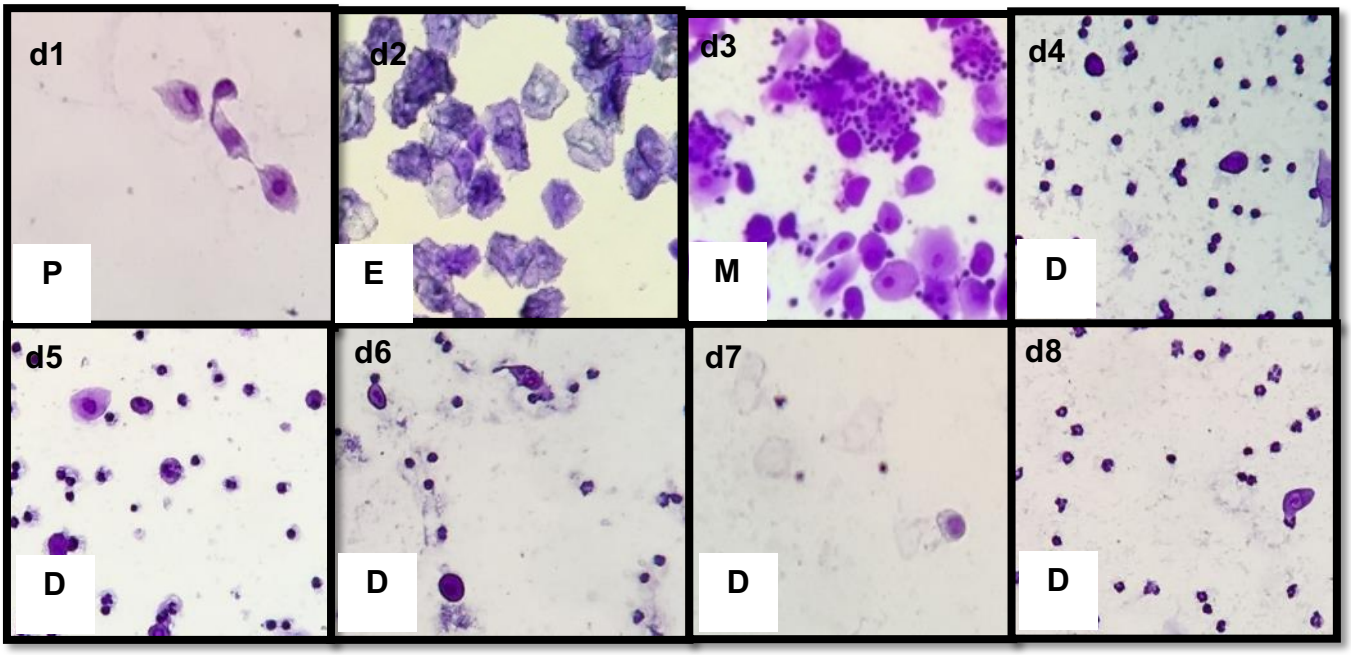

B

	FVB normal ovulation						***Gw* normal ovulation**						***Gw* oligo-ovulation**				
Mouse ID	1	2	3	4	5		1	2	3	4	5		1	2	3	4	5
Two months	M	M	D	D	E		M	D	D	E	E		M	D	P	D	D
	D	D	P	P	E		D	D	D	E	M		D	D	E	P	P
	D	P	E	E	E		D	D	P	E	D		D	D	M	E	P
	D	E	E	M	M		P	P	E	M	D		P	D	D	M	E
	P	E	E	D	D		E	P	M	D	P		E	D	D	D	E
	E	M	M	D	D		M	E	D	D	E		M	D	D	D	M
	E	D	P	D	E		D	D	D	P	M		D	D	D	D	D
	E	D	E	P	E		D	D	P	E	D		D	P	D	D	D
	M	E	E	E	M		P	P	E	M	D		P	E	D	D	P
	D	E	M	M	D		E	E	M	D	P		E	E	P	D	E
	D	M	D	D	D		M	M	D	D	E		E	M	E	P	E
	P	D	D	D	P		D	D	D	P	M		M	D	M	P	M
	E	D	P	P	E		D	D	P	E	D		D	D	D	M	D
	M	P	E	E	M		P	P	E	M	D		D	P	D	D	D
	D	E	M	E	D		E	E	M	D	P		D	E	P	D	D
	D	M	D	M	D		M	M	D	D	E		P	M	M	D	D
No. of cycles	2	3	3	3	3		3	3	3	3	3		2	2	2	1	2
Mouse ID	1	2	3	4	5		1	2	3	4	5		1	2	3	4	5
Four months	D	D	M	D	E		D	E	D	P	P		M	M	D	D	D
	D	P	D	D	M		D	M	P	E	E		M	D	D	D	P
	P	P	P	D	D		P	D	E	M	M		M	D	D	P	p
	E	E	E	P	D		E	D	M	D	D		D	P	P	P	M
	E	M	E	P	P		E	P	D	D	D		D	E	E	E	D
	E	D	E	E	E		E	E	D	P	P		D	M	M	M	D
	E	P	M	M	M		M	E	P	E	E		D	D	D	D	P
	M	P	D	D	D		D	E	E	M	M		P	D	D	D	E

	D	E	P	D	D		P	M	M	M	D		E	D	D	P	M
	P	M	E	E	P		E	D	D	M	D		D	D	P	E	D
	E	D	M	E	E		E	P	D	D	P		D	D	E	M	D
	M	D	M	M	E		M	P	P	D	E		P	D	M	M	P
	D	P	D	D	M		D	E	E	D	M		P	D	D	D	E
	D	E	D	P	D		D	M	M	D	D		E	D	D	D	M
	P	E	P	P	P		P	D	D	P	D		M	P	P	D	D
	E	M	E	E	E		E	D	D	E	P		D	E	P	P	D
No. of cycles	3	3	3	3	4		3	3	3	3	3		2	2	2	2	2
Mouse ID	1	2	3	4	5		1	2	3	4	5		1	2	3	4	5
Six months	E	E	D	E	D		P	P	D	E	P		D	D	M	M	D
	E	M	P	E	P		P	E	E	E	E		D	D	M	D	D
	E	D	E	E	E		E	M	E	M	E		D	D	D	D	P
	M	P	E	E	M		M	M	E	D	M		P	D	P	P	E
	D	E	E	M	D		D	D	E	D	M		E	D	E	E	M
	P	E	E	P	E		D	P	M	E	D		M	D	M	M	M
	E	E	M	P	M		P	M	D	E	P		M	M	M	M	M
	E	M	P	E	D		E	M	P	M	E		M	M	M	M	M
	M	D	E	M	P		M	D	E	M	E		D	D	M	M	M
	M	P	E	D	E		M	P	E	D	M		D	D	M	D	M
	D	E	M	D	E		D	E	D	P	D		E	P	D	D	D
	D	M	M	D	M		E	M	D	E	P		M	E	D	D	D
	P	D	M	P	D		E	D	P	E	E		D	E	D	D	D
	E	D	D	E	D		M	D	E	M	M		D	M	D	D	D
	E	P	P	E	P		D	P	M	M	M		D	M	P	D	D
	M	P	E	E	E		D	E	D	D	D		D	D	E	D	D
No. of Cycles	3	3	3	3	4		3	3	3	3	3		2	1	2	1	1

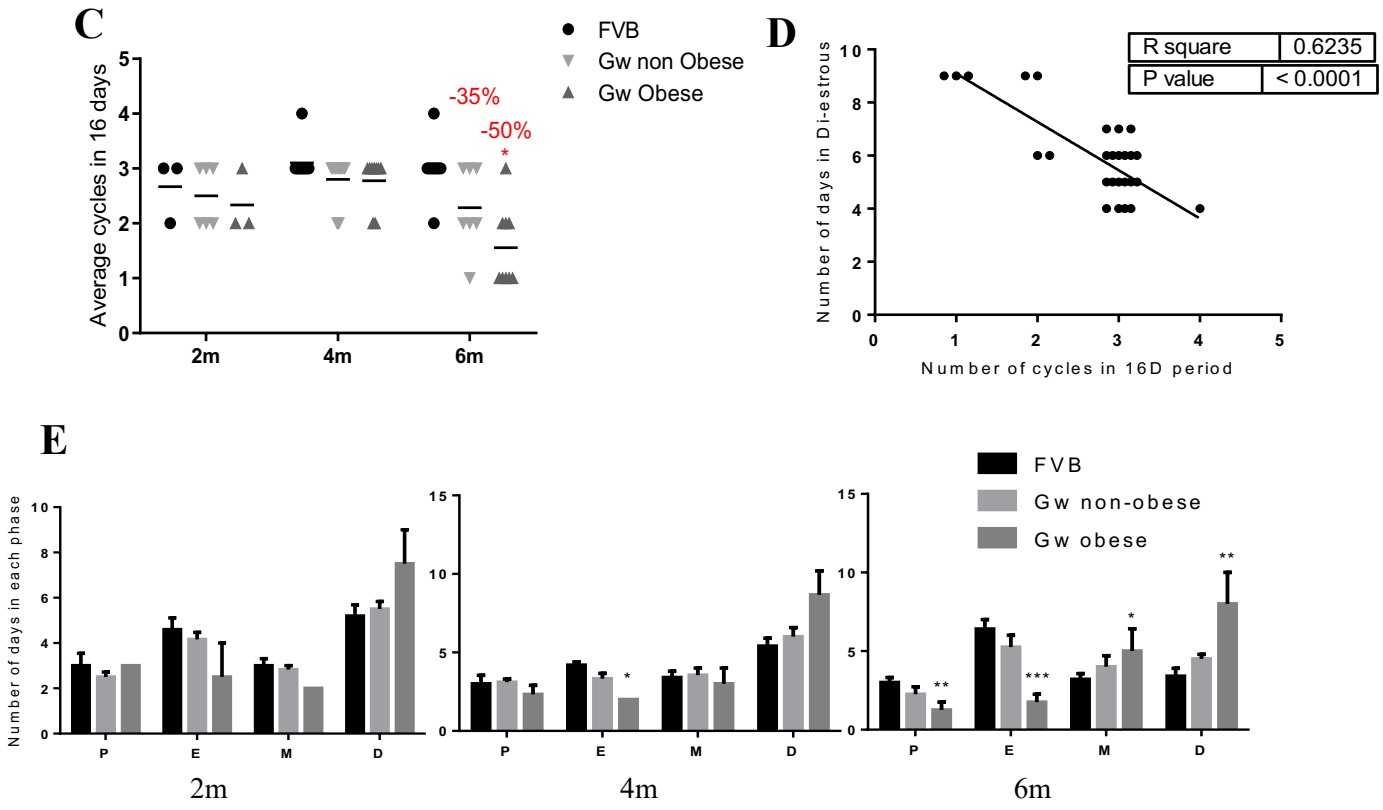

3.4 Estrous cycle features of *Gw* mice compared to FVB mice.

A Crystal violet-stained vaginal swabs of a six-month-old obese *Gw* mouse presenting different phases of a complete estrous cycle (Pro-estrous (P), Estrous (E), Met-estrous (M), and Di-estrous (D)), from day 1 to 8 (d1-d8). Phases of the estrous cycle were identified by the abundance of various cell types in vaginal lavage. **B** An estrous cycle follow-up sheet for FVB and *Gw* mice, with normal cycle/ovulation and *Gw* with oligo-cycles/ovulation. The di-estrous phase is highlighted in red and the estrous in blue to easily visualize the progressive prolongation of the di-estrous phase and shortening of the estrous with age and weight. **C** represents the number of cycles each mouse has in a period of 16 days (for FVB, *Gw* non-obese and *Gw* obese mice) at 2, 4, and 6 months of age. The graph also shows the average of each group as a horizontal line. **D** shows the inverse relationship between the number of days spent in the di-estrous phase of the cycle (Y-axis) and the overall number of cycles in 16 days (X-axis) identified by linear regression analysis, with an R^2 value of 0.62 and a p-value < 0.0001. **E** shows the average number of days each group of mice spent in each phase of the estrous cycle for 16 days. * p-value $\leqslant$ 0.05, ** p-value $\leqslant$ 0.01, *** p-value $\leqslant$ 0.001. Student t-test, two tails, was used for all statistical analyses.

3.3.1.2 A low number of pups, and oocytes anomalies, were observed in a sub-population of *Gw* mice.

Considering the direct relationship between uterine/vaginal cycles and ovarian cycles, anomalies of the latter were studied in the *Gw* mice to further characterize their fertility. The numbers of pups delivered by *Gw* female mice were counted and compared with the corresponding numbers of FVB mice, at 2, 3, 4, 5, and 6 months of age. Based on these numbers a subpopulation with significantly lower numbers of pups was identified among *Gw* mice (sub-fertile *Gw* mice), in both obese and non-obese mice. These numbers were plotted against different time points in Figure 3.5A, and the average of each group was presented as a horizontal line. The tendency of the average line of the sub-fertile group of *Gw* mice (in red) shows a progressive decline in their fertility with age and an increase in the overall number of sub-fertile mice with time. *Gw* mice were divided according to their weight into *Gw* obese (*Gw* O) and *Gw* non-obese (*Gw* NO), as detailed in section 3.3.2.1, to further highlight the effect of obesity on their fertility. The overall number of oocytes produced by each mouse following I.O was counted, and the average of each group was calculated. Fragmented and degenerated oocytes were identified based on previously established criteria (Swann 2014), and were counted as non-viable, Figure 3.5B (black and white arrows, respectively), the rest were counted as viable. The average number of oocytes produced by each group of mice was presented as a column with a black section representing abnormal oocytes (non-viable) in each group, at 4 and 6 months of age, Figure 3.5C. A significant reduction in the overall number of oocytes and increase in the percentage of non-viable oocytes were detected in *Gw* mice as early as 4 months of age. Interestingly these anomalies were more prominent among *Gw* obese mice compared to *Gw* non-obese and FVB mice, Figure 3.5C.

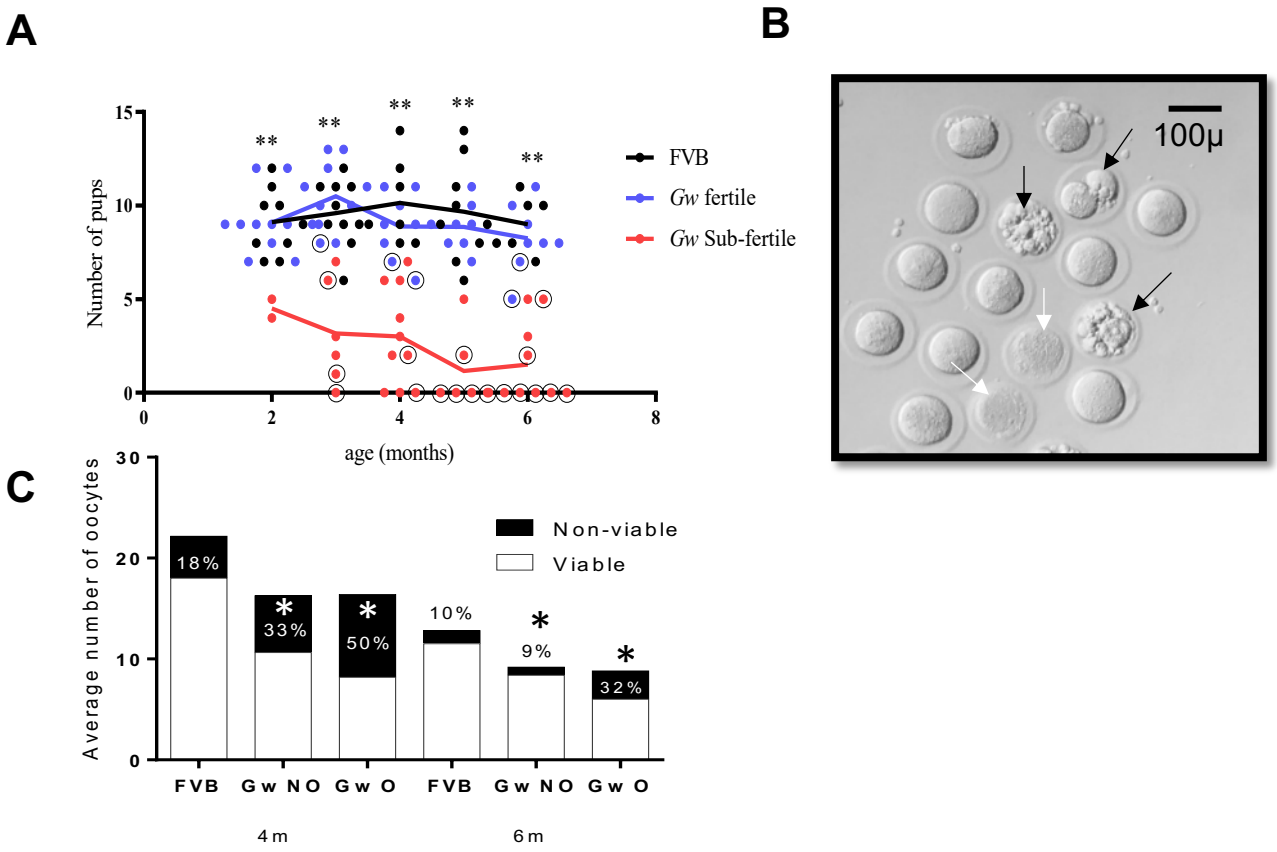

3.5 Number of pups and oocytes produced by *Gw* mice compared to FVB mice.

A Representation of the overall number of pups produced by each mouse in the three test groups (FVB (black), *Gw* fertile (blue), and *Gw* sub-fertile (red)) at 2, 3, 4, 5, and 6 months of age. Each dot represents one mouse, and the horizontal lines represent the average of each group through time. Mice encircled were obese mice. **B** Demonstrates the products of IO of a 6-months-old *Gw* obese mouse examined under a Leica microscope (20X objective) to highlight the morphology of fragmented (black arrows) and degenerated (white arrows) oocytes, scale bar is 100µm. The rest of the oocytes in the photo are of normal morphology. **C** Each column plots the average number of oocytes produced by each of the three test groups (FVB, *Gw* non-obese (*Gw* NO), and *Gw* obese (*Gw* O) mice) following IO, at 4 and 6 months of age, (n=10 in each group). The black part of each column is the average number of non-viable oocytes in each group (with the percentage written inside, or just above), while the white part represents viable oocytes. An asterisk inside the black part of a column indicates a statistically significant difference in the number of oocytes in that part compared to the corresponding part in the FVB group (at the same age point). As asterisk above a column compare the whole group of mice to corresponding FVB mice at the same age point. * p-value $\leqslant$ 0.05, ** p-value $\leqslant$ 0.01. Student t-test, two tails, was used for all statistical analyses.

3.3.1.3 Multiple cyst formation and PCOM in *Gw* ovaries

Cyst formation in the ovaries is a common feature of PCOS. Ovarian cysts in PCOS develop secondary to hormonal imbalances (Rosenfield and Ehrmann 2016). High GnRH levels and pulse frequencies favor the production of LH over FSH, which, in turn, leads to developmental defects in ovarian follicles. In the presence of low FSH levels, growing follicles cannot attain maturity, and those who rarely succeed, cannot achieve ovulation, due to persistently high LH levels and the absence of its natural surge (Rosenfield and Ehrmann 2016). Arrested follicles at different stages of growth gradually degrade, starting with the death of their oocytes followed by the absorption of their follicular cells. This transformation generates empty cysts, hence the PCOM (Qiao and Feng 2010). Histological sections of *Gw* mice ovaries at an age as early as two months old showed abnormal cyst formation both in obese and non-obese mice compared to FVB mice ovaries, Figure 3.6A, B, and C (FVB, *Gw* non-obese, and *Gw* obese respectively). Arrows point towards growing follicles while arrowheads point at cysts. As mice got older, the phenotype was accentuated with further reduction in the numbers of growing follicles and increased numbers of cysts, Figure 3.6D-I. Detailed quantification of different types of growing follicles, cysts, and CL, is shown in Figure 3.6J (n=5 mice in each test group). The significant increase in cyst formation was associated with a substantial reduction in the numbers of CL and a relative reduction in the number of growing follicles (including large antral follicles) in *Gw* mice (obese and non-obese) compared to FVB mice at all time points, Figure 3.6J. Fewer oocytes were able to reach maturity and further ovulate forming CL from the remainder of the follicle. Interestingly, *Gw* mice ovaries had significantly higher numbers of atretic follicles compared to FVB mice ovaries, as shown in the same Figure. The identification of various stages of growing follicles, CL, and cysts was based on their morphology as previously described (Myers, Britt et al. 2004, Caldwell, Middleton et al. 2014). Additional photo in Appendix A, Fig. 5.3.

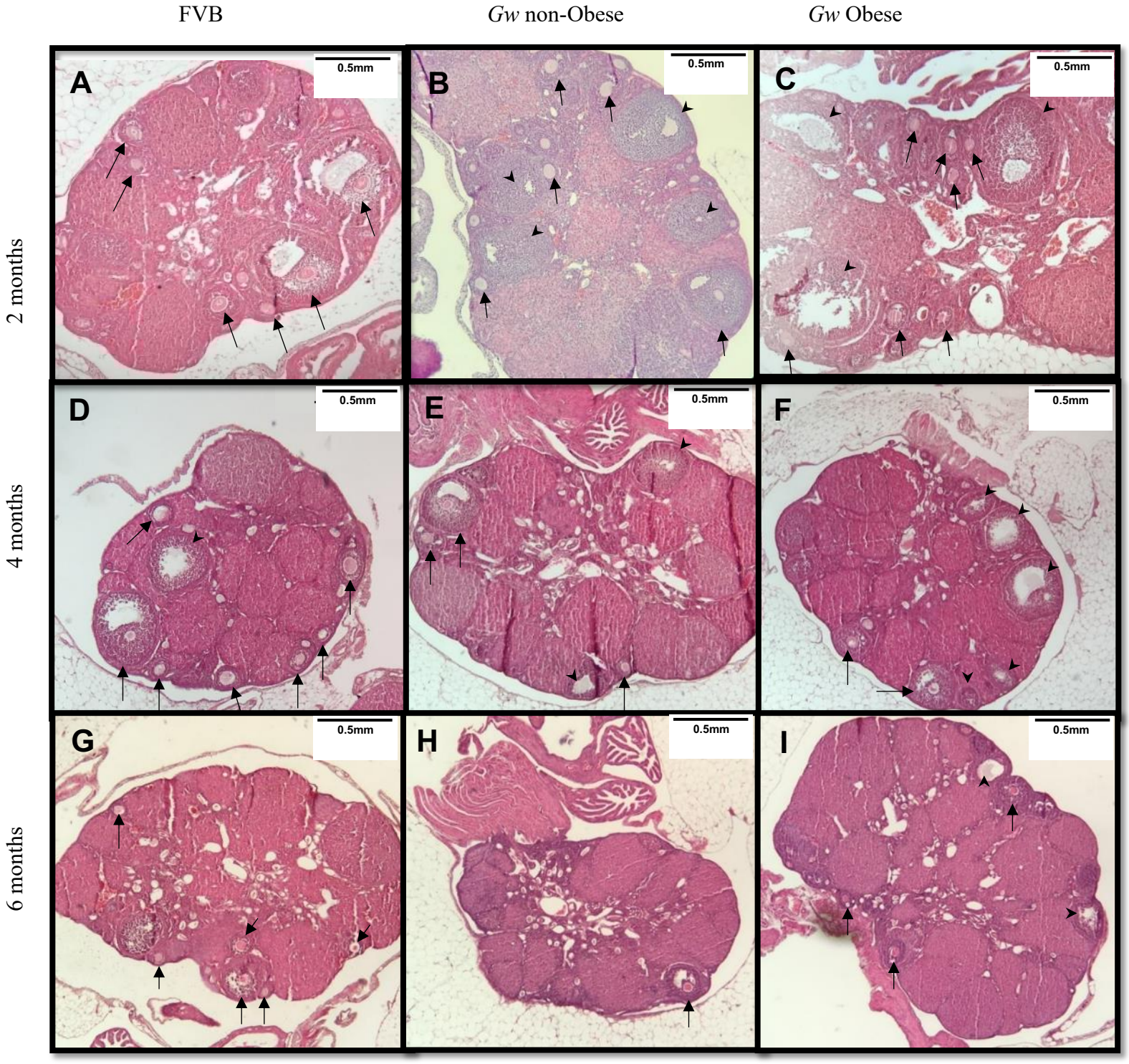
FVB
Gw non-Obese
Gw Obese
2 months
4 months
6 months
A
B
C
D
E
F
G
H
I
0.5mm

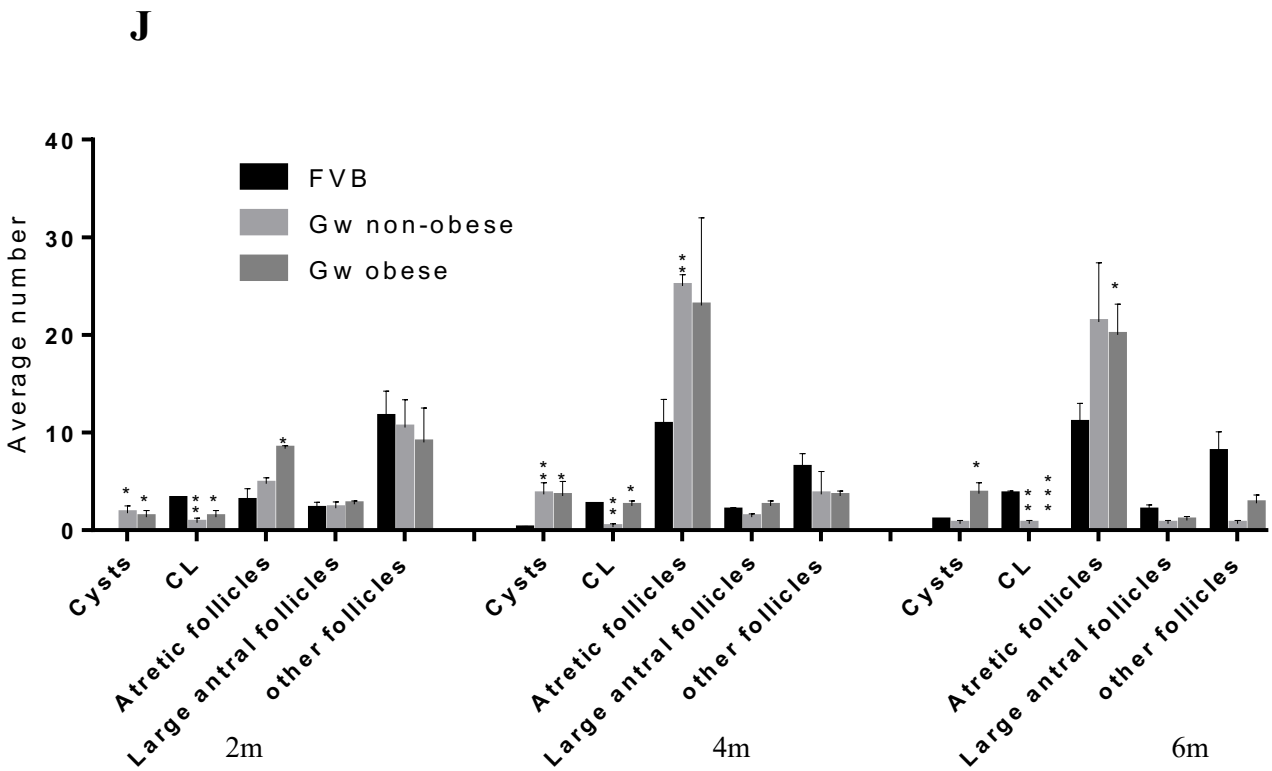

3.6 PCOM in *Gw* mice.

A-I Hematoxylin and eosin-stained histological sections of ovaries from 2-, 4- and 6-months-old FVB, *Gw* obese, and *Gw* non-obese mice, scale bar is 0.5 mm. Arrows indicate growing follicles, and arrowheads point out cysts. Representative pictures of n=5 mice in each group. **J** A representation of the average number of cysts, CL, atretic follicles, large antral follicles, and other follicles, in each group of mice at various time points (2, 4 and 6 months). Histological sections were examined using a Leica microscope with a 10X objective. The asterisk above each column represents a statistically significant difference of the marked column compared to the corresponding FVB group at the same time point. * p-value $\leqslant$ 0.05, ** p-value $\leqslant$ 0.01, *** p-value $\leqslant$ 0.001. Student t-test, two tails, was used for all statistical analyses.

3.3.1.4 Hormonal profile of female *Gw* mice compared to female FVB mice

In either PCOS patients or mouse models of PCOS, high T hormone levels cause follicular atresia and participate in follicular growth arrest, and subsequently reduce fertility (Rosenfield and Ehrmann 2016). On the other hand, persistently elevated LH levels is the main cause for anovulation and antral follicle degradation (Rosenfield and Ehrmann 2016). High LH level secondary to high GnRH pulse frequency is associated with a low FSH level (high LH/FSH ratio), causing follicular growth arrest in PCOS (Chaudhari, Dawalbhakta et al. 2018). The large cohort of growing follicles in PCOS patients and mouse models generates high plasma levels of E2 (produced by granulosa cells) prompting the hypothalamus to switch GnRH pulse frequency from low to high, to start ovulation. Plasma levels of E2, LH, and T hormone were measured in *Gw* mice to identify any irregularities in their hormonal profile. Furthermore, plasma levels of AMH were also tested in *Gw* mice for their potential to be used as a diagnostic test for PCOS, (Bani Mohammad and Majdi Seghinsara , Sahmay, Aydin et al. 2014). Tail plasma samples were collected from mice (FVB, *Gw* obese and *Gw* non-obese) at various time points (2-, 4-, and 6-months of age) at the Met-estrous phase of their estrous cycle.

For each of the three tested hormones (LH, T, and E2), a subgroup of *Gw* mice (obese and non-obese), had higher plasma levels compared to the highest value of the corresponding hormone in FVB mice, highlighted in red, Figure 3.7A, B and C**,** respectively. Interestingly a significant number of *Gw* mice had high E2, LH, and T levels simultaneously. AMH levels, on the other hand, were not higher in *Gw* mice compared to FVB mice, though they were lower in obese and aged mice, Figure 3.7D.

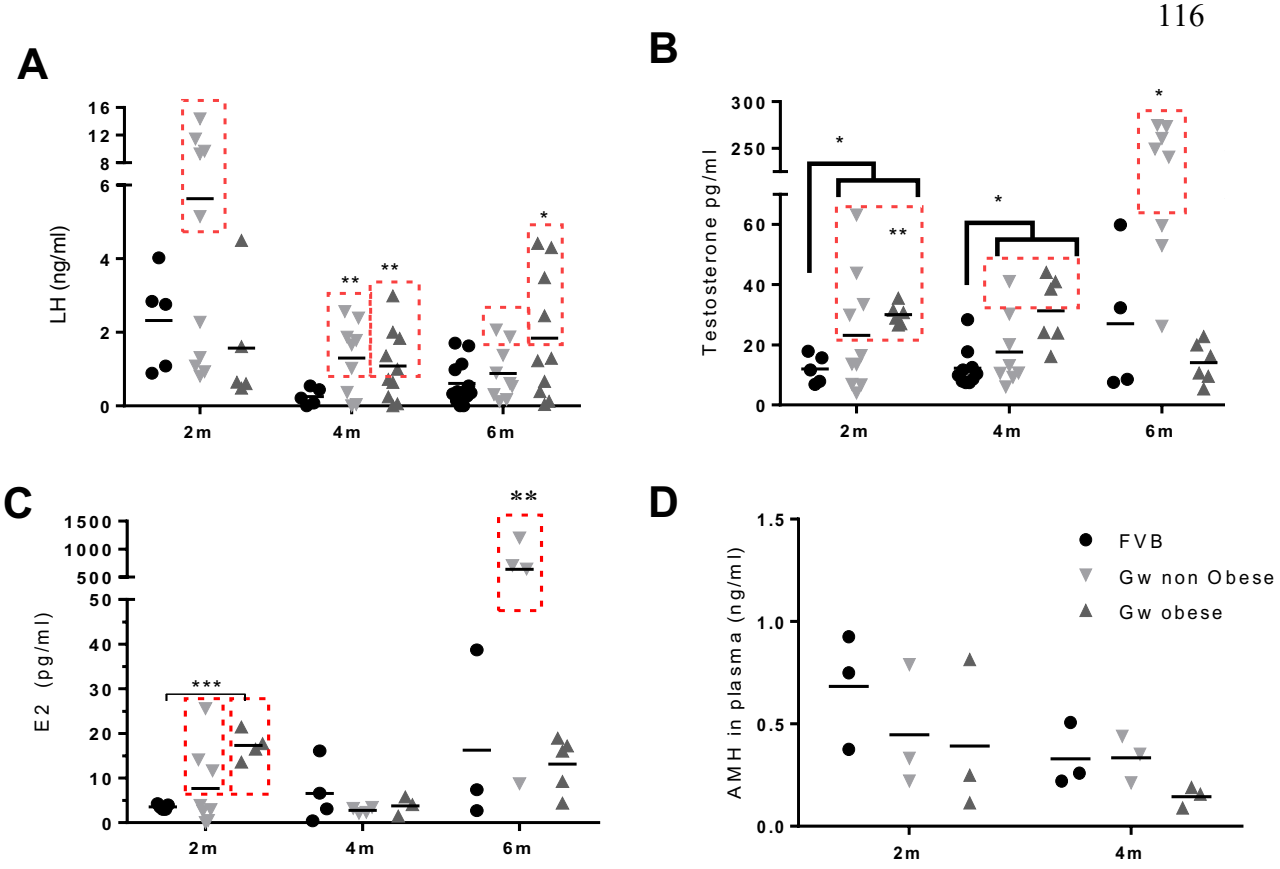

3.7 Hormonal profile of *Gw* female mice.

ELISA technique was used to measure different hormone levels (**LH (A), T (B), E2 (C), and AMH (D)**) from previously preserved frozen (at -80°C) plasma samples collected by a distal tail cut at the met-estrous phase of each mouse estrous cycle. All mice used for hormonal profile tests were virgin and did not participate in other experiments, except for the weigh follow-up to classify them into obese and non-obese, and estrous cycles follow-up to identify the met-estrous phase where blood was collected. Mice in the red dashed rectangles had hormone level values above the highest value of the corresponding hormone level of FVB mice. A horizontal line inside each group presents the average of the hormone level values in each group. An asterisk above a group indicates the statistical significance of the marked group compared to the corresponding FVB group at the same time point. Grouped data, with black brackets, were compared as one set of data against the corresponding FVB in panels **B** (2 and 4 months) and **C** (2 months). * p-value $\leqslant$ 0.05, ** p-value $\leqslant$ 0.01, *** p-value $\leqslant$ 0.001. Student t-test, two tails, was used for all statistical analyses.

3.3.2 Metabolic profile of *Gw* female mice

Gw mice showed signs of metabolic anomalies manifested as various degrees of being overweight and obesity. Obesity, impaired glucose and insulin tolerance, and insulin resistance were all tested in *Gw* mice, as they are common metabolic features of PCOS.

3.3.2.1 Obesity and food consumption anomalies in *Gw* mice

Gw and FVB female mice weight charts were generated starting from the age of 3 weeks and till the age of 29 weeks. A significant proportion of *Gw* female mice (~ 50%) gained significantly more weight than the average of the rest of the mice at the age of 17 weeks (20% extra weight), and became overweight, according to the human overweight and obesity classification (Division of Nutrition 2017). *Gw* overweight mice continued to gain extra weight at rates higher than those of FVB and *Gw* non-obese mice as they grew older (35% extra weight at 25 weeks of age) and were, therefore, considered obese mice (Division of Nutrition 2017). Figure 3.8A represents weight averages of FVB, *Gw* non-obese and *Gw* obese, female mice (n=10 in each group) from the age of 3 to 29 weeks. These weight anomalies were not detected among *Gw* male mice at any time point compared to FVB male mice, Figure 3.8B. The food consumption of the three test groups was then evaluated to identify the origin of the excessive weight gain. High food consumption levels were evident among all *Gw* mice, with the obese mice levels reaching statistical significance when compared to FVB mice, Figure 3.8C. Leptin hormone has a crucial role in regulating satiety, food consumption, and obesity, therefore, leptin hormone levels were measured next in the three test groups (Hill, Elias et al. 2010, Chakrabarti 2013). Leptin hormone levels tended to be higher among *Gw* non-obese and obese mice, compared to FVB mice, without reaching statistical significance Figure 3.8D. Interestingly, *Gw* mice with the highest rates of food consumption in Figure 3.8C, were the ones with the highest weight gain and the highest levels of Leptin hormone among tested mice in Figure 3.8D.

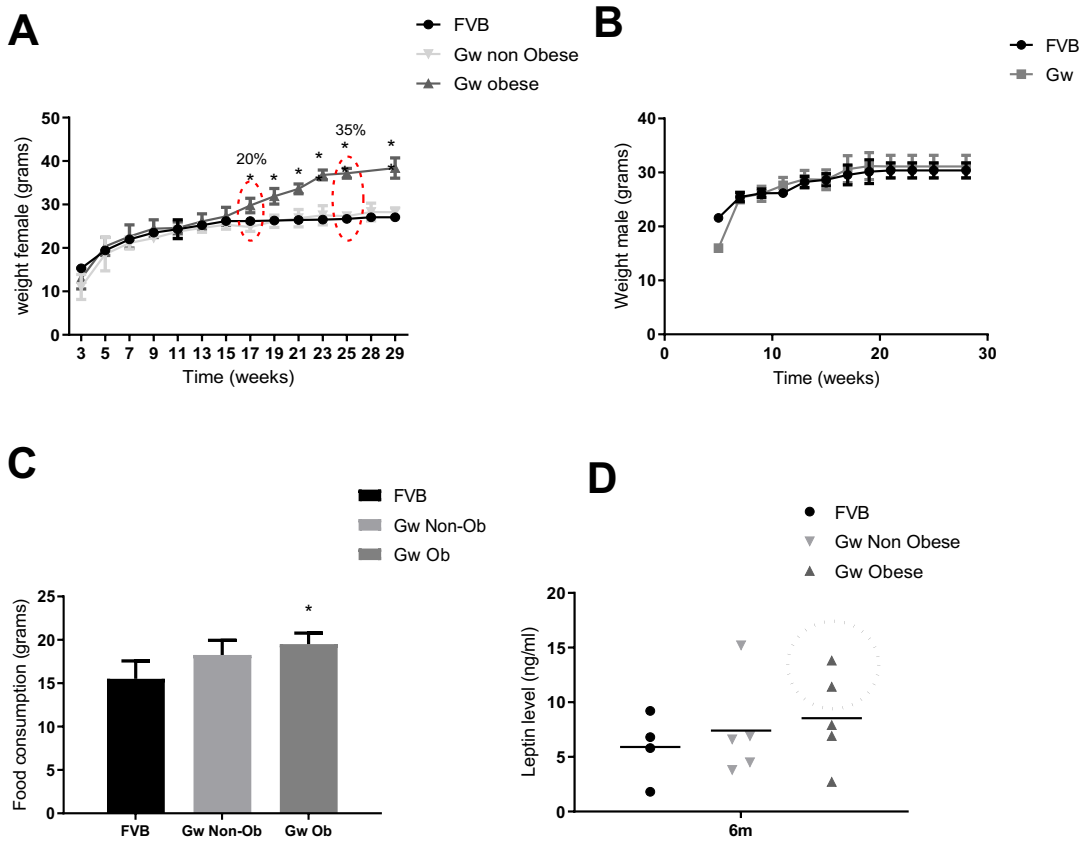

3.8 Obesity and food consumption anomalies among *Gw* female mice.

Female and male FVB and *Gw* mice weights were measured every two weeks starting from the age of 3 weeks until 29 weeks. The averages of weights of each group of mice, at each time point, are presented in panels **A** and **B** (females and males, respectively). The 1st red dotted oval shape at the age of 17 weeks (**A**) marks the onset of a statistically significant weight difference between *Gw* obese mice and *Gw* non-obese and FVB mice with 20% extra weight gain, while the 2nd at the age of 25w, marks stage II obesity, with 35% excess weight gain. **C** is a representation of the average food consumption of each mouse in the three test groups (n=12 per group) per 4 days period over 1 month. **D** represents Leptin hormone levels (collected by tail blood sampling and measured using an ELISA kit) of 6 hours fasting mice from the three test groups, with the average presented as a horizontal line. Mice encircled have Leptin hormone values above the highest value of FVB mice. * Indicates a p-value $\leqslant 0.05$, ** indicates p-value $\leqslant 0.01$. The student t-test, two tails, was used for all statistical analyses.

In obese PCOS patients, extra weight gain is mainly centered in the abdomen (male pattern obesity), (Hirshfeld-Cytron, Barnes et al. 2009, Rosenfield and Ehrmann 2016). *Gw* mice (obese and non-obese) were dissected, and fat depots weights and adipocytes sizes were compared to those of dissected FVB mice to study their fat accumulation patterns, (n=5 in each group). *Gw* obese mice gained a significant part of their weight in the parametrial and the para-ovarian fat depots, while other fat depots did not show a noticeable increase in their weight or size, including mesenteric, peri-hepatic, peri-renal, pericardial, and sub-cutaneous ones.

Representative photos of six-month-old mice, from the three test groups, were shown in Figure 3.9A to demonstrate the significant differences in parametrial (black arrows) fat depots sizes among *Gw* obese, *Gw* non-obese and FVB mice. On the other hand, mesenteric fat depots (white dashed arrows) were not showing noticeable differences in size between the three mice. Para-ovarian fat depots were not visible in these photos. The weight averages of parametrial fat depots for the three test groups (n=5 mice in each group) are presented in Figure 3.9B. The figure shows a significantly higher, parametrial fat depots weight average, in *Gw* obese mice compared to *Gw* non-obese and FVB mice**.**

Histologically both parametrial and para-ovarian fat depots, from *Gw* obese and *Gw* non-obese mice, had larger adipocytes in comparison with FVB mice, Fig. 3.9C. The average surface area of adipocytes, from both fat depots, of *Gw* obese and *Gw* non-obese mice, shows again that *Gw* mice had significantly larger adipocytes than FVB mice in both fat depots, Fig. 3.9D.

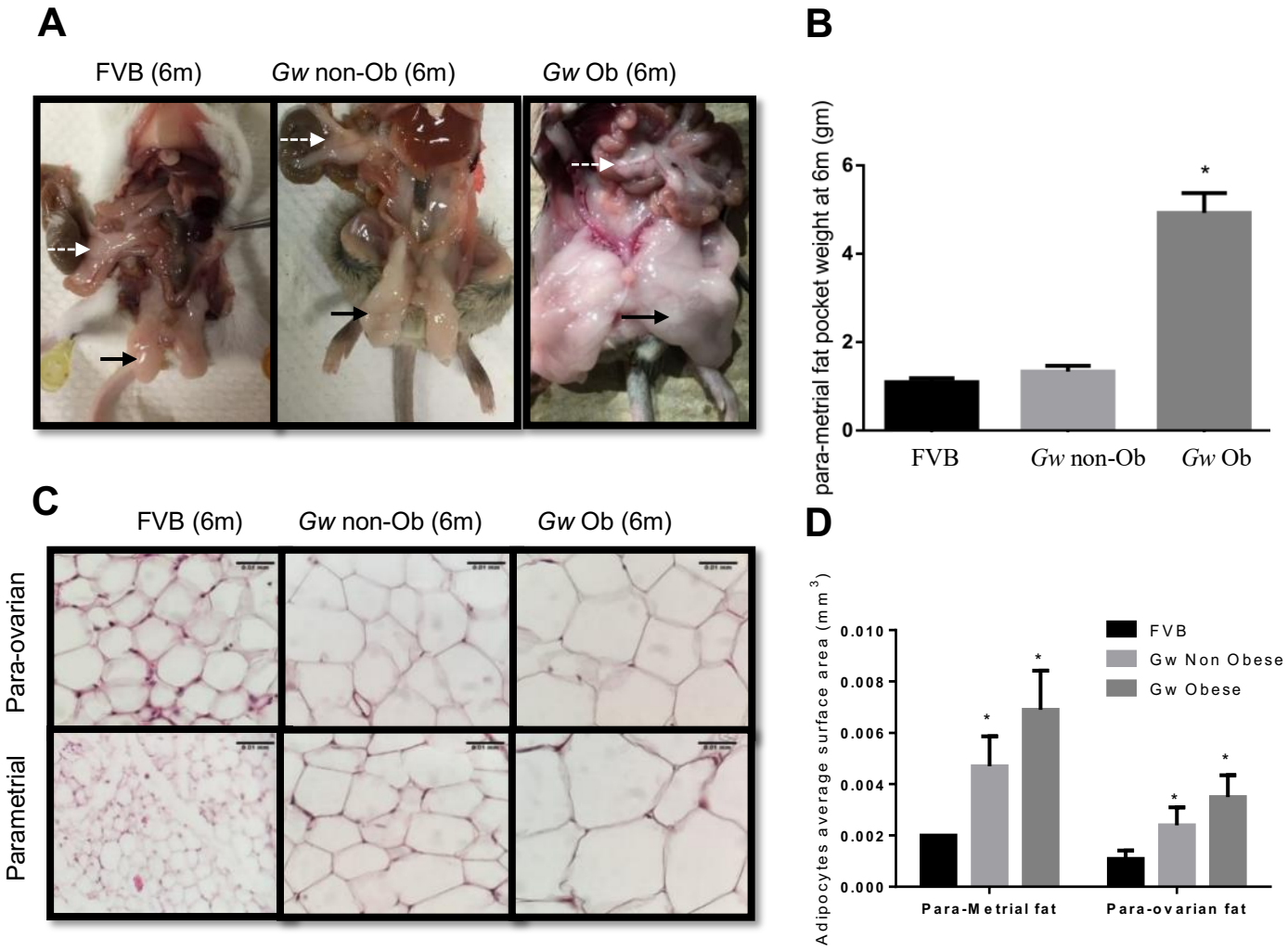

3.9 Fat distribution in *Gw* obese and non-obese mice in comparison with FVB mice.

A Representative photographs of three dissected 6-months-old mice, one from each of the test groups, showing the different sizes of parametrial (black arrows) and mesenteric (white dashed arrows) fat depots. Weights averages of parametrial fat depots from five mice in each group are presented in panel **B**. Hematoxylin and eosin-stained histological sections of parametrial and para-ovarian fat depots were used to demonstrate differences in adipocytes sizes among the three test groups, **C,** (scale bar is 0.01mm). The averages of the surface area of 100 adipocytes, from 5 mice in each group, are presented in **D**. * indicates p-value ≤ 0.05, ** indicates p-value ≤ 0.01. The student t-test, two tails, was used for all statistical analyses.

3.3.2.2 Ovarian pathologies in *Gw* obese mice

Considering the significant increase in the size of para-ovarian and parametrial fat depots observed in *Gw* obese mice, plus the well-established lipotoxic effect of excessive FFAs on tissues, ovaries from the three groups of mice were further analyzed for fat infiltration. *Gw* obese mice had a prominent peri-follicular fat infiltration in their ovaries compared to *Gw* non-obese and FVB mice. Figure 3.10 shows representative photos of oil red-stained, histological sections of ovaries from 6-months-old mice from the three test groups. The upper panels of the figure (4X) show whole ovaries with fat deposits (in red) predominantly existing around growing follicles. The lower panels of the figure (10X) are a 2.5X magnification of peri-follicular areas highlighted in black boxes in corresponding upper panels. *Gw* obese mice had larger amount of peri-follicular fat deposition compared to *Gw* non-obese and FVB mice. These deposits have a direct lipotoxic effect on growing follicles, affecting their maturation and their overall viability, as previously discussed in the introduction. Excessive FFAs and fat deposition induce pathological changes to surrounding tissues by increasing ER stress levels and reducing mitochondrial DNA copy numbers in involved cells (Wu, Russell et al. 2015). Further photos of oil-red stained histology sections of ovaries, from the three test groups, are shown in appendix A, Fig. 5.4.

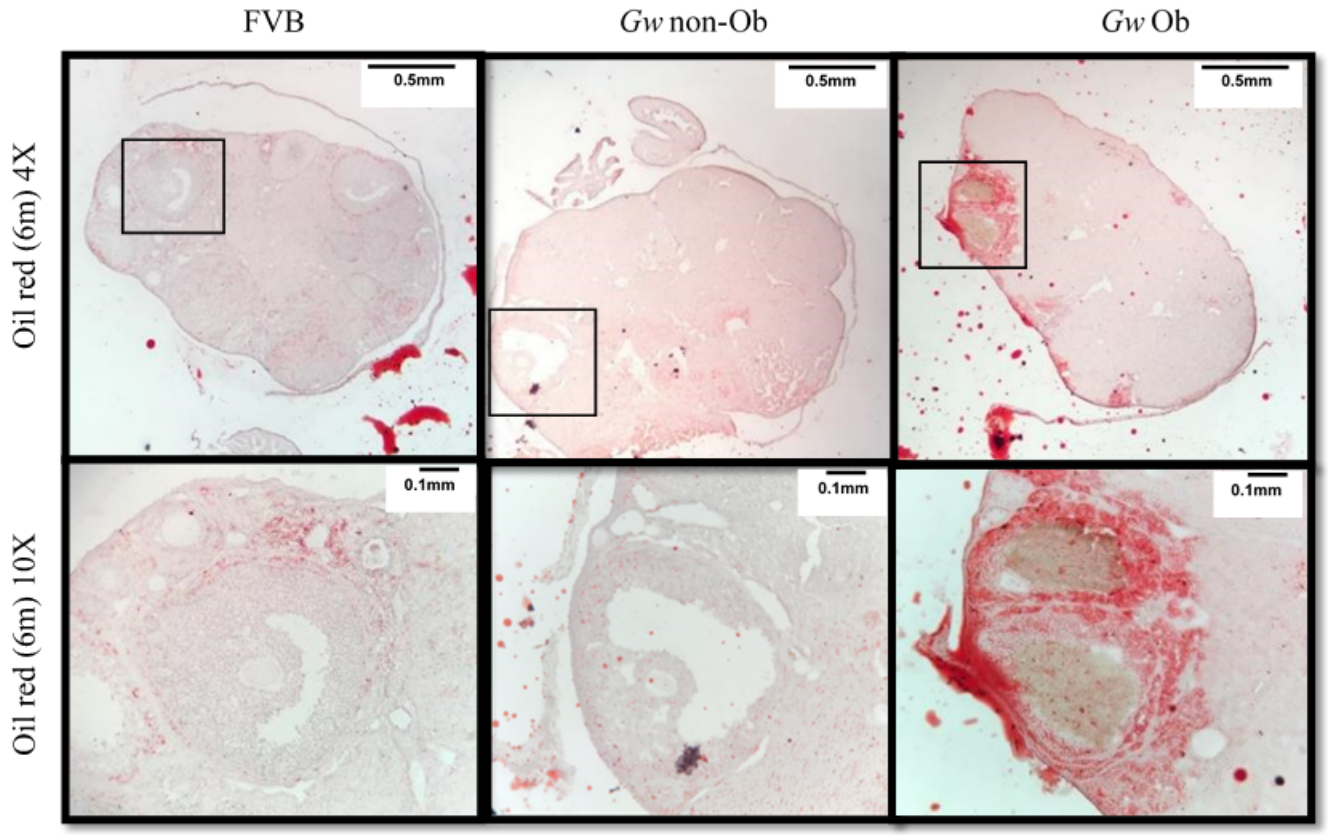

3.10 Fat accumulates in the ovaries of *Gw* and FVB mice.

The upper panels of the figure show representative photos of oil red-stained, histology sections of ovaries, from 6-months-old mice from each of the three test groups, examined under a Leica microscope using the 4X objective (scale bar is 0.5mm). The lower panels are a 2.5X magnification of the black-boxed area in each of the photos of the upper panel, surrounding a growing follicle. A 10X objective was used (scale bar is 0.1mm).

3.3.2.3 Impaired glucose tolerance in *Gw* mice

Impaired glucose tolerance is an early metabolic anomaly that predicts the likelihood of diabetes (Shaw, Zimmet et al. 1999). The capacity of the body to regulate glucose loads depends mainly on the ability of beta cells of the pancreas to produce enough insulin to allow various cells to process glucose. High blood sugar levels have toxic effects on various organs, including the heart, liver, eyes, nervous system, kidneys, and growing embryos (Scott-Drechsel, Rugonyi et al. 2013, Daryabor, Atashzar et al. 2020).

Six-hour fasting blood sugar (FBS) levels were measured for mice (n=5) from each of the three test groups, before being injected with 10% glucose solution (intraperitoneally (IP)) 1.0 mg/g of body weight. Blood sugar levels were measured again following the injection at 30 minutes, 1 and 2 hours. The averages of FBS and post glucose injection values (at each time point) for each of the three test groups, at four months and six months of age, are presented in Figure 3.11A and Figure 3.11B**,** respectively. Blood samples were collected from end tail cuts at each point according to standard protocol in mice.

Gw obese mice had relatively higher blood glucose values compared to *Gw* non-obese and FVB mice at almost all time points (30 minutes, 1 and 2 hours) at 6-month of age. These high blood glucose levels (of *Gw* obese mice) reached statistical significance among the 6-month-old mice at all time points except the fasting time point. The areas under the curve for the three test groups, at 6-months of age, were presented in Figure 3.11C. At 4-month of age there were not many differences noted among all three test groups.

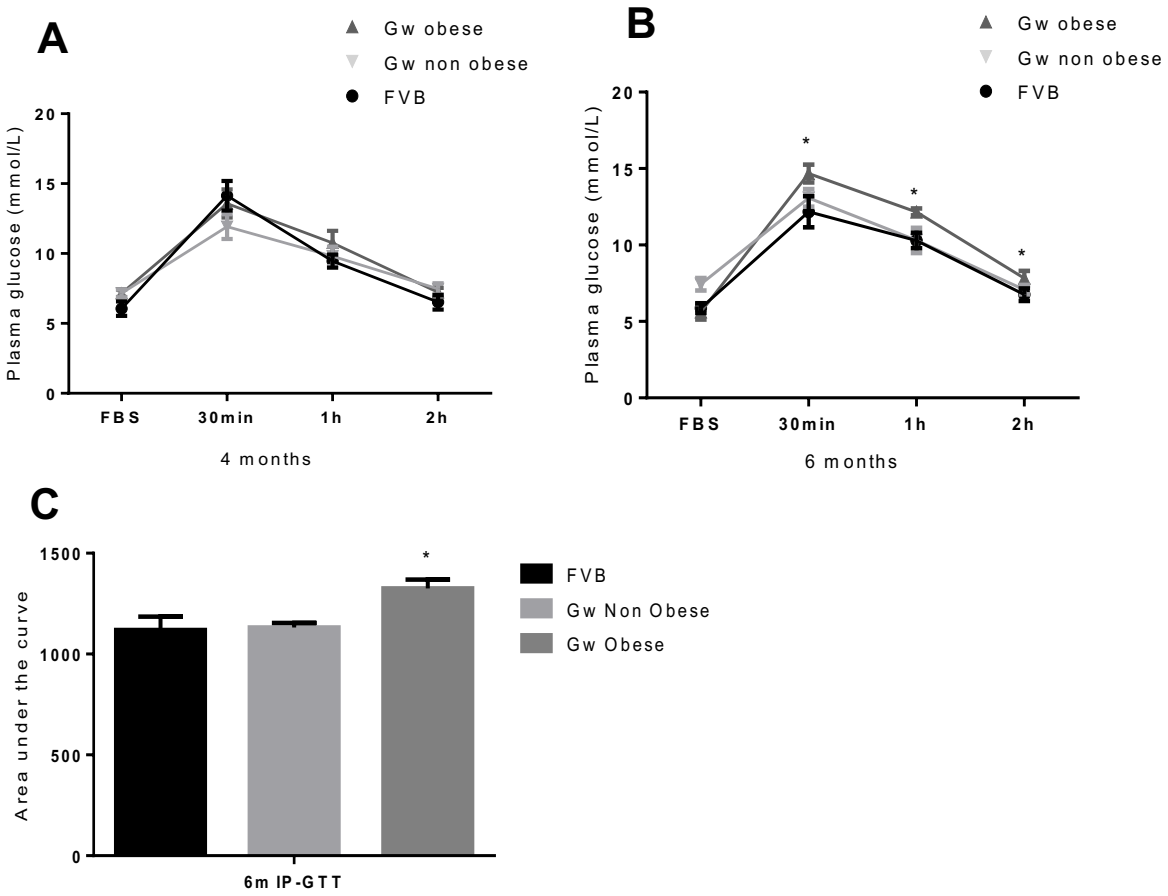

3.11 Glucose tolerance (GTT) in *Gw* and FVB female mice.

Five mice were used in each test group, at each time point (Fasting (FBS), 30 minutes, 1 and 2 hours), and age point (four- and six-month-old). Mice were kept fasted for 6 hours and tail blood samples were collected to measure fasting blood sugar levels (FBS) using an Accu-Chek machine. A loading dose of 1.0 mg/g of body weight of 10% glucose solution was then injected intraperitoneally (IP) and blood glucose levels were measured again at 30 minutes, 1 and 2 hours after the IP. Averages of measured blood sugar values (in mmol/L) at various time points for the 4- and 6-months-old mice groups were plotted in panels **A**, and **B** respectively. Areas under the curve for each of the 6-months-old test groups were presented in **C**. * indicates p-value $\leqslant$ 0.05, ** indicates p-value $\leqslant$ 0.01. The student t-test, two tails, was used for all statistical analyses.

3.3.2.4 Impaired insulin tolerance and hyperinsulinemia among *Gw* mice

The response of *Gw* mice to insulin was assessed next to understand the origin of their impaired glucose tolerance and to further complement their metabolic profile. Patients suffering from PCOS are known to have high plasma insulin levels and insulin resistance, irrespective of their weight (Dunaif, Segal et al. 1989). Both are known to play key roles in the development of PCOS pathology (Nestler 1997, Cree-Green, Rahat et al. 2017).

Mice were tested at the 6-month-old age point because obesity and impaired glucose tolerance are prominent at this age. FBS (4h) was measured for at least 5 mice in each of the three test groups, followed by IP injection of insulin (0.5 mU/g of body weight), and measurement of blood sugar was repeated at 30 minutes, 1 and 2 hours post IP insulin load. Mice were kept fasting for 4 hours only during the insulin tolerance test to avoid the development of severe hypoglycemia following the IP injection of insulin.

The average blood glucose values were blotted, in mmol/L, for the three test groups against each time point in Figure 3.12A. Interestingly, despite insulin load, *Gw* obese mice were still not able to reduce their blood sugar levels and maintained statistically significant higher levels of blood glucose compared to *Gw* non-obese and FVB mice, at all time-points, Fig 3.12A. The areas under the curves, of blood glucose values, for each group, are presented in Figure 3.12B. Insulin levels were then measured for mice from the three test groups after fasting for 6 hours (4- and 6-month-old) and values were presented in Figure 3.12C, with the average of each group presented as a horizontal line. Interestingly, most of *Gw* obese and non-obese mice had higher fasting insulin levels (and group averages) compared to corresponding FVB mice, at both time points, red rectangles in Fig. 3.12C.

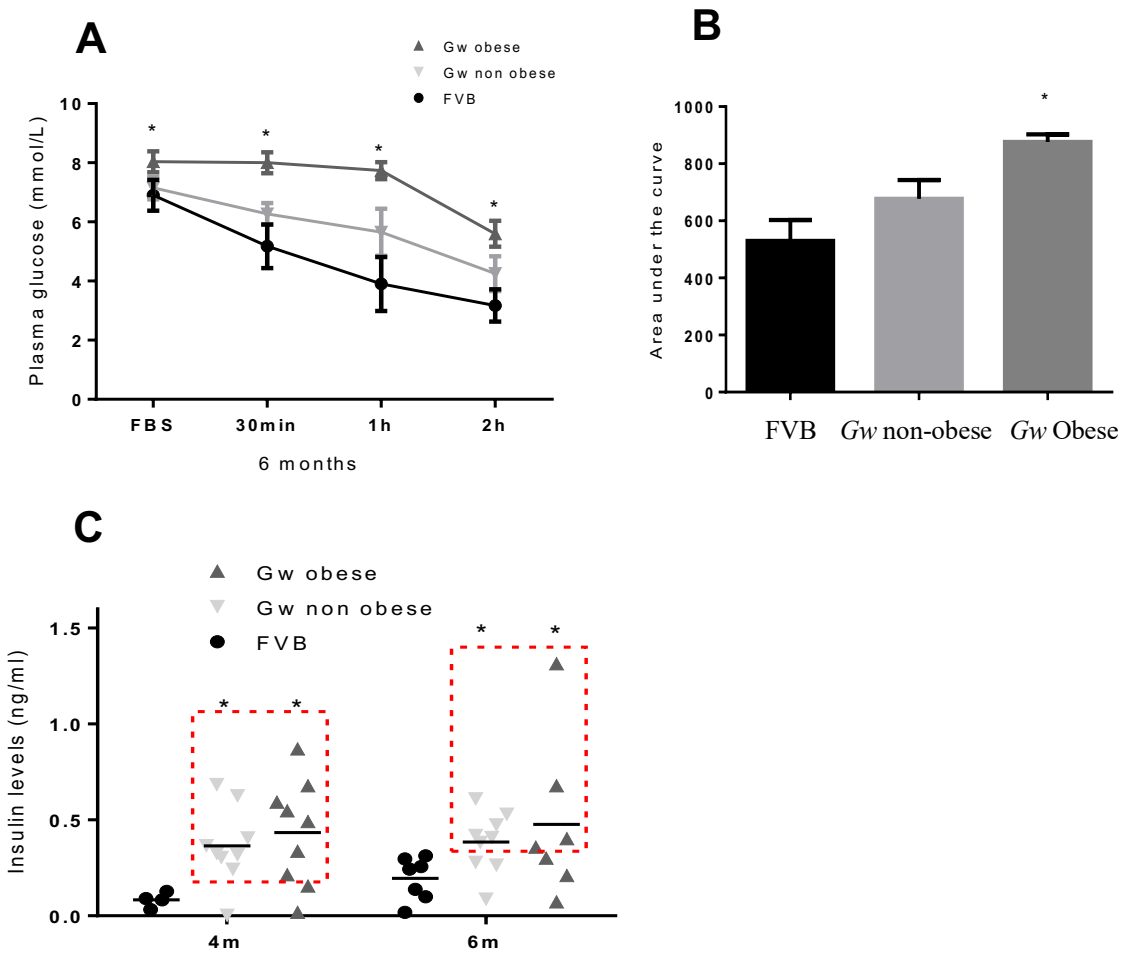

3.12 Impaired insulin tolerance in *Gw* female mice.

Averages of blood sugar values for (n=5) mice from each of the three test groups (FVB, *Gw* obese and non-obese) at fasting, 30 minutes, 1- and 2-hours post IP insulin injection, were calculated, and presented in panel **A**. Blood samples were collected by terminal tail cuts and glucose levels were measured using an Accu-Chek glucose reader as before. The areas under the curves for average blood glucose values of the three groups were presented in panel **B**. An ELISA kit was used next to measure 6 hours fasting insulin levels of mice from the three test groups at 4- and 6-months of age, **C**. Red rectangles in panel **C** highlight mice with fasting insulin levels above the highest value of the corresponding FVB group. * Indicates p-value $\leqslant$ 0.05, ** indicates p-value $\leqslant$ 0.01. The student t-test, two tails, was used for all statistical analyses.

3.3.3 Prevalence of obesity and sub-fertility among *Gw* mice

The two main pathologies observed among *Gw* mice were obesity and sub-fertility. In *Gw* mice, sub-fertility was mainly manifested with estrous irregularities, reflecting underlying hormonal anomalies and follicular maturation and ovulation defects. The prevalence of each of these two main features, among *Gw* mice, were analyzed as mice progressed in age, Figure 3.12. At a young age (2-months-old) sub-fertility was evident in 32% of the *Gw* mice population, with only 14% of the *Gw* population being obese and sub-fertile. Meanwhile, 18% of the *Gw* mice population were either subfertile or obese. At that time point, 50% of the *Gw* mice population maintained normal weight and fertility.

As mice progressed in age (4-, and 6-months-old) the sub-fertile proportion of *Gw* mice increased to 44%, and 58%, respectively. Interestingly, the obese sub-fertile proportion of the *Gw* population concomitantly increased with age to 20%, and 40%, at 4-, and 6-months, respectively. In contrast, the non-obese sub-fertile mice proportion was almost stable, ranging from 18% to 24% and back to 18% again of the *Gw* mice population, at 2-, 4- and 6-months of age, respectively. Concurrently, the percentage of the obese mice among the whole *Gw* mice population increased steadily with age from 32% to 46% and 56% at 2-, 4-, and 6-months of age, respectively.

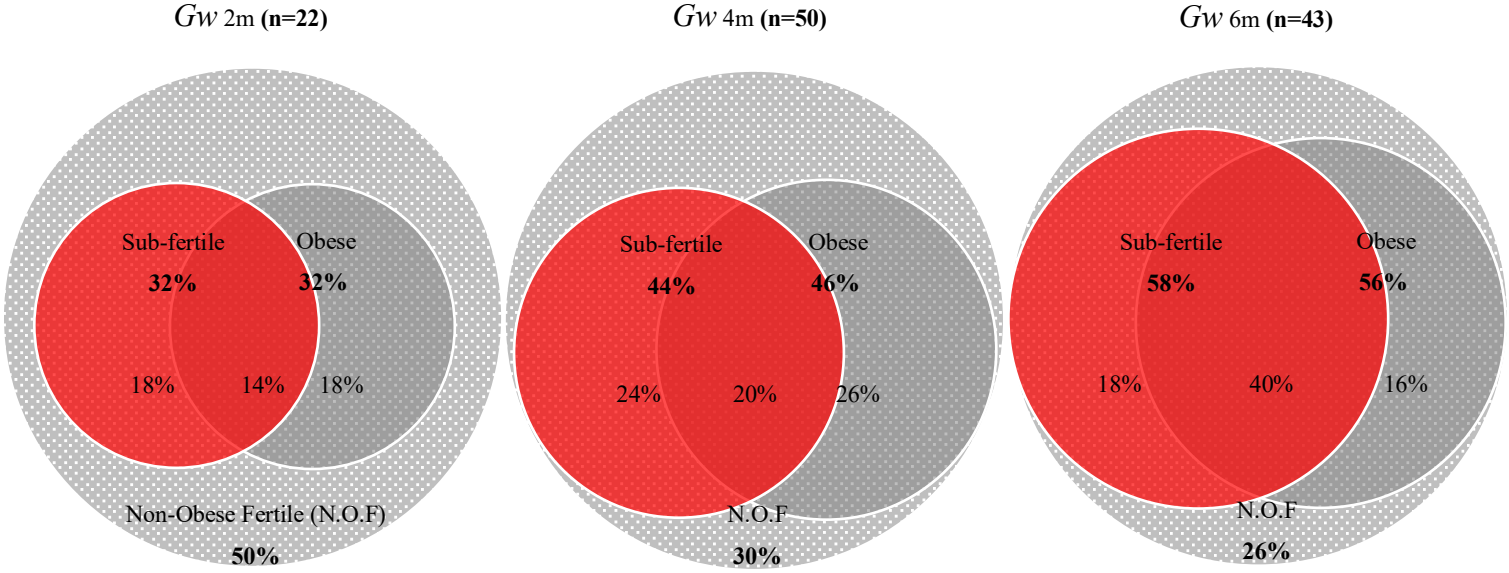

3.13 Obesity and subfertility progression with age among *Gw* female mice.

Estrous cycle follow-up (for 16 days) was used to identify the sub-fertile proportion of the *Gw* female mice population, and weight charts (every 2 weeks) to determine the obese and non-obese mice. N= 22, 50 and 43 mice were used for the 2-, 4-, and 6-months-old time points (2m, 4m, and 6m, respectively). Mice with a total number of cycles below the average for the rest of the *Gw* mice and the FVB controls were counted as sub-fertile. Non-obese fertile *Gw* mice (N.O.F) proportions were presented in the lower part of the *Gw* population circle, at each time point.

3.3.4 *Gw* mouse model phenotype compared to most used mouse models of PCOS and the human phenotype.

Androgen-induced mouse models are among the most used animal models for PCOS, and the most representative of the human phenotype. These are generated either by DHT or LET injection, (Chen, Chou et al. 2015, Kauffman, Thackray et al. 2015). A comparison between the main features of these models and the *Gw* mouse model plus the human phenotype of PCOS was presented in Table 3.1. Some of the features of DHT and LET mice were non-reproducible (Caldwell, Middleton et al. 2014) and were therefore listed as conflicting data in the table. Conflicting data were not counted towards calculating the overall similarity of each mouse model to the human phenotype.

Twenty-three identified features and pathologies of the human phenotype of PCOS were used as benchmarks to score the degree of similarity of different mouse models to the human phenotype. Some of the syndrome features (in humans) were absent in mouse models and were, therefore, listed as 'no data' and have not been included in the scoring system. The *Gw* mouse model had the highest degree of similarity to the human phenotype with a 74% similarity score, followed by the LET model (64%), the postnatal DHT model (45%), and the prenatal DHT model (36%). Worth mentioning here is that every single feature used for the similarity score calculation has been given a single point regardless of its weight.

3.2 Summary of main features of most prominent PCOS mouse models and the *Gw* mouse model in comparison with the human phenotype.

Phenotype	**PCOS patients** (Nikolaou and Gilling-Smith 2004, Wickenheisser, Nelson-Degrave et al. 2005, Chakrabarti 2013, Takahashi, Harada et al. 2017).	***Gw* mouse model**	**LET mouse model** (Caldwell, Middleton et al. 2014, Kauffman, Thackray et al. 2015)	**Prenatal DHT mouse model** (Roland, Nunemaker et al. 2010, Habib, Richards et al. 2012, Moore, Prescott et al. 2013, Caldwell, Middleton et al. 2014, Fornes, Maliqueo et al. 2017)	**Postnatal DHT mouse model** (Manneras, Cajander et al. 2007, van Houten, Kramer et al. 2012, Caldwell, Middleton et al. 2014)
Polycystic ovary	Y	Y	Y	N	N
Enlarged ovary	Y	N	Y	N	N
Increased atretic follicles	Y	Y	Y	Y	Y
Increased antral follicles	Y	N	Y	N	Y
Anovulation/oligo-ovulation	Y	Y (oligo)	Y	Y (oligo)	Y (oligo)
Irregular/absent cycles	Y	Y	Y	Y	Y
Infertility/sub-fertile	Y	Y (sub-fertile)	Y	Y (sub-fertile)	No data
Hyperandrogenaemia (T)	Y	Y	Y	Conflicting data	N

Elevated LH	Y	Y	Conflicting data	Conflicting data	N
Reduced FSH	Y	No data	Y	N	N
Elevated Cyp17	Y	No data	Y	No data	No data
Elevated FSHr in the ovary	Y	No data	Y	No data	No data
P4 resistance	Y	No data	No data	Y	No data
Obesity	Y	Y	Conflicting data	N	Y
Increased adipose weights	Y	Y	Conflicting data	N	Y
Enlarged adipocyte size	Y	Y	Conflicting data	Y	Y
Leptin	Y	Y	N	Y	Y
Inflammation (Ovarian or adipose tissue)	Y	Y	Y	No data	No data
Ovarian fibrosis	Y	Y	No data	Y	Y
Hyperinsulinemia	Y	Y	N	No data	No data
Insulin resistance	Y	Y	N	N	N
Glucose intolerance	Y	Y	Y	Conflicting data	Y
Percentage of similarity to human phenotype	100%	74%	64%	36%	45%
Y = yes; N = no, T = testosterone, LH = luteinizing hormone, FSH = follicle-stimulating hormone, Cyp17 = a steroidogenic enzyme, FSHr = FSH receptor gene, P4 = progesterone.					

3.4 Multi-receptor resistance, an ongoing hypothesis for the development of PCOS

Considering the rising evidence of multi-organ resistance to feedback signals in PCOS patients and mouse models (Diamanti-Kandarakis 2006, Al-Sabbagh, Lam et al. 2012, Moore, Prescott et al. 2013, Moore, Prescott et al. 2015, Lian, Zhao et al. 2016), and the observed insulin and leptin resistance among *Gw* mice, we revisited the multi-receptor resistance hypothesis as the origin of PCOS. The focus of this work was mainly to investigate hypothalamic resistance among *Gw* mice. Hypothalamic resistance to feedback signals could be due to either downregulation of the expression of genes coding for hypothalamic receptors or impaired receptor's function.

We first examined the expression patterns of genes coding for various reproductive hormones receptors in the ARC nuclei of the hypothalamus (of *Gw* and FVB mice), at different time points. The functions of GnRH neurons (in the pre-optic area (POA) are tightly regulated through a neuroendocrine circuit of adjacent neurons in POA and the ARC (Foecking, Szabo et al. 2005, Blank, McCartney et al. 2006, Clarkson, Han et al. 2017). These neurons express receptors for various reproductive hormones, allowing their detection and adjustment of GnRH production and pulse frequency accordingly (Cheng and Leung 2005, Herbison 2008). We then examined the expression patterns of various genes coding for feeding and satiety regulating peptides in the ARC nuclei. Finally, the expression patterns of the *Gata4* gene were also examined in the ARC nuclei, to evaluate the effect of the transgene insertion on this process. Mice were examined initially at 4-months of age as most of the anomalies observed among *Gw* mice are fully developed at that age. Other time points were added (E11.5, and P14d) to assess the onset and the progression of the gene expression anomalies.

3.4.1 Anomalies in the expression of genes coding for reproductive hormone receptors in *Gw* mice

The qPCR technique was used to quantify mRNA levels of genes coding for various reproductive hormone receptors including, E2 (*Esr1)*, P4 (*Pgr*), FSH (*Fshr*), LH (*Lhr*), and GnRH (*Gnrhr*), plus GnRH, in the ARC nuclei of 4 months old *Gw* and FVB mice, Figure 3.14A**.** For mice that were E11.5 and P14d old, whole brains were used instead of the ARC due to technical difficulties associated with dissection at these age points. Interestingly, all tested receptors were significantly under-expressed in the ARC nuclei of *Gw* mice compared to the FVB mice, except for the *Pgr* gene that did not reach a statistical significance of under-expression, Fig. 3.14A. On the other hand, expression levels of the *Gnrh* gene tended to be higher in *Gw* mice compared to FVB mice, Fig. 3.14A.

The timeline of *Esr1* expression in *Gw* mice, compared to FVB mice, showed an initial over-expression at embryonic age (E11.5), then a progressive under-expression at two weeks (P14d), and four months of age (P4m), Figure 3.14B. A similar pattern was observed in the expression levels of *Pgr,* but without statistical significance, Figure 3.14C. *Fshr* gene expression levels were lower in *Gw* mice compared to the FVB mice from as early as E11.5 days and they progressed to further lower levels at P14d and P4m, Figure 3.14D. *Lhr* expression levels followed a similar pattern to that of the *Esr1* with initially higher levels (in *Gw* mice compared to the FVB) at E11.5 and then became progressively lower as mice progressed in age to P14d and P4m, Figure 3.14E. *Gnrhr*, on the other hand, followed the same expression pattern as that of the *Fshr* at all time points, Figure 3.14F. Finally, *Gnrh* mRNA expression levels were higher in *Gw* mice compared to FVB mice at the age of E11.5 and P4m, but lower than FVB mice at the age of P14d, without reaching statistical significance at any time point, Figure 3.14G.

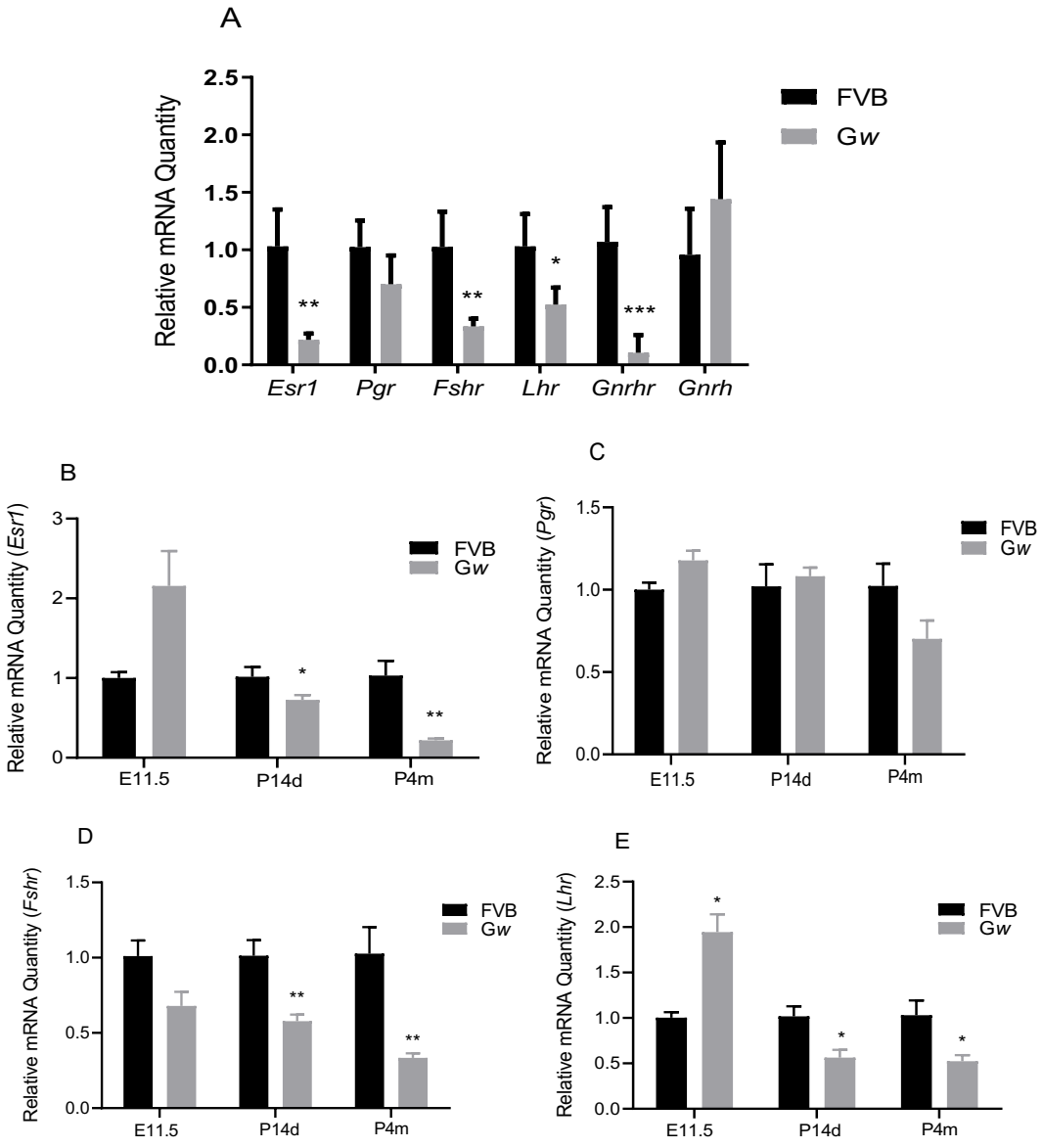
A
Relative mRNA Quantity
2.5
2.0
1.5
1.0
0.5
0.0
FVB
Gw
**
**
*
***
Esr1
Pgr
Fshr
Lhr
Gnrhr
Gnrh
B
Relative mRNA Quantity (Esr1)
3
2
1
0
FVB
Gw
*
**
E11.5
P14d
P4m
C
Relative mRNA Quantity (Pgr)
1.5
1.0
0.5
0.0
FVB
Gw
E11.5
P14d
P4m
D
Relative mRNA Quantity (Fshr)
1.5
1.0
0.5
0.0
FVB
Gw
**
**
E11.5
P14d
P4m
E
Relative mRNA Quantity (Lhr)
2.5
2.0
1.5
1.0
0.5
0.0
FVB
Gw
*
*
*
E11.5
P14d
P4m

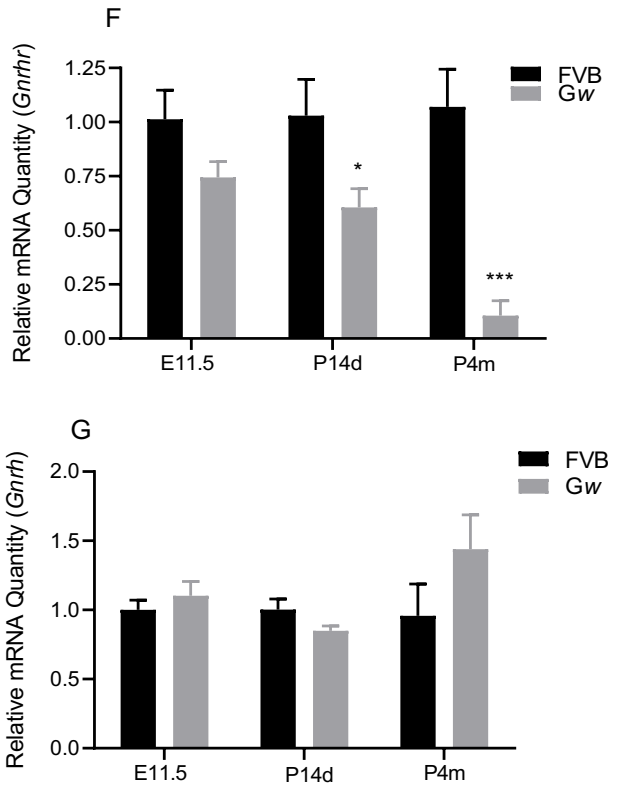

3.14 Expression levels of various genes coding for reproductive hormone receptors in the brain of *Gw* and FVB mice.

A relative quantification of mRNA levels, using qPCR, was done to evaluate the expression levels of genes coding for various reproductive hormone receptors including, *Esr1*, P4 (*Pgr*), FSH (*Fshr*), LH (*Lhr*), and GnRH (*Gnrhr*), plus the *Gnrh* gene, in the ARC nuclei of 4 months old (P4m) *Gw* and FVB mice (n=5), **A**. Two more time points (11.5 days of embryonic age (E11.5), and two weeks old post-natal (P14d)) were tested next to identify the onset and the progression of observed anomalies, including, *Esr1* **(B)**, *Pgr* **(C)**, *Fshr* **(D)**, *Lhr* **(E)**, *Gnrhr* **(F)**, and *Gnrh* **(G)**. Whole-brain samples were used at the age of E11.5 and P14d, instead of ARC nuclei, because of the technical difficulties associated with brain dissection at these age points. * Indicates p-value $\leqslant 0.05$, ** indicates p-value $\leqslant 0.01$. The student t-test, two tails, was used for all statistical analyses.

3.4.2 Dysregulation of the expression of genes coding for satiety and feeding regulating neuropeptides in *Gw* mice

POMC neurons in the ARC play a crucial role in activating satiety (by suppressing the feeding center in the lateral hypothalamus) and regulating energy expenditure in response to leptin (Millington 2007). On the other hand, NPY and AgRP neurons activate the feeding center in response to leptin (Ahima and Antwi 2008). The expression levels of the genes coding for these three neuropeptides, in the ARC of 4-months-old *Gw* and FVB mice, were assessed to understand the origin of observed overfeeding and obesity phenotypes among around 50% of the *Gw* mice population, Figure 3.15A. *Gw* mice showed significantly lower levels of *Pomc* mRNA compared to FVB mice. Interestingly, no significant differences, in the expression levels of *Npy* and *Agrp* genes, were observed among *Gw* and FVB mice, Fig. 3.15A. The three tested genes were also analyzed at the two other time points tested above (E11.5 and P14d). The expression levels of the *Pomc* gene did not show significant differences among *Gw* and FVB mice in earlier time points (E11.5 and P14d), Figure 3.15B. The expression levels of the *Npy* gene tended to be lower among *Gw* mice compared to FVB mice at the P14d time point, while interestingly, these levels were significantly higher at E11.5, Fig. 3.15C. Finally, the expression levels of the *Agrp* gene were slightly lower among *Gw* mice compared to FVB mice at E11.5 and P14d age points, with statistical significance at E11.5, Fig. 3.14D.

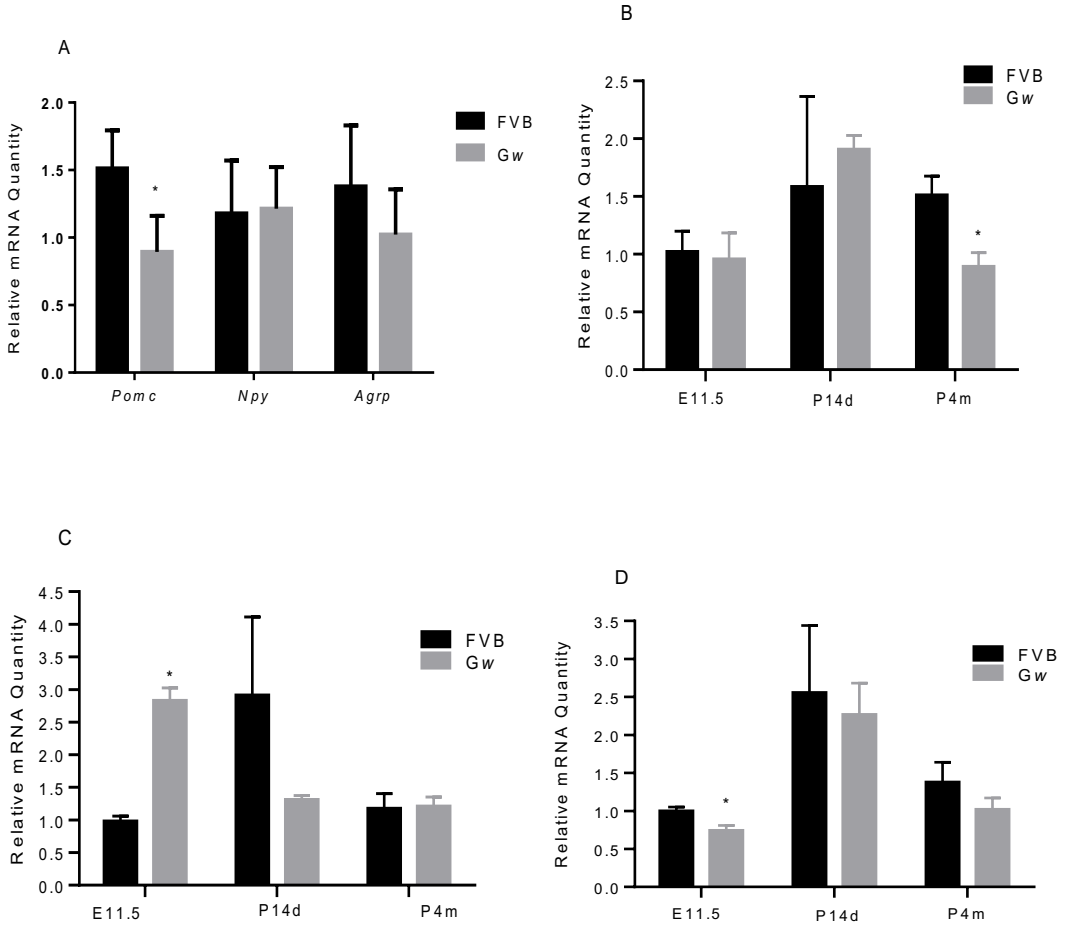

3.15 Expression levels of various genes coding for feeding and satiety regulating neuropeptides in the brain of *Gw* and FVB mice.

The qPCR technique was used to quantify the expression levels of three different genes coding feeding and satiety regulating neuropeptides among *Gw* and FVB mice (n=5), *Pomc, Npy,* and *Agrp*. **A** shows relative mRNA levels of the three tested genes for 4-months-old mice. Further time points were tested (E11.5 and P14d) to identify the onset and the progression of the observed anomalies in *Pomc, Npy* and *Agrp*; **B, C, and D**, respectively. ARC nuclei were dissected for each mouse at the age of 4 months, while whole brains were used for the E11.5 and P14d age points. * Indicates p-value $\leqslant 0.05$, ** indicates p-value $\leqslant 0.01$. The student t-test, two tails, was used for all statistical analyses.

3.5 Disruption of intrinsic *Gata4* gene expression is another hypothesis for the development of PCOS phenotype in *Gw* mice

GATA4 transcription factor is involved in the development of reproductive organs and in the regulation of their functions (Kyronlahti, Euler et al. 2011, Kyrönlahti, Vetter et al. 2011, Efimenko, Padua et al. 2013). It has also been linked to the regulation of the expression of various genes coding for reproductive hormone receptors like *Lhr* and *Esr1* (Rahman, Kiiveri et al. 2001, Miranda-Carboni, Guemes et al. 2011, Scott M 2018). Considering that the transgene used to generate the *Gw* mouse model contained a *Gata4* promoter (Gata4p), the possibility for a competition between the extrinsic and the intrinsic promoters (over the upstream transcription factors) was next investigated. The expression levels of the *Gata4* gene were evaluated in *Gw* and FVB mice, using the ARC nuclei of adult (P4m), whole brains of embryonic (E11.5) and early postnatal (P14d) mice. *Gata4* gene expression levels were significantly lower in *Gw* mice, at all time-points, compared to FVB mice, Figure 3.16. Interestingly, the differences between the expression levels of the *Gata4* gene in *Gw* and FVB mice became more important with age. An evaluation of the levels of the GATA4 protein in ARC nuclei, and ovaries of *Gw* and FVB mice, was later done by colleagues in the laboratory of Dr. Pilon. The GATA4 protein was not present in the ARC nuclei of *Gw* mice compared to FVB mice. Interestingly there was no differences in protein levels in the ovaries of *Gw* and FVB mice, S. Fig 5.5.

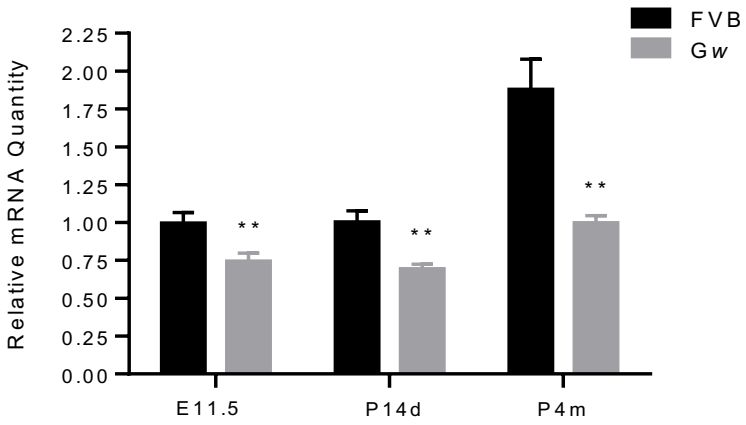

3.16 Expression levels of the *Gata4* gene in the brain of *Gw* and FVB mice.

The qPCR technique was used to quantify mRNA levels of the *Gata4* gene in *Gw* and FVB mice. RNA extracts from ARC nuclei of 4-months-old mice (P4m) or whole-brain of embryos at 11.5 days post-conception (E11.5) and 14 days postnatal mice (P14d) were used for this experiment. The averages of the relative quantification (of n=5 mice) are presented here. ** Indicates p-value $\leqslant$ 0.01. The student t-test, two tails, was used for all statistical analyses.

3.6 Pathologies of the *Gw* mice ovarian microenvironment

An extensive review of the literature was done to identify reversible pathologies among PCOS patients and animal models, and treatments used to achieve it. Among the most important pathologies affecting oocyte viability and fertility in PCOS patients and mouse models is the high level of ER stress (Wu, Russell et al. 2015, Azhary, Harada et al. 2019). High ER stress levels, in PCOS mouse models have been successfully reversed in multiple studies using various molecules, with some improvement of their fertility (Wu, Russell et al. 2015, Takahashi, Harada et al. 2017, Uppala, Gani et al. 2017). None of the ER stress inhibiting molecules was used in PCOS patients before, except for Metformin, which acts as an indirect inhibitor for ER stress through the reduction of the levels of T hormone (Jin, Ma et al. 2020).

TUDCA, a direct ER stress inhibitor, had a favourable effect on the fertility of PCOS mouse models, in various studies (Wu, Russell et al. 2015, Takahashi, Harada et al. 2017, Uppala, Gani et al. 2017). Moreover, it has also been used, with great success in some medical conditions, including pulmonary and renal fibrosis (Panella, Ierardi et al. 1995, Invernizzi, Setchell et al. 1999, clinicaltrials.gov 2019). Together, these criteria made TUDCA the best candidate molecule for further studying as a potential therapeutic for PCOS, especially since it had the Food and Drug Administration approval for human use, with a minimal side effects profile (Kusaczuk 2019). Further analysis of the ovarian microenvironment of *Gw* mice was done to validate ER stress levels in their ovaries and their reversibility using TUDCA and Metformin.

3.6.1 High peri-follicular ER stress levels in the ovaries of *Gw* mice

Immunofluorescence (IF) staining of ovarian histology sections, from the three test groups (*Gw* (obese and non-obese) and FVB mice), using three different ER stress markers (CHOP, ATF6, and IRE1), was used to evaluate ER stress levels in the ovarian microenvironment of these mice. ER stress positive GCs of these mice were evaluated against the number of growing follicles, at 4- and 6-months of age (n=5 mice) to estimates their ER stress levels.

Representative photos of IF sections from the three test groups, stained for each ER stress marker, at 4 and 6 months of age, were shown in Figures 3.17A, and C, respectively. ER stress positive GCs were identified using a red fluorescent secondary antibody against each ER stress marker primary antibody. Cell nuclei were counterstained in blue with DAPI (DNA stain). The averages of ER stress positive cells per growing follicle, hence ER stress levels were higher in *Gw* obese and non-obese mice compared to FVB mice at 4 and 6 months of age, (Figure 3.17B and 3.17D**,** respectively) for each marker separately. Interestingly, ER stress levels were more elevated among *Gw* obese mice compared to *Gw* non-obese mice at both age points, for all three markers, Figure 3.17B and 3.17D**,** respectively.

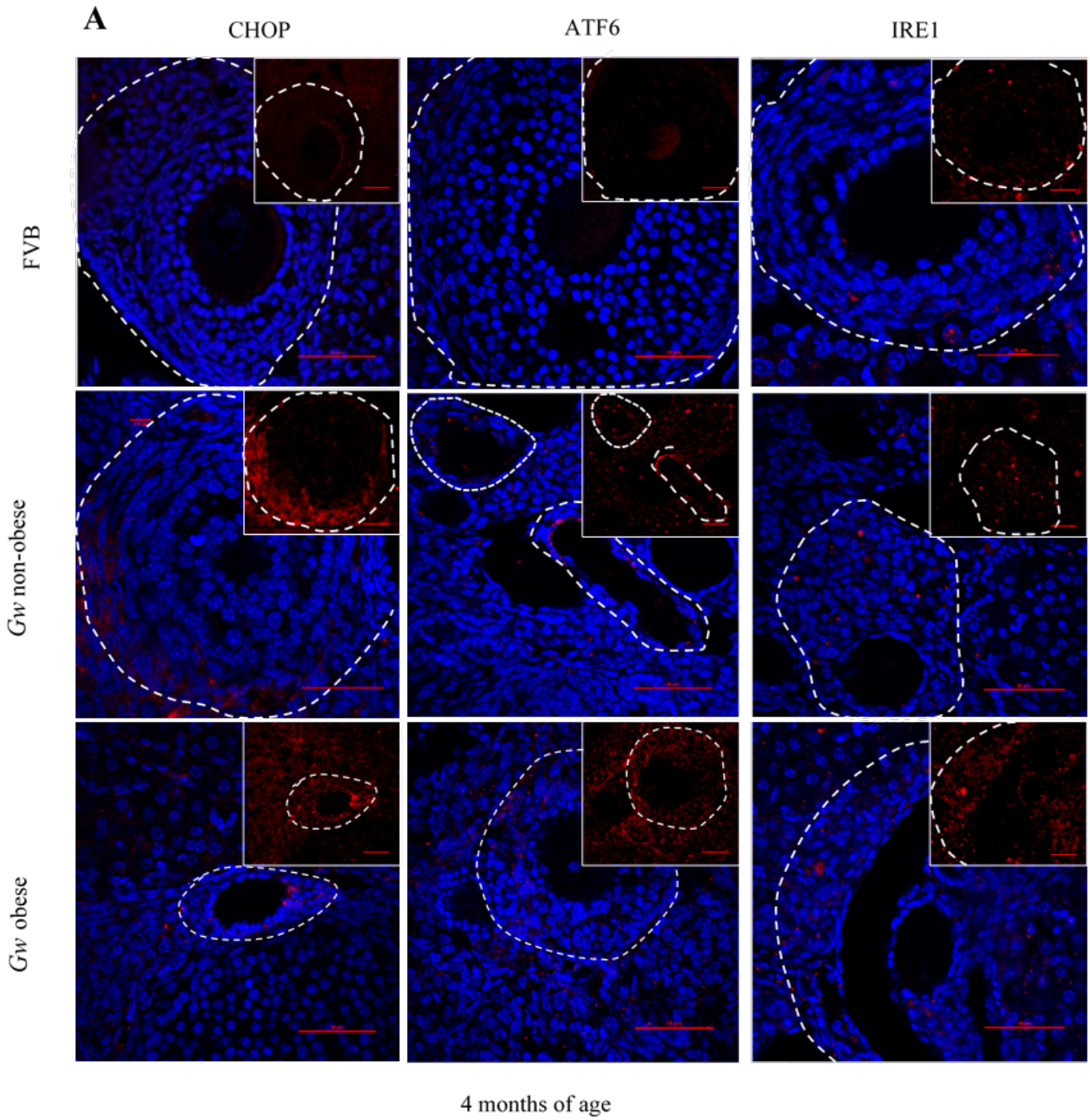
A
CHOP
ATF6
IRE1
FVB
Gw non-obese
Gw obese
4 months of age

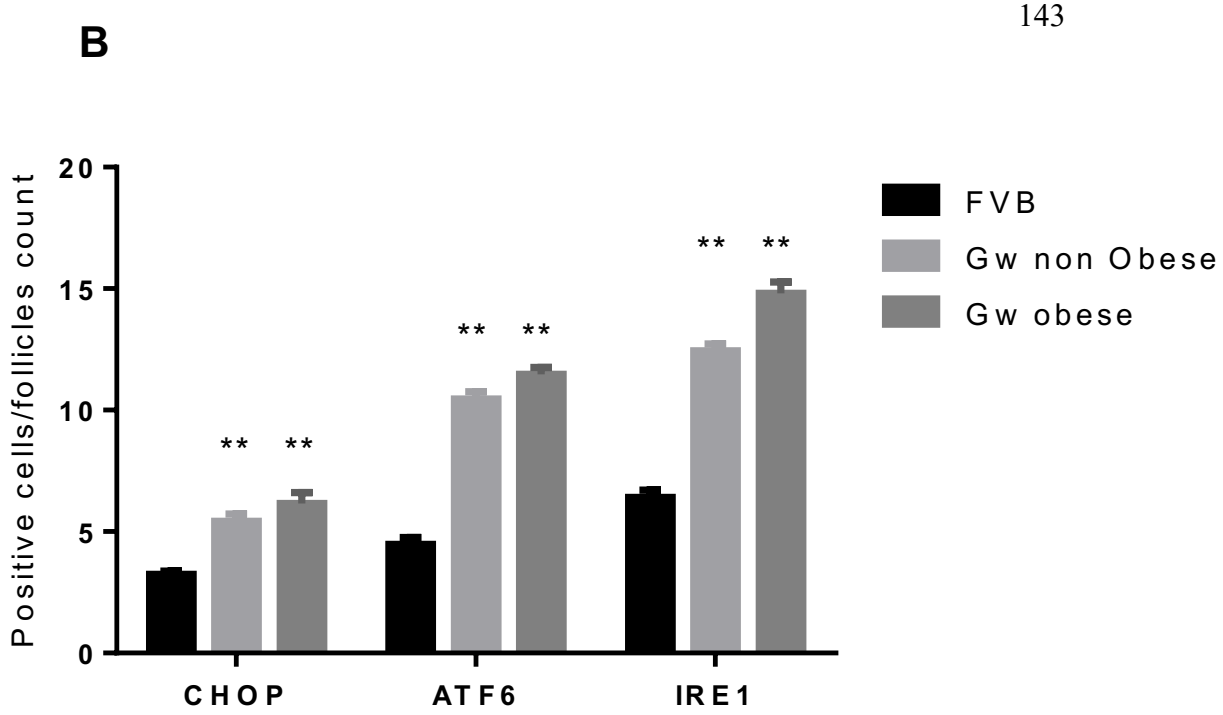
B
Positive cells/follicles count
20
15
10
5
0
**
**
**
**
**
**
CHOP
ATF6
IRE1
FVB
Gw non Obese
Gw obese

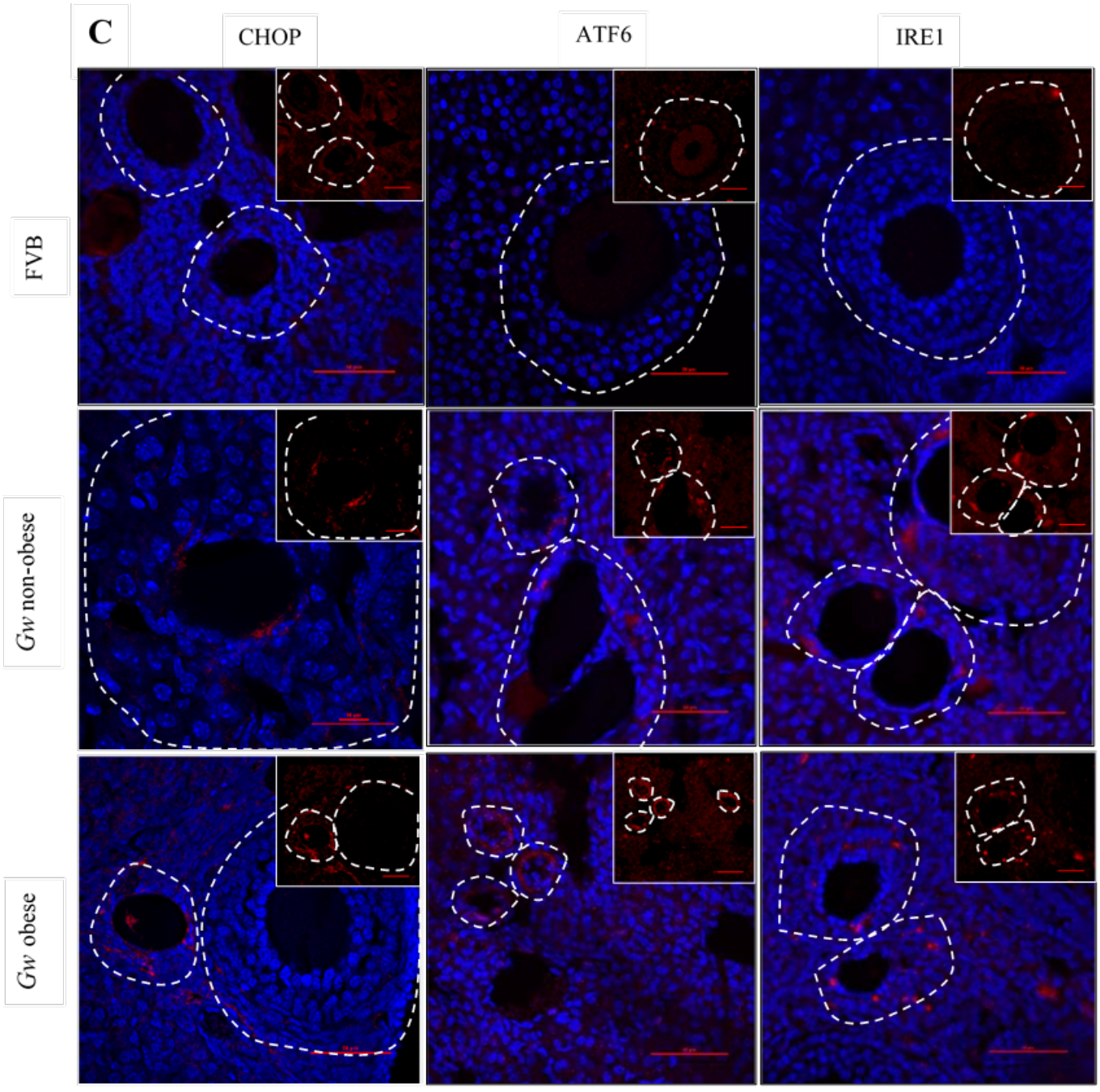
C
CHOP
ATF6
IRE1
FVB
Gw non-obese
Gw obese
6 months of age

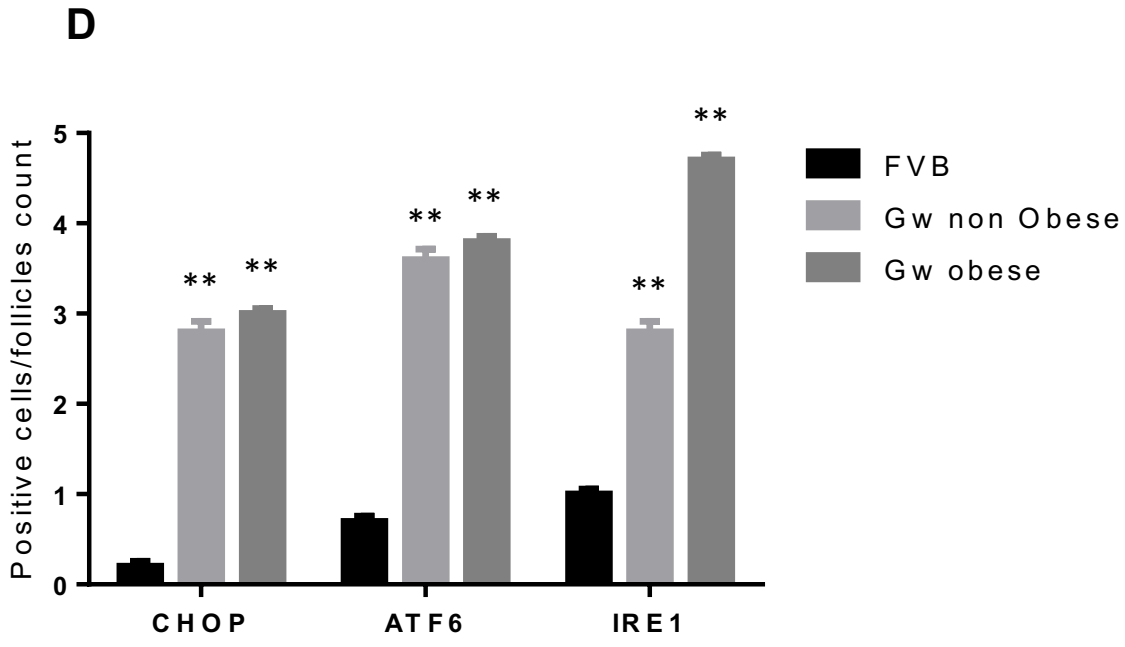

3.17 ER stress levels in ovaries of *Gw* and FVB mice at 4 and 6 months of age.

Representative IF sections of one mouse from each test group (*Gw* obese and non-obese and FVB), and each ER stress marker (CHOP, ATF6 and IRE1) are shown in panels **A** and **C** for 4- and 6-months-old mice, respectively. The white dashed line in each section outlines the outer limit of a growing follicle. The square in the right upper corner within each slide is a red fluorescent only vintage of the whole section to highlight the abundance of ER stress positive cells. The scale bar for the main sections is 50µm, and for the squared area is 10µm. Relative quantification of average ER stress levels (ER stress positive cells/growing follicle) for each ES stress marker, and each test group, were presented in panels **B** and **D,** for 4- and 6-months-old mice, respectively. ** indicates p-value $\leqslant$ 0.01. The student t-test, two tails, was used for all statistical analyses.

3.6.2 Collagen abundance within *Gw* mice ovaries

Persistently high ER stress levels eventually cause ovarian fibrosis secondary to a chronic inflammatory process (Takahashi, Harada et al. 2017). The three test groups were evaluated for the relative abundance of collagen within their ovaries at the age of 6 months using trichrome stain of histology sections from their ovaries, Figure 3.18A. Quantification of the average amount of collagen in each group (using ImageJ software) showed significantly higher levels of collagen in *Gw* mice ovaries, compared to the FVB mice, Figure 3.18B (n=5 mice in each group). Interestingly, *Gw* obese mice showed higher levels of collagen within their ovaries compared to *Gw* non-obese mice and FVB mice, Fig. 3.18B.

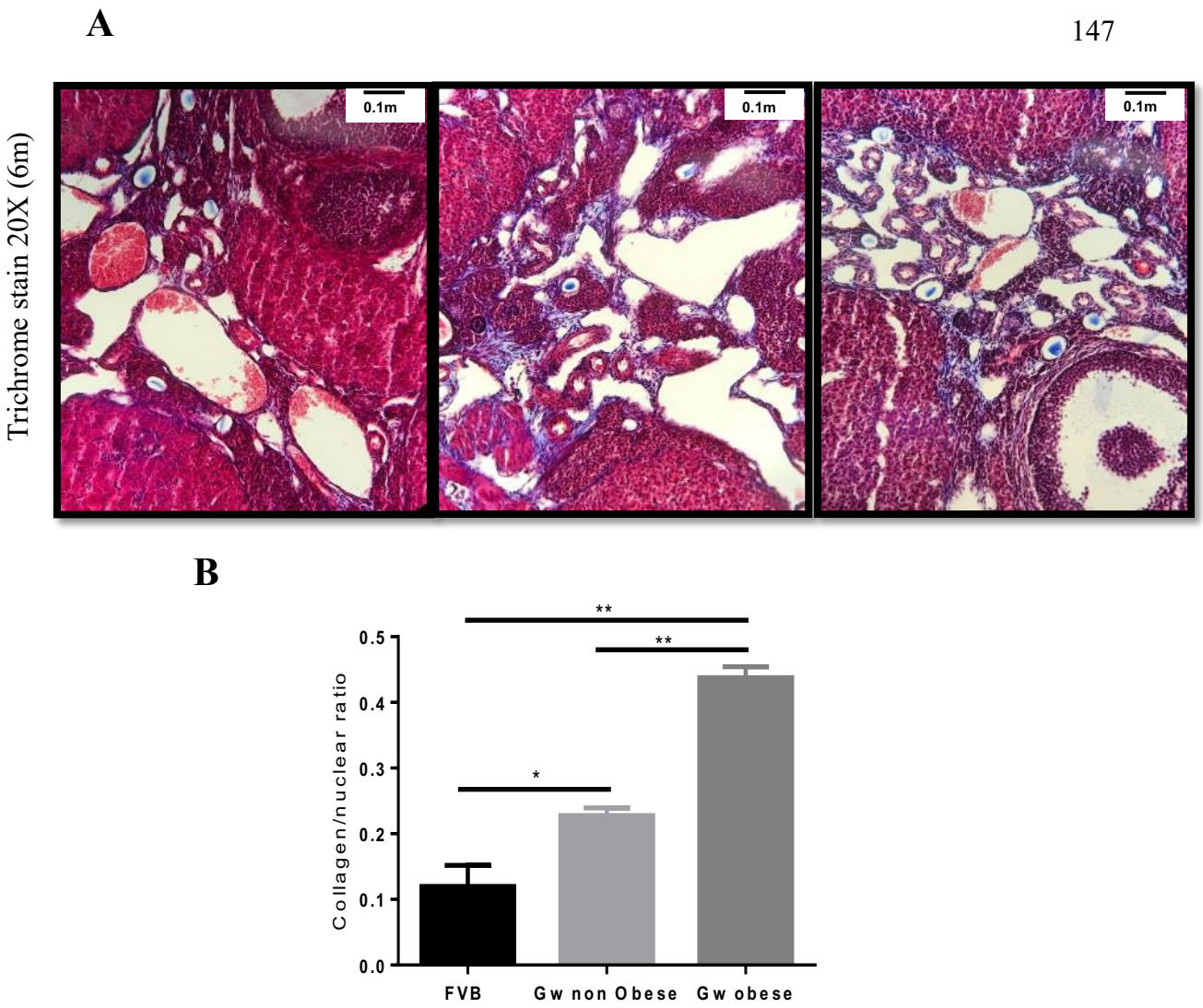

3.18 *Gw* female mice ovarian stroma fibrosis at six months of age.

Representative photos of histology sections of ovaries from *Gw* (obese and non-obese) and FVB mice, stained with the trichrome stain plus a hematoxylin and eosin counterstain, demonstrate collagen deposition (blue) within each mouse ovary in panel **A**. Relative quantification of the amount of collagen in each slide was done by counting blue pixels (collagen) against black pixels (nuclei) per high power field (20X) for each mouse ovarian stroma, using ImageJ software (n=5 mice in each group and 3 high power fields per mouse). The average amounts of collagen in the ovarian stroma of each group of mice was presented in panel **B**. * Indicates p-value $\leqslant 0.05$, ** indicates p-value $\leqslant 0.01$. The student t-test, two tails, was used for all statistical analyses.

3.7 TUDCA, Metformin and their combination improve *Gw* mice overall reproductivity

Considering the high levels of ER stress, and collagen deposition, detected in the ovaries of *Gw* mice (particularly obese mice), compared to FVB mice, TUDCA and Metformin (separately or combined) were tested to improve *Gw* mice fertility. TUDCA (an ER stress inhibitor) and Metformin both had shown some evidence of reducing ER stress levels and improving fertility in PCOS and obesity mouse models, and humans as well (Metformin only) (Velazquez, Mendoza et al. 1994, Wu, Russell et al. 2015, Desquiret-Dumas, Clement et al. 2017, Jin, Ma et al. 2020).

Gw mice of 2-months-old were identified and their weight and estrous cyclicity were followed up for one month. Only *Gw* mice with estrous cycle anomalies (either 1 or 2 cycles per 16 days, or diestrous arrest (≥4 days/cycle)) were selected for the treatment and vehicle (control) groups. In all experiments, the treatment group results were compared against two control groups, *Gw* mice treated with vehicle only, and FVB mice treated with vehicle only. Each treatment and control group included at least n=5 mice. *Gw* mice with estrous cycle anomalies were then divided into obese and non-obese according to their weight, using the predetermined cutoff from previous results.

Three different groups were generated for TUDCA only, Metformin only, and a combined TUDCA and Metformin treatment group. Each treatment was delivered in drinking water provided to mice at predetermined doses from previous literature (Sabatini, Guo et al. 2011, Takahashi, Harada et al. 2017). Mice in each group were treated for one month, and water (including the medication) was changed every two days as usual. After a month of treatment, mice were subjected to IO and IVF, according to standard protocols, using freshly thawed sperms from 2-months-old male FVB mice, previously validated as fertile.

The overall number of oocytes generated by IO at day zero (D0) were counted, and the number of abnormal oocytes was noted, for each mouse. Viable and non-viable oocytes were decided according to their morphology as shown in previous results, Fig. 3.5B, and using previously established criteria from the literature (Swann 2014). Collected oocytes were next fertilized in-vitro using sperms from a 2-months-old FVB mouse and were then incubated according to standard protocol (at 37ºC and 5% CO_2). Fertilized oocytes were followed up daily for various stages of zygote development until day four post-fertilization (D4). The numbers of zygotes that successfully reached the expected growth stage, at each day, were noted and compared to FVB mice. Zygotes that started dividing but failed to reach the blastocyst stage in the expected time (D4) were counted as arrested growth oocytes. On the other hand, 'morphologically' viable oocytes that failed to divide were counted as non-fertilized oocytes. The final count of non-fertilized oocytes at D4 did not include the oocytes previously identified as non-viable, 'morphologically' also, at D0. Various stages of zygote growth were identified according to established criteria in the literature (Gardner and Balaban 2016).

On day zero (IO day), *Gw* non-treated mice had significantly lower overall numbers of oocytes, and higher percentages of non-viable oocytes, compared to FVB mice, Figure 3.19A. *Gw* mice treated with TUDCA (obese and non-obese) had a significant increase in their overall oocytes production, and a relative reduction of the percentage of non-viable oocytes, compared to the corresponding non-treated *Gw* mice, Fig. 3.19A. This increase in oocytes production even reached levels similar to those of FVB mice following IO, with almost the same percentages of the non-viable oocytes, Fig. 3.19A. On the other hand, Metformin treated *Gw* mice showed similar results to those of TUDCA treated mice, but mainly among the *Gw* obese mice (increased overall oocytes production), compared to non-treated *Gw* and FVB mice, Fig. 3.19A. Metformin-treated *Gw* mice, obese and non-obese, both had relatively lower percentages of non-

viable oocytes compared to corresponding non-treated *Gw* mice, Fig. 3.19A. *Gw* mice treated with a combination of TUDCA and Metformin had higher overall numbers of oocytes, produced in response to IO than those of all other corresponding mice groups, Fig. 3.19A. Interestingly, the percentage of non-viable oocytes, in the double (T+M) treatment group, was higher among *Gw* obese mice compared to every other test and control group, Fig. 3.19A. This was not observed among *Gw* non-obese mice with the same double treatment, Fig. 3.19A.

On day four ((D4), 5 days following the IO and IVF), blastocysts, growth-arrested zygotes and non-fertilized oocytes were counted for each of the treatment and control groups. Data showed significantly lower numbers of zygotes that reached the stage of blastocysts among the non-treated *Gw* mice, with a significant increase in the percentage of zygotes with arrested growth (particularly among *Gw* obese mice), compared to FVB mice, Figure 3.19B. TUDCA treated *Gw* mice (obese and non-obese) showed a slight improvement in the overall numbers of zygotes that successfully reached the stage of blastocysts at day 4, compared to corresponding non-treated *Gw* mice groups, but these numbers were still below the average numbers of FVB mice, Fig. 3.19B. Furthermore, the percentages of zygotes that had arrested growth, among the TUDCA treated *Gw* mice, were slightly lower in both *Gw* obese and non-obese mice, compared to non treated *Gw* mice, Fig. 3.19B. Surprisingly, the numbers of non-fertilizable oocytes among the TUDCA treated *Gw* mice were higher than those numbers from the non-treated *Gw* and FVB mice, particularly for the obese *Gw* mice which reached a statistical significance Fig. 3.19B.

Metformin treatment also induced an increase in the final numbers of blastocysts of *Gw* mice, particularly in the obese group which reached a statistical significance compared to the corresponding non-treated *Gw* mice, Fig. 3.19B. Furthermore, Metformin-treated *Gw* mice also had a relative reduction in the percentage of zygotes

with arrested growth, and non-fertilizable oocytes, compared to non-treated *Gw* mice, Fig. 3.19B.

The combination of TUDCA and Metformin (T+M) treatment showed the most promising results in improving the fertility and reproductivity of *Gw* mice. *Gw* mice treated with T+M had significantly higher numbers of blastocysts (at D4), particularly among the obese mice, compared to the corresponding non-treated *Gw* mice, Fig. 3.19B. They also had a significant reduction in the percentage of zygotes with arrested growth, but they failed to show a reduction in the numbers of non-fertilizable oocytes, compared to non-treated *Gw* mice, Fig. 3.19B. Interestingly the T+M treatment rather increased the percentage of non-fertilizable oocytes to a significant level among treated *Gw* non-obese mice, compared to non-treated *Gw* mice, Fig. 3.19B. Figure 3.19C shows representative photos, obtained using Leica microscope (10X objective), of various stages of zygote development from D0 to D4 (following IO and IVF) of one of the T+M treated *Gw* obese mice compared to a non-treated *Gw* obese mouse and an FVB mouse. No clear correlation could be identified between the numbers of estrous cycles *Gw* mice had, and their overall number of oocytes produced in response to IO, or the percentage of the viable and non-viable oocytes, or even the numbers of blastocysts they had at D4, regardless of the treatment they had, Fig. 3.19D**.** Worth mentioning here is that the correlation results are preliminary and an increase in the number of mice is still required to confirm this initial finding. Table 3.3 summarizes the statistical analysis of the results of various treatment groups compared to the non-treated *Gw* mice, and to the FVB mice.

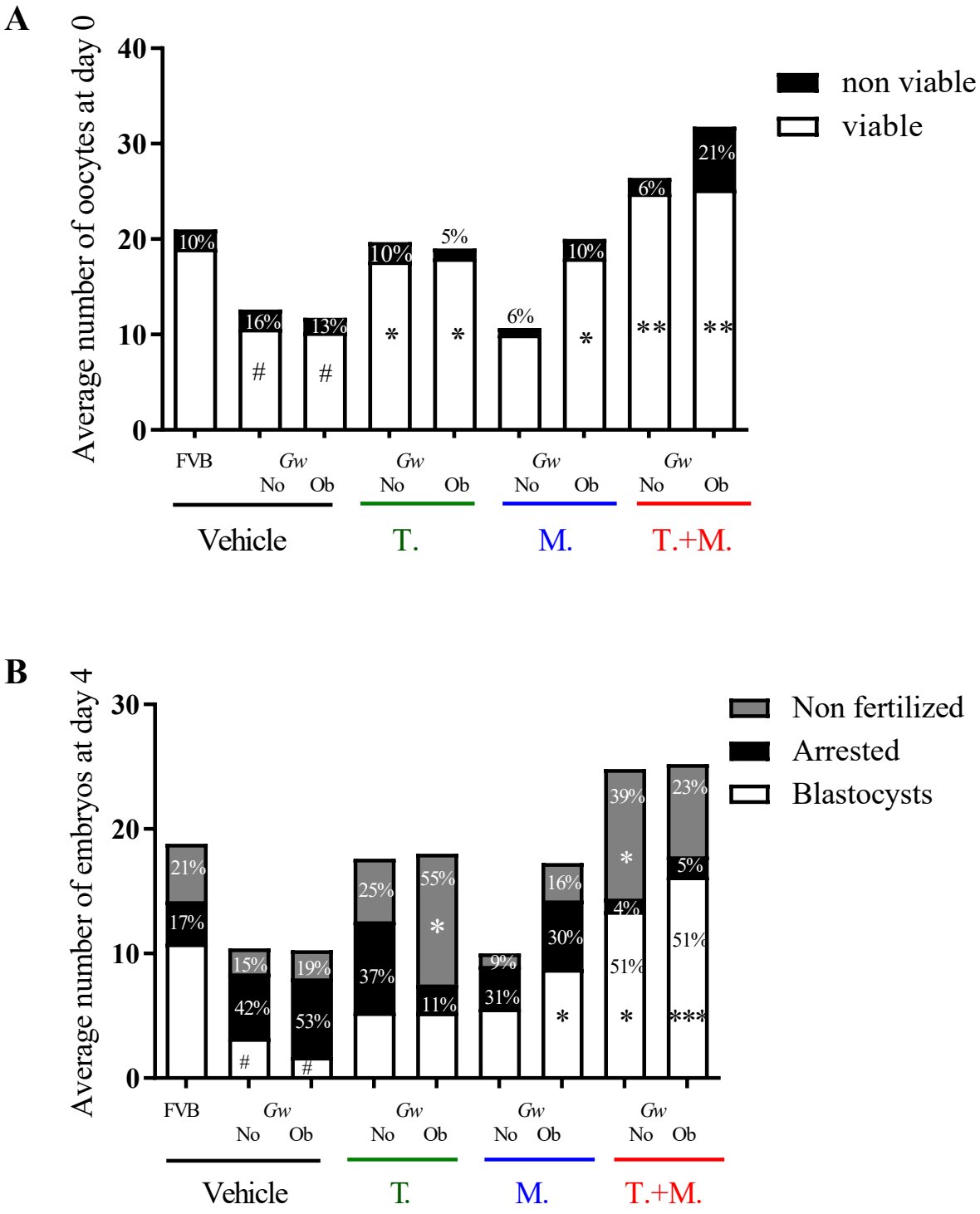
A
Average number of oocytes at day 0
40
30
20
10
0
non viable
viable
10%
16%
13%
10%
5%
6%
10%
6%
21%
#
#
*
*
*
**
**
FVB
Gw
No
Ob
Vehicle
T.
M.
T.+M.
B
Average number of embryos at day 4
30
20
10
0
Non fertilized
Arrested
Blastocysts
21%
17%
15%
42%
19%
53%
25%
37%
55%
11%
9%
31%
16%
30%
39%
4%
51%
23%
5%
51%
#
#
*
*
*
*
***
FVB
Gw
No
Ob
Vehicle
T.
M.
T.+M.

C

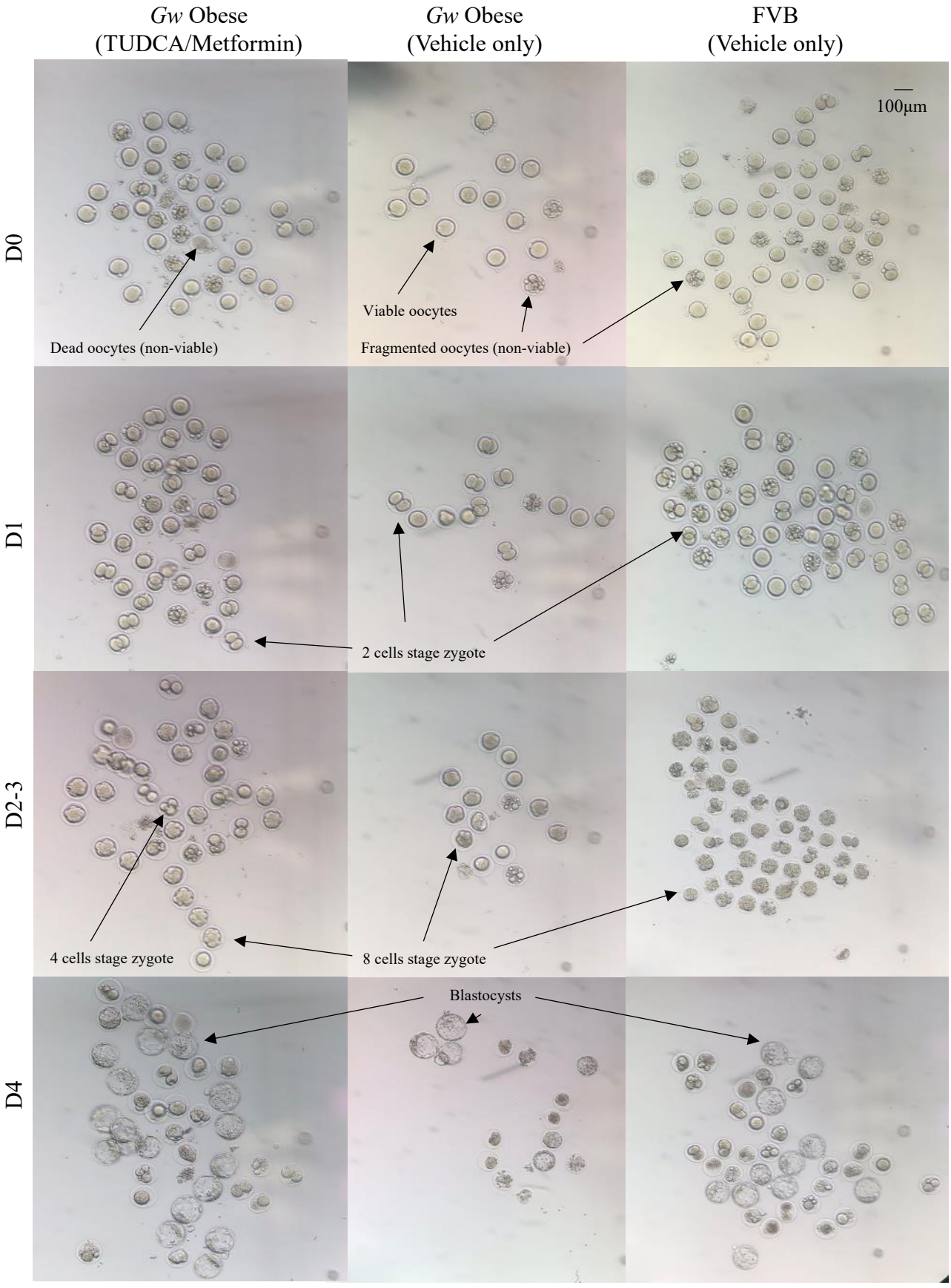
Gw Obese
(TUDCA/Metformin)
Gw Obese
(Vehicle only)
FVB
(Vehicle only)
D0
D1
D2-3
D4
100µm
Dead oocytes (non-viable)
Viable oocytes
Fragmented oocytes (non-viable)
2 cells stage zygote
4 cells stage zygote
8 cells stage zygote
Blastocysts

D

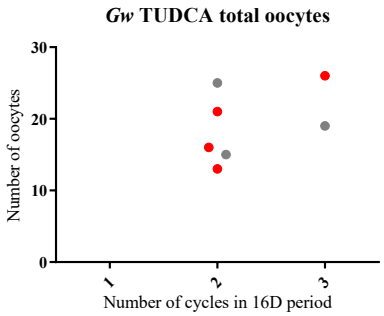
Gw TUDCA total oocytes
Number of oocytes
Number of cycles in 16D period

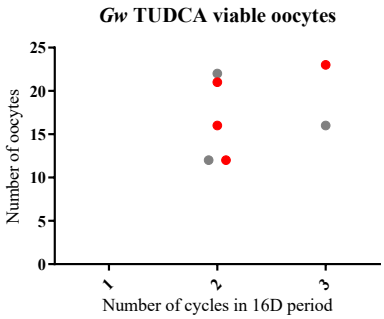
Gw TUDCA viable oocytes
Number of oocytes
Number of cycles in 16D period

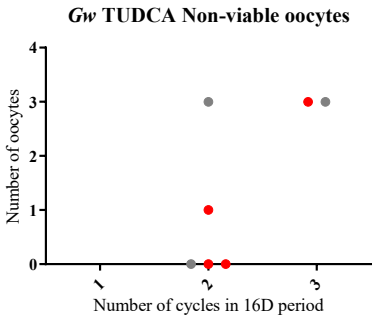
Gw TUDCA Non-viable oocytes
Number of oocytes
Number of cycles in 16D period

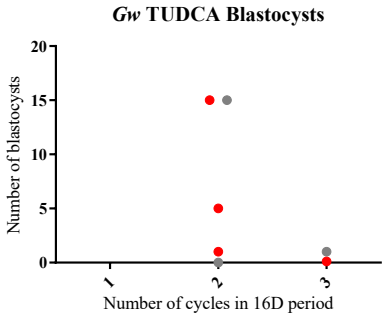
Gw TUDCA Blastocysts
Number of blastocysts
Number of cycles in 16D period

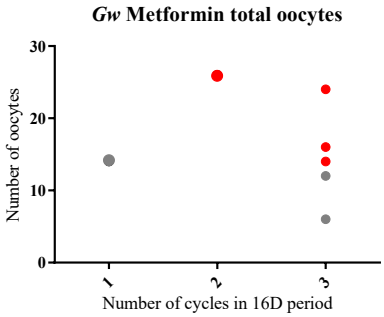
Gw Metformin total oocytes
Number of oocytes
Number of cycles in 16D period

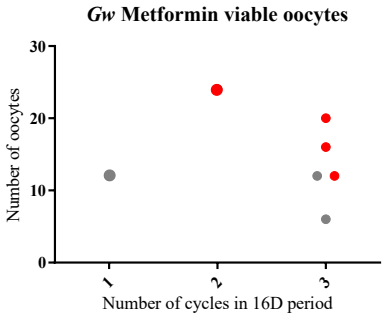
Gw Metformin viable oocytes
Number of oocytes
Number of cycles in 16D period

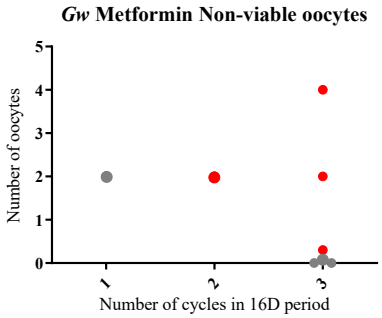
Gw Metformin Non-viable oocytes
Number of oocytes
Number of cycles in 16D period

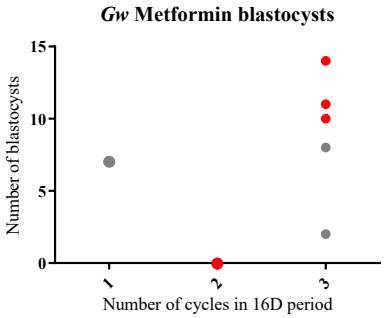
Gw Metformin blastocysts
Number of blastocysts
Number of cycles in 16D period

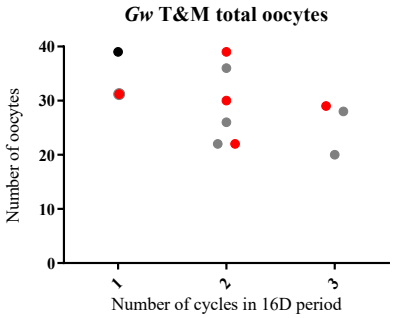
Gw T&M total oocytes
Number of oocytes
Number of cycles in 16D period

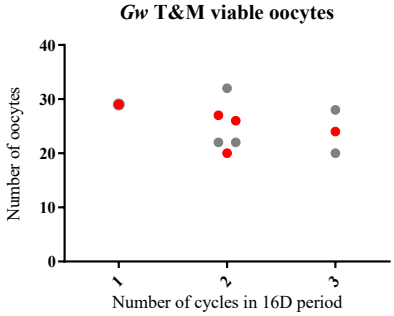
Gw T&M viable oocytes
Number of oocytes
Number of cycles in 16D period

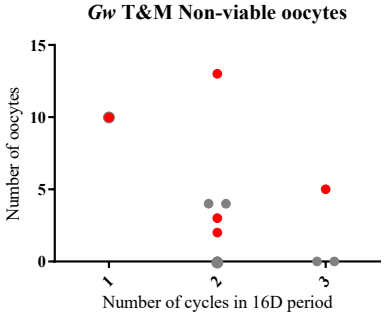
Gw T&M Non-viable oocytes
Number of oocytes
Number of cycles in 16D period

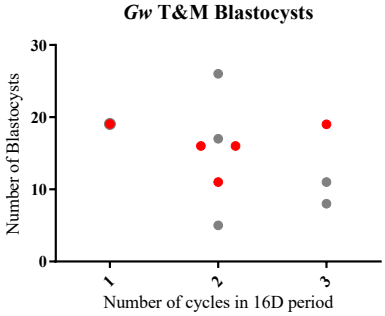
Gw T&M Blastocysts
Number of Blastocysts
Number of cycles in 16D period

3.3 Summary of p-values of various treatment groups against the corresponding non-treated *Gw* mice and FVB mice.

		No treatment	**Metformin**		**TUDCA**		**TUDCA + Metformin**	
		Against FVB	Against FVB	Against *Gw* non-treated	Against FVB	Against *Gw* non-treated	Against FVB	Against *Gw* non-treated
All *Gw*	total	ns	ns	ns	ns	**	ns	****
	Viable	#	ns	ns	ns	**	ns	****
	Non-viable	ns	ns	ns	ns	ns	ns	ns
	Blastocysts	#	ns	*	ns	ns	ns	****
	Non-fertilizable	ns	ns	ns	ns	*	ns	**
	Arrested	ns	ns	ns	ns	ns	ns	*
Gw non-obese	total	ns	ns	ns	ns	ns	ns	**
	Viable	#	ns	ns	ns	*ǂ	ns	**
	Non-viable	ns	ns	ns	ns	ns	ns	ns

	Blastocysts	#	ns	ns	ns	ns	ns	*
	Non-fertilizable	ns	ns	ns	ns	ns	ns	*
	Arrested	ns	ns	ns	ns	ns	ns	ns
Gw obese	total	ns	ns	ns	ns	ns	ns	**
	Viable	#	ns	*ǂ	ns	*ǂ	ns	**
	Non-viable	ns	ns	ns	ns	ns	ns	ns
	Blastocysts	#	ns	ns	ns	ns	ns	***
	Non-fertilizable	ns	ns	ns	ns	*	ns	ns
	Arrested	ns	ns	ns	ns	ns	ns	ns

*, (# against FVB) indicates a p-value ≤ 0.05, ** p-value ≤ 0.01, *** p-value ≤ 0.001, **** p-value ≤ 0.0001, ns = non-significant. All statistical analysis were done using the student t-test 2 tailed, except for those marked with ǂ which were analysed with one tailed student t-test.

3.19 TUDCA and Metformin effects on *Gw* female mice fertility and reproductivity.

Two-month-old *Gw* and FVB female mice were followed up for their weight and estrous cycle for 16 days. *Gw* mice were divided into obese (Ob) and non-obese (No), according to weight cut-off from previous results in Figure 3.8A. *Gw* mice (obese and non-obese) were divided into four groups and a vehicle only (water), TUDCA (T), Metformin (M), or TUDCA + Metformin (T+M), were served to each group in drinking water for 1 month. FVB mice had only the vehicle and were included with every test group as a second control (*Gw* non-treated mice were the 1st control). After the treatment duration, mice were subjected to IO and IVF as per protocols. Oocytes generated in response to IO were counted in each group and viable and non-viable oocytes were microscopically identified as previously explained in Figure 3.5B. The average number of oocytes generated in each group at day zero (D0) and the percentage of non-viable oocytes were presented in panel **A**. Oocytes were then fertilized in-vitro using freshly towed sperms from 2-months-old FVB mice, on D0. Zygotes were incubated at 37C^{o} in the presence of 5% CO_2, for four more days, and zygotes development was followed till day 4 (D4). The average number of blastocysts, the average percentage of non-fertilized oocytes (grey), and zygotes with arrested growth (black) (from the overall oocytes produced by IO) are presented in panel **B**, for each group at D4. **C** showed representative photos of the progression of zygotes, from D0 (oocytes) to D4 (blastocysts), from two obese *Gw* mice, one treated with T+M and the second with vehicle only, plus an FVB mouse, scale bar is100µm. Various stages of zygote growth were pointed out with arrows. The numbers of total oocytes, viable and non-viable oocytes, and blastocysts were separately plotted against the numbers of estrous cycles of individual *Gw* mice (obese (red dots) and non-obese (grey dots)) from each treatment group in **D**, to identify possible correlations between estrous and ovulation anomalies. A representative number of mice from each group was used. Statistical analysis of results from each of the treatment groups in comparison to *Gw* non-treated mice (1st control, (*, and **)), and FVB mice (2nd control, (#)) were presented in **Table 3.3**. The student t-test, two tails, was used for all statistical analyses with the *, (#) indicates a p-value $\leqslant$ 0.05, and the ** indicates a p-value $\leqslant$ 0.01, ns indicates non-significance, and the symbol ǂ indicates significance only when a one-tailed Student-t test is used.

CHAPTER IV: DISCUSSION AND FUTURE WORK

4.1.1 Phenotypic characterization of the *Gw* mouse model highlights its representability for the metabolic subtype of PCOS.

Rotterdam criteria are the most used criteria to diagnose PCOS (Boyle and Teede 2012). Two of its three criteria (together) are enough to diagnose PCOS in humans and to validate animal models of the syndrome as well (Bani Mohammad and Majdi Seghinsara , 2004). Our results highlighted the presence of hyperandrogenism, PCOM, and oligo-ovulation, in around 60% of *Gw* mice with various degrees of severity.

Persistently high GnRH levels are known to cause persistently high LH levels, and therefore a lack of an efficient LH surge which in turn causes oligo and/or anovulation, besides persistently low FSH levels which cause follicular growth arrest, in PCOS patients (Rosenfield and Ehrmann 2016, Chaudhari, Dawalbhakta et al. 2018). Persistently high LH levels are also a direct cause of hyperandrogenaemia in PCOS patients, among other causes (Rosenfield and Ehrmann 2016, Arao, Hamilton et al. 2019). High plasma T levels directly inhibit follicular growth and increase atretic follicles in PCOS patients (Chen, Chou et al. 2015, Rosenfield and Ehrmann 2016). Our results showed high LH and T levels, oligo-ovulation, and high numbers of atretic follicles among a large proportion of *Gw* mice compared to FVB mice. LH and T levels were measured at a single time point initially in this work, and they were still significantly higher among *Gw* mice compared to FVB mice (at 2-, 4-, and 6- months

of age). Considering the pulsatile nature of the LH hormone, a detailed evaluation of LH levels and pulse frequencies was done, after the initial submission of this work, by collaborating colleagues, and was later added as a supplementary figure with the permission of Prof. N. Pilon, S.Fig. 5.1. LH hormone pulse frequency and plasma levels were both higher among *Gw* mice compared to FVB mice, which is confirmatory and complementary to our initial results. Further supplementary images were also added in Appendix A to highlight cysts formation in the ovaries of *Gw* mice, and the abundance of fat deposits in their peri-follicular area, S. Fig 5.3, 5.4, respectively.

PCOS patients are also known to have a wide range of metabolic anomalies including, impaired glucose tolerance, hyperinsulinemia, and insulin resistance, plus obesity among a large proportion of them (Diamanti-Kandarakis 2006, Sam 2007, Rojas, Chávez et al. 2014). Both hyperinsulinemia and impaired insulin tolerance are prominent in PCOS patients, regardless of their weight (Cree-Green et al., 2017). Interestingly obesity among PCOS patients is not always present but it is rather an important aggravating factor (Goyal and Dawood 2017). Further characterization of the *Gw* mouse model led to the identification of similar metabolic anomalies, in a similarly large cohort of the mice, including obesity, impaired glucose and insulin tolerance, increased adipocytes size and number, and high plasma levels of leptin and insulin hormones. *Gw* mice also showed reduced numbers of pups, and oocytes (upon IO), plus estrous cycle anomalies, and hormonal irregularities, regardless of their weight, with most of these anomalies being more severe among obese mice. Further work would be needed to validate the presence of insulin resistance among *Gw* mice as our results are only suggestive of it. This could be achieved by relative quantification of insulin receptor gene expression levels and insulin receptor signalling pathway study. On a molecular level, *Gw* mice showed high ER stress levels and significant collagen deposition in the stroma of their ovaries (compared to FVB mice), with these pathologies being more severe among the obese mice as well. This is again consistent

with what is known in PCOS patients and mouse models, (Zhou, Shi et al. 2017, Azhary, Harada et al. 2020).

Trials are currently going on to study AMH levels in PCOS patients and evaluate their use as early diagnostic markers for this syndrome (Bani Mohammad and Majdi Seghinsara). Plasma levels of AMH were found to be higher among PCOS patients compared to healthy females of the same age and weight (Sahmay, Aydin et al. 2014). Interestingly, *Gw* mice did not show the high levels of AMH known in PCOS patients (Sahmay, Aydin et al. 2014, Zadehmodarres, Heidar et al. 2015, Carmina, Guastella et al. 2016), while they maintained the usual patterns of healthy people where AMH levels decrease with age and obesity (Moy, Jindal et al. 2015). This discrepancy in AMH levels between PCOS patients and *Gw* mice could be attributed to the wide variability of different features of the syndrome in *Gw* mice which could affect AMH levels. For example, AMH levels, in humans, are known to be sensitive to obesity and androgen levels, which are widely variable in *Gw* mice (Moy, Jindal et al. 2015, Rosenfield and Ehrmann 2016). Worth mentioning here that AMH is not currently used as a diagnostic criterion or considered as a constant feature of PCOS in humans until the time of writing of this thesis because of its wide variability between patients (Carmina, Guastella et al. 2016, Bani Mohammad and Majdi Seghinsara 2017).

Detailed characterization of the *Gw* mouse model and careful comparison to phenotypes of most used mouse models, as well as the human phenotype, led us to identify a 74% similarity to the human phenotype, particularly the metabolic spectrum of the syndrome. The criteria used for this evaluation were obtained from an extensive review of the literature to identify most of the documented features of the syndrome in humans and the three most used mouse models (Nikolaou and Gilling-Smith 2004, Wickenheisser, Nelson-Degrave et al. 2005, Manneras, Cajander et al. 2007, Roland, Nunemaker et al. 2010, Habib, Richards et al. 2012, van Houten, Kramer et al. 2012,

Chakrabarti 2013, Moore, Prescott et al. 2013, Caldwell, Middleton et al. 2014, Kauffman, Thackray et al. 2015, Fornes, Maliqueo et al. 2017, Takahashi, Harada et al. 2017). The closest next mouse model to the human phenotype was the LET-induced mouse model with a similarity of 64%. Considering the wide spectrum of PCOS presenting symptoms and the close similarity between the metabolic anomalies of *Gw* mice and those of PCOS patients, we concluded that the *Gw* mouse model is highly representative of the metabolic spectrum of the PCOS.

4.1.2 Genotypic characterization of the *Gw* mouse model leads to a new hypothesis for PCOS development.

4.1.2.1 Transgene insertion site and affected gene in *Gw* mice

We confirmed the transgene insertion site using whole genome sequencing and 10X linked reads sequencing techniques, and by the amplification of the transition events from gDNA to the transgene and backward. The main query we had here was whether the observed phenotype, among *Gw* mice, was caused only by the disruption of the *Gm10800* gene, or were there other factors involved? Whole-genome sequencing and mapping analysis confirmed a single insertion site for the transgene, with no other genomic anomalies detected. We analyzed the *Gm10800* gene and extracted the ORF within its sequence and confirmed it using the RACE protocol to identify its predicted protein. Amino acid sequence analysis of the predicted protein showed five transmembrane domains containing receptor-like protein like a human PIRO protein. In humans, the *PIRO* family of genes codes for proteins responsible for forming multinucleated giant osteoclasts (Oh, Kim et al. 2015). We successfully subcloned the cDNA of the predicted ORF with a *Myc*-tag on the 3’ end (in one construct) and the 5’ ends (in another construct) in an expression vector. Our trials did not show any protein translated from the identified ORF in either N2A or COS7 cells. All experiments were validated by a co-transfected *Gfp* expressing vector. A further validation step for the

sub-cloning and cell expression was done using another construct containing the cDNA of a FAM172 protein (family with sequence similarity 172 member A) with success. We concluded that the ORF identified within the *Gm10800* gene does not code for any protein. We did an extensive review of the literature and protein libraries and there were not many studies available on this gene, its gene family, or even its predicted protein in general. Furthermore, there was no data in the literature about any successful isolation of the predicted protein of the *Gm10800* gene. The expression levels of the *Gm10800* gene were assessed in only one study by Kim et al. in 2015 (Oh, Kim et al. 2015).

4.1.2.2 The role of the transgene in the phenotype of *Gw* mice

We next generated a KO of the *Gm10800* gene mouse model, using CRISPR technology and characterized it, $Gm10800^{KO/KO}$. Our analysis of the weight charts and number of pups generated by this new mouse model did not show any of the previously observed phenotypic anomalies among *Gw* mice. We, therefore, concluded that the disruption of the *Gm10800* gene, by transgene insertion, is not the only factor causing the fertility and metabolic anomalies observed in *Gw* mice. Worth mentioning here that multiple other mouse models were generated using the same transgene and insertion technique and none of them developed PCOS phenotype (Pilon, Raiwet et al. 2008). This fact excludes that the transgene sequence is responsible alone for the phenotype of *Gw* mice. Hence, we hypothesized that the transgene sequence (*Gata4* promoter) together with this insertion site (within the *Gm10800* gene) generated the observed phenotype of *Gw* mice. We hypothesized that the *Gata4* promoter component of the transgene is competing with the intrinsic *Gata4* promoter (which drives the intrinsic *Gata4* gene) for upstream transcription factor family of factors, like USF2 that normally binds to the critical E-box motif to activate the intrinsic *Gata4* promoter (Mazaud Guittot, Tetu et al. 2007).

We concluded that other mice, with the same transgene (Pilon, Raiwet et al. 2008), did not develop a similar phenotype to that of *Gw* mice because of the differences in the transgene insertion sites, and the difference in the 4 dimensional chromatin structure between various cells, according to their function. DNA in eukaryotes cells is condensed in a form of compact chromatin to minimize its size, protect it from oxidative damage and allow for selective genes transcription based on various cell functions (Chung, Ketharnathan et al. 2016). Chromatin regions are unfolded during different phases of the cell cycle, and depending on its function, to allow the access of various transcription factors to needed genes (Tark-Dame, van Driel et al. 2011). Cell identity is defined by the specific set of genes it expresses, which determines cell organelles, receptors, enzymes, and functions. It is possible that the neurons of the ARC nuclei, of *Gw* mice, unfold their genome around the transgene insertion site (within the *Gm10800* gene), exposing the transgene in the process. This allows for the exposed transgene to compete with the intrinsic *Gata4* promoter, of various other transcription available genes, over upstream transcription factors. In other mouse models, the transgene was most likely inserted in a region that, when unfolded, exposes the transgene to genes not dependent on the consumed upstream transcription factors. This can be further validated in future work through chromosome conformation capture technology.

4.1.2.3 *Gata4* gene under expression dysregulates the expression of various genes in *Gw* mice

The *Gata4* gene codes the GATA4 transcription factor which is a member of a large family of factors known as the GATA family. The role of the GATA4, along with other members of the GATA family of transcription factors, in the development, reproduction, and fertility is well established in the literature (Viger, Guittot et al. 2008, Kyronlahti, Euler et al. 2011, Efimenko, Padua et al. 2013). Multiple studies have identified binding sites for members of this family within the promoter region of the

Gnrhr gene in the pituitary (Pincas, Amoyel et al. 2001), and the placenta, (Cheng, Chow et al. 2001) (GATA factors 2 and 3, respectively). GATA4 transcription factor was found to be expressed in the developing GnRH neurons in the hypothalamus (Lawson and Mellon 1998). Another study also found GATA4 having a vital role in regulating the GnRH pulse frequency through its binding to the neuron-specific enhancer portion of the *Gnrh* gene promoter (Leclerc, Bose et al. 2008). GATA4 is also known to play a crucial role in controlling the expression of FSH and LH hormone receptors in the testicles (Rahman, Kiiveri et al. 2004, Hermann and Heckert 2005). Furthermore, multiple GWAS identified the *GATA4* gene as one of the persistent gene loci among PCOS patient common genetic susceptibility loci (Hayes, Urbanek et al. 2015, McAllister, Legro et al. 2015, Hayes, Urbanek et al. 2020).

Our results have shown that the expression levels of the *Gata4* gene in the brains/ARC nuclei of *Gw* mice were significantly lower than that of FVB mice since early development and at E11.5, P14d, and P4m points of age. This could be due to the binding of the upstream transcription factors to the extrinsic *Gata4* promoter, making them less available for the intrinsic promoter of the *Gata4* gene, and other genes as well. Worth mentioning here that a single transcription factor can bind to the promoter region of multiple different genes (Bhattacharjee, Renganaath et al. 2013), therefore the extent of affected genes by the scarcity of the above-mentioned transcription factors is yet undiscovered. We also predict that the observed reduction in the expression levels of the GATA4 transcription factor in the ARC of the *Gw* mice, along with potentially other transcription factors dysregulation, are responsible for the observed decrease in the expression levels of different reproductive hormones receptors genes, including *Esr1, Pgr, Fshr, Lhr,* and *Gnrhr,* in the ARC as well. This under expression of receptors may have caused some degree of hypothalamic resistance to hormonal feedback signals which may have consequently caused the hormonal dysregulations observed among *Gw* mice. These hormonal irregularities included high *Gnrh* gene expression level (in

the ARC neurons), and elevated plasma levels of E2, T and LH at different age points. Interestingly, high levels of *Gnrh* gene expression were observed in *Gw* mice around the age of 4 months, concomitantly with low levels of *Gnrhr* gene expression at the same age point. These results suggest some degree of hypothalamic resistance to GnRH autoregulatory negative feedback signals, caused by the under expression of the *Gnrhr* gene, and eventually leading to a compensatory persistently high *Gnrh* gene expression, and GnRH levels, at four months of age.

The hypothalamus and the pituitary have reproductive hormone receptors to sense positive and negative feedback signals from the ovaries and the pituitary to maintain the delicate hormonal balance needed for reproduction. The under expression of genes coding for these receptors (*Esr1, Pgr, Fshr, Lhr,* and *Gnrhr*), in the *Gw* mice ARC nuclei, made *Gw* mice less sensitive to the E2 hormone feedback signals (among others), which, in turn, leads to a disinhibition of the *Gnrh* gene expression as shown in the results. The GATA4 transcription factor (under expressed in the *Gw* mice), through its binding to the neuro-specific enhancer portion of the *Gnrh* gene promotor, increases its expression (Leclerc, Bose et al. 2008). This finding means that we should have observed a concomitant under expression of the *Gnrh* gene with the under expression of the *Gata4* gene observed in *Gw* mice. This discrepancy could be due to the complexity of the *Gnrh* gene expression regulation process. This process includes multiple other factors besides the GATA4, for example, insulin-like growth factor, in humans (Zhen, Zakaria et al. 1997, Mancini, Howard et al. 2019), Kisspeptin, in humans and mice, (Messager, Chatzidaki et al. 2005, Navarro, Gottsch et al. 2009, Kirilov, Clarkson et al. 2013), plus, E2 receptor-beta, orthodenticle homeobox 2, early growth response protein 1, and insulin, in mice, (Cameron and Nosbisch 1991, Huang and Harlan 1993, Topilko, Schneider-Maunoury et al. 1998, Rave-Harel, Givens et al. 2004). These factors exert their effect through different binding sites on the *Gnrh* gene promoter region. Furthermore, the enhancer and suppressor regions (upstream of the

promoter) regulate *Gnrh* gene expression. These regions are subjected to multiple regulatory factors, including, Octamer-binding site 1, Pbx/Prep1, GATA, CCAAT enhancer-binding proteins in rats (Nuñez, Faught et al. 1998).

Among other important regulatory factors are tissue specificity cofactors in mice (Kim, Wolfe et al. 2002). Cofactors bind to variable transcription factors to regulate *Gnrh* production in a tissue-specific manner in GnRH neurons and ovaries (Biggin and McGinnis 1997). Enhancer region factors also influence *Gnrh* gene episodic expression, in close relation to GnRH pulsatile release (Kepa, Spaulding et al. 1996, Lee, Lee et al. 2008). From another side, the *Gnrh* gene overexpression in *Gw* mice could also be due to some degree of hypothalamic/ARC resistance to regulatory feedback signals, which is suggested by our results through the under expression of variable reproductive hormones receptors in the hypothalamus/ARC. FSH and LH both downregulate *Gnrh* gene expression in Gnrh neurons via hypothalamic neurons that possess their receptors (Lei and Rao 1994, Lei and Rao 1995, Lee, Lee et al. 2008). E2 and P4, through their nuclear receptors, exerts a dual effect on *Gnrh* gene expression through specific binding sites on *Gnrh* gene promoter, depending on the hormone level and when in the cycle the gene expression was measured (Lee, Smith et al. 1990, O'Byrne, Thalabard et al. 1991, Radovick, Ticknor et al. 1991, Roy, Angelini et al. 1999). Multiple other hormones and peptides influence *Gnrh* gene expression and pulse frequency, including, insulin, insulin-like growth factor, melatonin, nitric oxide, GABA, and retinoic acid (Lee, Lee et al. 2008).

The effects of the under expression of the *Gata4* gene on the regulation of the *Gnrh* gene expression and pulse frequency are yet to be fully explored to better understand the origin of the phenotype of *Gw* mice. As a future step, we could evaluate the expression levels of genes coding other regulatory factors in the hypothalamus/ARC of *Gw* mice by qPCR in comparison to FVB mice. Worth mentioning here is that the

mRNA expression levels of KNDy neuropeptides, in ARC neurons of *Gw* mice, were later evaluated in the laboratory of professor N. Pilon and the results were consistent with our hypothesis of neuroendocrine circuit disturbance in *Gw* mice. All 3 KNDy neuropeptides were deregulated in *Gw* mice compared to FVB mice where Kiss and NKB neuropeptides were overexpressed, and the Dyn neuropeptide was under expressed in *Gw* mice, S. Fig 5.2. IF technique can also be used to map the *Gnrh* neuroendocrine regulatory network in *Gw* mice to identify any existing developmental anomalies compared to FVB mice. This should be first tested on adult mice hypothalamus to identify any neuronal rearrangement in the neuroendocrine circuit regulating GnRH release, then followed up in embryonic brain samples. POMC and SF1 can be used as specific markers for ARC and VMH nuclei, respectively.

On a metabolic level, anomalies were identified in the expression of various genes coding for metabolic neuropeptides in the ARC nuclei of *Gw* mice compared to FVB mice, at E11.5, P14d, and P4m points of age. The expression level of the *Pomc* gene was the only one that reached a statistically significant low level in *Gw* mice compared to FVB mice, at four months of age. POMC is a well-known neuropeptide that induces satiety in the hypothalamus and increases energy expenditure (Millington 2007), therefore, *Pomc* under expression in the ARC of *Gw* mice could explain their overfeeding (polyphagia) behaviour compared to the FVB mice. Interestingly, mice with polyphagia also had high plasma levels of leptin hormone (particularly *Gw* obese mice), a satiety hormone (Hill, Elias et al. 2010). The presence of polyphagia and overweight, and high leptin hormone levels, in the same mouse, suggests hypothalamic resistance to leptin, which was supposed to inhibit the feeding centre in the hypothalamus of the *Gw* mice. In literature, PCOS rat models, induced using LET injection present with leptin resistance and polyphagia (Lian, Zhao et al. 2016). Furthermore, PCOS patients are known to have high levels of leptin hormone, which is positively correlated with their obesity and insulin hormone levels (Chakrabarti

2013). Finally, leptin hormone has also been found to play a key role in post-transcriptional regulation of GnRH levels, hence, leptin receptor deficient mice are infertile (Odle, Akhter et al. 2018).

On the other hand, neuropeptides coded by *Agrp* and *Nyp* genes stimulate the feeding centre and decrease energy expenditure, inducing, therefore, weight gain (Ahima and Antwi 2008). Interestingly, expression levels of these two last genes, in ARC nuclei, were not significantly different between *Gw* and FVB mice, at four months of age. During development, expression levels of the *Agrp* gene were significantly lower in the brains of *Gw* mice compared to FVB mice, at E11.5. On the other hand, the levels of the *Nyp* gene were significantly higher in *Gw* mice compared to FVB mice at the same embryonic age point. These early high levels of *Npy* gene expression could be explained by the high developmental need to suppress energy expenditure during the embryonic period to allow weight gain at this time point (E11.5). A possible further analysis of these results could be done by evaluating the expression levels of these two genes in obese and non-obese *Gw* mice separately and comparing them to FVB mice, at the age of 4 months, to exclude the factor of weight. These tests are not feasible at earlier time points as obesity starts at 2 months of age and reaches a significant level at 4 months of age. Our results strongly suggest a genetic origin for this syndrome, which causes some degree of hypothalamic resistance to reproductive hormones, and metabolic neuropeptides signals, with a possible peripheral tissue resistance as well. In humans, genetic susceptibility is potentiated by environmental factors that promote obesity, which is a significant aggravating factor for various PCOS pathologies (Rojas, Chávez et al. 2014, Rosenfield and Ehrmann 2016).

A detailed characterization of brains of *Gw* mice, particularly hypothalamic neurons, is still needed to better understand the origin and the extent of observed hormonal receptors gene expression anomalies in *Gw* mice ARC nuclei. Furthermore, the study

of the migration of GnRH neurons, during embryogenesis, would help to detect developmental anomalies in *Gw* mice. Mapping adult *Gw* mice hypothalamic neurons (using IF), and comparing them to FVB mice, could also give valuable information about possible neuronal arrangement anomalies in various hypothalamic nuclei. To validate and further characterize the hypothesis of hypothalamic and peripheral tissues resistance, the function of hormone receptors (*Esr1, Pgr, Fshr, Lhr,* and *Gnrhr*) could be analyzed in ARC nuclei of adult *Gw* mice, alongside insulin signalling in peripheral tissues as well. Insulin signalling can be assessed on multiple levels, for example, the phosphorylation patterns of serine residues of IRS1 and AKT. The study of the neuroendocrine circuit regulating the secretion and pulse frequency of GnRH could also give an insight into the observed high levels of *Gnrh* gene expression in the ARC nuclei of *Gw* mice.

4.1.3 High ER stress level, in *Gw* mice ovaries, is a key reversible event and a route for a new therapeutic for PCOS.

One of the most prominent molecular events identified among PCOS patients and mouse models is the elevated levels of ER stress, which causes low-grade chronic inflammation in their ovaries. This chronic inflammation affects the competency (viability) of oocytes, alters their growth and increases the rates of failed IVF attempts in PCOS patients as well (Metwally, Cutting et al. 2007, Wu, Russell et al. 2015). Chronic inflammation also leads to ovarian fibrosis in the long term (Qiao and Feng 2011, Palomba, Daolio et al. 2017). High ER stress levels in PCOS patients and mouse models are attributed to multiple factors including hyperinsulinemia, high T. hormone levels, and the direct lipotoxic effect of excess fat deposition in the ovaries (Nestler 1997, Cui, Ma et al. 2013, Chen, Chou et al. 2015, Wu, Russell et al. 2015, Rosenfield and Ehrmann 2016, Cree-Green, Rahat et al. 2017, Lima, Nivet et al. 2018, Azhary, Harada et al. 2019).

Our IF results have shown higher ER stress levels in the peri-follicular area of ovaries from *Gw* mice compared to FVB mice, using three different ER stress markers, CHOP, ATF6, and IRE1, at four months of age. These levels got even higher as mice progressed in age to 6-months-old. These findings are in line with what is known in PCOS patients and mouse models. Ovaries of *Gw* mice also showed higher collagen deposition levels compared to ovaries of FVB mice, at six months of age, which is again consistent with what is found in PCOS patients. Our IO and IVF results had also shown that *Gw* mice have higher numbers of non-viable oocytes (fragmented or dead) and zygotes with arrested growth than FVB mice. The presence of these key pathologies in *Gw* mice further validated the model as a representative mouse model for PCOS and strongly suggests that the same pathophysiology of PCOS patients occurs in *Gw* mice.

TUDCA, an ER stress inhibitor, is a modified molecule of ursodeoxycholic acid (taurine conjugated) that is approved by the Food and Drug Administration for treating some biliary conditions, like primary biliary cholangitis, with promising results and minimal side effects profile (Bahar, Wong et al. 2018, Mahabadi3. 2020). Multiple studies and clinical trials are currently testing TUDCA for various other medical conditions (Vang, Longley et al. 2014, clinicaltrials.gov 2019). ER stress inhibitors (salubrinal, BGP-15, and TUDCA) have been showing promising results in improving oocytes viability by reducing ER stress levels in various PCOS mouse models, and by reducing the lipotoxic effect of FFAs on oocytes in obesity mouse models (Wu, Russell et al. 2015, Azhary, Harada et al. 2019). Our results have shown that TUDCA was able to increase the overall number of oocytes, and the percentage of viable oocytes, produced by *Gw* mice in response to IO to a similar level to that of the FVB mice. These results are consistent with what has been shown in the literature using various ER stress inhibitors, in PCOS and obesity mouse models, improving ER stress levels, and oocytes viability (Azhary, Harada et al. 2019, Takahashi, Harada et al. 2019,

Azhary, Harada et al. 2020). The Metformin treatment, an insulin sensitizer, and a reducer of hepatic gluconeogenesis had a similar effect to that of TUDCA in improving the overall number of oocytes and the percentage of viable oocytes, but only among obese *Gw* mice, and to a lesser extent compared to TUDCA, at D0. The fact that the effect of Metformin treatment (at D0) was observed only among obese *Gw* mice is consistent with its mechanism of action as an insulin sensitizer, which improves insulin resistance and hyperinsulinemia, while it could not reverse other causes of high ER stress in non-obese *Gw* mice (Velazquez, Mendoza et al. 1994). Finally, the combination of TUDCA and Metformin had a synergistic effect in improving the overall number of oocytes, and the percentage of viable oocytes, produced by *Gw* mice (obese and non-obese) in response to IO.

IVF experiments had two main goals, first to double-check the viability of the apparently normal oocytes produced by IO, second to test the effect of various treatments on embryo development until the blastocyst stage, on the 4th day of IVF (D4). Surprisingly, although TUDCA increased the overall number of oocytes, a significant percentage of 'apparently' viable oocytes were non-fertilizable following IVF, and this percentage was higher than the percentage in non-treated *Gw* and FVB mice. On the other hand, the percentage of zygotes with arrested growth had improved significantly among treated *Gw* mice, compared to non-treated *Gw* mice. We think that the limited effect of TUDCA on obese *Gw* mice is probably secondary to the added lipotoxicity caused by excessive free fatty acids in obese mice. The overall increase in oocytes numbers, produced by TUDCA treated *Gw* mice, was large enough to compensate for the high percentage of non-viable oocytes and to improve the overall subfertility of *Gw* mice, manifested by the higher number of blastocysts, at D4, compared to non-treated *Gw* mice. TUDCA results at D0 reached FVB mice numbers, but not at D4, which makes the TUDCA effect only partial in improving *Gw* mice subfertility.

Metformin treatment, on the other hand, improved the final percentage of non-fertilizable oocytes, zygotes with arrested growth, and blastocysts (at D4) among treated *Gw* mice compared to the non-treated *Gw* mice. The effect of Metformin at D4 was also more prominent among treated obese *Gw* mice compared to treated non-obese *Gw* mice, which is consistent with our observation at D0 and its mechanism of action. Results from clinical trials on PCOS patients were variable regarding the efficacy of Metformin in improving IO and IVF outcomes (Palomba, Falbo et al. 2014, Tso, Costello et al. 2014, Christianson, Wu et al. 2015). Metformin treatment in PCOS mouse models, on the other hand, had similar results to ours, with only a partial rescue of the PCOS phenotype, particularly oocytes viability, and mainly among obese mice (Huang, Yu et al. 2015).

The combination of TUDCA and Metformin treatment had a synergistic effect on improving the overall numbers of blastocysts, reducing zygotes with arrested growth, and non-fertilizable oocytes, among treated *Gw* mice (obese and non-obese). The results of the combination treatment reached levels higher than those of FVB mice, at D4. These results suggest a promising role for TUDCA, in improving the responsiveness of PCOS patients to IO and IVF, particularly when used in combination with Metformin. This would eventually reduce the number of IVF attempts needed to treat PCOS patients, which are usually very costly.

Further work is needed to test the effect of TUDCA, separately and in combination with Metformin, on naturally occurring pregnancy in *Gw* and other PCOS mouse models. Next, the side effects profile, of each treatment, on *Gw*, FVB, and other PCOS mouse models, would also need to be studied before progressing into clinical trials of this new molecule. We did not observe any side effects in any test mouse from various treatment groups, till the time of writing of the work. Metformin in humans is known to cause minimal side effects like mild abdominal pain, appetite reduction, occasional

diarrhea, nausea, and vomiting (BNF 2021). TUDCA on the other hand does not have any reported side effects in the limited number of studies done on it (Pan, Zhao et al. 2013).

Gene therapies also represent a promising chance for a definitive cure for this syndrome. This could be done by an attempt to rescue the expression of the *Gata4* gene in the ARC nuclei of *Gw* mice and possibly other PCOS mouse models. A neurotropic virus envelope can be used to deliver a genetic core, composed of a *Gata4* gene driven by a neuro/ARC specific promoter, specifically to neurons of ARC nuclei in the hypothalamus of *Gw* mice. This virus can be directly injected into the hypothalamus through micro-surgery or into the cerebrospinal fluid that circulates the brain. The viral construct and infection techniques could be tested and validated *in vitro* using immortalized GnRH-expressing neuronal cells, for example, the GT1 cell line (Cheng and Leung 2005).

CONCLUSIONS

We conclude that the *Gw* mouse model is a representative mouse model for the metabolic spectrum of PCOS. We also conclude that obesity is not the primary pathology causing the sub/infertility phenotype among *Gw* mice but rather an important aggravating factor. Our hypothalamic results suggest a central origin for PCOS evidenced by the *Gata4* gene expression anomalies identified in *Gw* mice, plus the under expression of various hormonal receptor genes in their ARC. This brain involvement is new to the known *Gata4* expression anomalies identified in ovaries of PCOS patients. These results also support our emerging hypothesis of hypothalamic resistance, possibly with some peripheral tissues resistance, as well, as the origin of this syndrome. We also predict that the transgene sequence, alone, does not produce the phenotype, but rather the combination of the transgene sequence (*Gata4* promoter) and its insertion site (within the *Gm10800* gene) is responsible for the phenotype. We finally conclude that TUDA, particularly when used in combination with Metformin, has a promising effect on improving the response of PCOS patients and mouse models to IO and IVF, through increasing their producibility of oocytes and enhancing oocytes quality/viability.

APPENDIX A

SUPPLEMENTARY FIGURES

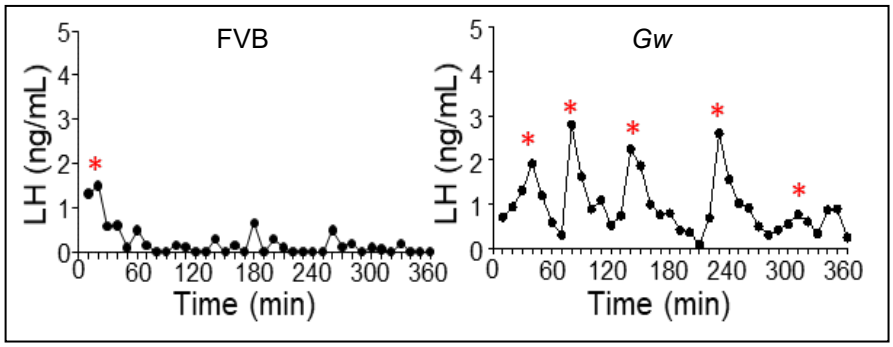

5.1 LH pulse frequency differences between *Gw* and FVB mice.

A representative figure of plasma LH levels for 6 hours analysis of one FVB and one *Gw* mouse. Red asterisks mark peaks of LH level in each mouse. N=8 mice were tested in total, and the figure shows the results of a one represents mouse from each group. This experiment was done after the initial submission of this work by a colleague in the laboratory of professor N. Pilon (S. Nawaito) in collaboration with professor D.B and was added to Appendix A after her permission and that of professor N. Pilon.

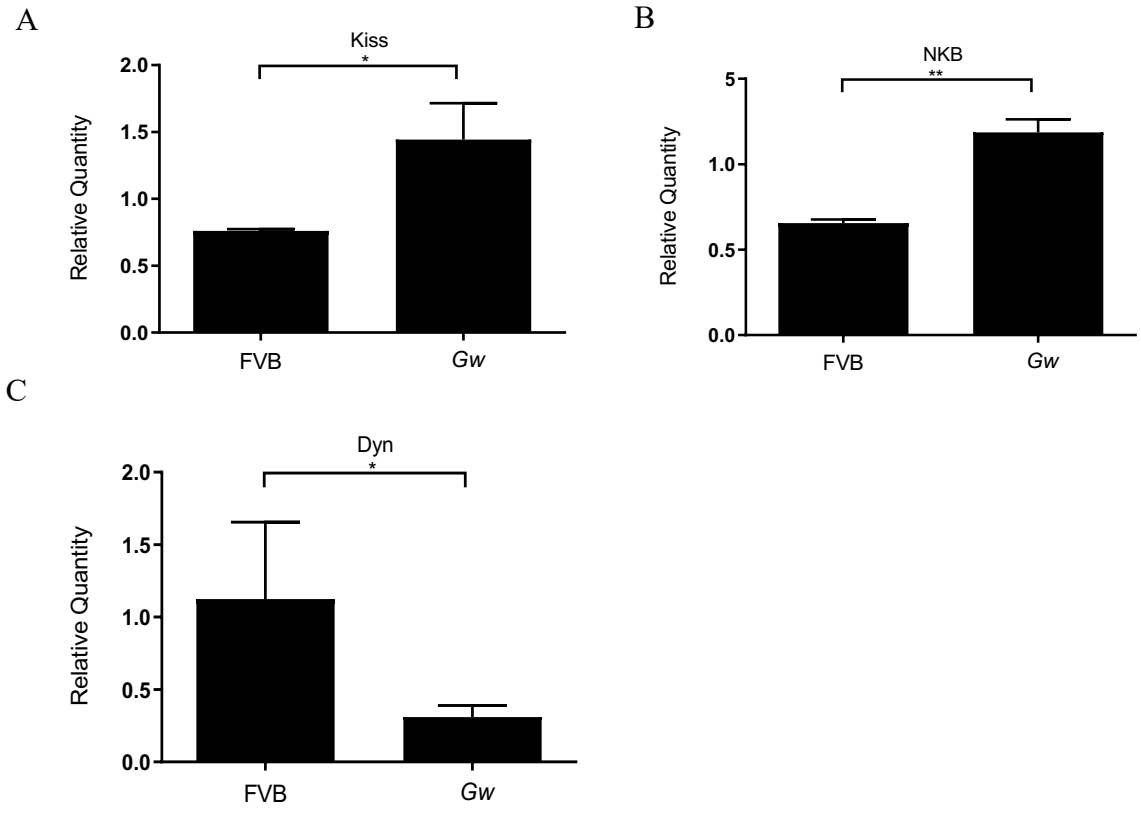

5.2 KNDy mRNA levels in *Gw* and FVB mice ARC neurons.

The figure represents the average quantification of Kisspeptin, NKB and Dyn's mRNA levels (**A, B,** and **C** respectively), by qPCR, in *Gw* and FVB mice hypothalamus (n=5 mice per group). These experiments were also done after the initial submission of this work by a colleague in the laboratory of professor N. Pilon (S. Nawaito) and were later added to Appendix A after her permission and that of professor N. Pilon.

5.3 *Gw* obese mouse ovary with cystic changes.

Hematoxylin and eosin-stained histological section of an ovary from a 6-months-old *Gw* obese mouse showing cystic changes characteristic of PCOS. No growing follicles or CL were identified in this section. Asterisks mark cysts.

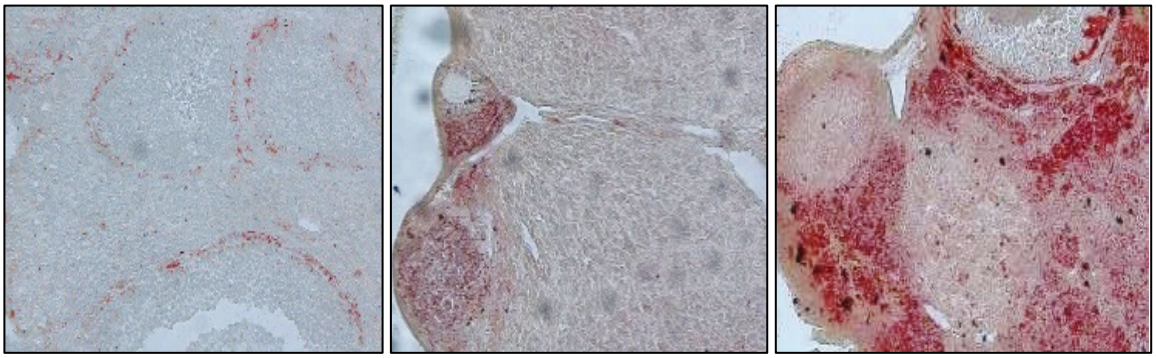

FVB *Gw* non-obese *Gw* obese

5.4 Fat distribution in the peri-follicular area of ovaries of *Gw* and FVB mice.

Oil red-stained histology sections of ovaries from 6-months-old FVB, *Gw* non-obese and *Gw* obese mice show higher levels of peri-follicular fat deposits in both the *Gw* non-obese and obese mice, compared to FVB mice. Like previously shown results in Fig. 3.10, ovaries of *Gw* obese mice showed the highest levels of peri-follicular fat deposits.

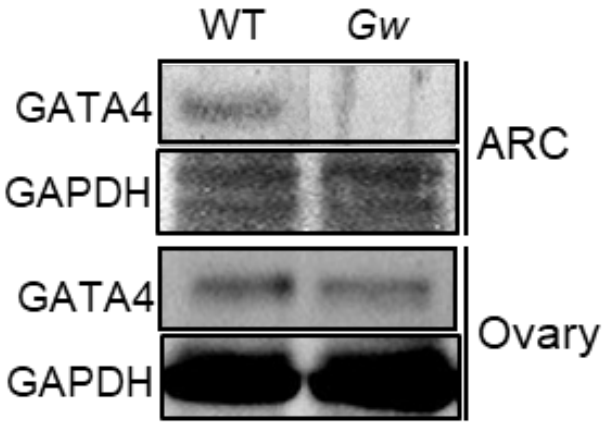

5.5 *GATA4* protein levels in the ovaries and ARC nuclei of *Gw* and FVB mice.

Western Blot results demonstrate the differences in the GATA4 protein levels in the ARC nuclei (decreased) and ovaries (no change) of *Gw* compared to FVB mice at the age of 4 months. GAPDH was used as a reference protein in both experiments.

APPENDIX B

PRESENTATIONS AND SCIENTIFIC DAYS AND CONFERENCES

- Esmael M, Karl-F. Bergeron, Robert Viger, Catherine Mounier and Nicolas Pilon (2018-19). *G4* (the old name for the *Gw* mouse model) Transgenic Mouse Model for PCOS Responding to Metformin and ER Stress Inhibitor (TUDCA) Treatment.
  - → The Society of reproductive investigation conference, in Paris, France March 2019.
  - → *G4* is a new transgenic mouse model for polycystic ovary syndrome.
  - → 'Fertility 2018' conference, Liverpool, UK, oral presentation.
  - → SQLNM, Magog, Canada, February 2018, poster presentation.
  - → 'Society of reproductive investigation, (SRI)' conference, San Diego, March 2018, late-breaking abstract, poster presentation.
- Esmael M, Karl-F. Bergeron, Robert Viger, Catherine Mounier and Nicolas Pilon (201-16). Characterization of a new genetically induced mouse model for PCOS.
  - → 8eme Symposium de Réseau Québécois en reproduction (RQR), Montréal, 2015.
  - → Société Québécoise de Lipidologie de Nutrition et métabolisme (SQLNM) réunion annuelle, 2016.
  - → Centre de recherche du diabète de Montréal (CRDM) réunion annuelle, 2016.

→ Le 84e Congrès de L'Association Francophone Pour Le Savoir (l'Acfas), 2016.

- Esmael, M (2015). Regulation of Lipocalin Prostaglandin-D Synthase expression by interleukin-1β in Human chondrocytes. Oral presentation of my master's project at Cr-CHUM scientific day.
- Esmael, M (2014). LKB1-Mutant and Lung Cancer. Oral presentation at McGill University, Canada.
- Esmael, M (2014). Self-organizing optic-cup morphogenesis in three-dimensional culture. Oral presentation at McGill University, Canada.
- Esmael, M (2014). PET scan and its role in research. Oral presentation at McGill University, Canada.
- Esmael, M (2014). Peer assessment committee member at McGill University.
- Participated in research ethics training at Case Western Reserve University, Ohio, USA, 2010, emergency medicine department.
- Observe-ship at Cleveland Clinic, Ohio, USA, 2010, obstetrics and gynecology department).
- Esmael M (2005-2010). Clinical guidelines and up-to-date practice skills. Presentations and scientific journal presentations as part of continuous medical education (CME) during my medical residency program in Egypt.

APPENDIX C

SCHOLARSHIPS AND AWARDS

- Pfizer-SRI President's Presenter's Award 2019
- Travel award, Biochemistry department, UQAM. 2018
- Réseau Québécois en reproduction CIRD scholarship 2018
- Centre d'évaluation des diplômés internationaux en santé. 2016
- Bourse D'excellence, University of Montreal, Canada. 2014

REFERENCES

(2004). "Revised 2003 consensus on diagnostic criteria and long-term health risks related to polycystic ovary syndrome (PCOS)." Hum Reprod **19**(1): 41-47.
Abbott, D. H., A. F. Tarantal and D. A. Dumesic (2009). "Fetal, infant, adolescent and adult phenotypes of polycystic ovary syndrome in prenatally androgenized female rhesus monkeys." Am J Primatol **71**(9): 776-784.
Adams, D. J. (2012). "The Valley of Death in anticancer drug development: a reassessment." Trends Pharmacol Sci **33**(4): 173-180.
Adams, J. M., A. E. Taylor, W. F. Crowley, Jr. and J. E. Hall (2004). "Polycystic ovarian morphology with regular ovulatory cycles: insights into the pathophysiology of polycystic ovarian syndrome." J Clin Endocrinol Metab **89**(9): 4343-4350.
Agarwal, A., A. Mulgund, A. Hamada and M. R. Chyatte (2015). "A unique view on male infertility around the globe." Reproductive biology and endocrinology : RB&E **13**: 37-37.
Aghajanova, L., J. Hoffman, E. Mok-Lin and C. N. Herndon (2017). "Obstetrics and Gynecology Residency and Fertility Needs." Reprod Sci **24**(3): 428-434.
Ahima, R. S. and D. A. Antwi (2008). "Brain regulation of appetite and satiety." Endocrinology and metabolism clinics of North America **37**(4): 811-823.
Al-Sabbagh, M., E. W. Lam and J. J. Brosens (2012). "Mechanisms of endometrial progesterone resistance." Mol Cell Endocrinol **358**(2): 208-215.
Almawi, W. Y., E. Gammoh, Z. H. Malalla and S. A. Al-Madhi (2016). "Analysis of VEGFA Variants and Changes in VEGF Levels Underscores the Contribution of VEGF to Polycystic Ovary Syndrome." PLoS One **11**(11): e0165636.
Ambele, M. A., C. Dessels, C. Durandt and M. S. Pepper (2016). "Genome-wide analysis of gene expression during adipogenesis in human adipose-derived stromal cells reveals novel patterns of gene expression during adipocyte differentiation." Stem Cell Research **16**(3): 725-734.
Amer, S. A., J. Smith, A. Mahran, P. Fox and A. Fakis (2017). "Double-blind randomized controlled trial of letrozole versus clomiphene citrate in subfertile women with polycystic ovarian syndrome." Hum Reprod **32**(8): 1631-1638.
Arao, Y., K. J. Hamilton, S. P. Wu, M. J. Tsai, F. J. DeMayo and K. S. Korach (2019). "Dysregulation of hypothalamic-pituitary estrogen receptor alpha-mediated signaling causes episodic LH secretion and cystic ovary." FASEB J: fj201802653RR.
Arceci, R. J., A. A. King, M. C. Simon, S. H. Orkin and D. B. Wilson (1993). "Mouse GATA-4: a retinoic acid-inducible GATA-binding transcription factor expressed in endodermally derived tissues and heart." Mol Cell Biol **13**(4): 2235-2246.

Asuncion, M., R. M. Calvo, J. L. San Millan, J. Sancho, S. Avila and H. F. Escobar-Morreale (2000). "A prospective study of the prevalence of the polycystic ovary syndrome in unselected Caucasian women from Spain." J Clin Endocrinol Metab **85**(7): 2434-2438.

Au - McLean, A. C., N. Au - Valenzuela, S. Au - Fai and S. A. L. Au - Bennett (2012). "Performing Vaginal Lavage, Crystal Violet Staining, and Vaginal Cytological Evaluation for Mouse Estrous Cycle Staging Identification." JoVE(67): e4389.

Azhary, J. M. K., M. Harada, C. Kunitomi, A. Kusamoto, N. Takahashi, E. Nose, N. Oi, O. Wada-Hiraike, Y. Urata, T. Hirata, Y. Hirota, K. Koga, T. Fujii and Y. Osuga (2020). "Androgens Increase Accumulation of Advanced Glycation End Products in Granulosa Cells by Activating ER Stress in PCOS." Endocrinology **161**(2).

Azhary, J. M. K., M. Harada, N. Takahashi, E. Nose, C. Kunitomi, H. Koike, T. Hirata, Y. Hirota, K. Koga, O. Wada-Hiraike, T. Fujii and Y. Osuga (2019). "Endoplasmic Reticulum Stress Activated by Androgen Enhances Apoptosis of Granulosa Cells via Induction of Death Receptor 5 in PCOS." Endocrinology **160**(1): 119-132.

Azziz, R. (2016). "PCOS in 2015: New insights into the genetics of polycystic ovary syndrome." Nat Rev Endocrinol **12**(3): 183.

Azziz, R., E. Carmina, D. Dewailly, E. Diamanti-Kandarakis, H. F. Escobar-Morreale, W. Futterweit, O. E. Janssen, R. S. Legro, R. J. Norman, A. E. Taylor and S. F. Witchel (2006). "Positions statement: criteria for defining polycystic ovary syndrome as a predominantly hyperandrogenic syndrome: an Androgen Excess Society guideline." J Clin Endocrinol Metab **91**(11): 4237-4245.

Azziz, R., D. Ehrmann, R. S. Legro, R. W. Whitcomb, R. Hanley, A. G. Fereshetian, M. O'Keefe and M. N. Ghazzi (2001). "Troglitazone improves ovulation and hirsutism in the polycystic ovary syndrome: a multicenter, double blind, placebo-controlled trial." J Clin Endocrinol Metab **86**(4): 1626-1632.

Azziz, R., L. A. Sanchez, E. S. Knochenhauer, C. Moran, J. Lazenby, K. C. Stephens, K. Taylor and L. R. Boots (2004). "Androgen excess in women: experience with over 1000 consecutive patients." J Clin Endocrinol Metab **89**(2): 453-462.

Bagis, T., A. Gokcel, H. B. Zeyneloglu, E. Tarim, E. B. Kilicdag and B. Haydardedeoglu (2002). "The effects of short-term medroxyprogesterone acetate and micronized progesterone on glucose metabolism and lipid profiles in patients with polycystic ovary syndrome: a prospective randomized study." J Clin Endocrinol Metab **87**(10): 4536-4540.

Bahar, R., K. A. Wong, C. H. Liu and C. L. Bowlus (2018). "Update on New Drugs and Those in Development for the Treatment of Primary Biliary Cholangitis." Gastroenterology & hepatology **14**(3): 154-163.

Balen, A. H. (1993). "Hypersecretion of luteinizing hormone and the polycystic ovary syndrome." Hum Reprod **8 Suppl 2**: 123-128.

Banhegyi, G., P. Baumeister, A. Benedetti, D. Dong, Y. Fu, A. S. Lee, J. Li, C. Mao, E. Margittai, M. Ni, W. Paschen, S. Piccirella, S. Senesi, R. Sitia, M. Wang and W. Yang (2007). "Endoplasmic reticulum stress." Ann N Y Acad Sci **1113**: 58-71.

Bani Mohammad, M. and A. Majdi Seghinsara "Polycystic Ovary Syndrome (PCOS), Diagnostic Criteria, and AMH." Asian Pacific journal of cancer prevention : APJCP **18**(1): 17-21.
Bani Mohammad, M. and A. Majdi Seghinsara (2017). "Polycystic Ovary Syndrome (PCOS), Diagnostic Criteria, and AMH." Asian Pacific journal of cancer prevention : APJCP **18**(1): 17-21.
Barber, T. M., M. I. McCarthy, J. A. Wass and S. Franks (2006). "Obesity and polycystic ovary syndrome." Clin Endocrinol (Oxf) **65**(2): 137-145.
Barnes, R. B., R. L. Rosenfield, D. A. Ehrmann, J. F. Cara, L. Cuttler, L. L. Levitsky and I. M. Rosenthal (1994). "Ovarian hyperandrogynism as a result of congenital adrenal virilizing disorders: evidence for perinatal masculinization of neuroendocrine function in women." J Clin Endocrinol Metab **79**(5): 1328-1333.
Bellver, J., Y. Ayllon, M. Ferrando, M. Melo, E. Goyri, A. Pellicer, J. Remohi and M. Meseguer (2010). "Female obesity impairs in vitro fertilization outcome without affecting embryo quality." Fertil Steril **93**(2): 447-454.
Bellver, J., F. Cruz, M. C. Martinez, J. Ferro, J. F. Ramirez, A. Pellicer and N. Garrido (2011). "Female overweight is not associated with a higher embryo euploidy rate in first trimester miscarriages karyotyped by hysteroembryoscopy." Fertil Steril **96**(4): 931-933.
Bellver, J., M. A. Melo, E. Bosch, V. Serra, J. Remohi and A. Pellicer (2007). "Obesity and poor reproductive outcome: the potential role of the endometrium." Fertil Steril **88**(2): 446-451.
Belsham, D. D. and P. L. Mellon (2000). "Transcription factors Oct-1 and C/EBPbeta (CCAAT/enhancer-binding protein-beta) are involved in the glutamate/nitric oxide/cyclic-guanosine 5'-monophosphate-mediated repression of mediated repression of gonadotropin-releasing hormone gene expression." Mol Endocrinol **14**(2): 212-228.
Bergeron, K. F., C. M. Nguyen, T. Cardinal, B. Charrier, D. W. Silversides and N. Pilon (2016). "Upregulation of the Nr2f1-A830082K12Rik gene pair in murine neural crest cells results in a complex phenotype reminiscent of Waardenburg syndrome type 4." Dis Model Mech **9**(11): 1283-1293.
Bhattacharjee, S., K. Renganaath, R. Mehrotra and S. Mehrotra (2013). "Combinatorial control of gene expression." BioMed research international **2013**: 407263-407263.
Biggin, M. D. and W. McGinnis (1997). "Regulation of segmentation and segmental identity by Drosophila homeoproteins: the role of DNA binding in functional activity and specificity." Development **124**(22): 4425-4433.
Blank, S. K., C. R. McCartney and J. C. Marshall (2006). "The origins and sequelae of abnormal neuroendocrine function in polycystic ovary syndrome." Human Reproduction Update **12**(4): 351-361.
BNF (2021). "Metformin ".
Boomsma, C. M., M. J. Eijkemans, E. G. Hughes, G. H. Visser, B. C. Fauser and N. S. Macklon (2006). "A meta-analysis of pregnancy outcomes in women with polycystic ovary syndrome." Hum Reprod Update **12**(6): 673-683.

Boucher, J., A. Kleinridders and C. R. Kahn (2014). "Insulin receptor signaling in normal and insulin-resistant states." Cold Spring Harb Perspect Biol **6**(1).
Boyle, J. and H. Teede (2012). "Polycystic ovary syndrome An update." Australian Family Physician **41**: 752-756.
Britt, K. L., A. E. Drummond, V. A. Cox, M. Dyson, N. G. Wreford, M. E. Jones, E. R. Simpson and J. K. Findlay (2000). "An age-related ovarian phenotype in mice with targeted disruption of the Cyp 19 (aromatase) gene." Endocrinology **141**(7): 2614-2623.
Broekmans, F. J., J. A. Visser, J. S. Laven, S. L. Broer, A. P. Themmen and B. C. Fauser (2008). "Anti-Mullerian hormone and ovarian dysfunction." Trends Endocrinol Metab **19**(9): 340-347.
Burt Solorzano, C. M., C. R. McCartney, S. K. Blank, K. L. Knudsen and J. C. Marshall (2010). "Hyperandrogenaemia in adolescent girls: origins of abnormal gonadotropin-releasing hormone secretion." BJOG **117**(2): 143-149.
Buse, J. B., R. A. DeFronzo, J. Rosenstock, T. Kim, C. Burns, S. Skare, A. Baron and M. Fineman (2016). "The Primary Glucose-Lowering Effect of Metformin Resides in the Gut, Not the Circulation: Results From Short-term Pharmacokinetic and 12-Week Dose-Ranging Studies." Diabetes Care **39**(2): 198-205.
Bushnik, T., J. L. Cook, A. A. Yuzpe, S. Tough and J. Collins (2012). "Estimating the prevalence of infertility in Canada." Human reproduction (Oxford, England) **27**(3): 738-746.
Byers, S. L., M. V. Wiles, S. L. Dunn and R. A. Taft (2012). "Mouse estrous cycle identification tool and images." PloS one **7**(4): e35538-e35538.
Caldwell, A. S., L. J. Middleton, M. Jimenez, R. Desai, A. C. McMahon, C. M. Allan, D. J. Handelsman and K. A. Walters (2014). "Characterization of reproductive, metabolic, and endocrine features of polycystic ovary syndrome in female hyperandrogenic mouse models." Endocrinology **155**(8): 3146-3159.
Caldwell, A. S. L., M. C. Edwards, R. Desai, M. Jimenez, R. B. Gilchrist, D. J. Handelsman and K. A. Walters (2017). "Neuroendocrine androgen action is a key extraovarian mediator in the development of polycystic ovary syndrome." Proc Natl Acad Sci U S A **114**(16): E3334-e3343.
Caldwell, A. S. L., L. J. Middleton, M. Jimenez, R. Desai, A. C. McMahon, C. M. Allan, D. J. Handelsman and K. A. Walters (2014). "Characterization of Reproductive, Metabolic, and Endocrine Features of Polycystic Ovary Syndrome in Female Hyperandrogenic Mouse Models." Endocrinology **155**(8): 3146-3159.
Caligioni, C. S. (2009). "Assessing reproductive status/stages in mice." Current protocols in neuroscience **Appendix 4**: Appendix-4I.
Cameron, J. L. and C. Nosbisch (1991). "Suppression of pulsatile luteinizing hormone and testosterone secretion during short term food restriction in the adult male rhesus monkey (Macaca mulatta)." Endocrinology **128**(3): 1532-1540.
Carmina, E., E. Guastella and R. A. Longo (2016). "Advances in the Diagnosis and Treatment of PCOS." Curr Pharm Des **22**(36): 5508-5514.

Cawley, K., S. Deegan, A. Samali and S. Gupta (2011). Chapter Two - Assays for Detecting the Unfolded Protein Response. Methods in Enzymology. P. M. Conn, Academic Press. **490:** 31-51.
Cawley, N. X., Z. Li and Y. P. Loh (2016). "60 YEARS OF POMC: Biosynthesis, trafficking, and secretion of pro-opiomelanocortin-derived peptides." Journal of molecular endocrinology **56**(4): T77-T97.
Chakrabarti, J. (2013). "Serum Leptin Level in Women with Polycystic Ovary Syndrome: Correlation with Adiposity, Insulin, and Circulating Testosterone." Annals of Medical and Health Sciences Research **3**(2): 191-196.
Chalasani, N., X. Guo, R. Loomba, M. O. Goodarzi, T. Haritunians, S. Kwon, J. Cui, K. D. Taylor, L. Wilson, O. W. Cummings, Y.-D. I. Chen and J. I. Rotter (2010). "Genome-Wide Association Study Identifies Variants Associated With Histologic Features of Nonalcoholic Fatty Liver Disease." Gastroenterology **139**(5): 1567-1576.e1566.
Chaudhari, N., M. Dawalbhakta and L. Nampoothiri (2018). "GnRH dysregulation in polycystic ovarian syndrome (PCOS) is a manifestation of an altered neurotransmitter profile." Reproductive Biology and Endocrinology **16**(1): 37.
Chen, M.-J., C.-H. Chou, S.-U. Chen, W.-S. Yang, Y.-S. Yang and H.-N. Ho (2015). "The effect of androgens on ovarian follicle maturation: Dihydrotestosterone suppress FSH-stimulated granulosa cell proliferation by upregulating PPARγ-dependent PTEN expression." Scientific Reports **5**: 18319.
Chen, M.-J., C.-H. Chou, S.-U. Chen, W.-S. Yang, Y.-S. Yang and H.-N. Ho (2015). "The effect of androgens on ovarian follicle maturation: Dihydrotestosterone suppress FSH-stimulated granulosa cell proliferation by upregulating PPARγ-dependent PTEN expression." Scientific Reports **5**(1): 18319.
Chen, Y. H., S. Heneidi, J. M. Lee, L. C. Layman, D. W. Stepp, G. M. Gamboa, B. S. Chen, G. Chazenbalk and R. Azziz (2013). "miRNA-93 inhibits GLUT4 and is overexpressed in adipose tissue of polycystic ovary syndrome patients and women with insulin resistance." Diabetes **62**(7): 2278-2286.
Chen, Z.-J., H. Zhao, L. He, Y. Shi, Y. Qin, Y. Shi, Z. Li, L. You, J. Zhao, J. Liu, X. Liang, X. Zhao, J. Zhao, Y. Sun, B. Zhang, H. Jiang, D. Zhao, Y. Bian, X. Gao, L. Geng, Y. Li, D. Zhu, X. Sun, J.-e. Xu, C. Hao, C.-e. Ren, Y. Zhang, S. Chen, W. Zhang, A. Yang, J. Yan, Y. Li, J. Ma and Y. Zhao (2010). "Genome-wide association study identifies susceptibility loci for polycystic ovary syndrome on chromosome 2p16.3, 2p21 and 9q33.3." Nature Genetics **43**: 55.
Chen, Z. J., H. Zhao, L. He, Y. Shi, Y. Qin, Y. Shi, Z. Li, L. You, J. Zhao, J. Liu, X. Liang, X. Zhao, J. Zhao, Y. Sun, B. Zhang, H. Jiang, D. Zhao, Y. Bian, X. Gao, L. Geng, Y. Li, D. Zhu, X. Sun, J. E. Xu, C. Hao, C. E. Ren, Y. Zhang, S. Chen, W. Zhang, A. Yang, J. Yan, Y. Li, J. Ma and Y. Zhao (2011). "Genome-wide association study identifies susceptibility loci for polycystic ovary syndrome on chromosome 2p16.3, 2p21 and 9q33.3." Nat Genet **43**(1): 55-59.

Cheng, C. K. and P. C. Leung (2005). "Molecular biology of gonadotropin-releasing hormone (GnRH)-I, GnRH-II, and their receptors in humans." Endocr Rev **26**(2): 283-306.
Cheng, K. W., B. K. Chow and P. C. Leung (2001). "Functional mapping of a placenta-specific upstream promoter for human gonadotropin-releasing hormone receptor gene." Endocrinology **142**(4): 1506-1516.
Cheong, R. Y., R. Porteous, P. Chambon, I. Abraham and A. E. Herbison (2014). "Effects of neuron-specific estrogen receptor (ER) alpha and ERbeta deletion on the acute estrogen negative feedback mechanism in adult female mice." Endocrinology **155**(4): 1418-1427.
Chhabra, S., C. R. McCartney, R. Y. Yoo, C. A. Eagleson, R. J. Chang and J. C. Marshall (2005). "Progesterone Inhibition of the Hypothalamic Gonadotropin-Releasing Hormone Pulse Generator: Evidence for Varied Effects in Hyperandrogenemic Adolescent Girls." The Journal of Clinical Endocrinology & Metabolism **90**(5): 2810-2815.
Christianson, M. S., H. Wu, Y. Zhao, M. Yemini, M. Leong and Z. Shoham (2015). "Metformin use in patients undergoing in vitro fertilization treatment: results of a worldwide web-based survey." Journal of assisted reproduction and genetics **32**(3): 401-406.
Chumduri, C. and M. Turco (2021). "Organoids of the female reproductive tract." Journal of Molecular Medicine: 1-23.
Chung, I.-M., S. Ketharnathan, S.-H. Kim, M. Thiruvengadam, M. K. Rani and G. Rajakumar (2016). "Making Sense of the Tangle: Insights into Chromatin Folding and Gene Regulation." Genes **7**(10): 71.
Clark, M. E. and P. L. Mellon (1995). "The POU homeodomain transcription factor Oct-1 is essential for activity of the gonadotropin-releasing hormone neuron-specific enhancer." Mol Cell Biol **15**(11): 6169-6177.
Clarkson, J., S. Y. Han, R. Piet, T. McLennan, G. M. Kane, J. Ng, R. W. Porteous, J. S. Kim, W. H. Colledge, K. J. Iremonger and A. E. Herbison (2017). "Definition of the hypothalamic GnRH pulse generator in mice." Proceedings of the National Academy of Sciences **114**(47): E10216-E10223.
clinicaltrials.gov (2019). "TUDCA clinical trials search results."
Copps, K. D. and M. F. White (2012). "Regulation of insulin sensitivity by serine/threonine phosphorylation of insulin receptor substrate proteins IRS1 and IRS2." Diabetologia **55**(10): 2565-2582.
Cosma, M., B. A. Swiglo, D. N. Flynn, D. M. Kurtz, M. L. Labella, R. J. Mullan, M. B. Elamin, P. J. Erwin and V. M. Montori (2008). "Clinical review: Insulin sensitizers for the treatment of hirsutism: a systematic review and metaanalyses of randomized controlled trials." J Clin Endocrinol Metab **93**(4): 1135-1142.
Costello, M. F., M. L. Misso, A. Balen, J. Boyle, L. Devoto, R. M. Garad, R. Hart, L. Johnson, C. Jordan, R. S. Legro, R. J. Norman, E. Mocanu, J. Qiao, R. J. Rodgers, L. Rombauts, E. C. Tassone, S. Thangaratinam, E. Vanky, H. J. Teede and P. N.

International (2019). "Evidence summaries and recommendations from the international evidence-based guideline for the assessment and management of polycystic ovary syndrome: assessment and treatment of infertility." Human Reproduction Open **2019**(1): hoy021.
Couse, J. F., D. O. Bunch, J. Lindzey, D. W. Schomberg and K. S. Korach (1999). "Prevention of the polycystic ovarian phenotype and characterization of ovulatory capacity in the estrogen receptor-alpha knockout mouse." Endocrinology **140**(12): 5855-5865.
Couse, J. F., M. M. Yates, V. R. Walker and K. S. Korach (2003). "Characterization of the hypothalamic-pituitary-gonadal axis in estrogen receptor (ER) Null mice reveals hypergonadism and endocrine sex reversal in females lacking ERalpha but not ERbeta." Mol Endocrinol **17**(6): 1039-1053.
Coutinho, E. A. and A. S. Kauffman (2019). "The Role of the Brain in the Pathogenesis and Physiology of Polycystic Ovary Syndrome (PCOS)." Med Sci (Basel) **7**(8).
Cree-Green, M., H. Rahat, B. R. Newcomer, B. C. Bergman, M. S. Brown, G. V. Coe, L. Newnes, Y. Garcia-Reyes, S. Bacon, J. E. Thurston, L. Pyle, A. Scherzinger and K. J. Nadeau (2017). "Insulin Resistance, Hyperinsulinemia, and Mitochondria Dysfunction in Nonobese Girls With Polycystic Ovarian Syndrome." Journal of the Endocrine Society **1**(7): 931-944.
Crosignani, P. G., G. Ragni, F. Parazzini, H. Wyssling, G. Lombroso and L. Perotti (1994). "Anthropometric indicators and response to gonadotrophin for ovulation induction." Hum Reprod **9**(3): 420-423.
Cui, W., J. Ma, X. Wang, W. Yang, J. Zhang and Q. Ji (2013). "Free fatty acid induces endoplasmic reticulum stress and apoptosis of beta-cells by Ca2+/calpain-2 pathways." PLoS One **8**(3): e59921.
d'Anglemont de Tassigny, X., L. A. Fagg, J. P. C. Dixon, K. Day, H. G. Leitch, A. G. Hendrick, D. Zahn, I. Franceschini, A. Caraty, M. B. L. Carlton, S. A. J. R. Aparicio and W. H. Colledge (2007). "Hypogonadotropic hypogonadism in mice lacking a functional Kiss1 gene." Proceedings of the National Academy of Sciences **104**(25): 10714-10719.
Dağ, Z. Ö. and B. Dilbaz (2015). "Impact of obesity on infertility in women." Journal of the Turkish German Gynecological Association **16**(2): 111-117.
Daryabor, G., M. R. Atashzar, D. Kabelitz, S. Meri and K. Kalantar (2020). "The Effects of Type 2 Diabetes Mellitus on Organ Metabolism and the Immune System." Frontiers in immunology **11**: 1582-1582.
Dasen, J. S., S. M. O'Connell, S. E. Flynn, M. Treier, A. S. Gleiberman, D. P. Szeto, F. Hooshmand, A. K. Aggarwal and M. G. Rosenfeld (1999). "Reciprocal interactions of Pit1 and GATA2 mediate signaling gradient-induced determination of pituitary cell types." Cell **97**(5): 587-598.
Day, F., T. Karaderi, M. R. Jones, C. Meun, C. He, A. Drong, P. Kraft, N. Lin, H. Huang, L. Broer, R. Magi, R. Saxena, T. Laisk, M. Urbanek, M. G. Hayes, G. Thorleifsson, J. Fernandez-Tajes, A. Mahajan, B. H. Mullin, B. G. A. Stuckey, T. D.

Spector, S. G. Wilson, M. O. Goodarzi, L. Davis, B. Obermayer-Pietsch, A. G. Uitterlinden, V. Anttila, B. M. Neale, M.-R. Jarvelin, B. Fauser, I. Kowalska, J. A. Visser, M. Andersen, K. Ong, E. Stener-Victorin, D. Ehrmann, R. S. Legro, A. Salumets, M. I. McCarthy, L. Morin-Papunen, U. Thorsteinsdottir, K. Stefansson, T. the 23andMe Research, U. Styrkarsdottir, J. R. B. Perry, A. Dunaif, J. Laven, S. Franks, C. M. Lindgren and C. K. Welt (2018). "Large-scale genome-wide meta-analysis of polycystic ovary syndrome suggests shared genetic architecture for different diagnosis criteria." PLOS Genetics **14**(12): e1007813.

Day, F. R., D. A. Hinds, J. Y. Tung, L. Stolk, U. Styrkarsdottir, R. Saxena, A. Bjonnes, L. Broer, D. B. Dunger, B. V. Halldorsson, D. A. Lawlor, G. Laval, I. Mathieson, W. L. McCardle, Y. Louwers, C. Meun, S. Ring, R. A. Scott, P. Sulem, A. G. Uitterlinden, N. J. Wareham, U. Thorsteinsdottir, C. Welt, K. Stefansson, J. S. E. Laven, K. K. Ong and J. R. B. Perry (2015). "Causal mechanisms and balancing selection inferred from genetic associations with polycystic ovary syndrome." Nature Communications **6**: 8464.

Day, F. R., D. A. Hinds, J. Y. Tung, L. Stolk, U. Styrkarsdottir, R. Saxena, A. Bjonnes, L. Broer, D. B. Dunger, B. V. Halldorsson, D. A. Lawlor, G. Laval, I. Mathieson, W. L. McCardle, Y. Louwers, C. Meun, S. Ring, R. A. Scott, P. Sulem, A. G. Uitterlinden, N. J. Wareham, U. Thorsteinsdottir, C. Welt, K. Stefansson, J. S. E. Laven, K. K. Ong and J. R. B. Perry (2015). "Causal mechanisms and balancing selection inferred from genetic associations with polycystic ovary syndrome." Nat Commun **6**: 8464.

de Luca, C. and J. M. Olefsky (2008). "Inflammation and insulin resistance." FEBS Lett **582**(1): 97-105.

DeFazio, R. A., S. Heger, S. R. Ojeda and S. M. Moenter (2002). "Activation of A-Type γ-Aminobutyric Acid Receptors Excites Gonadotropin-Releasing Hormone Neurons." Molecular Endocrinology **16**(12): 2872-2891.

Desbuquois, B., N. Carre and A. F. Burnol (2013). "Regulation of insulin and type 1 insulin-like growth factor signaling and action by the Grb10/14 and SH2B1/B2 adaptor proteins." FEBS J **280**(3): 794-816.

Desquiret-Dumas, V., A. Clement, V. Seegers, L. Boucret, V. Ferre-L'Hotellier, P. E. Bouet, P. Descamps, V. Procaccio, P. Reynier and P. May-Panloup (2017). "The mitochondrial DNA content of cumulus granulosa cells is linked to embryo quality." Hum Reprod **32**(3): 607-614.

Deswal, R., A. Yadav and A. S. Dang (2018). "Sex hormone binding globulin - an important biomarker for predicting PCOS risk: A systematic review and meta-analysis." Systems Biology in Reproductive Medicine **64**(1): 12-24.

DeUgarte, C. M., A. A. Bartolucci and R. Azziz (2005). "Prevalence of insulin resistance in the polycystic ovary syndrome using the homeostasis model assessment." Fertil Steril **83**(5): 1454-1460.

Devin, J. K., J. E. Johnson, M. Eren, L. A. Gleaves, W. S. Bradham, J. R. Bloodworth, Jr. and D. E. Vaughan (2007). "Transgenic overexpression of plasminogen activator

inhibitor-1 promotes the development of polycystic ovarian changes in female mice." J Mol Endocrinol **39**(1): 9-16.
Diamanti-Kandarakis, E. (2006). "Insulin resistance in PCOS." Endocrine **30**(1): 13-17.
Diamanti-Kandarakis, E. and A. Dunaif (2012). "Insulin resistance and the polycystic ovary syndrome revisited: an update on mechanisms and implications." Endocr Rev **33**(6): 981-1030.
Dieterle, A. M., P. Böhler, H. Keppeler, S. Alers, N. Berleth, S. Drießen, N. Hieke, S. Pietkiewicz, A. S. Löffler, C. Peter, A. Gray, N. R. Leslie, H. Shinohara, T. Kurosaki, M. Engelke, J. Wienands, M. Bonin, S. Wesselborg and B. Stork (2014). "PDK1 controls upstream PI3K expression and PIP3 generation." Oncogene **33**(23): 3043-3053.
Ding, Y., G. Zhuo, C. Zhang and J. Leng (2016). "Point mutation in mitochondrial tRNA gene is associated with polycystic ovary syndrome and insulin resistance." Mol Med Rep **13**(4): 3169-3172.
Dissen, G. A., C. Garcia-Rudaz, A. Paredes, C. Mayer, A. Mayerhofer and S. R. Ojeda (2009). "Excessive ovarian production of nerve growth factor facilitates development of cystic ovarian morphology in mice and is a feature of polycystic ovarian syndrome in humans." Endocrinology **150**(6): 2906-2914.
Division of Nutrition, P. A., and Obesity, National Center for Chronic Disease Prevention and Health Promotion. (2017). "Defining Adult Overweight and Obesity."
Do, R., R. Kiss, D. Gaudet and J. Engert (2009). "Squalene synthase: a critical enzyme in the cholesterol biosynthesis pathway." Clinical Genetics **75**(1): 19-29.
Dokras, A., D. H. Jagasia, M. Maifeld, C. A. Sinkey, B. J. VanVoorhis and W. G. Haynes (2006). "Obesity and insulin resistance but not hyperandrogenism mediates vascular dysfunction in women with polycystic ovary syndrome." Fertil Steril **86**(6): 1702-1709.
Du, X., R. L. Rosenfield and K. Qin (2009). "KLF15 Is a transcriptional regulator of the human 17beta-hydroxysteroid dehydrogenase type 5 gene. A potential link between regulation of testosterone production and fat stores in women." J Clin Endocrinol Metab **94**(7): 2594-2601.
Dumesic, D. A., S. E. Oberfield, E. Stener-Victorin, J. C. Marshall, J. S. Laven and R. S. Legro (2015). "Scientific Statement on the Diagnostic Criteria, Epidemiology, Pathophysiology, and Molecular Genetics of Polycystic Ovary Syndrome." Endocr Rev **36**(5): 487-525.
Dunaif, A. (1997). "Insulin resistance and the polycystic ovary syndrome: mechanism and implications for pathogenesis." Endocr Rev **18**(6): 774-800.
Dunaif, A. (1999). "Insulin action in the polycystic ovary syndrome." Endocrinol Metab Clin North Am **28**(2): 341-359.
Dunaif, A., K. R. Segal, W. Futterweit and A. Dobrjansky (1989). "Profound peripheral insulin resistance, independent of obesity, in polycystic ovary syndrome." Diabetes **38**(9): 1165-1174.

Durlinger, A. L., P. Kramer, B. Karels, F. H. de Jong, J. T. Uilenbroek, J. A. Grootegoed and A. P. Themmen (1999). "Control of primordial follicle recruitment by anti-Mullerian hormone in the mouse ovary." Endocrinology **140**(12): 5789-5796.
Dyson, J. M., C. G. Fedele, E. M. Davies, J. Becanovic and C. A. Mitchell (2012). "Phosphoinositide phosphatases: just as important as the kinases." Subcell Biochem **58**: 215-279.
Eagleson, C. A., M. B. Gingrich, C. L. Pastor, T. K. Arora, C. M. Burt, W. S. Evans and J. C. Marshall (2000). "Polycystic ovarian syndrome: evidence that flutamide restores sensitivity of the gonadotropin-releasing hormone pulse generator to inhibition by estradiol and progesterone." J Clin Endocrinol Metab **85**(11): 4047-4052.
Efimenko, E., M. B. Padua, N. L. Manuylov, S. C. Fox, D. A. Morse and S. G. Tevosian (2013). "The transcription factor GATA4 is required for follicular development and normal ovarian function." Developmental Biology **381**(1): 144-158.
Eftekhar, M., R. Deghani Firoozabadi, P. Khani, E. Ziaei Bideh and H. Forghani (2016). "Effect of Laparoscopic Ovarian Drilling on Outcomes of In Vitro Fertilization in Clomiphene-Resistant Women with Polycystic Ovary Syndrome." Int J Fertil Steril **10**(1): 42-47.
Ehrmann, D. A., R. B. Barnes and R. L. Rosenfield (1995). "Polycystic ovary syndrome as a form of functional ovarian hyperandrogenism due to dysregulation of androgen secretion." Endocr Rev **16**(3): 322-353.
Ehrmann, D. A., D. R. Liljenquist, K. Kasza, R. Azziz, R. S. Legro and M. N. Ghazzi (2006). "Prevalence and predictors of the metabolic syndrome in women with polycystic ovary syndrome." J Clin Endocrinol Metab **91**(1): 48-53.
Elchebly, M., P. Payette, E. Michaliszyn, W. Cromlish, S. Collins, A. L. Loy, D. Normandin, A. Cheng, J. Himms-Hagen, C. C. Chan, C. Ramachandran, M. J. Gresser, M. L. Tremblay and B. P. Kennedy (1999). "Increased insulin sensitivity and obesity resistance in mice lacking the protein tyrosine phosphatase-1B gene." Science **283**(5407): 1544-1548.
Elsea, S. H. and R. E. Lucas (2002). "The mousetrap: what we can learn when the mouse model does not mimic the human disease." ILAR J **43**(2): 66-79.
Engin, A. (2017). "The Pathogenesis of Obesity-Associated Adipose Tissue Inflammation." Adv Exp Med Biol **960**: 221-245.
Fauser, B. C. and A. M. Van Heusden (1997). "Manipulation of human ovarian function: physiological concepts and clinical consequences." Endocr Rev **18**(1): 71-106.
Fedorcsak, P., P. O. Dale, R. Storeng, G. Ertzeid, S. Bjercke, N. Oldereid, A. K. Omland, T. Abyholm and T. Tanbo (2004). "Impact of overweight and underweight on assisted reproduction treatment." Hum Reprod **19**(11): 2523-2528.
Feingold KR, A. B., Boyce A, et al. (2018). The Normal Menstrual Cycle and the Control of Ovulation. . South Dartmouth (MA), MDText.com, Inc.; 2000.

Flegal, K. M. and B. I. Graubard (2009). "Estimates of excess deaths associated with body mass index and other anthropometric variables." The American journal of clinical nutrition **89**(4): 1213-1219.
Foecking, E. M., M. Szabo, N. B. Schwartz and J. E. Levine (2005). "Neuroendocrine consequences of prenatal androgen exposure in the female rat: absence of luteinizing hormone surges, suppression of progesterone receptor gene expression, and acceleration of the gonadotropin-releasing hormone pulse generator." Biol Reprod **72**(6): 1475-1483.
Fornes, R., M. Maliqueo, M. Hu, L. Hadi, J. M. Jimenez-Andrade, K. Ebefors, J. Nyström, F. Labrie, T. Jansson, A. Benrick and E. Stener-Victorin (2017). "The effect of androgen excess on maternal metabolism, placental function and fetal growth in obese dams." Scientific Reports **7**: 8066.
Foster, H. L., J. D. Small and J. G. Fox (2014). The Mouse in Biomedical Research: Normative biology, immunology, and husbandry, Academic Press.
Franik, S., S. M. Eltrop, J. A. Kremer, L. Kiesel and C. Farquhar (2018). "Aromatase inhibitors (letrozole) for subfertile women with polycystic ovary syndrome." Cochrane Database Syst Rev **5**: CD010287.
Freedman, D. S., C. L. Ogden and B. K. Kit (2015). "Interrelationships between BMI, skinfold thicknesses, percent body fat, and cardiovascular disease risk factors among U.S. children and adolescents." BMC pediatrics **15**: 188-188.
Fu, S., S. M. Watkins and G. S. Hotamisligil (2012). "The role of endoplasmic reticulum in hepatic lipid homeostasis and stress signaling." Cell Metab **15**(5): 623-634.
Fulghesu, A. M., R. Manca, S. Loi and F. Fruzzetti (2015). "Insulin resistance and hyperandrogenism have no substantive association with birth weight in adolescents with polycystic ovary syndrome." Fertil Steril **103**(3): 808-814.
Gardner, C. D., J. F. Trepanowski, L. C. Del Gobbo, M. E. Hauser, J. Rigdon, J. P. A. Ioannidis, M. Desai and A. C. King (2018). "Effect of Low-Fat vs Low-Carbohydrate Diet on 12-Month Weight Loss in Overweight Adults and the Association With Genotype Pattern or Insulin Secretion: The DIETFITS Randomized Clinical Trial." JAMA **319**(7): 667-679.
Gardner, D. K. and B. Balaban (2016). "Assessment of human embryo development using morphological criteria in an era of time-lapse, algorithms and 'OMICS': is looking good still important?" Molecular Human Reproduction **22**(10): 704-718.
Garfinkel, B. P. and G. S. Hotamisligil (2017). "ER Stress Promotes Inflammation through Re-wIREd Macrophages in Obesity." Mol Cell **66**(6): 731-733.
George, J. T., R. Kakkar, J. Marshall, M. L. Scott, R. D. Finkelman, T. W. Ho, J. Veldhuis, K. Skorupskaite, R. A. Anderson, S. McIntosh and L. Webber (2016). "Neurokinin B Receptor Antagonism in Women With Polycystic Ovary Syndrome: A Randomized, Placebo-Controlled Trial." The Journal of Clinical Endocrinology & Metabolism **101**(11): 4313-4321.

Gesink Law, D. C., R. F. Maclehose and M. P. Longnecker (2007). "Obesity and time to pregnancy." Hum Reprod **22**(2): 414-420.
Gieske, M. C., H. J. Kim, S. J. Legan, Y. Koo, A. Krust, P. Chambon and C. Ko (2008). "Pituitary gonadotroph estrogen receptor-alpha is necessary for fertility in females." Endocrinology **149**(1): 20-27.
Givens, M. L., R. Kurotani, N. Rave-Harel, N. L. Miller and P. L. Mellon (2004). "Phylogenetic footprinting reveals evolutionarily conserved regions of the gonadotropin-releasing hormone gene that enhance cell-specific expression." Mol Endocrinol **18**(12): 2950-2966.
Givens, M. L., N. Rave-Harel, V. D. Goonewardena, R. Kurotani, S. E. Berdy, C. H. Swan, J. L. Rubenstein, B. Robert and P. L. Mellon (2005). "Developmental regulation of gonadotropin-releasing hormone gene expression by the MSX and DLX homeodomain protein families." J Biol Chem **280**(19): 19156-19165.
Gonzalez, F., J. P. Kirwan, N. S. Rote and J. Minium (2013). "Elevated circulating levels of tissue factor in polycystic ovary syndrome." Clin Appl Thromb Hemost **19**(1): 66-72.
Goodman, R. L., M. N. Lehman, J. T. Smith, L. M. Coolen, C. V. R. de Oliveira, M. R. Jafarzadehshirazi, A. Pereira, J. Iqbal, A. Caraty, P. Ciofi and I. J. Clarke (2007). "Kisspeptin Neurons in the Arcuate Nucleus of the Ewe Express Both Dynorphin A and Neurokinin B." Endocrinology **148**(12): 5752-5760.
Gottsch, M. L., D. K. Clifton and R. A. Steiner (2006). "Kisspepeptin-GPR54 signaling in the neuroendocrine reproductive axis." Molecular and Cellular Endocrinology **254-255**: 91-96.
Gottsch, M. L., M. J. Cunningham, J. T. Smith, S. M. Popa, B. V. Acohido, W. F. Crowley, S. Seminara, D. K. Clifton and R. A. Steiner (2004). "A Role for Kisspeptins in the Regulation of Gonadotropin Secretion in the Mouse." Endocrinology **145**(9): 4073-4077.
Goyal, M. and A. S. Dawood (2017). "Debates Regarding Lean Patients with Polycystic Ovary Syndrome: A Narrative Review." Journal of human reproductive sciences **10**(3): 154-161.
Greenaway, J., J. Lawler, R. Moorehead, P. Bornstein, J. LaMarre and J. Petrik (2007). "Thrombospondin-1 inhibits VEGF levels in the ovary directly by binding and internalization via the low density lipoprotein receptor-related protein-1 (LRP-1)." Journal of Cellular Physiology **210**(3): 807-818.
Gribble, F. M. (2005). "Metabolism: a higher power for insulin." Nature **434**(7036): 965-966.
Groome, N. P., P. J. Illingworth, M. O'Brien, R. Pai, F. E. Rodger, J. P. Mather and A. S. McNeilly (1996). "Measurement of dimeric inhibin B throughout the human menstrual cycle." J Clin Endocrinol Metab **81**(4): 1401-1405.
Group, R. E. A.-S. P. C. W. (2004). "Revised 2003 consensus on diagnostic criteria and long-term health risks related to polycystic ovary syndrome." Fertil Steril **81**(1): 19-25.

Guerrero-Hernandez, A., D. Leon-Aparicio, J. Chavez-Reyes, J. A. Olivares-Reyes and S. DeJesus (2014). "Endoplasmic reticulum stress in insulin resistance and diabetes." Cell Calcium **56**(5): 311-322.
Guidelines, N. I. P. (2018). "Draft Summary and Recommendations of International Evidenced-Based Guideline for the Assessment and Management of Polycystic Ovary Syndrome."
Gupta, S., L. Cuffe, E. Szegezdi, S. E. Logue, C. Neary, S. Healy and A. Samali (2010). "Mechanisms of ER Stress-Mediated Mitochondrial Membrane Permeabilization." International journal of cell biology **2010**: 170215-170215.
Gutierrez-Rodelo, C., A. Roura-Guiberna and J. A. Olivares-Reyes (2017). "[Molecular Mechanisms of Insulin Resistance: An Update]." Gac Med Mex **153**(2): 214-228.
Habib, A. M., P. Richards, L. S. Cairns, G. J. Rogers, C. A. M. Bannon, H. E. Parker, T. C. E. Morley, G. S. H. Yeo, F. Reimann and F. M. Gribble (2012). "Overlap of Endocrine Hormone Expression in the Mouse Intestine Revealed by Transcriptional Profiling and Flow Cytometry." Endocrinology **153**(7): 3054-3065.
Hanson, B., E. Johnstone, J. Dorais, B. Silver, C. M. Peterson and J. Hotaling (2017). "Female infertility, infertility-associated diagnoses, and comorbidities: a review." Journal of assisted reproduction and genetics **34**(2): 167-177.
Hardarson, T., L. Van Landuyt and G. Jones (2012). "The blastocyst." Human Reproduction **27**(suppl_1): i72-i91.
Harno, E., T. Gali Ramamoorthy, A. P. Coll and A. White (2018). "POMC: The Physiological Power of Hormone Processing." Physiological reviews **98**(4): 2381-2430.
Harris, H. R., A. Babic, P. M. Webb, C. M. Nagle, S. J. Jordan, H. A. Risch, M. A. Rossing, J. A. Doherty, M. T. Goodman, F. Modugno, R. B. Ness, K. B. Moysich, S. K. Kjaer, E. Hogdall, A. Jensen, J. M. Schildkraut, A. Berchuck, D. W. Cramer, E. V. Bandera, N. Wentzensen, J. Kotsopoulos, S. A. Narod, C. M. Phelan, J. R. McLaughlin, H. Anton-Culver, A. Ziogas, C. L. Pearce, A. H. Wu and K. L. Terry (2018). "Polycystic Ovary Syndrome, Oligomenorrhea, and Risk of Ovarian Cancer Histotypes: Evidence from the Ovarian Cancer Association Consortium." Cancer Epidemiol Biomarkers Prev **27**(2): 174-182.
Hartz, A. J., P. N. Barboriak, A. Wong, K. P. Katayama and A. A. Rimm (1979). "The association of obesity with infertility and related menstural abnormalities in women." Int J Obes **3**(1): 57-73.
Hayes, M. G., M. Urbanek, D. A. Ehrmann, L. L. Armstrong, J. Y. Lee, R. Sisk, T. Karaderi, T. M. Barber, M. I. McCarthy, S. Franks, C. M. Lindgren, C. K. Welt, E. Diamanti-Kandarakis, D. Panidis, M. O. Goodarzi, R. Azziz, Y. Zhang, R. G. James, M. Olivier, A. H. Kissebah, R. Alvero, H. X. Barnhart, V. Baker, K. T. Barnhart, G. W. Bates, R. G. Brzyski, B. R. Carr, S. A. Carson, P. Casson, N. A. Cataldo, G. Christman, C. Coutifaris, M. P. Diamond, E. Eisenberg, G. G. Gosman, L. C. Giudice, D. J. Haisenleder, H. Huang, S. A. Krawetz, S. Lucidi, P. G. McGovern, E. R. Myers, J. E. Nestler, D. Ohl, N. Santoro, W. D. Schlaff, P. Snyder, M. P. Steinkampf, J. C.

Trussell, R. Usadi, Q. Yan, H. Zhang, E. Stener-Victorin, R. S. Legro, A. Dunaif and N. Reproductive Medicine (2015). "Genome-wide association of polycystic ovary syndrome implicates alterations in gonadotropin secretion in European ancestry populations." Nature Communications **6**(1): 7502.

Hayes, M. G., M. Urbanek, D. A. Ehrmann, L. L. Armstrong, J. Y. Lee, R. Sisk, T. Karaderi, T. M. Barber, M. I. McCarthy, S. Franks, C. M. Lindgren, C. K. Welt, E. Diamanti-Kandarakis, D. Panidis, M. O. Goodarzi, R. Azziz, Y. Zhang, R. G. James, M. Olivier, A. H. Kissebah, R. Alvero, H. X. Barnhart, V. Baker, K. T. Barnhart, G. W. Bates, R. G. Brzyski, B. R. Carr, S. A. Carson, P. Casson, N. A. Cataldo, G. Christman, C. Coutifaris, M. P. Diamond, E. Eisenberg, G. G. Gosman, L. C. Giudice, D. J. Haisenleder, H. Huang, S. A. Krawetz, S. Lucidi, P. G. McGovern, E. R. Myers, J. E. Nestler, D. Ohl, N. Santoro, W. D. Schlaff, P. Snyder, M. P. Steinkampf, J. C. Trussell, R. Usadi, Q. Yan, H. Zhang, E. Stener-Victorin, R. S. Legro, A. Dunaif and N. Reproductive Medicine (2020). "Publisher Correction: Genome-wide association of polycystic ovary syndrome implicates alterations in gonadotropin secretion in European ancestry populations." Nature Communications **11**(1): 2158.

Hayes, M. G., M. Urbanek, D. A. Ehrmann, L. L. Armstrong, J. Y. Lee, R. Sisk, T. Karaderi, T. M. Barber, M. I. McCarthy, S. Franks, C. M. Lindgren, C. K. Welt, E. Diamanti-Kandarakis, D. Panidis, M. O. Goodarzi, R. Azziz, Y. Zhang, R. G. James, M. Olivier, A. H. Kissebah, N. Reproductive Medicine, R. Alvero, H. X. Barnhart, V. Baker, K. T. Barnhart, G. W. Bates, R. G. Brzyski, B. R. Carr, S. A. Carson, P. Casson, N. A. Cataldo, G. Christman, C. Coutifaris, M. P. Diamond, E. Eisenberg, G. G. Gosman, L. C. Giudice, D. J. Haisenleder, H. Huang, S. A. Krawetz, S. Lucidi, P. G. McGovern, E. R. Myers, J. E. Nestler, D. Ohl, N. Santoro, W. D. Schlaff, P. Snyder, M. P. Steinkampf, J. C. Trussell, R. Usadi, Q. Yan, H. Zhang, E. Stener-Victorin, R. S. Legro and A. Dunaif (2015). "Genome-wide association of polycystic ovary syndrome implicates alterations in gonadotropin secretion in European ancestry populations." Nature Communications **6**: 7502.

Hayes, M. G., M. Urbanek, D. A. Ehrmann, L. L. Armstrong, J. Y. Lee, R. Sisk, T. Karaderi, T. M. Barber, M. I. McCarthy, S. Franks, C. M. Lindgren, C. K. Welt, E. Diamanti-Kandarakis, D. Panidis, M. O. Goodarzi, R. Azziz, Y. Zhang, R. G. James, M. Olivier, A. H. Kissebah, E. Stener-Victorin, R. S. Legro and A. Dunaif (2015). "Genome-wide association of polycystic ovary syndrome implicates alterations in gonadotropin secretion in European ancestry populations." Nat Commun **6**: 7502.

Herbison, A., M. J. Skynner and J. A. Sim (2001). "Erratum: Lack of detection of estrogen receptor-α transcripts in mouse gonadotropin-releasing hormone neurons (Endocrinology (1999) 140 (5195-5201)." Endocrinology **142**: 493-493.

Herbison, A. E. (2008). "Estrogen positive feedback to gonadotropin-releasing hormone (GnRH) neurons in the rodent: the case for the rostral periventricular area of the third ventricle (RP3V)." Brain research reviews **57**(2): 277-287.

Hermann, B. P. and L. L. Heckert (2005). "Silencing of Fshr Occurs through a Conserved, Hypersensitive Site in the First Intron." Molecular Endocrinology **19**(8): 2112-2131.
Hewlett, M., E. Chow, A. Aschengrau and S. Mahalingaiah (2017). "Prenatal Exposure to Endocrine Disruptors: A Developmental Etiology for Polycystic Ovary Syndrome." Reprod Sci **24**(1): 19-27.
Hill, J. W., C. F. Elias, M. Fukuda, K. W. Williams, E. D. Berglund, W. L. Holland, Y. R. Cho, J. C. Chuang, Y. Xu, M. Choi, D. Lauzon, C. E. Lee, R. Coppari, J. A. Richardson, J. M. Zigman, S. Chua, P. E. Scherer, B. B. Lowell, J. C. Bruning and J. K. Elmquist (2010). "Direct insulin and leptin action on pro-opiomelanocortin neurons is required for normal glucose homeostasis and fertility." Cell Metab **11**(4): 286-297.
Hirosumi, J., G. Tuncman, L. Chang, C. Z. Gorgun, K. T. Uysal, K. Maeda, M. Karin and G. S. Hotamisligil (2002). "A central role for JNK in obesity and insulin resistance." Nature **420**(6913): 333-336.
Hirshfeld-Cytron, J., R. B. Barnes, D. A. Ehrmann, A. Caruso, M. M. Mortensen and R. L. Rosenfield (2009). "Characterization of functionally typical and atypical types of polycystic ovary syndrome." J Clin Endocrinol Metab **94**(5): 1587-1594.
Hoff, J. D., M. E. Quigley and S. S. Yen (1983). "Hormonal dynamics at midcycle: a reevaluation." J Clin Endocrinol Metab **57**(4): 792-796.
Homburg, R. (2004). "Management of infertility and prevention of ovarian hyperstimulation in women with polycystic ovary syndrome." Best Pract Res Clin Obstet Gynaecol **18**(5): 773-788.
Homburg, R., A. Gudi, A. Shah and M. L. A (2017). "A novel method to demonstrate that pregnant women with polycystic ovary syndrome hyper-expose their fetus to androgens as a possible stepping stone for the developmental theory of PCOS. A pilot study." Reprod Biol Endocrinol **15**(1): 61.
Hrabovszky, E., A. r. Steinhauser, K. Barabás, P. J. Shughrue, S. L. Petersen, I. n. Merchenthaler and Z. Liposits (2001). "Estrogen Receptor-β Immunoreactivity in Luteinizing Hormone-Releasing Hormone Neurons of the Rat Brain." Endocrinology **142**(7): 3261-3264.
Hruby, A. and F. B. Hu (2015). "The Epidemiology of Obesity: A Big Picture." PharmacoEconomics **33**(7): 673-689.
Hsueh, A. J., K. Kawamura, Y. Cheng and B. C. Fauser (2015). "Intraovarian control of early folliculogenesis." Endocr Rev **36**(1): 1-24.
Hu, P., Z. Han, A. D. Couvillon, R. J. Kaufman and J. H. Exton (2006). "Autocrine tumor necrosis factor alpha links endoplasmic reticulum stress to the membrane death receptor pathway through IRE1alpha-mediated NF-kappaB activation and down-regulation of TRAF2 expression." Mol Cell Biol **26**(8): 3071-3084.
Huang, X. and R. E. Harlan (1993). "Absence of androgen receptors in LHRH immunoreactive neurons." Brain Res **624**(1-2): 309-311.
Huang, X. and R. E. Harlan (1993). "Absence of androgen receptors in LHRH immunoreactive neurons." Brain Research **624**(1): 309-311.

Huang, Y., Y. Yu, J. Gao, R. Li, C. Zhang, H. Zhao, Y. Zhao and J. Qiao (2015). "Impaired oocyte quality induced by dehydroepiandrosterone is partially rescued by metformin treatment." PloS one **10**(3): e0122370-e0122370.
Hubbard, S. R. (2013). "The insulin receptor: both a prototypical and atypical receptor tyrosine kinase." Cold Spring Harb Perspect Biol **5**(3): a008946.
Huhtaniemi, I., S. Rulli, P. Ahtiainen and M. Poutanen (2005). "Multiple sites of tumorigenesis in transgenic mice overproducing hCG." Mol Cell Endocrinol **234**(1-2): 117-126.
Ibanez, L., S. E. Oberfield, S. Witchel, R. J. Auchus, R. J. Chang, E. Codner, P. Dabadghao, F. Darendeliler, N. S. Elbarbary, A. Gambineri, C. Garcia Rudaz, K. M. Hoeger, A. Lopez-Bermejo, K. Ong, A. S. Pena, T. Reinehr, N. Santoro, M. Tena-Sempere, R. Tao, B. O. Yildiz, H. Alkhayyat, A. Deeb, D. Joel, R. Horikawa, F. de Zegher and P. A. Lee (2017). "An International Consortium Update: Pathophysiology, Diagnosis, and Treatment of Polycystic Ovarian Syndrome in Adolescence." Horm Res Paediatr **88**(6): 371-395.
Ibanez, L., N. Potau, I. Francois and F. de Zegher (1998). "Precocious pubarche, hyperinsulinism, and ovarian hyperandrogenism in girls: relation to reduced fetal growth." J Clin Endocrinol Metab **83**(10): 3558-3562.
infrafrontier (2018). "IVF and sperms cryopreservation protocols."
Invernizzi, P., K. D. Setchell, A. Crosignani, P. M. Battezzati, A. Larghi, N. C. O'Connell and M. Podda (1999). "Differences in the metabolism and disposition of ursodeoxycholic acid and of its taurine-conjugated species in patients with primary biliary cirrhosis." Hepatology **29**(2): 320-327.
Jackson_Laboratory (1966). Biology of the Laboratory Mouse, DOVER PUBLICATIONS, INC., NEW YORK.
Jakimiuk, A. J., S. R. Weitsman, A. Navab and D. A. Magoffin (2001). "Luteinizing hormone receptor, steroidogenesis acute regulatory protein, and steroidogenic enzyme messenger ribonucleic acids are overexpressed in thecal and granulosa cells from polycystic ovaries." J Clin Endocrinol Metab **86**(3): 1318-1323.
Janssen, I. (2013). "The public health burden of obesity in Canada." Can J Diabetes **37**(2): 90-96.
Jensen, M. and P. De Meyts (2009). "Molecular mechanisms of differential intracellular signaling from the insulin receptor." Vitam Horm **80**: 51-75.
Jeppesen, J. V., R. A. Anderson, T. W. Kelsey, S. L. Christiansen, S. G. Kristensen, K. Jayaprakasan, N. Raine-Fenning, B. K. Campbell and C. Yding Andersen (2013). "Which follicles make the most anti-Müllerian hormone in humans? Evidence for an abrupt decline in AMH production at the time of follicle selection." Molecular Human Reproduction **19**(8): 519-527.
Jin, J., Y. Ma, X. Tong, W. Yang, Y. Dai, Y. Pan, P. Ren, L. Liu, H.-Y. Fan, Y. Zhang and S. Zhang (2020). "Metformin inhibits testosterone-induced endoplasmic reticulum stress in ovarian granulosa cells via inactivation of p38 MAPK." Human Reproduction **35**(5): 1145-1158.

Jo, J., O. Gavrilova, S. Pack, W. Jou, S. Mullen, A. E. Sumner, S. W. Cushman and V. Periwal (2009). "Hypertrophy and/or Hyperplasia: Dynamics of Adipose Tissue Growth." PLoS computational biology **5**(3): e1000324-e1000324.
Johnson, A. M. and J. M. Olefsky (2013). "The origins and drivers of insulin resistance." Cell **152**(4): 673-684.
Jungheim, E. S., J. L. Travieso, K. R. Carson and K. H. Moley (2012). "Obesity and reproductive function." Obstet Gynecol Clin North Am **39**(4): 479-493.
Jungheim, E. S., J. L. Travieso and M. M. Hopeman (2013). "Weighing the impact of obesity on female reproductive function and fertility." Nutr Rev **71 Suppl 1**: S3-8.
Kadowaki, T., T. Yamauchi, N. Kubota, K. Hara, K. Ueki and K. Tobe (2006). "Adiponectin and adiponectin receptors in insulin resistance, diabetes, and the metabolic syndrome." J Clin Invest **116**(7): 1784-1792.
Kammoun, H. L., H. Chabanon, I. Hainault, S. Luquet, C. Magnan, T. Koike, P. Ferre and F. Foufelle (2009). "GRP78 expression inhibits insulin and ER stress-induced SREBP-1c activation and reduces hepatic steatosis in mice." J Clin Invest **119**(5): 1201-1215.
Kandaraki, E., A. Chatzigeorgiou, S. Livadas, E. Palioura, F. Economou, M. Koutsilieris, S. Palimeri, D. Panidis and E. Diamanti-Kandarakis (2011). "Endocrine disruptors and polycystic ovary syndrome (PCOS): elevated serum levels of bisphenol A in women with PCOS." J Clin Endocrinol Metab **96**(3): E480-484.
Kars, M., L. Yang, M. F. Gregor, B. S. Mohammed, T. A. Pietka, B. N. Finck, B. W. Patterson, J. D. Horton, B. Mittendorfer, G. S. Hotamisligil and S. Klein (2010). "Tauroursodeoxycholic Acid may improve liver and muscle but not adipose tissue insulin sensitivity in obese men and women." Diabetes **59**(8): 1899-1905.
Katulski, K., A. Podfigurna, A. Czyzyk, B. Meczekalski and A. D. Genazzani (2018). "Kisspeptin and LH pulsatile temporal coupling in PCOS patients." Endocrine **61**(1): 149-157.
Kauffman, A. S., M. L. Gottsch, J. Roa, A. C. Byquist, A. Crown, D. K. Clifton, G. E. Hoffman, R. A. Steiner and M. Tena-Sempere (2007). "Sexual Differentiation of Kiss1 Gene Expression in the Brain of the Rat." Endocrinology **148**(4): 1774-1783.
Kauffman, A. S., V. G. Thackray, G. E. Ryan, K. P. Tolson, C. A. Glidewell-Kenney, S. J. Semaan, M. C. Poling, N. Iwata, K. M. Breen, A. J. Duleba, E. Stener-Victorin, S. Shimasaki, N. J. Webster and P. L. Mellon (2015). "A Novel Letrozole Model Recapitulates Both the Reproductive and Metabolic Phenotypes of Polycystic Ovary Syndrome in Female Mice." Biol Reprod **93**(3): 69.
Kauffman, A. S., V. G. Thackray, G. E. Ryan, K. P. Tolson, C. A. Glidewell-Kenney, S. J. Semaan, M. C. Poling, N. Iwata, K. M. Breen, A. J. Duleba, E. Stener-Victorin, S. Shimasaki, N. J. Webster and P. L. Mellon (2015). "A Novel Letrozole Model Recapitulates Both the Reproductive and Metabolic Phenotypes of Polycystic Ovary Syndrome in Female Mice1." Biology of Reproduction **93**(3).

Kawwass, J. F., K. M. Sanders, T. L. Loucks, L. C. Rohan and S. L. Berga (2017). "Increased cerebrospinal fluid levels of GABA, testosterone and estradiol in women with polycystic ovary syndrome." Human Reproduction **32**(7): 1450-1456.
Kelley, C., H. Blumberg, L. I. Zon and T. Evans (1993). "GATA-4 is a novel transcription factor expressed in endocardium of the developing heart." Development **118**(3): 817-827.
Kelley, C. G., M. L. Givens, N. Rave-Harel, S. B. Nelson, S. Anderson and P. L. Mellon (2002). "Neuron-restricted expression of the rat gonadotropin-releasing hormone gene is conferred by a cell-specific protein complex that binds repeated CAATT elements." Mol Endocrinol **16**(11): 2413-2425.
Kepa, J. K., A. J. Spaulding, B. M. Jacobsen, Z. Fang, X. Xiong, S. Radovick and M. E. Wierman (1996). "Structure of the distal human gonadotropin releasing hormone (hGnrh) gene promoter and functional analysis in Gt1-7 neuronal cells." Nucleic acids research **24**(18): 3614-3620.
Kero, J. T., E. Savontaus, M. Mikola, U. Pesonen, M. Koulu, R. A. Keri, J. H. Nilson, M. Poutanen and I. T. Huhtaniemi (2003). "Obesity in transgenic female mice with constitutively elevated luteinizing hormone secretion." Am J Physiol Endocrinol Metab **285**(4): E812-818.
Kim, H. H., A. Wolfe, G. R. Smith, S. A. Tobet and S. Radovick (2002). "Promoter sequences targeting tissue-specific gene expression of hypothalamic and ovarian gonadotropin-releasing hormone in vivo." J Biol Chem **277**(7): 5194-5202.
Kirilov, M., J. Clarkson, X. Liu, J. Roa, P. Campos, R. Porteous, G. Schütz and A. E. Herbison (2013). "Dependence of fertility on kisspeptin–Gpr54 signaling at the GnRH neuron." Nature Communications **4**: 2492.
Kommagani, R., M. M. Szwarc, Y. M. Vasquez, M. C. Peavey, E. C. Mazur, W. E. Gibbons, R. B. Lanz, F. J. DeMayo and J. P. Lydon (2016). "The Promyelocytic Leukemia Zinc Finger Transcription Factor Is Critical for Human Endometrial Stromal Cell Decidualization." PLOS Genetics **12**(4): e1005937.
Kong, L., M. Tang, T. Zhang, D. Wang, K. Hu, W. Lu, C. Wei, G. Liang and Y. Pu (2014). "Nickel Nanoparticles Exposure and Reproductive Toxicity in Healthy Adult Rats." International Journal of Molecular Sciences **15**(11): 21253-21269.
Korhonen, S., M. Hippelainen, L. Niskanen, M. Vanhala and S. Saarikoski (2001). "Relationship of the metabolic syndrome and obesity to polycystic ovary syndrome: a controlled, population-based study." Am J Obstet Gynecol **184**(3): 289-296.
Kosidou, K., C. Dalman, L. Widman, S. Arver, B. K. Lee, C. Magnusson and R. M. Gardner (2016). "Maternal polycystic ovary syndrome and the risk of autism spectrum disorders in the offspring: a population-based nationwide study in Sweden." Mol Psychiatry **21**(10): 1441-1448.
Kumar, A., K. S. Woods, A. A. Bartolucci and R. Azziz (2005). "Prevalence of adrenal androgen excess in patients with the polycystic ovary syndrome (PCOS)." Clin Endocrinol (Oxf) **62**(6): 644-649.

Kumar, T. R., G. Palapattu, P. Wang, T. K. Woodruff, I. Boime, M. C. Byrne and M. M. Matzuk (1999). "Transgenic models to study gonadotropin function: the role of follicle-stimulating hormone in gonadal growth and tumorigenesis." Mol Endocrinol **13**(6): 851-865.
Kuroda, M. and H. Sakaue (2017). "Adipocyte Death and Chronic Inflammation in Obesity." J Med Invest **64**(3.4): 193-196.
Kusaczuk, M. (2019). "Tauroursodeoxycholate-Bile Acid with Chaperoning Activity: Molecular and Cellular Effects and Therapeutic Perspectives." Cells **8**(12): 1471.
Kwon, H. and J. E. Pessin (2013). "Adipokines mediate inflammation and insulin resistance." Front Endocrinol (Lausanne) **4**: 71.
Kyronlahti, A., R. Euler, M. Bielinska, E. L. Schoeller, K. H. Moley, J. Toppari, M. Heikinheimo and D. B. Wilson (2011). "GATA4 regulates Sertoli cell function and fertility in adult male mice." Mol Cell Endocrinol **333**(1): 85-95.
Kyrönlahti, A., M. Vetter, R. Euler, M. Bielinska, P. Y. Jay, M. Anttonen, M. Heikinheimo and D. B. Wilson (2011). "GATA4 deficiency impairs ovarian function in adult mice." Biology of reproduction **84**(5): 1033-1044.
Ladson, G., W. C. Dodson, S. D. Sweet, A. E. Archibong, A. R. Kunselman, L. M. Demers, N. I. Williams, P. Coney and R. S. Legro (2011). "The effects of metformin with lifestyle therapy in polycystic ovary syndrome: a randomized double-blind study." Fertil Steril **95**(3): 1059-1066 e1051-1057.
Landres, I. V., A. A. Milki and R. B. Lathi (2010). "Karyotype of miscarriages in relation to maternal weight." Hum Reprod **25**(5): 1123-1126.
Lansdown, A. and D. A. Rees (2012). "The sympathetic nervous system in polycystic ovary syndrome: a novel therapeutic target?" Clin Endocrinol (Oxf) **77**(6): 791-801.
Lapatto, R., J. C. Pallais, D. Zhang, Y.-M. Chan, A. Mahan, F. Cerrato, W. W. Le, G. E. Hoffman and S. B. Seminara (2007). "Kiss1−/− Mice Exhibit More Variable Hypogonadism than Gpr54−/− Mice." Endocrinology **148**(10): 4927-4936.
Lashen, H., K. Fear and D. W. Sturdee (2004). "Obesity is associated with increased risk of first trimester and recurrent miscarriage: matched case-control study." Hum Reprod **19**(7): 1644-1646.
Laverriere, A. C., C. MacNeill, C. Mueller, R. E. Poelmann, J. B. Burch and T. Evans (1994). "GATA-4/5/6, a subfamily of three transcription factors transcribed in developing heart and gut." J Biol Chem **269**(37): 23177-23184.
Lawson, M. A. and P. L. Mellon (1998). "Expression of GATA-4 in migrating gonadotropin-releasing neurons of the developing mouse." Mol Cell Endocrinol **140**(1-2): 157-161.
Lawson, M. A., D. B. Whyte, S. A. Eraly and P. L. Mellon (1995). "Hypothalamus-specific regulation of gonadotropin-releasing hormone gene expression." Recent Prog Horm Res **50**: 459-463.
Lawson, M. A., D. B. Whyte and P. L. Mellon (1996). "GATA factors are essential for activity of the neuron-specific enhancer of the gonadotropin-releasing hormone gene." Mol Cell Biol **16**(7): 3596-3605.

Leaver, R. B. (2016). "Male infertility: an overview of causes and treatment options." Br J Nurs **25**(18): S35-S40.
Lebovitz, H. E. (2001). "Insulin resistance: definition and consequences." Exp Clin Endocrinol Diabetes **109 Suppl 2**: S135-148.
Lebrun, P. and E. Van Obberghen (2008). "SOCS proteins causing trouble in insulin action." Acta Physiol (Oxf) **192**(1): 29-36.
Leclerc, G. M. and F. R. Boockfor (2005). "Identification of a novel OCT1 binding site that is necessary for the elaboration of pulses of rat GnRH promoter activity." Mol Cell Endocrinol **245**(1-2): 86-92.
Leclerc, G. M., S. K. Bose and F. R. Boockfor (2008). "Specific GATA-Binding Elements in the GnRH Promoter Are Required for Gene Expression Pulse Activity: Role of GATA-4 and GATA-5 in This Intermittent Process." Neuroendocrinology **88**(1): 1-16.
Lee, V. H., L. T. Lee and B. K. Chow (2008). "Gonadotropin-releasing hormone: regulation of the GnRH gene." FEBS J **275**(22): 5458-5478.
Lee, W.-S., M. S. Smith and G. E. Hoffman (1990). "PROGESTERONE ENHANCES THE SURGE OF LUTEINIZING HORMONE BY INCREASING THE ACTIVATION OF LUTEINIZING HORMONE-RELEASING HORMONE NEURONS." Endocrinology **127**(5): 2604-2606.
Legro, R. S., D. Driscoll, J. F. Strauss, 3rd, J. Fox and A. Dunaif (1998). "Evidence for a genetic basis for hyperandrogenemia in polycystic ovary syndrome." Proc Natl Acad Sci U S A **95**(25): 14956-14960.
Legro, R. S., D. Finegood and A. Dunaif (1998). "A fasting glucose to insulin ratio is a useful measure of insulin sensitivity in women with polycystic ovary syndrome." J Clin Endocrinol Metab **83**(8): 2694-2698.
Legro, R. S., A. R. Kunselman, W. C. Dodson and A. Dunaif (1999). "Prevalence and predictors of risk for type 2 diabetes mellitus and impaired glucose tolerance in polycystic ovary syndrome: a prospective, controlled study in 254 affected women." J Clin Endocrinol Metab **84**(1): 165-169.
Lei, Z. M. and C. V. Rao (1994). "Novel presence of luteinizing hormone/human chorionic gonadotropin (hCG) receptors and the down-regulating action of hCG on gonadotropin-releasing hormone gene expression in immortalized hypothalamic GT1-7 neurons." Mol Endocrinol **8**(8): 1111-1121.
Lei, Z. M. and C. V. Rao (1995). "Signaling and transacting factors in the transcriptional inhibition of gonadotropin releasing hormone gene by human chorionic gonadotropin in immortalized hypothalamic GT1-7 neurons." Molecular and cellular endocrinology **109**(2): 151-157.
Li, L., J. Zhang, Q. Deng, J. Li, Z. Li, Y. Xiao, S. Hu, T. Li, Q. Tan, X. Li, B. Luo and H. Mo (2016). "Proteomic Profiling for Identification of Novel Biomarkers Differentially Expressed in Human Ovaries from Polycystic Ovary Syndrome Patients." PLoS One **11**(11): e0164538.

Lian, Y., F. Zhao and W. Wang (2016). "Central leptin resistance and hypothalamic inflammation are involved in letrozole-induced polycystic ovary syndrome rats." Biochem Biophys Res Commun **476**(4): 306-312.
Lima, P. D. A., A. L. Nivet, Q. Wang, Y. A. Chen, A. Leader, A. Cheung, C. R. Tzeng and B. K. Tsang (2018). "Polycystic ovary syndrome: possible involvement of androgen-induced, chemerin-mediated ovarian recruitment of monocytes/macrophages." Biol Reprod.
Liu, H. Y., Y. L. Huang, J. Q. Liu and Q. Huang (2016). "Transcription factormicroRNA synergistic regulatory network revealing the mechanism of polycystic ovary syndrome." Mol Med Rep **13**(5): 3920-3928.
Liu, Y. X. and A. J. Hsueh (1986). "Synergism between granulosa and theca-interstitial cells in estrogen biosynthesis by gonadotropin-treated rat ovaries: studies on the two-cell, two-gonadotropin hypothesis using steroid antisera." Biol Reprod **35**(1): 27-36.
Long, Y. C., Z. Cheng, K. D. Copps and M. F. White (2011). "Insulin receptor substrates Irs1 and Irs2 coordinate skeletal muscle growth and metabolism via the Akt and AMPK pathways." Mol Cell Biol **31**(3): 430-441.
Lord, J. M., I. H. Flight and R. J. Norman (2003). "Insulin-sensitising drugs (metformin, troglitazone, rosiglitazone, pioglitazone, D-chiro-inositol) for polycystic ovary syndrome." Cochrane Database Syst Rev(3): CD003053.
Lovelace, D. L., Z. Gao, K. Mutoji, Y. C. Song, J. Ruan and B. P. Hermann (2016). "The regulatory repertoire of PLZF and SALL4 in undifferentiated spermatogonia." Development **143**(11): 1893.
Mahabadi3., T. G. O. A. A. O. S. N. (2020). Ursodeoxycholic Acid In: StatPearls Treasure Island (FL): StatPearls Publishing.
Malin, S. K., J. P. Kirwan, C. L. Sia and F. Gonzalez (2015). "Pancreatic beta-cell dysfunction in polycystic ovary syndrome: role of hyperglycemia-induced nuclear factor-kappaB activation and systemic inflammation." Am J Physiol Endocrinol Metab **308**(9): E770-777.
Maliqueo, M., T. Sir-Petermann, V. Perez, B. Echiburu, A. L. de Guevara, C. Galvez, N. Crisosto and R. Azziz (2009). "Adrenal function during childhood and puberty in daughters of women with polycystic ovary syndrome." J Clin Endocrinol Metab **94**(9): 3282-3288.
Maliqueo, M., M. Sun, J. Johansson, A. Benrick, F. Labrie, H. Svensson, M. Lonn, A. J. Duleba and E. Stener-Victorin (2013). "Continuous administration of a P450 aromatase inhibitor induces polycystic ovary syndrome with a metabolic and endocrine phenotype in female rats at adult age." Endocrinology **154**(1): 434-445.
Mancini, A., S. R. Howard, C. P. Cabrera, M. R. Barnes, A. David, K. Wehkalampi, S. Heger, A. Lomniczi, L. Guasti, S. R. Ojeda and L. Dunkel (2019). "EAP1 regulation of GnRH promoter activity is important for human pubertal timing." Hum Mol Genet **28**(8): 1357-1368.

Manneras, L., S. Cajander, A. Holmang, Z. Seleskovic, T. Lystig, M. Lonn and E. Stener-Victorin (2007). "A new rat model exhibiting both ovarian and metabolic characteristics of polycystic ovary syndrome." Endocrinology **148**(8): 3781-3791.
Marieb, E. N. (2001). Human anatomy & physiology. San Francisco, Benjamin Cummings.
Marino, J. S., J. Iler, A. R. Dowling, S. Chua, J. C. Bruning, R. Coppari and J. W. Hill (2012). "Adipocyte dysfunction in a mouse model of polycystic ovary syndrome (PCOS): evidence of adipocyte hypertrophy and tissue-specific inflammation." PLoS One **7**(10): e48643.
Masson, O., C. Chavey, C. Dray, A. Meulle, D. Daviaud, D. Quilliot, C. Muller, P. Valet and E. Liaudet-Coopman (2009). "LRP1 Receptor Controls Adipogenesis and Is Up-Regulated In Human and Mouse Obese Adipose Tissue." PLOS ONE **4**(10): e7422.
Matzuk, M. M., F. J. DeMayo, L. A. Hadsell and T. R. Kumar (2003). "Overexpression of human chorionic gonadotropin causes multiple reproductive defects in transgenic mice." Biol Reprod **69**(1): 338-346.
Mazaud Guittot, S., A. Tetu, E. Legault, N. Pilon, D. W. Silversides and R. S. Viger (2007). "The proximal Gata4 promoter directs reporter gene expression to sertoli cells during mouse gonadal development." Biol Reprod **76**(1): 85-95.
McAllister, J. M., R. S. Legro, B. P. Modi and J. F. Strauss, 3rd (2015). "Functional genomics of PCOS: from GWAS to molecular mechanisms." Trends Endocrinol Metab **26**(3): 118-124.
McAllister, J. M., B. Modi, B. A. Miller, J. Biegler, R. Bruggeman, R. S. Legro and J. F. Strauss, 3rd (2014). "Overexpression of a DENND1A isoform produces a polycystic ovary syndrome theca phenotype." Proc Natl Acad Sci U S A **111**(15): E1519-1527.
McCartney, C. R. and J. C. Marshall (2016). "CLINICAL PRACTICE. Polycystic Ovary Syndrome." N Engl J Med **375**(1): 54-64.
McLean, A. C., N. Valenzuela, S. Fai and S. A. L. Bennett (2012). "Performing Vaginal Lavage, Crystal Violet Staining, and Vaginal Cytological Evaluation for Mouse Estrous Cycle Staging Identification." Journal of Visualized Experiments : JoVE(67): 4389.
Meehan, T. P., B. G. Harmon, M. E. Overcast, K. K. Yu, S. A. Camper, D. Puett and P. Narayan (2005). "Gonadal defects and hormonal alterations in transgenic mice expressing a single chain human chorionic gonadotropin-lutropin receptor complex." J Mol Endocrinol **34**(2): 489-503.
Mesiano, S., S. L. Katz, J. Y. Lee and R. B. Jaffe (1997). "Insulin-like growth factors augment steroid production and expression of steroidogenic enzymes in human fetal adrenal cortical cells: implications for adrenal androgen regulation." J Clin Endocrinol Metab **82**(5): 1390-1396.
Messager, S., E. E. Chatzidaki, D. Ma, A. G. Hendrick, D. Zahn, J. Dixon, R. R. Thresher, I. Malinge, D. Lomet, M. B. L. Carlton, W. H. Colledge, A. Caraty and S. A. J. R. Aparicio (2005). "Kisspeptin directly stimulates gonadotropin-releasing hormone

release via G protein-coupled receptor 54." Proceedings of the National Academy of Sciences of the United States of America **102**(5): 1761-1766.
Messer, C., R. Boston, D. Leroith, E. Geer, J. D. Miller, M. Messer and W. Futterweit (2012). "Pancreatic beta-cell dysfunction in polycystic ovary syndrome: the role of metformin." Endocr Pract **18**(5): 685-693.
Methot, D., T. L. Reudelhuber and D. W. Silversides (1995). "Evaluation of tyrosinase minigene co-injection as a marker for genetic manipulations in transgenic mice." Nucleic Acids Res **23**(22): 4551-4556.
Metwally, M., R. Cutting, A. Tipton, J. Skull, W. L. Ledger and T. C. Li (2007). "Effect of increased body mass index on oocyte and embryo quality in IVF patients." Reprod Biomed Online **15**(5): 532-538.
Metwally, M., T. C. Li and W. L. Ledger (2007). "The impact of obesity on female reproductive function." Obes Rev **8**(6): 515-523.
Metwally, M., E. M. Tuckerman, S. M. Laird, W. L. Ledger and T. C. Li (2007). "Impact of high body mass index on endometrial morphology and function in the peri-implantation period in women with recurrent miscarriage." Reprod Biomed Online **14**(3): 328-334.
Miller, B. and J. Takahashi (2013). Central Circadian Control of Female Reproductive Function.
Millington, G. W. (2007). "The role of proopiomelanocortin (POMC) neurones in feeding behaviour." Nutrition & metabolism **4**: 18-18.
Miranda-Carboni, G. A., M. Guemes, S. Bailey, E. Anaya, M. Corselli, B. Peault and S. A. Krum (2011). "GATA4 regulates estrogen receptor-alpha-mediated osteoblast transcription." Molecular endocrinology (Baltimore, Md.) **25**(7): 1126-1136.
Mitra, S., P. K. Nayak and S. Agrawal (2015). "Laparoscopic ovarian drilling: An alternative but not the ultimate in the management of polycystic ovary syndrome." J Nat Sci Biol Med **6**(1): 40-48.
Molkentin, J. D. (2000). "The zinc finger-containing transcription factors GATA-4, -5, and -6. Ubiquitously expressed regulators of tissue-specific gene expression." J Biol Chem **275**(50): 38949-38952.
Montgomery, M. K. and N. Turner (2015). "Mitochondrial dysfunction and insulin resistance: an update." Endocrine connections **4**(1): R1-R15.
Moore, A. M., L. M. Coolen, D. T. Porter, R. L. Goodman and M. N. Lehman (2018). "KNDy Cells Revisited." Endocrinology **159**(9): 3219-3234.
Moore, A. M., M. Prescott and R. E. Campbell (2013). "Estradiol negative and positive feedback in a prenatal androgen-induced mouse model of polycystic ovarian syndrome." Endocrinology **154**(2): 796-806.
Moore, A. M., M. Prescott, C. J. Marshall, S. H. Yip and R. E. Campbell (2015). "Enhancement of a robust arcuate GABAergic input to gonadotropin-releasing hormone neurons in a model of polycystic ovarian syndrome." Proceedings of the National Academy of Sciences **112**(2): 596-601.

Moran, L. J., S. K. Hutchison, R. J. Norman and H. J. Teede (2011). "Lifestyle changes in women with polycystic ovary syndrome." Cochrane Database Syst Rev(2): CD007506.
Morino, K., K. F. Petersen, S. Dufour, D. Befroy, J. Frattini, N. Shatzkes, S. Neschen, M. F. White, S. Bilz, S. Sono, M. Pypaert and G. I. Shulman (2005). "Reduced mitochondrial density and increased IRS-1 serine phosphorylation in muscle of insulin-resistant offspring of type 2 diabetic parents." J Clin Invest **115**(12): 3587-3593.
Morrisey, E. E., H. S. Ip, M. M. Lu and M. S. Parmacek (1996). "GATA-6: a zinc finger transcription factor that is expressed in multiple cell lineages derived from lateral mesoderm." Dev Biol **177**(1): 309-322.
Moy, V., S. Jindal, H. Lieman and E. Buyuk (2015). "Obesity adversely affects serum anti-müllerian hormone (AMH) levels in Caucasian women." Journal of Assisted Reproduction and Genetics **32**(9): 1305-1311.
Myers, M., K. L. Britt, N. G. M. Wreford, F. J. P. Ebling and J. B. Kerr (2004). "Methods for quantifying follicular numbers within the mouse ovary." Reproduction **127**(5): 569-580.
Mykhalchenko, K., D. Lizneva, T. Trofimova, W. Walker, L. Suturina, M. P. Diamond and R. Azziz (2017). "Genetics of polycystic ovary syndrome." Expert Rev Mol Diagn **17**(7): 723-733.
Nagy A., G. M., Vintersten K. and Behringer R. (2003). " Manipulating the Mouse Embryo." Cold Spring Harbor Laboratory Press.(3rd edition).
Navarro, V. M. (2013). "Interactions between kisspeptins and neurokinin B." Advances in experimental medicine and biology **784**: 325-347.
Navarro, V. M., M. L. Gottsch, C. Chavkin, H. Okamura, D. K. Clifton and R. A. Steiner (2009). "Regulation of Gonadotropin-Releasing Hormone Secretion by Kisspeptin/Dynorphin/Neurokinin B Neurons in the Arcuate Nucleus of the Mouse." The Journal of Neuroscience **29**(38): 11859-11866.
Nestler, J. E. (1997). "Role of hyperinsulinemia in the pathogenesis of the polycystic ovary syndrome, and its clinical implications." Semin Reprod Endocrinol **15**(2): 111-122.
Nestler, J. E., D. J. Jakubowicz, A. F. de Vargas, C. Brik, N. Quintero and F. Medina (1998). "Insulin stimulates testosterone biosynthesis by human thecal cells from women with polycystic ovary syndrome by activating its own receptor and using inositolglycan mediators as the signal transduction system." J Clin Endocrinol Metab **83**(6): 2001-2005.
Nestler, J. E., L. P. Powers, D. W. Matt, K. A. Steingold, S. R. Plymate, R. S. Rittmaster, J. N. Clore and W. G. Blackard (1991). "A direct effect of hyperinsulinemia on serum sex hormone-binding globulin levels in obese women with the polycystic ovary syndrome." J Clin Endocrinol Metab **72**(1): 83-89.
Ng, Y. K., K. M. George, J. D. Engel and D. I. Linzer (1994). "GATA factor activity is required for the trophoblast-specific transcriptional regulation of the mouse placental lactogen I gene." Development **120**(11): 3257-3266.

Nikolaou, D. and C. Gilling-Smith (2004). "Early ovarian ageing: are women with polycystic ovaries protected?" Human Reproduction **19**(10): 2175-2179.
Nilsson, C., M. Jiang, K. Pettersson, A. Iitia, M. Makela, H. Simonsen, S. Easteal, R. J. Herrera and I. Huhtaniemi (1998). "Determination of a common genetic variant of luteinizing hormone using DNA hybridization and immunoassays." Clin Endocrinol (Oxf) **49**(3): 369-376.
Nimrod, A., G. F. Erickson and K. J. Ryan (1976). "A specific FSH receptor in rat granulosa cells: properties of binding in vitro." Endocrinology **98**(1): 56-64.
Nuñez, L., W. J. Faught and L. S. Frawley (1998). "Episodic gonadotropin-releasing hormone gene expression revealed by dynamic monitoring of luciferase reporter activity in single, living neurons." Proceedings of the National Academy of Sciences **95**(16): 9648-9653.
O'Byrne, K. T., J. C. Thalabard, P. M. Grosser, R. C. Wilson, C. L. Williams, M. D. Chen, D. Ladendorf, J. Hotchkiss and E. Knobil (1991). "Radiotelemetric monitoring of hypothalamic gonadotropin-releasing hormone pulse generator activity throughout the menstrual cycle of the rhesus monkey." Endocrinology **129**(3): 1207-1214.
Odle, A. K., N. Akhter, M. M. Syed, M. L. Allensworth-James, H. Beneš, A. I. Melgar Castillo, M. C. MacNicol, A. M. MacNicol and G. V. Childs (2018). "Leptin Regulation of Gonadotrope Gonadotropin-Releasing Hormone Receptors As a Metabolic Checkpoint and Gateway to Reproductive Competence." Frontiers in endocrinology **8**: 367-367.
Oh, J., J. Y. Kim, H. S. Kim, J. C. Oh, Y. H. Cheon, J. Park, K. H. Yoon, M. S. Lee and B. S. Youn (2015). "Progranulin and a five transmembrane domain-containing receptor-like gene are the key components in receptor activator of nuclear factor κB (RANK)-dependent formation of multinucleated osteoclasts." J Biol Chem **290**(4): 2042-2052.
OpenStax (2013). Anatomy and Physiology, OpenStax.
Osuka, S., A. Iwase, T. Nakahara, M. Kondo, A. Saito, Bayasula, T. Nakamura, S. Takikawa, M. Goto, T. Kotani and F. Kikkawa (2016). "Kisspeptin in the Hypothalamus of 2 Rat Models of Polycystic Ovary Syndrome." Endocrinology **158**(2): 367-377.
Ozawa, K., M. Miyazaki, M. Matsuhisa, K. Takano, Y. Nakatani, M. Hatazaki, T. Tamatani, K. Yamagata, J. Miyagawa, Y. Kitao, O. Hori, Y. Yamasaki and S. Ogawa (2005). "The endoplasmic reticulum chaperone improves insulin resistance in type 2 diabetes." Diabetes **54**(3): 657-663.
Ozcan, U., E. Yilmaz, L. Ozcan, M. Furuhashi, E. Vaillancourt, R. O. Smith, C. Z. Görgün and G. S. Hotamisligil (2006). "Chemical chaperones reduce ER stress and restore glucose homeostasis in a mouse model of type 2 diabetes." Science (New York, N.Y.) **313**(5790): 1137-1140.
Padmanabhan, V. and A. Veiga-Lopez (2013). "Sheep models of polycystic ovary syndrome phenotype." Mol Cell Endocrinol **373**(1-2): 8-20.

Pagel-Langenickel, I., J. Bao, L. Pang and M. N. Sack (2010). "The role of mitochondria in the pathophysiology of skeletal muscle insulin resistance." Endocr Rev **31**(1): 25-51.
Palomba, S., J. Daolio and G. B. La Sala (2017). "Oocyte Competence in Women with Polycystic Ovary Syndrome." Trends Endocrinol Metab **28**(3): 186-198.
Palomba, S., A. Falbo and G. B. La Sala (2014). "Metformin and gonadotropins for ovulation induction in patients with polycystic ovary syndrome: a systematic review with meta-analysis of randomized controlled trials." Reproductive biology and endocrinology : RB&E **12**: 3-3.
Pan, X. L., L. Zhao, L. Li, A. H. Li, J. Ye, L. Yang, K. S. Xu and X. H. Hou (2013). "Efficacy and safety of tauroursodeoxycholic acid in the treatment of liver cirrhosis: a double-blind randomized controlled trial." J Huazhong Univ Sci Technolog Med Sci **33**(2): 189-194.
Panella, C., E. Ierardi, M. F. De Marco, M. Barone, F. W. Guglielmi, L. Polimeno and A. Francavilla (1995). "Does tauroursodeoxycholic acid (TUDCA) treatment increase hepatocyte proliferation in patients with chronic liver disease?" Ital J Gastroenterol **27**(5): 256-258.
Pastor, C. L., M. L. Griffin-Korf, J. A. Aloi, W. S. Evans and J. C. Marshall (1998). "Polycystic Ovary Syndrome: Evidence for Reduced Sensitivity of the Gonadotropin-Releasing Hormone Pulse Generator to Inhibition by Estradiol and Progesterone1." The Journal of Clinical Endocrinology & Metabolism **83**(2): 582-590.
Patient, R. K. and J. D. McGhee (2002). "The GATA family (vertebrates and invertebrates)." Curr Opin Genet Dev **12**(4): 416-422.
Pavone, M. E. and S. E. Bulun (2013). "Clinical review: The use of aromatase inhibitors for ovulation induction and superovulation." J Clin Endocrinol Metab **98**(5): 1838-1844.
Perlman, R. L. (2016). "Mouse models of human disease: An evolutionary perspective." Evolution, medicine, and public health **2016**(1): 170-176.
Perseghin, G., K. Petersen and G. I. Shulman (2003). "Cellular mechanism of insulin resistance: potential links with inflammation." Int J Obes Relat Metab Disord **27 Suppl 3**: S6-11.
Pigny, P., S. Jonard, Y. Robert and D. Dewailly (2006). "Serum anti-Mullerian hormone as a surrogate for antral follicle count for definition of the polycystic ovary syndrome." J Clin Endocrinol Metab **91**(3): 941-945.
Pigny, P., E. Merlen, Y. Robert, C. Cortet-Rudelli, C. Decanter, S. Jonard and D. Dewailly (2003). "Elevated serum level of anti-mullerian hormone in patients with polycystic ovary syndrome: relationship to the ovarian follicle excess and to the follicular arrest." J Clin Endocrinol Metab **88**(12): 5957-5962.
Pilon, N., D. Raiwet, R. S. Viger and D. W. Silversides (2008). "Novel pre- and post-gastrulation expression of Gata4 within cells of the inner cell mass and migratory neural crest cells." Dev Dyn **237**(4): 1133-1143.

Pincas, H., K. Amoyel, R. Counis and J.-N. l. Laverrière (2001). "Proximal cis-Acting Elements, Including Steroidogenic Factor 1, Mediate the Efficiency of a Distal Enhancer in the Promoter of the Rat Gonadotropin-Releasing Hormone Receptor Gene." Molecular Endocrinology **15**(2): 319-337.
Plant, T. M. (2015). "60 YEARS OF NEUROENDOCRINOLOGY: The hypothalamo-pituitary-gonadal axis." The Journal of endocrinology **226**(2): T41-T54.
Polak, K., A. Czyzyk, T. Simoncini and B. Meczekalski (2017). "New markers of insulin resistance in polycystic ovary syndrome." J Endocrinol Invest **40**(1): 1-8.
Qiao, J. and H. L. Feng (2010). "Extra- and intra-ovarian factors in polycystic ovary syndrome: impact on oocyte maturation and embryo developmental competence." Human Reproduction Update **17**(1): 17-33.
Qiao, J. and H. L. Feng (2011). "Extra- and intra-ovarian factors in polycystic ovary syndrome: impact on oocyte maturation and embryo developmental competence." Human reproduction update **17**(1): 17-33.
Radovick, S., C. M. Ticknor, Y. Nakayama, A. C. Notides, A. Rahman, B. D. Weintraub, G. B. Cutler, Jr. and F. E. Wondisford (1991). "Evidence for direct estrogen regulation of the human gonadotropin-releasing hormone gene." The Journal of clinical investigation **88**(5): 1649-1655.
Rahman, N. A., S. Kiiveri, A. Rivero-Müller, J. r. m. Levallet, S. Vierre, J. Kero, D. B. Wilson, M. Heikinheimo and I. Huhtaniemi (2004). "Adrenocortical Tumorigenesis in Transgenic Mice Expressing the Inhibin α-Subunit Promoter/Simian Virus 40 T-Antigen Transgene: Relationship between Ectopic Expression of Luteinizing Hormone Receptor and Transcription Factor GATA-4." Molecular Endocrinology **18**(10): 2553-2569.
Rahman, N. A., S. Kiiveri, S. Siltanen, J. Levallet, J. Kero, T. Lensu, D. B. Wilson, M. T. Heikinheimo and I. T. Huhtaniemi (2001). "Adrenocortical tumorigenesis in transgenic mice: the role of luteinizing hormone receptor and transcription factors GATA-4 and GATA-61." Reprod Biol **1**(1): 5-9.
Rave-Harel, N., M. L. Givens, S. B. Nelson, H. A. Duong, D. Coss, M. E. Clark, S. B. Hall, M. P. Kamps and P. L. Mellon (2004). "TALE homeodomain proteins regulate gonadotropin-releasing hormone gene expression independently and via interactions with Oct-1." J Biol Chem **279**(29): 30287-30297.
Rave-Harel, N., M. L. Givens, S. B. Nelson, H. A. Duong, D. Coss, M. E. Clark, S. B. Hall, M. P. Kamps and P. L. Mellon (2004). "TALE homeodomain proteins regulate gonadotropin-releasing hormone gene expression independently and via interactions with Oct-1." The Journal of biological chemistry **279**(29): 30287-30297.
Rebar, R., H. L. Judd, S. S. Yen, J. Rakoff, G. Vandenberg and F. Naftolin (1976). "Characterization of the inappropriate gonadotropin secretion in polycystic ovary syndrome." J Clin Invest **57**(5): 1320-1329.
Reid, S. P., C.-N. Kao, L. Pasch, K. Shinkai, M. I. Cedars and H. G. Huddleston (2017). "Ovarian morphology is associated with insulin resistance in women with polycystic ovary syndrome: a cross sectional study." Fertility Research and Practice **3**(1): 8.

Rena, G., E. R. Pearson and K. Sakamoto (2013). "Molecular mechanism of action of metformin: old or new insights?" Diabetologia **56**(9): 1898-1906.
Rice, G. M. and R. D. Steiner (2016). "Inborn Errors of Metabolism (Metabolic Disorders)." Pediatr Rev **37**(1): 3-15; quiz 16-17, 47.
Rice, S., A. Elia, Z. Jawad, L. Pellatt and H. D. Mason (2013). "Metformin inhibits follicle-stimulating hormone (FSH) action in human granulosa cells: relevance to polycystic ovary syndrome." J Clin Endocrinol Metab **98**(9): E1491-1500.
Rich-Edwards, J. W., M. B. Goldman, W. C. Willett, D. J. Hunter, M. J. Stampfer, G. A. Colditz and J. E. Manson (1994). "Adolescent body mass index and infertility caused by ovulatory disorder." Am J Obstet Gynecol **171**(1): 171-177.
Risma, K. A., C. M. Clay, T. M. Nett, T. Wagner, J. Yun and J. H. Nilson (1995). "Targeted overexpression of luteinizing hormone in transgenic mice leads to infertility, polycystic ovaries, and ovarian tumors." Proc Natl Acad Sci U S A **92**(5): 1322-1326.
Rittenberg, V., S. Seshadri, S. K. Sunkara, S. Sobaleva, E. Oteng-Ntim and T. El-Toukhy (2011). "Effect of body mass index on IVF treatment outcome: an updated systematic review and meta-analysis." Reprod Biomed Online **23**(4): 421-439.
Robinson, S., D. Kiddy, S. V. Gelding, D. Willis, R. Niththyananthan, A. Bush, D. G. Johnston and S. Franks (1993). "The relationship of insulin insensitivity to menstrual pattern in women with hyperandrogenism and polycystic ovaries." Clin Endocrinol (Oxf) **39**(3): 351-355.
Rogers, J. and G. W. Mitchell, Jr. (1952). "The relation of obesity to menstrual disturbances." N Engl J Med **247**(2): 53-55.
Rojas, J., M. Chávez, L. Olivar, M. Rojas, J. Morillo, J. Mejías, M. Calvo and V. Bermúdez (2014). "Polycystic ovary syndrome, insulin resistance, and obesity: navigating the pathophysiologic labyrinth." International journal of reproductive medicine **2014**: 719050-719050.
Rojas, J., M. Chávez, L. Olivar, M. Rojas, J. Morillo, J. Mejías, M. Calvo and V. Bermúdez (2014). "Polycystic Ovary Syndrome, Insulin Resistance, and Obesity: Navigating the Pathophysiologic Labyrinth." International Journal of Reproductive Medicine **2014**: 719050.
Roland, A. V. and S. M. Moenter (2011). "Prenatal androgenization of female mice programs an increase in firing activity of gonadotropin-releasing hormone (GnRH) neurons that is reversed by metformin treatment in adulthood." Endocrinology **152**(2): 618-628.
Roland, A. V. and S. M. Moenter (2011). "Prenatal Androgenization of Female Mice Programs an Increase in Firing Activity of Gonadotropin-Releasing Hormone (GnRH) Neurons That Is Reversed by Metformin Treatment in Adulthood." Endocrinology **152**(2): 618-628.
Roland, A. V., C. S. Nunemaker, S. R. Keller and S. M. Moenter (2010). "Prenatal androgen exposure programs metabolic dysfunction in female mice." J Endocrinol **207**(2): 213-223.

Roque, M., A. C. Tostes, M. Valle, M. Sampaio and S. Geber (2015). "Letrozole versus clomiphene citrate in polycystic ovary syndrome: systematic review and meta-analysis." Gynecol Endocrinol **31**(12): 917-921.
Rosenfield, R. L. and D. A. Ehrmann (2016). "The Pathogenesis of Polycystic Ovary Syndrome (PCOS): The Hypothesis of PCOS as Functional Ovarian Hyperandrogenism Revisited." Endocrine Reviews **37**(5): 467-520.
Rosenfield, R. L. and D. A. Ehrmann (2016). "The Pathogenesis of Polycystic Ovary Syndrome (PCOS): The Hypothesis of PCOS as Functional Ovarian Hyperandrogenism Revisited." Endocr Rev **37**(5): 467-520.
Roy, D., N. L. Angelini and D. D. Belsham (1999). "Estrogen directly respresses gonadotropin-releasing hormone (GnRH) gene expression in estrogen receptor-alpha (ERalpha)- and ERbeta-expressing GT1-7 GnRH neurons." Endocrinology **140**(11): 5045-5053.
Ruderman, N. B., D. Carling, M. Prentki and J. M. Cacicedo (2013). "AMPK, insulin resistance, and the metabolic syndrome." The Journal of clinical investigation **123**(7): 2764-2772.
Rulli, S. B., A. Kuorelahti, O. Karaer, L. J. Pelliniemi, M. Poutanen and I. Huhtaniemi (2002). "Reproductive disturbances, pituitary lactotrope adenomas, and mammary gland tumors in transgenic female mice producing high levels of human chorionic gonadotropin." Endocrinology **143**(10): 4084-4095.
Rutkowska, A. Z. and E. Diamanti-Kandarakis (2016). "Polycystic ovary syndrome and environmental toxins." Fertil Steril **106**(4): 948-958.
Sabatini, M. E., L. Guo, M. P. Lynch, J. O. Doyle, H. Lee, B. R. Rueda and A. K. Styer (2011). "Metformin therapy in a hyperandrogenic anovulatory mutant murine model with polycystic ovarian syndrome characteristics improves oocyte maturity during superovulation." Journal of Ovarian Research **4**: 8-8.
Sahmay, S., Y. Aydin, M. Oncul and L. M. Senturk (2014). "Diagnosis of Polycystic Ovary Syndrome: AMH in combination with clinical symptoms." Journal of assisted reproduction and genetics **31**(2): 213-220.
Saisho, Y. (2016). "Pancreas Volume and Fat Deposition in Diabetes and Normal Physiology: Consideration of the Interplay Between Endocrine and Exocrine Pancreas." The review of diabetic studies : RDS **13**(2-3): 132-147.
Sakumoto, T., Y. Tokunaga, H. Tanaka, M. Nohara, E. Motegi, T. Shinkawa, A. Nakaza and M. Higashi (2010). "Insulin resistance/hyperinsulinemia and reproductive disorders in infertile women." Reproductive medicine and biology **9**(4): 185-190.
Sam, S. (2007). "Obesity and Polycystic Ovary Syndrome." Obesity management **3**(2): 69-73.
Sarwar, R., N. Pierce and S. Koppe (2018). "Obesity and nonalcoholic fatty liver disease: current perspectives." Diabetes, metabolic syndrome and obesity : targets and therapy **11**: 533-542.
Sawetawan, C., B. R. Carr, E. McGee, I. M. Bird, T. L. Hong and W. E. Rainey (1996). "Inhibin and activin differentially regulate androgen production and 17 alpha-

hydroxylase expression in human ovarian thecal-like tumor cells." J Endocrinol **148**(2): 213-221.
Scott M, C. (2018). Role of GATA4, GATA6, and SP1 on Luteal Function and LH Receptor Expression.
Scott-Drechsel, D. E., S. Rugonyi, D. L. Marks, K. L. Thornburg and M. T. Hinds (2013). "Hyperglycemia slows embryonic growth and suppresses cell cycle via cyclin D1 and p21." Diabetes **62**(1): 234-242.
Sen, A. and S. R. Hammes (2010). "Granulosa cell-specific androgen receptors are critical regulators of ovarian development and function." Mol Endocrinol **24**(7): 1393-1403.
Senn, J. J., P. J. Klover, I. A. Nowak, T. A. Zimmers, L. G. Koniaris, R. W. Furlanetto and R. A. Mooney (2003). "Suppressor of cytokine signaling-3 (SOCS-3), a potential mediator of interleukin-6-dependent insulin resistance in hepatocytes." J Biol Chem **278**(16): 13740-13746.
Shaw, J. E., P. Z. Zimmet, M. de Courten, G. K. Dowse, P. Chitson, H. Gareeboo, F. Hemraj, D. Fareed, J. Tuomilehto and K. G. Alberti (1999). "Impaired fasting glucose or impaired glucose tolerance. What best predicts future diabetes in Mauritius?" Diabetes Care **22**(3): 399-402.
Shi, Y., H. Zhao, Y. Shi, Y. Cao, D. Yang, Z. Li, B. Zhang, X. Liang, T. Li, J. Chen, J. Shen, J. Zhao, L. You, X. Gao, D. Zhu, X. Zhao, Y. Yan, Y. Qin, W. Li, J. Yan, Q. Wang, J. Zhao, L. Geng, J. Ma, Y. Zhao, G. He, A. Zhang, S. Zou, A. Yang, J. Liu, W. Li, B. Li, C. Wan, Y. Qin, J. Shi, J. Yang, H. Jiang, J.-e. Xu, X. Qi, Y. Sun, Y. Zhang, C. Hao, X. Ju, D. Zhao, C.-e. Ren, X. Li, W. Zhang, Y. Zhang, J. Zhang, D. Wu, C. Zhang, L. He and Z.-J. Chen (2012). "Genome-wide association study identifies eight new risk loci for polycystic ovary syndrome." Nature Genetics **44**: 1020.
Shi, Y. H., D. N. Zhao, J. L. Zhao, L. You, H. Liu, M. Sun and Z. J. Chen (2010). "[Characteristics of glucose metabolism in non-obese and obese women with polycystic ovarian syndrome]." Zhonghua Fu Chan Ke Za Zhi **45**(8): 575-577.
Shorakae, S., S. Ranasinha, S. Abell, G. Lambert, E. Lambert, B. de Courten and H. Teede (2018). "Inter-related effects of insulin resistance, hyperandrogenism, sympathetic dysfunction and chronic inflammation in PCOS." Clin Endocrinol (Oxf) **89**(5): 628-633.
Silva, M. S. B., M. Prescott and R. E. Campbell (2018). "Ontogeny and reversal of brain circuit abnormalities in a preclinical model of PCOS." JCI Insight **3**(7).
Silvestris, E., G. de Pergola, R. Rosania and G. Loverro (2018). "Obesity as disruptor of the female fertility." Reproductive biology and endocrinology : RB&E **16**(1): 22-22.
Simonis-Bik, A. M., G. Nijpels, T. W. van Haeften, J. J. Houwing-Duistermaat, D. I. Boomsma, E. Reiling, E. C. van Hove, M. Diamant, M. H. Kramer, R. J. Heine, J. A. Maassen, P. E. Slagboom, G. Willemsen, J. M. Dekker, E. M. Eekhoff, E. J. de Geus and L. M. t Hart (2010). "Gene variants in the novel type 2 diabetes loci CDC123/CAMK1D, THADA, ADAMTS9, BCL11A, and MTNR1B affect different aspects of pancreatic beta-cell function." Diabetes **59**(1): 293-301.

Singh, S. P., A. Wolfe, Y. Ng, S. A. DiVall, C. Buggs, J. E. Levine, F. E. Wondisford and S. Radovick (2009). "Impaired estrogen feedback and infertility in female mice with pituitary-specific deletion of estrogen receptor alpha (ESR1)." Biol Reprod **81**(3): 488-496.
Sirmans, S. M. and K. A. Pate (2013). "Epidemiology, diagnosis, and management of polycystic ovary syndrome." Clin Epidemiol **6**: 1-13.
Smith, J. T., M. J. Cunningham, E. F. Rissman, D. K. Clifton and R. A. Steiner (2005). "Regulation of Kiss1 Gene Expression in the Brain of the Female Mouse." Endocrinology **146**(9): 3686-3692.
Snider, A. P. and J. R. Wood (2019). "Obesity Induces Ovarian Inflammation and Reduces Oocyte Quality." Reproduction.
Sommerweiss, D., T. Gorski, S. Richter, A. Garten and W. Kiess (2013). "Oleate rescues INS-1E beta-cells from palmitate-induced apoptosis by preventing activation of the unfolded protein response." Biochem Biophys Res Commun **441**(4): 770-776.
Stephens, S. B. Z., K. P. Tolson, M. L. Rouse, Jr., M. C. Poling, M. K. Hashimoto-Partyka, P. L. Mellon and A. S. Kauffman (2015). "Absent Progesterone Signaling in Kisspeptin Neurons Disrupts the LH Surge and Impairs Fertility in Female Mice." Endocrinology **156**(9): 3091-3097.
Steyn, F. J., Y. Wan, J. Clarkson, J. D. Veldhuis, A. E. Herbison and C. Chen (2013). "Development of a Methodology for and Assessment of Pulsatile Luteinizing Hormone Secretion in Juvenile and Adult Male Mice." Endocrinology **154**(12): 4939-4945.
Suh, H., P. J. Gage, J. Drouin and S. A. Camper (2002). "Pitx2 is required at multiple stages of pituitary organogenesis: pituitary primordium formation and cell specification." Development **129**(2): 329-337.
Sullivan, S. D. and S. M. Moenter (2004). "Prenatal androgens alter GABAergic drive to gonadotropin-releasing hormone neurons: Implications for a common fertility disorder." Proceedings of the National Academy of Sciences of the United States of America **101**(18): 7129-7134.
Sun, H., B. A. Rowan, P. J. Flood, R. Brandt, J. Fuss, A. M. Hancock, R. W. Michelmore, B. Huettel and K. Schneeberger (2019). "Linked-read sequencing of gametes allows efficient genome-wide analysis of meiotic recombination." Nature Communications **10**(1): 4310.
Suzuki, E., T. Evans, J. Lowry, L. Truong, D. W. Bell, J. R. Testa and K. Walsh (1996). "The human GATA-6 gene: structure, chromosomal location, and regulation of expression by tissue-specific and mitogen-responsive signals." Genomics **38**(3): 283-290.
Swann, K. (2014). Effects of ovarian stimulation on oocyte development and embryo quality.
Swerdloff, R. S., R. E. Dudley, S. T. Page, C. Wang and W. A. Salameh (2017). "Dihydrotestosterone: Biochemistry, Physiology, and Clinical Implications of Elevated Blood Levels." Endocr Rev **38**(3): 220-254.

Takahashi, N., M. Harada, J. M. K. Azhary, C. Kunitomi, E. Nose, H. Terao, H. Koike, O. Wada-Hiraike, T. Hirata, Y. Hirota, K. Koga, T. Fujii and Y. Osuga (2019). "Accumulation of advanced glycation end products in follicles is associated with poor oocyte developmental competence." Mol Hum Reprod **25**(11): 684-694.
Takahashi, N., M. Harada, Y. Hirota, E. Nose, J. M. Azhary, H. Koike, C. Kunitomi, O. Yoshino, G. Izumi, T. Hirata, K. Koga, O. Wada-Hiraike, R. J. Chang, S. Shimasaki, T. Fujii and Y. Osuga (2017). "Activation of Endoplasmic Reticulum Stress in Granulosa Cells from Patients with Polycystic Ovary Syndrome Contributes to Ovarian Fibrosis." Sci Rep **7**(1): 10824.
Takahashi, N., M. Harada, Y. Hirota, E. Nose, J. M. K. Azhary, H. Koike, C. Kunitomi, O. Yoshino, G. Izumi, T. Hirata, K. Koga, O. Wada-Hiraike, R. J. Chang, S. Shimasaki, T. Fujii and Y. Osuga (2017). "Activation of Endoplasmic Reticulum Stress in Granulosa Cells from Patients with Polycystic Ovary Syndrome Contributes to Ovarian Fibrosis." Scientific Reports **7**: 10824.
Tantin, D., C. Schild-Poulter, V. Wang, R. J. G. Haché and P. A. Sharp (2005). "The Octamer Binding Transcription Factor Oct-1 Is a Stress Sensor." Cancer Research **65**(23): 10750-10758.
Tark-Dame, M., R. van Driel and D. W. Heermann (2011). "Chromatin folding--from biology to polymer models and back." J Cell Sci **124**(Pt 6): 839-845.
Tata, B., N. E. H. Mimouni, A.-L. Barbotin, S. A. Malone, A. Loyens, P. Pigny, D. Dewailly, S. Catteau-Jonard, I. Sundström-Poromaa, T. T. Piltonen, F. Dal Bello, C. Medana, V. Prevot, J. Clasadonte and P. Giacobini (2018). "Elevated prenatal anti-Müllerian hormone reprograms the fetus and induces polycystic ovary syndrome in adulthood." Nature Medicine **24**(6): 834-846.
Taylor, A. E., B. McCourt, K. A. Martin, E. J. Anderson, J. M. Adams, D. Schoenfeld and J. E. Hall (1997). "Determinants of abnormal gonadotropin secretion in clinically defined women with polycystic ovary syndrome." J Clin Endocrinol Metab **82**(7): 2248-2256.
Teede, H., A. Deeks and L. Moran (2010). "Polycystic ovary syndrome: a complex condition with psychological, reproductive and metabolic manifestations that impacts on health across the lifespan." BMC Med **8**: 41.
Terasawa, E., J. P. Garcia, S. B. Seminara and K. L. Keen (2018). "Role of Kisspeptin and Neurokinin B in Puberty in Female Non-Human Primates." Frontiers in Endocrinology **9**(148).
Thompson, I. R. and U. B. Kaiser (2014). "GnRH pulse frequency-dependent differential regulation of LH and FSH gene expression." Molecular and cellular endocrinology **385**(1-2): 28-35.
Timper, K. and J. C. Brüning (2017). "Hypothalamic circuits regulating appetite and energy homeostasis: pathways to obesity." Disease models & mechanisms **10**(6): 679-689.
Topaloglu, A. K., F. Reimann, M. Guclu, A. S. Yalin, L. D. Kotan, K. M. Porter, A. Serin, N. O. Mungan, J. R. Cook, S. Imamoglu, N. S. Akalin, B. Yuksel, S. O'Rahilly

and R. K. Semple (2009). "TAC3 and TACR3 mutations in familial hypogonadotropic hypogonadism reveal a key role for Neurokinin B in the central control of reproduction." Nat Genet **41**(3): 354-358.
Topilko, P., S. Schneider-Maunoury, G. Levi, A. Trembleau, D. Gourdji, M. A. Driancourt, C. V. Rao and P. Charnay (1998). "Multiple pituitary and ovarian defects in Krox-24 (NGFI-A, Egr-1)-targeted mice." Mol Endocrinol **12**(1): 107-122.
Tortoriello, D. V., J. McMinn and S. C. Chua (2004). "Dietary-induced obesity and hypothalamic infertility in female DBA/2J mice." Endocrinology **145**(3): 1238-1247.
Treloar, A. E., R. E. Boynton, B. G. Behn and B. W. Brown (1967). "Variation of the human menstrual cycle through reproductive life." Int J Fertil **12**(1 Pt 2): 77-126.
Tso, L. O., M. F. Costello, L. E. T. Albuquerque, R. B. Andriolo and C. R. Macedo (2014). "Metformin treatment before and during IVF or ICSI in women with polycystic ovary syndrome." The Cochrane database of systematic reviews **2014**(11): CD006105-CD006105.
Tzivion, G., M. Dobson and G. Ramakrishnan (2011). "FoxO transcription factors; Regulation by AKT and 14-3-3 proteins." Biochim Biophys Acta **1813**(11): 1938-1945.
Uppala, J. K., A. R. Gani and K. V. A. Ramaiah (2017). "Chemical chaperone, TUDCA unlike PBA, mitigates protein aggregation efficiently and resists ER and non-ER stress induced HepG2 cell death." Scientific Reports **7**(1): 3831.
Vagi, S. J., E. Azziz-Baumgartner, A. Sjodin, A. M. Calafat, D. Dumesic, L. Gonzalez, K. Kato, M. J. Silva, X. Ye and R. Azziz (2014). "Exploring the potential association between brominated diphenyl ethers, polychlorinated biphenyls, organochlorine pesticides, perfluorinated compounds, phthalates, and bisphenol A in polycystic ovary syndrome: a case-control study." BMC Endocr Disord **14**: 86.
van Houten, E. L., P. Kramer, A. McLuskey, B. Karels, A. P. Themmen and J. A. Visser (2012). "Reproductive and metabolic phenotype of a mouse model of PCOS." Endocrinology **153**(6): 2861-2869.
Vang, S., K. Longley, C. J. Steer and W. C. Low (2014). "The Unexpected Uses of Urso- and Tauroursodeoxycholic Acid in the Treatment of Non-liver Diseases." Global advances in health and medicine **3**(3): 58-69.
Vazquez-Martinez, R., G. M. Leclerc, M. E. Wierman and F. R. Boockfor (2002). "Episodic activation of the rat GnRH promoter: role of the homeoprotein oct-1." Mol Endocrinol **16**(9): 2093-2100.
Velazquez, E. M., S. Mendoza, T. Hamer, F. Sosa and C. J. Glueck (1994). "Metformin therapy in polycystic ovary syndrome reduces hyperinsulinemia, insulin resistance, hyperandrogenemia, and systolic blood pressure, while facilitating normal menses and pregnancy." Metabolism **43**(5): 647-654.
Viger, R. S., S. M. Guittot, M. Anttonen, D. B. Wilson and M. Heikinheimo (2008). "Role of the GATA family of transcription factors in endocrine development, function, and disease." Molecular endocrinology (Baltimore, Md.) **22**(4): 781-798.

Vink, J. M., S. Sadrzadeh, C. B. Lambalk and D. I. Boomsma (2006). "Heritability of polycystic ovary syndrome in a Dutch twin-family study." J Clin Endocrinol Metab **91**(6): 2100-2104.
Waldstreicher, J., N. F. Santoro, J. E. Hall, M. Filicori and W. F. Crowley, Jr. (1988). "Hyperfunction of the hypothalamic-pituitary axis in women with polycystic ovarian disease: indirect evidence for partial gonadotroph desensitization." J Clin Endocrinol Metab **66**(1): 165-172.
Wang, N., G. D. Frank, R. Ding, Z. Tan, A. Rachakonda, P. P. Pandolfi, T. Senbonmatsu, E. J. Landon and T. Inagami (2012). "Promyelocytic Leukemia Zinc Finger Protein Activates GATA4 Transcription and Mediates Cardiac Hypertrophic Signaling from Angiotensin II Receptor 2." PLOS ONE **7**(4): e35632.
Wang, T., S. Han, W. Tian, M. Zhao and H. Zhang (2019). "Effects of kisspeptin on pathogenesis and energy metabolism in polycystic ovarian syndrome (PCOS)." Gynecological Endocrinology **35**(9): 807-810.
Wang, W., J. Cai, L. Liu, Y. Xu, Z. Liu, J. Chen, X. Jiang, X. Sun and J. Ren (2020). "Does the transfer of a poor quality embryo with a good quality embryo benefit poor prognosis patients?" Reproductive Biology and Endocrinology **18**(1): 97.
Waterston, R. H., K. Lindblad-Toh, E. Birney, J. Rogers, J. F. Abril, P. Agarwal, R. Agarwala, R. Ainscough, M. Alexandersson, P. An, S. E. Antonarakis, J. Attwood, R. Baertsch, J. Bailey, K. Barlow, S. Beck, E. Berry, B. Birren, T. Bloom, P. Bork, M. Botcherby, N. Bray, M. R. Brent, D. G. Brown, S. D. Brown, C. Bult, J. Burton, J. Butler, R. D. Campbell, P. Carninci, S. Cawley, F. Chiaromonte, A. T. Chinwalla, D. M. Church, M. Clamp, C. Clee, F. S. Collins, L. L. Cook, R. R. Copley, A. Coulson, O. Couronne, J. Cuff, V. Curwen, T. Cutts, M. Daly, R. David, J. Davies, K. D. Delehaunty, J. Deri, E. T. Dermitzakis, C. Dewey, N. J. Dickens, M. Diekhans, S. Dodge, I. Dubchak, D. M. Dunn, S. R. Eddy, L. Elnitski, R. D. Emes, P. Eswara, E. Eyras, A. Felsenfeld, G. A. Fewell, P. Flicek, K. Foley, W. N. Frankel, L. A. Fulton, R. S. Fulton, T. S. Furey, D. Gage, R. A. Gibbs, G. Glusman, S. Gnerre, N. Goldman, L. Goodstadt, D. Grafham, T. A. Graves, E. D. Green, S. Gregory, R. Guigo, M. Guyer, R. C. Hardison, D. Haussler, Y. Hayashizaki, L. W. Hillier, A. Hinrichs, W. Hlavina, T. Holzer, F. Hsu, A. Hua, T. Hubbard, A. Hunt, I. Jackson, D. B. Jaffe, L. S. Johnson, M. Jones, T. A. Jones, A. Joy, M. Kamal, E. K. Karlsson, D. Karolchik, A. Kasprzyk, J. Kawai, E. Keibler, C. Kells, W. J. Kent, A. Kirby, D. L. Kolbe, I. Korf, R. S. Kucherlapati, E. J. Kulbokas, D. Kulp, T. Landers, J. P. Leger, S. Leonard, I. Letunic, R. Levine, J. Li, M. Li, C. Lloyd, S. Lucas, B. Ma, D. R. Maglott, E. R. Mardis, L. Matthews, E. Mauceli, J. H. Mayer, M. McCarthy, W. R. McCombie, S. McLaren, K. McLay, J. D. McPherson, J. Meldrim, B. Meredith, J. P. Mesirov, W. Miller, T. L. Miner, E. Mongin, K. T. Montgomery, M. Morgan, R. Mott, J. C. Mullikin, D. M. Muzny, W. E. Nash, J. O. Nelson, M. N. Nhan, R. Nicol, Z. Ning, C. Nusbaum, M. J. O'Connor, Y. Okazaki, K. Oliver, E. Overton-Larty, L. Pachter, G. Parra, K. H. Pepin, J. Peterson, P. Pevzner, R. Plumb, C. S. Pohl, A. Poliakov, T. C. Ponce, C. P. Ponting, S. Potter, M. Quail, A. Reymond, B. A. Roe, K. M. Roskin, E. M. Rubin, A. G. Rust,

R. Santos, V. Sapojnikov, B. Schultz, J. Schultz, M. S. Schwartz, S. Schwartz, C. Scott, S. Seaman, S. Searle, T. Sharpe, A. Sheridan, R. Shownkeen, S. Sims, J. B. Singer, G. Slater, A. Smit, D. R. Smith, B. Spencer, A. Stabenau, N. Stange-Thomann, C. Sugnet, M. Suyama, G. Tesler, J. Thompson, D. Torrents, E. Trevaskis, J. Tromp, C. Ucla, A. Ureta-Vidal, J. P. Vinson, A. C. Von Niederhausern, C. M. Wade, M. Wall, R. J. Weber, R. B. Weiss, M. C. Wendl, A. P. West, K. Wetterstrand, R. Wheeler, S. Whelan, J. Wierzbowski, D. Willey, S. Williams, R. K. Wilson, E. Winter, K. C. Worley, D. Wyman, S. Yang, S. P. Yang, E. M. Zdobnov, M. C. Zody and E. S. Lander (2002). "Initial sequencing and comparative analysis of the mouse genome." Nature **420**(6915): 520-562.

Weems, P. W., L. M. Coolen, S. M. Hileman, S. Hardy, R. B. McCosh, R. L. Goodman and M. N. Lehman (2018). "Evidence That Dynorphin Acts Upon KNDy and GnRH Neurons During GnRH Pulse Termination in the Ewe." Endocrinology **159**(9): 3187-3199.

Weems, P. W., C. F. Witty, M. Amstalden, L. M. Coolen, R. L. Goodman and M. N. Lehman (2016). "κ-Opioid Receptor Is Colocalized in GnRH and KNDy Cells in the Female Ovine and Rat Brain." Endocrinology **157**(6): 2367-2379.

Weenen, C., J. S. Laven, A. R. Von Bergh, M. Cranfield, N. P. Groome, J. A. Visser, P. Kramer, B. C. Fauser and A. P. Themmen (2004). "Anti-Mullerian hormone expression pattern in the human ovary: potential implications for initial and cyclic follicle recruitment." Mol Hum Reprod **10**(2): 77-83.

Welch, W. J. and C. R. Brown (1996). "Influence of molecular and chemical chaperones on protein folding." Cell Stress Chaperones **1**(2): 109-115.

Welt, C. K., K. A. Martin, A. E. Taylor, G. M. Lambert-Messerlian, W. F. Crowley, Jr., J. A. Smith, D. A. Schoenfeld and J. E. Hall (1997). "Frequency modulation of follicle-stimulating hormone (FSH) during the luteal-follicular transition: evidence for FSH control of inhibin B in normal women." J Clin Endocrinol Metab **82**(8): 2645-2652.

Welt, C. K., Y. L. Pagan, P. C. Smith, K. B. Rado and J. E. Hall (2003). "Control of follicle-stimulating hormone by estradiol and the inhibins: critical role of estradiol at the hypothalamus during the luteal-follicular transition." J Clin Endocrinol Metab **88**(4): 1766-1771.

Wendy Kuohung, M. D. H., MD (2019). "Causes of female infertility ", from https://www.uptodate.com/contents/causes-of-female-infertility.

White, M. F. (2003). "Insulin signaling in health and disease." Science **302**(5651): 1710-1711.

WHO (1992). Recent Advances in Medically Assisted Conception **Number 820, 1992, pp 1-111.**

Wickenheisser, J. K., V. L. Nelson-Degrave and J. M. McAllister (2005). "Dysregulation of cytochrome P450 17alpha-hydroxylase messenger ribonucleic acid stability in theca cells isolated from women with polycystic ovary syndrome." J Clin Endocrinol Metab **90**(3): 1720-1727.

Willett, K., R. Jiang, E. Lenart, D. Spiegelman and W. Willett (2006). "Comparison of bioelectrical impedance and BMI in predicting obesity-related medical conditions." Obesity (Silver Spring) **14**(3): 480-490.
Wise, L. A., K. J. Rothman, E. M. Mikkelsen, H. T. Sorensen, A. Riis and E. E. Hatch (2010). "An internet-based prospective study of body size and time-to-pregnancy." Hum Reprod **25**(1): 253-264.
Witham, E. A., J. D. Meadows, S. Shojaei, A. S. Kauffman and P. L. Mellon (2012). "Prenatal exposure to low levels of androgen accelerates female puberty onset and reproductive senescence in mice." Endocrinology **153**(9): 4522-4532.
Wolf, W. M., R. A. Wattick, O. N. Kinkade and M. D. Olfert (2018). "Geographical Prevalence of Polycystic Ovary Syndrome as Determined by Region and Race/Ethnicity." International journal of environmental research and public health **15**(11): 2589.
Wu, L. L., K. R. Dunning, X. Yang, D. L. Russell, M. Lane, R. J. Norman and R. L. Robker (2010). "High-fat diet causes lipotoxicity responses in cumulus-oocyte complexes and decreased fertilization rates." Endocrinology **151**(11): 5438-5445.
Wu, L. L., D. L. Russell, S. L. Wong, M. Chen, T.-S. Tsai, J. C. St John, R. J. Norman, M. A. Febbraio, J. Carroll and R. L. Robker (2015). "Mitochondrial dysfunction in oocytes of obese mothers: transmission to offspring and reversal by pharmacological endoplasmic reticulum stress inhibitors." Development **142**(4): 681-691.
Xiao, C., A. Giacca and G. F. Lewis (2011). "Sodium phenylbutyrate, a drug with known capacity to reduce endoplasmic reticulum stress, partially alleviates lipid-induced insulin resistance and beta-cell dysfunction in humans." Diabetes **60**(3): 918-924.
Xu, Y., L. D. Faulkner and J. W. Hill (2011). "Cross-Talk between Metabolism and Reproduction: The Role of POMC and SF1 Neurons." Front Endocrinol (Lausanne) **2**: 98.
Yagel, S., A. Ben-Chetrit, E. Anteby, D. Zacut, D. Hochner-Celnikier and M. Ron (1992). "The effect of ethinyl estradiol on endometrial thickness and uterine volume during ovulation induction by clomiphene citrate." Fertil Steril **57**(1): 33-36.
Yalcin, A. and G. S. Hotamisligil (2013). "Impact of ER protein homeostasis on metabolism." Diabetes **62**(3): 691-693.
Yan, X., C. Yuan, N. Zhao, Y. Cui and J. Liu (2014). "Prenatal androgen excess enhances stimulation of the GNRH pulse in pubertal female rats." **222**(1): 73.
Yaswen, L., N. Diehl, M. B. Brennan and U. Hochgeschwender (1999). "Obesity in the mouse model of pro-opiomelanocortin deficiency responds to peripheral melanocortin." Nat Med **5**(9): 1066-1070.
Ye, J. (2013). "Mechanisms of insulin resistance in obesity." Front Med **7**(1): 14-24.
Youngren, J. F. (2007). "Regulation of insulin receptor function." Cell Mol Life Sci **64**(7-8): 873-891.

Yu, Y. Y., C. X. Sun, Y. K. Liu, Y. Li, L. Wang and W. Zhang (2015). "Genome-wide screen of ovary-specific DNA methylation in polycystic ovary syndrome." Fertil Steril **104**(1): 145-153 e146.
Yuan, M., N. Konstantopoulos, J. Lee, L. Hansen, Z. W. Li, M. Karin and S. E. Shoelson (2001). "Reversal of obesity- and diet-induced insulin resistance with salicylates or targeted disruption of Ikkbeta." Science **293**(5535): 1673-1677.
Zaadstra, B. M., J. C. Seidell, P. A. Van Noord, E. R. te Velde, J. D. Habbema, B. Vrieswijk and J. Karbaat (1993). "Fat and female fecundity: prospective study of effect of body fat distribution on conception rates." BMJ **306**(6876): 484-487.
Zadehmodarres, S., Z. Heidar, Z. Razzaghi, L. Ebrahimi, K. Soltanzadeh and F. Abed (2015). "Anti-mullerian hormon level and polycystic ovarian syndrome diagnosis." Iranian journal of reproductive medicine **13**(4): 227-230.
Zakar, T. and S. Mesiano (2011). "How Does Progesterone Relax the Uterus in Pregnancy?" New England Journal of Medicine **364**(10): 972-973.
Zawadzki, J. and A. Dunaif (1992). Polycystic Ovary Syndrome, Current Issues in Endocrinology and Metabolism, Boston: Blackwell Scientific Publications.
Zegers-Hochschild, F., G. D. Adamson, J. de Mouzon, O. Ishihara, R. Mansour, K. Nygren, E. Sullivan and S. Vanderpoel (2009). "International Committee for Monitoring Assisted Reproductive Technology (ICMART) and the World Health Organization (WHO) revised glossary of ART terminology, 2009[∗]." Fertility and Sterility **92**(5): 1520-1524.
Zeleznik, A. J., A. R. Midgley, Jr. and L. E. Reichert, Jr. (1974). "Granulosa cell maturation in the rat: increased binding of human chorionic gonadotropin following treatment with follicle-stimulating hormone in vivo." Endocrinology **95**(3): 818-825.
Zhang, D., J. Cong, H. Shen, Q. Wu and X. Wu (2014). "Genome-wide identification of aberrantly methylated promoters in ovarian tissue of prenatally androgenized rats." Fertil Steril **102**(5): 1458-1467.
Zhang_Lab. "Guide Design Resources." from https://zlab.bio/guide-design-resources.
Zhen, S., M. Zakaria, A. Wolfe and S. Radovick (1997). "Regulation of Gonadotropin-Releasing Hormone (GnRH) Gene Expression by Insulin-Like Growth Factor I in a Cultured GnRH-Expressing Neuronal Cell Line." Molecular Endocrinology **11**(8): 1145-1155.
Zhou, F., L. B. Shi and S. Y. Zhang (2017). "Ovarian Fibrosis: A Phenomenon of Concern." Chin Med J (Engl) **130**(3): 365-371.